

DISSERTATION

TURBULENT VELOCITY PROFILES IN CLEAR WATER AND
SEDIMENT-LADEN FLOWS

Submitted by

Junke Guo

Department of Civil Engineering

In partial fulfillment of the requirements

for the Degree of Doctor of Philosophy

Colorado State University

Fort Collins, Colorado

Spring 1998

COLORADO STATE UNIVERSITY

December 18, 1997

WE HEREBY RECOMMEND THAT THE DISSERTATION PREPARED UNDER OUR SUPERVISION BY **JUNKE GUO** ENTITLED **TURBULENT VELOCITY PROFILES IN CLEAR WATER AND SEDIMENT-LADEN FLOWS** BE ACCEPTED AS FULFILLING IN PART REQUIREMENTS FOR THE DEGREE OF DOCTOR OF PHILOSOPHY.

Committee on Graduate Work

Adviser

Department Head/Director

To my parents
my brothers and sisters
my wife Jun An and my son Hao

*“Everything should be made as simple as possible,
but not simpler.”*
—Albert Einstein

ABSTRACT OF DISSERTATION

TURBULENT VELOCITY PROFILES IN CLEAR WATER AND
SEDIMENT-LADEN FLOWS

This dissertation studies turbulent velocity profiles in pipes with clear water, and centerline velocity profiles in open-channels with clear water and sediment-laden flows. The main purpose is to find a suitable velocity profile law for the entire boundary layer, particularly near the water surface, and to study the effects of sediment suspension on the model parameters. As a prerequisite for the study of velocity profiles in open-channels, a theoretical method for determining the bed shear stress in smooth rectangular channels is presented.

The major findings are:

(1) A wall shear turbulent velocity profile, in a velocity defect form, consists of three parts: a log term, a wake correction term, and a boundary correction term which is a linear function. The first two terms are the same as those in the classical log-wake law. The third term is a major contribution of this study. This new velocity profile law is referred to as the *modified log-wake law*. The new law considers the upper derivative boundary condition, which is not satisfied in previous studies. Physically, the log term reflects the inertia effect, the wake term reflects the large scale turbulent mixing, and the linear term reflects the effect of the upper boundary condition. In open-channels, the log term reflects the effect of the channel bed; the wake term reflects the effect of the side-walls, which induce secondary flows in the corners and then produce large scale turbulent mixing.

(2) For clear water flows in pipes, the new law contains two universal constants: the von Karman constant $\kappa_0 = 0.406$ and the wake strength coefficient $\Omega_0 = 3.2$.

(3) For clear water flows in narrow channels, the boundary layer thickness δ is

defined as the distance from the bed to the maximum velocity. The velocity profile equation is similar to that in pipes except that the wake strength coefficient Ω_0 decreases with the aspect ratios. In particular, the new law can even reproduce the velocity profile measurements beyond the boundary layer thickness.

(4) For clear water flows in wide channels, the effect of the side-walls is weakened, also, the water surface limits large scale turbulent mixing, so the wake component may be neglected. The modified log-wake law reduces to a log-linear law. The von Karman constant κ_0 is still 0.406. The water surface shear stress is considered through the parameter λ_0 which is about a constant 0.065 for a smooth bed and small relative roughness, but increases with the relative roughness in very rough beds.

(5) The modified log-wake law is also valid in sediment-laden flows. Sediment suspension affects the velocity profile in two factors: concentration and density gradient (the Richardson number R_i). Both factors reduce the von Karman constant κ . However, if both concentration and density gradient near the water surface are very small, they have little effect on the wake strength coefficient Ω in narrow channels and the water surface shear effect factor λ in wide channels.

(6) The modified log-wake law, including its reduction in wide channels, compares quite well with over 100 experimental velocity profiles in pipes, narrow open-channels and wide open-channels. The correlation coefficients r are always over 0.99.

Junke Guo
Department of Civil Engineering
Colorado State University
Fort Collins, CO 80523
Spring 1998

ACKNOWLEDGMENTS

I would like to thank a number of people who contributed, directly or indirectly, to this dissertation. First, I would like to express gratitude to Prof. Pierre Y. Julien, my advisor, for his guidance, encouragement, friendship and financial support during this study. Working with him has been a rewarding and enjoyable experience.

Prof. Carl F. Nordin and Prof. Robert N. Meroney expressed much interest in this study. Their service in my graduate study committee and academic supports are greatly appreciated. Thanks do also go to Prof. Deborah J. Anthony at Department of Earth Resources for her service as the outside member in the committee.

The experimental data used in this dissertation were provided by Dr. Lex Smits and Dr. Mark V. Zagarola at Princeton University, Dr. Walter H. Graf at Swiss Federal Institute of Technology at Lausanne, Dr. Marian V. I. Muste at the University of Iowa, and Dr. Xang-Kui Wang and Prof. Yu-Jia Hui at Tsinghua University, China. These people are greatly acknowledged. Their valuable data sets are certainly important for this study.

I am also grateful to Dr. Virenda C. Patel, Distinguished Professor and Director of Iowa Institute of Hydraulic Research, the University of Iowa, and Prof. Yu-Jia Hui at the Sedimentation Lab, Tsinghua University, China, for their constant encouragement. Mr. Baosheng Wu, my classmate in both China and CSU, is also appreciated for his discussion, encouragement and friendship.

In addition, I particularly thank Dr. Hsieh Wen Shen, Professor of Civil and Environmental Engineering at the University of California, Berkeley, Member of National Academy of Engineering, for his support through the 1997-1998 H. W. Shen Water Resources Graduate Award.

Lastly, I would like to dedicate this work to my parents, brothers and sisters. Their twenty year supports make this dissertation possible. I would also like to dedicate

this work to my wife Jun An and my son Hao Guo for their patience, understanding, and love through the two years required for this effort.

Junke Guo
Division of Hydraulics and Fluid Mechanics
Department of Civil Engineering
Colorado State University
Fort Collins, CO 80523
jguo@lamar.colostate.edu

Contents

1	INTRODUCTION	1
1.1	Statement and significance of the problem	1
1.2	Background	1
1.3	Objectives	2
1.4	Limitations and assumptions	2
1.5	Outline	3
2	LITERATURE REVIEW	4
2.1	Introduction	4
2.2	Velocity Profile in Clear Water	4
2.2.1	Linear law in the viscous sublayer	5
2.2.2	Log law in the overlap	6
2.2.3	Parabolic law in the wake layer and upper boundary conditions	7
2.2.4	The law of the wall (general inner region law)	10
2.2.5	The law of the wake (general outer region law)	11
2.3	Velocity Profiles in Sediment-Laden Flows	12
2.3.1	Extension of the log law to sediment-laden flows	12
2.3.2	Extension of the log-wake law to sediment-laden flows	14
2.3.3	Log-linear law and others	16
2.4	Summary	17
3	SIMILARITY ANALYSIS OF CLEAR WATER VELOCITY PROFILES	18

3.1	Introduction	18
3.2	Four-step similarity analysis method	19
3.2.1	Dimensional analysis	19
3.2.2	Intermediate asymptotics	20
3.2.3	Wake correction (or wake function)	20
3.2.4	Boundary correction	21
3.3	Velocity profile analysis	23
3.3.1	Dimensional analysis	23
3.3.2	Intermediate asymptotics	24
3.3.3	Wake correction to the log law	25
3.3.4	Boundary correction to the log-wake law	26
3.4	Implication to turbulent eddy viscosity	27
3.5	Summary	28
4	SHEAR VELOCITY IN SMOOTH OPEN-CHANNELS	29
4.1	Introduction	29
4.2	Conformal mapping from a rectangular cross-section (z -plane) into a half upper plane (w -plane)	30
4.3	Bed shear stress distribution and centerline shear velocity	32
4.4	Average bed shear stress and average bed shear velocity	36
4.5	Summary	41
5	TEST OF THE MODIFIED LOG-WAKE LAW IN CLEAR WA- TER	42
5.1	Introduction	42
5.2	Test of the modified log-wake law in pipes	43
5.2.1	Modified log-wake law in pipes	43
5.2.2	Data selection	43
5.2.3	Methods for determining κ_0 and Ω_0	43
5.2.4	Test of the structure of the modified log-wake law	45
5.2.5	Test of κ_0 and Ω_0 with Reynolds number	45

5.2.6	Test of the eddy viscosity model	49
5.3	Test of the modified log-wake law in narrow open-channels	53
5.3.1	Data selection	53
5.3.2	Method for determining δ and $\bar{u}_{1\max}$	54
5.3.3	Test of the modified log-wake law	54
5.3.4	Test of the eddy viscosity model	60
5.4	Test of the modified log-wake law in wide open-channels	61
5.4.1	Data selection	61
5.4.2	Method for determining u_* , Ω_0 , and λ_0	61
5.4.3	Test of the modified log-wake law	61
5.4.4	Wake strength coefficient Ω_0 in open-channels	62
5.5	Simplification of the modified log-wake law and its test in wide open-channels	64
5.5.1	Simplification of the modified log-wake law (the log-linear law) in wide open-channels	64
5.5.2	Data selection	65
5.5.3	Method for determining u_* , λ_0 and $\bar{u}_{1\max}$	66
5.5.4	Test of the log-linear law	66
5.5.5	The water surface shear effect factor λ_0	67
5.5.6	Test of the eddy viscosity model	73
5.6	Summary	75
6	THEORETICAL ANALYSIS OF SEDIMENT-LADEN FLOWS	77
6.1	Introduction	77
6.2	Governing equations	77
6.2.1	Navier-Stokes equations in sediment-laden flows	77
6.2.2	Reynolds mean equations and turbulent equations in sediment-laden flows	79
6.3	Simplifications of governing equations in steady uniform 2D flows	82
6.4	Effects of sediment suspension on turbulence intensities	86

6.4.1	Turbulence intensity $\overline{u'_i u'_j}$ in sediment-laden flows	87
6.4.2	Turbulent kinetic energy budget and Richardson number in sediment-laden flows	89
6.4.3	Effects of sediment suspension on the vertical eddy viscosity .	91
6.5	Modification of the eddy viscosity model in sediment-laden flows . . .	93
6.6	Velocity profiles in sediment-laden flows	94
6.7	Summary	94
7	TEST OF THE MODIFIED LOG-WAKE LAW IN SEDIMENT- LADEN FLOWS	96
7.1	Introduction	96
7.2	Preliminary analysis of the model parameters	96
7.3	Test of the modified log-wake law in narrow open-channels	97
7.3.1	Effect of molecular viscosity	98
7.3.2	Effect of density gradient	104
7.3.3	Combination of the effects of molecular viscosity and density gradient	109
7.4	Test of the log-linear law in natural rivers	110
7.4.1	Test of the log-linear law in natural rivers	110
7.4.2	Conjecture of the effects of sediment suspension in wide open- channels	111
7.5	Summary	114
8	APPLICATIONS OF THE MODIFIED LOG-WAKE LAW	115
8.1	Applications of the modified log-wake law in pipes	115
8.1.1	Relation between the maximum velocity $\bar{u}_{1\max}$ and the average velocity U	115
8.1.2	Position of the average velocity U	116
8.1.3	Procedures for applying the modified log-wake law	116
8.2	Applications of the modified log-wake law in open-channels	117
8.2.1	Magnitude of the linear term in the log-linear law	118

8.2.2	Relation between the maximum velocity $\bar{u}_{1\max}$ and the average velocity U	118
8.2.3	Position of the average velocity U	119
8.2.4	Procedures for applying the log-linear law	120
9	SUMMARY AND CONCLUSIONS	122
9.1	Summary	122
9.2	Conclusions	123
9.2.1	Clear water flows	123
9.2.2	Sediment-laden flows	125
9.3	Recommendations	126
	REFERENCES	127
	APPENDICES	133
	A POWER-WAKE LAW IN TURBULENT PIPE FLOWS	133
	Development of the power-wake law	133
	Dimensional analysis	133
	Intermediate asymptotics	134
	Wake correction	134
	Boundary correction	134
	Determinations of α and C_o in the power-wake law	135
	Test of the power-wake law	136
	B MATLAB PROGRAMS	140
	Program for solving κ and Ω in the modified log-wake law	140
	Program for solving κ , $\bar{u}_{1\max}$ and λ in the log-linear law	143
	C ANALYSIS OF WANG-QIAN'S EXPERIMENTAL DATA	145
	Introduction of the experiments	145
	Measurements of velocity profile and concentration profile data (Wang and Qian, 1989)	146

Velocity profile analysis	146
D ANALYSIS OF COLEMAN'S EXPERIMENTAL DATA	173
E ANALYSIS OF KIRONOTO'S EXPERIMENTAL DATA	197
F ANALYSIS OF MUSTE'S EXPERIMENTAL DATA	216
G ANALYSIS OF McQUIVEY'S EXPERIMENTAL DATA	220
H ANALYSIS OF GUY, SIMONS AND RICHARDSON'S EXPERIMENTAL DATA	228
I MEASUREMENT DATA IN THE YELLOW RIVER AND THE YANGTZE RIVER	234
Measurements of velocity and concentration profiles at Hua-Yuan-Kou Hydrologic Station, the Yellow River, China	234
Measurements of velocity and concentration profiles at Feng-Jie Hydrologic Station, the Yangtze River, China	236

List of Tables

4.1	Comparison of side-wall correction factor with experiments	40
5.1	The model parameters in the modified log-wake law for individual velocity profiles (Velocity profile data source: Zagarola, 1996)	48
5.2	Calculated results of Wang-Qian’s clear and salt water experiments .	55
5.3	Calculated results of Coleman’s clear water experiments	55
5.4	Calculated results of Kironoto’s clear water experiments	59
5.5	Results of Kironoto’s wide channel experiments from the modified log-wake law	62
5.6	Results of Kironoto’s wide channel experiments	67
5.7	Results of Muste’s wide channel experiments	67
5.8	Results of McQuivey’s wide channel experiments	68
5.9	Results of Guy et al.’s wide channel experiments	68
7.1	Calculated results of Wang-Qian’s neutral particle experiments . . .	101
7.2	Calculated results of Wang-Qian’s quasi-neutral particle experiments	102
A.1	The model parameters in the power-wake law for individual velocity profiles (Velocity profile data source: Zagarola, 1996)	137
C.1	Wang-Qian’s (1989) measurements of velocity profiles in clear water and salt water	147
C.2	Wang-Qian’s (1989) measurements of velocity profiles in neutral particle-laden flows	148

C.3	Wang-Qian's (1989) measurements of velocity profiles in density sediment-laden flows	149
C.4	Wang-Qian's (1989) measurements of concentration profiles	151
D.1	Coleman's (1986) measurement data of velocity and concentration profiles	174
E.1	Kironoto's (1993) measurement data	198
F.1	Muste's (1995) ^a measurements of velocity profiles	217
G.1	McQuivey's (1971) measurements of velocity profiles	221
H.1	Selected experimental data of Guy, Simons and Richardson (1966) . .	229

List of Figures

2.1	Sketch of a representative velocity profile in open-channels	5
2.2	Upper derivative boundary conditions in pipes, narrow channels ($a/h < 5$), and wide channels ($a/h \geq 5$)	9
2.3	The velocity defect law in the outer region (After Hinze, 1975, p.631)	10
2.4	The law of the wall in the inner region (After White, 1991, p.416) . .	11
2.5	Effect of suspended sediment on the von Karman constant (After Einstein and Chien, 1955)	13
2.6	Effect of suspended sediment on the wake strength coefficient	15
4.1	Scheme of flow domain from a rectangular cross-section to a half upper plane	31
4.2	Scheme for computing bed shear stress distribution	33
4.3	Bed shear stress distribution versus aspect ratio	35
4.4	Scheme for computing average bed shear stress	37
4.5	Comparison of the theoretical side-wall correction factor with experimental data	39
5.1	Test of the structure of the modified log-wake law [(a) in a semilog coordinate system; (b) in a rectangular coordinate system.]	46
5.2	Comparison of the modified log-wake law and Zagarola's superpipe experimental profiles with $y^+ \geq 70$	47
5.3	(a) Variation of κ_0 versus Re_* ; (b) Variation of Ω_0 versus Re_*	50
5.4	Complete similarity: Comparison of the modified log-wake law with Zagarola's (1996) superpipe experimental data with $y^+ \geq 500$	51

5.5	Test of the eddy viscosity model from the modified log-wake law . . .	52
5.6	Comparison of the modified log-lake law with Wang-Qian's experiments [(a) in a semilog coordinate system, (b) in a rectangular coordinate system]	56
5.7	Comparison between the modified log-lake law and Coleman's experi- mental data [(a) in a semilog coordinate system , (b) in a rectangular coordinate system]	57
5.8	Comparison between the modified log-lake law and Kironoto's narrow flume data [(a) in a semilog coordinate system, (b) in a rectangular coordinate system]	58
5.9	Test of the eddy viscosity model from the modified log-wake law . . .	60
5.10	Comparison of the modified log-wake law with Kironoto's wide channel data [(a) in a rectangular coordinate, (b) in a semilog coordinate] . .	63
5.11	The wake strength coefficient Ω_0 versus the aspect ratio a/h	64
5.12	Comparison of the log-linear law with Kironoto's experimental data [(a) in a rectangular coordinate, (b) in a semilog coordinate]	69
5.13	Comparison between the log-linear law and Muste's experimental data [(a) in a rectangular coordinate, (b) in a semilog coordinate]	70
5.14	Comparison between the log-linear law and McQuivey's experimental data [(a) in a rectangular coordinate, (b) in a semilog coordinate] . .	71
5.15	Comparison between the log-linear law and Guy et al.'s experimental data [(a) in a rectangular coordinate system, (b) in a semilog coordi- nate system]	72
5.16	The water surface effect factor λ_0	74
5.17	Test of the eddy viscosity model from the log-linear law	75
6.1	Scheme of steady uniform 2D sediment-laden flows	83
7.1	A representative velocity profile of neutral sediment-laden flows in nar- row channels [(a) in a semilog coordinate; (b) in a rectangular coordi- nate]	99

7.2	The effect of molecular viscosity on the velocity profiles [o: Wang and Qian's data (1989); —: The modified log-wake law]	100
7.3	The effect of molecular viscosity on the von Karman constant	103
7.4	The effect of molecular viscosity on the wake strength coefficient	103
7.5	A representative velocity profile of sediment-laden flows in narrow channels [(a) in a semilog coordinate; (b) in a rectangular coordinate]	105
7.6	The effect of density gradient on velocity profiles [o: Coleman's data (1986); —: The modified log-wake law]	106
7.7	The effect of density gradient on the von Karman constant	109
7.8	The effect of density gradient on the wake strength coefficient	110
8.1	Position of the average velocity versus the water surface shear correction	119
A.1	Comparison among the power-wake law, the modified log-wake law and Zagarola's superpipe experimental data ($y^+ \geq 50$)	138
A.2	The variations of the model parameters with Reynolds number: (a) α versus Re_* , (b) C_o versus Re_*	139

List of Symbols

- A Constant in parabolic law (2.17)
- A_b, A_w Cross-section areas corresponding to the bed and the side-walls, respectively, see FIG. 4.2
- a Channel width
- a_1, a_2, a_3 Curve-fitting constant in the parabolic law (5.14)
- B (= 5.5) constant in Spalding's law (2.18); or boundary correction function in (3.6), (3.7) and (3.22)
- C Instantaneous volumetric sediment concentration
- \overline{C} Local time-mean volumetric sediment concentration
- \overline{C}_a Reference volumetric sediment concentration
- C_d Water surface drag coefficient in (2.10)
- C_i Parameter in the power law (A.4)
- C_o Parameter in the power law (A.5)
- C_1, C_2 Addictive constants in the log law (2.6) and (2.21)
- C_3 Constant in the log-wake law (3.21)
- C_4 Addictive constant in the power law (A.4)
- D Molecular sediment diffusion coefficient in (6.3)
- d Pipe diameter
- d_s Sediment diameter
- d_{50} Sediment medium diameter
- F Functional symbols in (3.9), (3.10) and (6.55)
- F_1, F_2 Functional symbols in (7.1), and (7.2)
- f Functional symbols in (3.8), (6.8) and FIG. (4.2)

G	($= \rho_s/\rho_0$) specific gravity; or functional symbols in (3.12) and (3.13)
g	The gravitational acceleration; or functional symbol in (3.11)
g_i	Component of the gravitational acceleration in the x_i -direction
h	Flow depth
i, j, k	Subscripts in tensor variables
k_s	Bed roughness
L_m	Monin-Obukhov length scale in (2.21)
m	Subscript for mixture water; or exponent in (7.9)
n	Sample number of a velocity profile measurements
p	Pressure
p_1, p_2, p_3	Curve-fitting constants in (5.20) and (5.25)
R	Pipe radius or hydraulic radius
R_i	Global Richardson number in (6.45)
r	Correlation coefficient of the modified log-wake law with measurement velocity profile data
Re	($= VR/\nu$) Reynolds number
Re $_*$	($= u_*\delta/\nu$) Reynolds number
S	Energy or bed slope; or the sum of the squares of residuals in the least-squares method (5.3)
t	Time
U	Pipe average velocity, or vertical average velocity in an open-channel
u_i	Instantaneous velocity in direction- i , and $i = 1, 2, 3$. “1” denotes the flow direction; “2” denotes the lateral direction; and “3” denotes the vertical direction
\bar{u}_i	Local time-mean; or sample data in a curve-fitting
u'_i	Turbulent velocity
u_*	Shear velocity
$\bar{u}_{1\max}$	The maximum velocity at the boundary layer margin $\xi = 1$
u^+	($= \bar{u}_1/u_*$) normalized velocity by the shear velocity
$\overline{u'_i u'_j}$	Turbulence intensity

V_{wind}	Wind velocity over the water surface
W	Wake function
w	A half-upper plane, complex variable $w = \xi + i\eta$
x_i	Coordinates
x_1	Flow direction coordinate; or a point in the bed of FIG. 4.2
x_{30}	Reference position in the Monin-Obukhov log-linear law in (2.21)
y^+	($= u_* x_3 / \nu$) normalized distance by the viscous length scale
z	Physical flow domain, complex variable $z = x + iy$

Greek Symbols

α	Coefficient in (7.5); or exponent in the power law (A.3)
α_i	Experimental exponents in a complete similarity (3.3)
β	Coefficient in (7.8)
Γ	Symbol of a boundary
δ	Boundary layer thickness, which is defined as the distance from the bed to the maximum velocity position
ε	Turbulent eddy viscosity
ε_m	Eddy viscosity in sediment-laden flows
ε^+	Dimensionless turbulent eddy viscosity
ε_m^+	Dimensionless eddy viscosity in sediment-laden flows
ε_s	Dimensionless turbulent sediment diffusion coefficient
ε_1^+	Dimensionless eddy viscosity at the water surface $\xi = 1$ for wide open-channels in (2.11)
κ	The von Karman constant in sediment-laden flows
κ_0	The von Karman constant in clear water ($\kappa_0 = 0.406$)
λ	Secondary flow correction for an average bed shear stress in (4.21) and (4.22); or water surface shear effect factor in the log-linear law in wide open-channels

λ_0	Water surface shear effect factor in the log-linear law in clear water flows
μ	The kinetic viscosity of clear water
μ_m	The kinetic viscosity of mixture water
ν	The kinematic viscosity of clear water
ν_m	The kinematic viscosity of mixture water
Π	The Coles wake strength coefficient in (2.19) or a dependable similarity parameter
Π_i	Independent similarity variables, and $i = 1, 2, 3, \dots, m$
ρ	Local sediment-water mixture density
ρ_0	The water density
ρ_{air}	Air density over a water surface, $\rho_{\text{air}} = 1.21 \text{ kg/m}^3$ is taken in this study
τ_b	Local bed shear stress
$\bar{\tau}_b$	Average bed shear stress
τ_{bc}	Channel centerline bed shear stress
τ_0	Bed shear stress in a 2D open-channel
ξ	(= x_3/δ) Sample data in a curve-fitting
$\bar{\xi}$	Position of the average velocity in a pipe or an open-channel flow
Ω	Wake strength coefficient
Ω_0	Wake strength coefficient in clear water flows
ω	Sediment settling velocity
Φ	Functional symbol of a similarity analysis in (3.1)
Φ_s	A concentration correction factor in the eddy viscosity model in (6.53)
ϕ_c	The side-wall correction factor for the centerline shear stress in (4.15)
ϕ_i	Dimensionless boundary conditions, and $i = 1, 2, 3, \dots, n$, in (3.2)
ϕ_m	The side-wall correction factor for average bed shear stress in (4.22)
θ	The angle between the channel bed and the datum

Chapter 1

INTRODUCTION

1.1 Statement and significance of the problem

The study of wall shear turbulent velocity profiles is a basic subject in fluid mechanics. In particular, the study of turbulent velocity profiles in sediment-laden flows is one of the most important subjects in sediment transport and river mechanics. This study addresses the problem: *what is the best functional form of the velocity profile equation in a pipe or open-channel, and how does sediment suspension affect the velocity profile in a sediment-laden flow?*

Since the problem is a fundamental subject, its thorough understanding is required to study flow resistance and sediment transport capacity. Furthermore, its accurate prediction is helpful for the analysis of a pipe flow, a river development and management, reservoir operation, flood protection, etc.

1.2 Background

To answer the above questions, extensive investigations have been reported for the last half century. The studies in clear water include Prandtl (Schlichting, 1979, p.596), von Karman (Schlichting, 1979, p.608), Nikuradse (1932), Keulegan (1938), Laufer (1954), Patel and Head (1969), Zagarola (1996), and many others. The studies in sediment-laden flows include Vanoni (1946), Einstein and Chien (1955), Vanoni and

Nomicos (1960), Elata and Ippen (1961), Coleman (1981, 1986), Janin (1986), Karim and Kennedy (1987), Woo, Julien and Richardson (1988), Lyn (1986, 1988), Wang and Qian(1989). All investigations of sediment-laden flows are to study the effects of sediment suspension on the model parameters in the log law, the log-wake law or the power law. However, a literature review shows that neither the log law, the log-wake law nor the power law is the best functional form of the velocity profile model in pipes and open-channels. This is because all of them do not satisfy the derivative boundary condition at the pipe axis, the water surface or the boundary layer margin, where the boundary layer thickness is defined as the distance from the bed to the maximum velocity position in narrow channels. Obviously, the subject of the velocity profiles in pipes and open-channels is still very challenging and a further research is indicated.

1.3 Objectives

The specific objectives addressed in this study are: (1) to establish a new velocity profile model in clear water flows using a new similarity analysis method; (2) to create a method for determining the bed shear stress (or the bed shear velocity) in a smooth rectangular channel, based on a conformal mapping method; (3) to determine the model parameters, i.e., the von Karman constant κ_0 , the wake strength coefficient Ω_0 , and the water surface shear effect factor λ_0 , in clear water flows, using a least-squares method; (4) to prove that the new velocity profile model from clear water flows is also valid in sediment-laden flows, based on the sediment-laden flow governing equations and a magnitude order analysis; and (5) to study the effects of sediment suspension on the model parameters, using a least-squares method.

1.4 Limitations and assumptions

This study is limited to the outer region velocity profiles in pipes and open-channels, i.e., the inner region (the viscous sublayer and the buffer layer), where the viscous shear stress is important, is excluded. In addition, the study assumes that: (1)

the flow is steady, uniform and 2D (two-dimensional); (2) the 2D flow results may be empirically extended to narrow channels; and (3) the volumetric concentration may be very high for neutral particle-laden flows, but relative dilute for natural sediment-laden flows, say, the volumetric concentration $\bar{C} < 0.1$.

1.5 Outline

This dissertation includes 9 chapters. Chapter 1 briefly introduces the subject and states the objectives. Chapter 2 reviews previous major achievements in pipes and open-channel flows. To meet Objective 1, Chapter 3 first presents a new similarity analysis method and then proposes a new velocity profile law, the *modified log-wake law*, in clear water. Chapter 4 discusses a method for determining the bed shear velocity in a smooth rectangular channel (Objective 2). Chapter 5 tests the modified log-wake law and studies the model parameters in clear water (Objective 3). Chapter 6 discusses the application of the velocity profile law from clear water to sediment-laden flows (Objective 4). Chapter 7 studies the effects of sediment suspension on the velocity profiles in sediment-laden flows (Objective 5). Chapter 8 illustrates the procedures for applying the modified log-wake law. Finally, Chapter 9 summarites the main results of this research. In addition, several appendixes, which show detailed programs or analyses, appear at the end of the dissertation.

Chapter 2

LITERATURE REVIEW

2.1 Introduction

This chapter reviews the previous principal achievements regarding velocity profiles in pipes and open-channels. The velocity profile in clear water is first reviewed in Section 2.2, Then, a review of the sediment-laden velocity profiles is followed in Section 2.3. Section 2.4 summarizes the previous major results and weaknesses.

2.2 Velocity Profile in Clear Water

Experimental evidence shows that all wall shear turbulent velocity profiles, such as pipe flows, open-channel flows, and boundary layer flows, over a smooth boundary can be divided into two regions (Coles, 1956): an inner region where turbulence is directly affected by the bed; and an outer region where the flow is only indirectly affected by the bed through its shear stress. The inner region can be further divided into a viscous sublayer, a buffer layer, and an overlap. Since the variation from the inner region to the outer region is gradual, the overlap is also a part of the outer regions (Kundu, 1990, p.451). Thus, the outer region can be further divided into the overlap and a wake layer. In brief, the flow domain in a wall shear turbulence can be divided into four layers (or subregions): viscous sublayer, buffer layer, overlap (or intermediate layer), and wake layer, shown in FIG. 2.1. The velocity profile in each

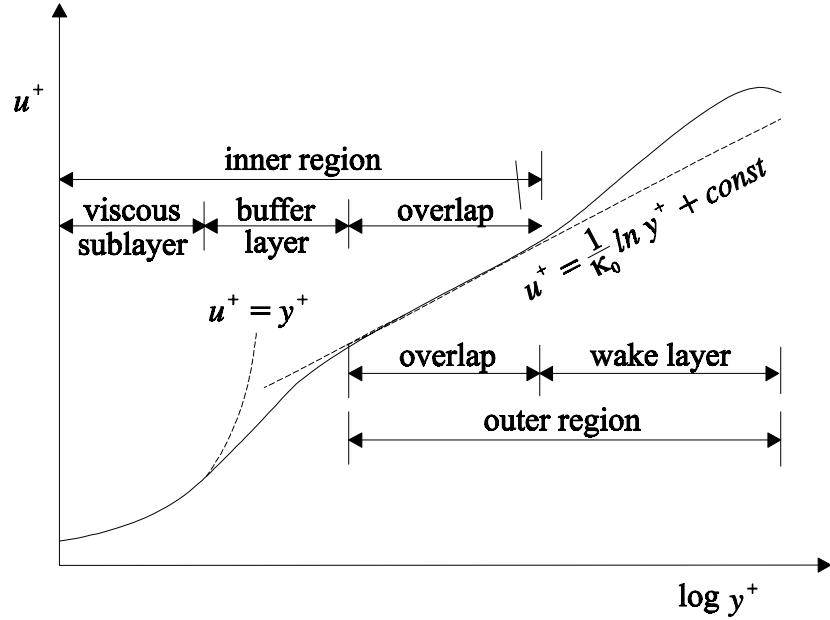


FIG. 2.1: Sketch of a representative velocity profile in open-channels

layer is reviewed below.

2.2.1 Linear law in the viscous sublayer

Assume that the velocity profile near the bed can be expressed as a Taylor series, i.e.

$$\bar{u}_1 = \bar{u}_1|_{x_3=0} + \left. \frac{d\bar{u}_1}{dx_3} \right|_{x_3=0} x_3 + \frac{1}{2} \left. \frac{d^2\bar{u}_1}{dx_3^2} \right|_{x_3=0} x_3^2 + \dots \quad (2.1)$$

where \bar{u}_1 is the time mean velocity in the flow direction; and x_3 is the distance from the bed. The no-slip condition at the bed requires that

$$\bar{u}_1|_{x_3=0} = 0 \quad (2.2)$$

According to Newton's frictional law, $\left. \frac{d\bar{u}_1}{dx_3} \right|_{x_3=0}$ is related to the bed shear stress τ_0 , i.e.

$$\tau_0 \equiv \rho_0 u_*^2 = \mu \left. \frac{d\bar{u}_1}{dx_3} \right|_{x_3=0}$$

or

$$\left. \frac{d\bar{u}_1}{dx_3} \right|_{x_3=0} = \frac{u_*^2}{\nu} \quad (2.3)$$

in which ρ_0 is the water density; $u_* = \sqrt{\tau_0/\rho_0}$ is the shear velocity; $\mu = \rho_0\nu$ is the water dynamic viscosity; and ν is the water kinematic viscosity.

Substituting (2.2) and (2.3) into (2.1) and neglecting the higher order terms yield the velocity profile near the bed as

$$\frac{\bar{u}_1}{u_*} = \frac{u_* x_3}{\nu}$$

or

$$u^+ = y^+ \quad (2.4)$$

in which $u^+ = \bar{u}_1/u_*$ and $y^+ = u_* x_3/\nu$ are the inner variables. Experiments (Schlichting, 1979, p.601) show that the above equation is valid in the range of $0 \leq y^+ \leq 5$.

The buffer layer velocity profile is very complicated and cannot be expressed using a simple function. It will be discussed in Subsection 2.2.4.

2.2.2 Log law in the overlap

Traditionally, the velocity profile in the overlap is expressed by the log law or the power law. The log law is usually regarded as a complete success since it can be derived from a complete similarity assumption (Kundu, 1990, p.451), i.e.

$$\bar{u}_1 = \frac{u_*}{\kappa_0} \ln x_3 + \text{const} \quad (2.5)$$

The above equation is usually expressed in terms of the inner variables as

$$u^+ = \frac{1}{\kappa_0} \ln y^+ + C_1 \quad (2.6)$$

in which $C_1 \approx 5$, or in terms of the outer variables as

$$\frac{\bar{u}_{1\max} - \bar{u}_1}{u_*} = -\frac{1}{\kappa_0} \ln \xi + C_2 \quad (2.7)$$

in which $\bar{u}_{1\max}$ = the velocity at the water surface for a wide channel or at the boundary layer margin for a narrow channel; $\xi = x_3/\delta$, and $C_2 \approx 1$. Experiments (Kundu, p.453) show that the log law is usually valid in the range of $y^+ > 30 - 70$ and $\xi < 0.15 - 0.2$, which is shown in FIG. 2.1.

Barenblatt (1996, p.271) has shown that the power law can be derived from an incomplete similarity assumption and the log law is only a special case of the power law. Zagarola (1996) experimentally shows that the power law has advantage over the log law in the range of $50 < y^+ < 500$. In practice, the log law may still be a good approximation.

2.2.3 Parabolic law in the wake layer and upper boundary conditions

The velocity profile near a water surface or a boundary layer margin can be expressed as a Taylor series, i.e.

$$\begin{aligned} \bar{u}_1 = & \bar{u}_1|_{\xi=1} + \frac{d\bar{u}_1}{d\xi} \Big|_{\xi=1} (\xi - 1) + \frac{1}{2!} \frac{d^2\bar{u}_1}{d\xi^2} \Big|_{\xi=1} (\xi - 1)^2 \\ & + \frac{1}{3!} \frac{d^3\bar{u}_1}{d\xi^3} \Big|_{\xi=1} (\xi - 1)^3 + \dots \end{aligned} \quad (2.8)$$

The boundary conditions at the water surface of a 2D channel can be expressed as:

$$\text{Velocity at the water surface: } \bar{u}_1|_{\xi=1} = \bar{u}_{1\max} \quad (2.9)$$

and the shear stress at the water surface (White, 1991, p.149):

$$\tau|_{\xi=1} = C_d \rho_{\text{air}} (V_{\text{wind}} - \bar{u}_{1\max})^2 \quad (2.10)$$

in which $\bar{u}_{1\max}$ = the maximum velocity; $\rho_{\text{air}} = 1.21 \text{ kg/m}^3$ is the air density in the standard atmosphere; V_{wind} is the wind velocity over the water; and C_d = the water surface drag coefficient which is in the order of 10^{-3} but difficult to determine accurately (Roll, 1965, p.160). On the other hand, the shear stress (turbulent shear stress) at the water surface relates to the velocity gradient by an eddy viscosity, i.e.

$$\tau|_{\xi=1} = \varepsilon_1^+ \rho_0 u_* \frac{d\bar{u}_1}{d\xi} \Big|_{\xi=1} \quad (2.11)$$

in which ε_1^+ is the dimensionless eddy viscosity at the water surface. From the above two equations, one derives that

$$\frac{d\bar{u}_1}{d\xi} \Big|_{\xi=1} = \frac{C_d \rho_{\text{air}} (V_{\text{wind}} - \bar{u}_{1\max})^2}{\varepsilon_1^+ \rho_0 u_*}$$

$$= \lambda_0 \frac{(V_{\text{wind}} - \bar{u}_{1 \text{ max}})^2}{u_*} \quad (2.12)$$

in which $\lambda_0 = C_d \rho_{\text{air}} / (\varepsilon_1^+ \rho_0)$ is called the water surface shear effect factor. The above equation shows that the shear stress at the water surface is usually nonzero except that the wind velocity over the water is equal to the water surface velocity.

However, the boundary layer thickness in a narrow channel is not the water depth, rather it is usually defined as the distance from the bed to the maximum velocity position. In this case, the velocity gradient at the maximum velocity must be zero, i.e.

$$\left. \frac{d\bar{u}_1}{d\xi} \right|_{\xi=1} = 0 \quad (2.13)$$

The above condition is also required in a circular pipe flow. (2.13) may also be expressed by (2.12) except that $\lambda_0 = 0$. (2.13) and (2.12) are shown in FIG. 2.2.

Now neglecting the 3rd and higher order terms in (2.8), one obtains

$$\bar{u}_1 = \bar{u}_{1 \text{ max}} + \left. \frac{d\bar{u}_1}{d\xi} \right|_{\xi=1} (\xi - 1) + \frac{1}{2!} \left. \frac{d^2\bar{u}_1}{d\xi^2} \right|_{\xi=1} (\xi - 1)^2 \quad (2.14)$$

or

$$\frac{\bar{u}_1}{u_*} = \frac{\bar{u}_{1 \text{ max}}}{u_*} + \frac{1}{u_*} \left. \frac{d\bar{u}_1}{d\xi} \right|_{\xi=1} (\xi - 1) + \frac{1}{2!} \frac{1}{u_*} \left. \frac{d^2\bar{u}_1}{d\xi^2} \right|_{\xi=1} (\xi - 1)^2 \quad (2.15)$$

The above equation can be rewritten as a defect form:

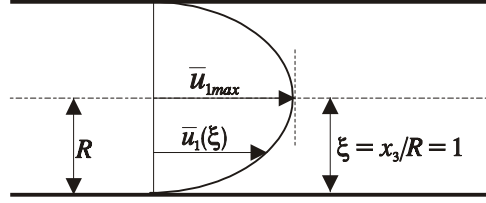
$$\frac{\bar{u}_{1 \text{ max}} - \bar{u}_1}{u_*} = \frac{1}{u_*} \left. \frac{d\bar{u}_1}{d\xi} \right|_{\xi=1} (1 - \xi) - \frac{1}{2!} \frac{1}{u_*} \left. \frac{d^2\bar{u}_1}{d\xi^2} \right|_{\xi=1} (1 - \xi)^2 \quad (2.16)$$

in which $\left. \frac{d\bar{u}_1}{d\xi} \right|_{\xi=1}$ is defined by (2.12) or (2.13); and $\frac{1}{2u_*} \left. \frac{d^2\bar{u}_1}{d\xi^2} \right|_{\xi=1}$ is determined experimentally.

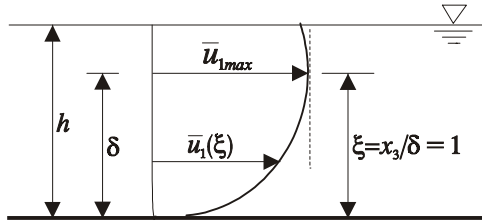
If (2.13) is used, the previous parabolic law is obtained

$$\frac{\bar{u}_{1 \text{ max}} - \bar{u}_1}{u_*} = A(1 - \xi)^2 \quad (2.17)$$

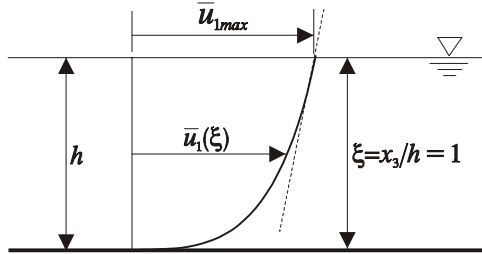
in which $A = -\frac{1}{2u_*} \left. \frac{d^2\bar{u}_1}{d\xi^2} \right|_{\xi=1}$ is determined experimentally. Bazin suggested $A = 6.3$ for wide open-channels (Hu and Hui, 1995, p.31), Hama gave $A = 9.6$ in plane boundary layers (Hinze, 1975, p.631) and Laufer proposed $A = 7.2$ in pipes (Hinze, 1975, p.732). The parabolic law is usually valid in $\xi > 0.15 - 0.2$, which is shown in



(a) Pipes: $\frac{d\bar{u}_1}{d\xi}\bigg|_{\xi=1} = 0$



(b) Narrow Channels: $\frac{d\bar{u}_1}{d\xi}\bigg|_{\xi=1} = 0$



(c) Wide channels: $\frac{d\bar{u}_1}{d\xi}\bigg|_{\xi=1} \propto \tau\bigg|_{\xi=1}$

FIG. 2.2: Upper derivative boundary conditions in pipes, narrow channels ($a/h < 5$), and wide channels ($a/h \geq 5$)

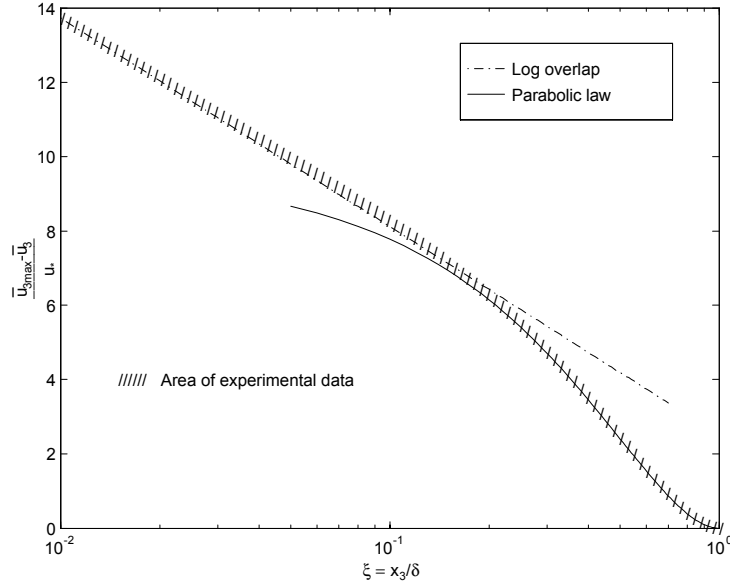


FIG. 2.3: The velocity defect law in the outer region (After Hinze, 1975, p.631)

FIG. 2.3. However, the velocity gradient at the water surface in a wide channel is not necessary to be zero, as indicated in (2.12).

Equations (2.4), (2.7) and (2.16) are independent of any turbulent models and are indeed three physical constraints to the velocity profile. A satisfactory turbulent model must meet them simultaneously. In practice, the viscous and the buffer layers may be neglected, in particular in a rough boundary. Therefore, (2.7) and (2.16) must be at least met.

2.2.4 The law of the wall (general inner region law)

To describe the velocity profile in the buffer layer ($5 \leq y^+ \leq 70$), Spalding (White, 1991, p.415) deduced a composite law of the wall, based on an asymptotic matching of (2.4) and (2.7), i.e.

$$y^+ = u^+ + e^{-\kappa_0 B} \left[e^{\kappa_0 u^+} - 1 - \kappa_0 u^+ - \frac{(\kappa_0 u^+)^2}{2} - \frac{(\kappa_0 u^+)^3}{6} \right] \quad (2.18)$$

in which $\kappa_0 = 0.4$, and $B = 5.5$. This equation smoothly merges the linear and the log laws and fits experimental data excellently, shown in FIG. 2.4. Therefore, it can be

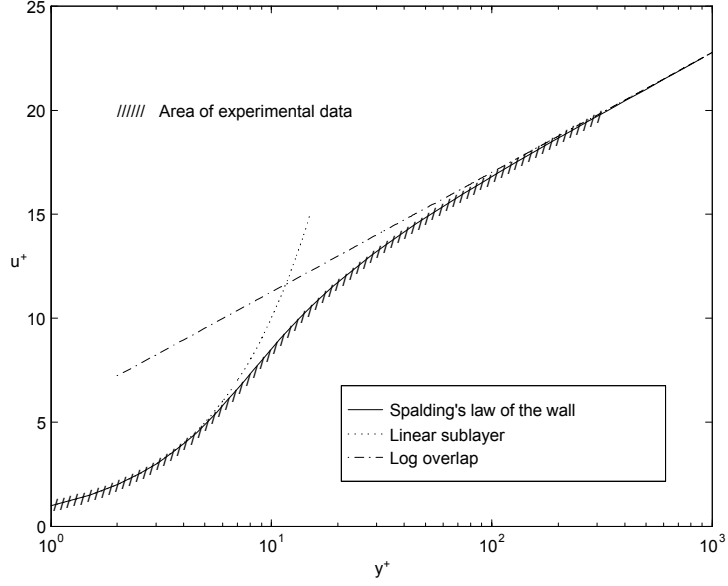


FIG. 2.4: The law of the wall in the inner region (After White, 1991, p.416)

regarded as a complete success in the inner region. The only weakness is its implicit functional relation.

2.2.5 The law of the wake (general outer region law)

The law of the wake or the log-wake law, proposed by Coles (1956, 1969), is a popular one in the outer region. Coles surveyed a lot of experiments of boundary layer flows, all experimental data showed that the velocity defect law in the outer region is a composite of two universal functions, i.e., the law of the wall and the law of the wake. That is,

$$\frac{\bar{u}_{1\max} - \bar{u}_1}{u_*} = \underbrace{\left[-\frac{1}{\kappa_0} \ln \xi + \frac{2\Pi}{\kappa_0} \right]}_{\text{The law of the wall}} - \underbrace{\frac{2\Pi}{\kappa_0} \sin^2 \left(\frac{\pi}{2} \xi \right)}_{\text{The law of the wake}} \quad (2.19)$$

in which Π is the Coles wake strength coefficient and varies with the pressure gradient in a boundary layer flow. The wake flow function is just a purely empirical function. For convenience of applications, an equivalent equation is often written as

$$\frac{\bar{u}_{1\max} - \bar{u}_1}{u_*} = -\frac{1}{\kappa_0} \ln \xi + \frac{2\Pi}{\kappa_0} \cos^2 \left(\frac{\pi}{2} \xi \right) \quad (2.20)$$

Several hydraulicians (Coleman, 1981, 1986; Nezu and Nakagawa, 1993) systematically examined it in open-channels. They found that the wake flow function can also improve the accuracy of velocity profiles in open-channels. For clear water, the Coles wake strength coefficient Π is about 0 – 0.2. Note that although many investigators regarded the log-wake law as a great success in the outer region, as Coles (1969) stated, it is not valid near the upper boundary layer edge ($\xi > 0.6 - 0.9$). This is because it does not satisfy the boundary condition (2.12) or (2.13).

In summary, no existing velocity profile equation satisfies (2.12) or (2.13).

2.3 Velocity Profiles in Sediment-Laden Flows

Because more independent variables, such as sediment concentration and density gradient, are involved in sediment-laden flow systems, velocity profiles in sediment-laden flows are much more complicated than those in clear water. In this section, only the applications of the log law and the log-wake law will be reviewed. The application of the power law is neglected here although several studies have been reported.

2.3.1 Extension of the log law to sediment-laden flows

Vanoni (1946), Einstein and Chien (1955), Vanoni and Nomicos (1960), Elata and Ippen (1961), and many others examined the log law in sediment-laden flows experimentally. They concluded that the log law remains valid except that κ , which is the von Karman constant in sediment-laden flow, decreases with sediment suspension. Furthermore, Einstein and Chien (1955) proposed a graphical relation to predict the von Karman constant κ based on an energy concept, as shown in FIG. 2.5. They also pointed out that the main effect of sediment suspension occurs near the bed.

Later, Vanoni and Nomicos (1960) modified the Einstein and Chien parameter with the average volumetric concentration near the bed. Barton and Lin (1955) discussed the variation of the von Karman constant κ from the view of density gradient. Chien and Wan (1983, p.396) unified various arguments with a Richardson number. However, their study could not explain Elata and Ippen's (1961) neutral particle ex-

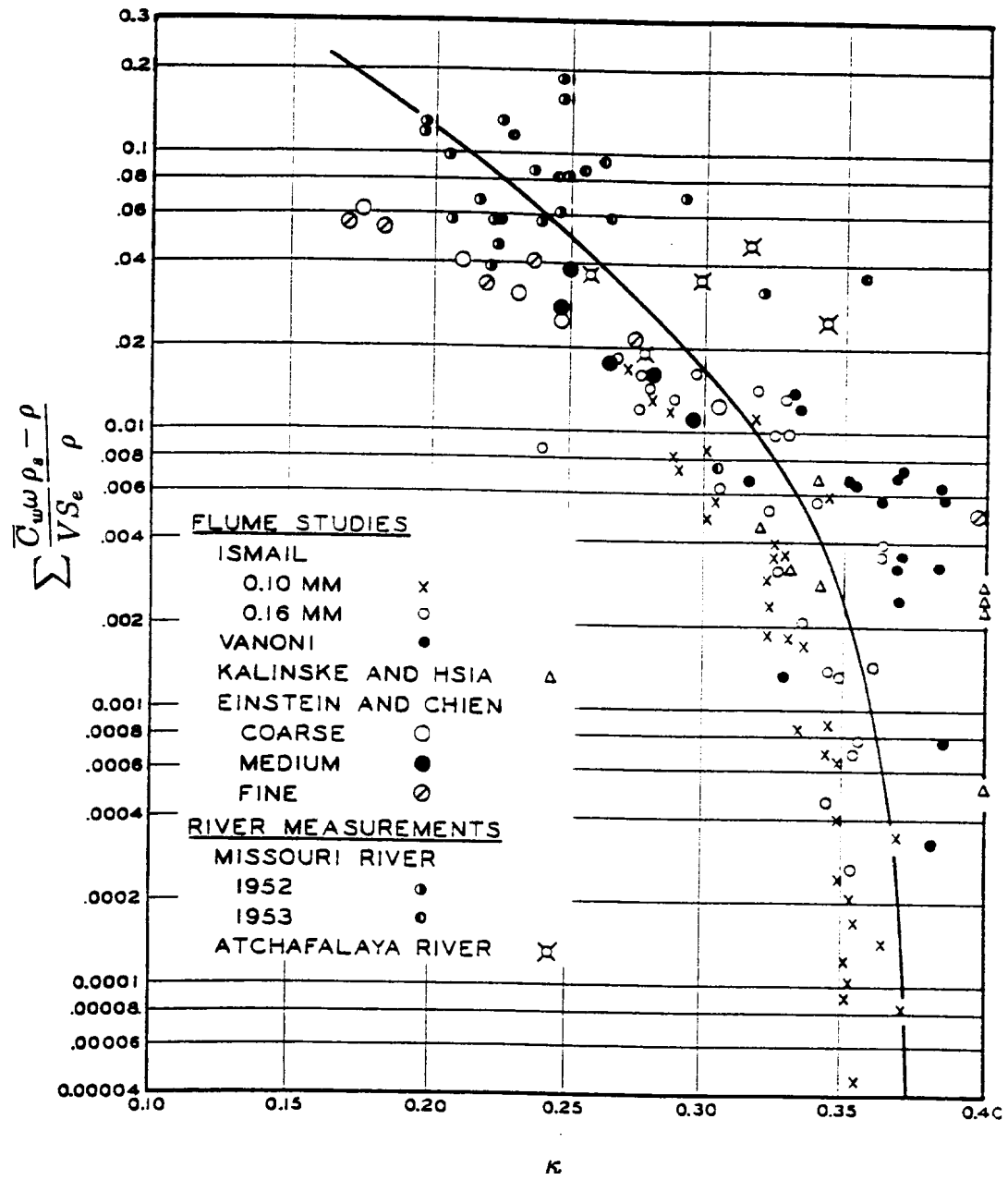


FIG. 2.5: Effect of suspended sediment on the von Karman constant (After Einstein and Chien, 1955)

periments. To explain his neutral particle experiments, Ippen (1971) argued that suspended sediment affects the velocity profile mainly by changing water viscosity. A good summary of this type of research can be found in the literature (Vanoni, 1975, p.83-91; Chien and Wan, 1983, p.391-401; Hu and Hui, 1995, p.130-137).

Almost at the same time as Einstein and Chien (1955), Kolmogorov (1954) and Barenblatt (1953, 1996) also analyzed the effect of sediment suspension on the log law from a view of complete similarity. They considered the momentum equation, the sediment concentration equation and the turbulent energy equation simultaneously and concluded that the log law is still valid in sediment-laden flows except that the von Karman constant becomes smaller. This is exactly the same conclusion as that drawn by Einstein and Chien (1955). Barenblatt (1996, p.270) further pointed out that the application of the log law in sediment-laden flows, as it in clear water, is limited to the overlap zone. In other words, the log law may not be valid in the wake layer and near the water surface.

2.3.2 Extension of the log-wake law to sediment-laden flows

Coleman (1981, 1986) introduced the log-wake law to open channels and studied the effect of suspended sediment on the parameters κ and Π . He argued that if the log-wake law is applied, the von Karman constant κ remains the same as that in clear water κ_0 , but the wake strength coefficient Π increases with a Richardson number, shown in FIG. 2.6. He further pointed out that the previous conclusion, i.e., κ decreases with sediment suspension, was obtained by incorrectly extending the log law to the wake layer.

Coleman's argument was supported by Parker and Coleman (1986), Cioffi and Gallerano (1991). A similar result was obtained at CSU by Janin (1986) in a large boundary layer wind tunnel. Coleman's conclusion is actually an analogy to the effect of pressure-gradient on boundary-layer flows. However, the pressure equation of a boundary layer flow in the normal direction is not similar to the sediment concentration equation in a sediment-laden flow. The pressure or pressure-gradient is regarded as a constant at a certain cross-section in a boundary layer flow while the sediment

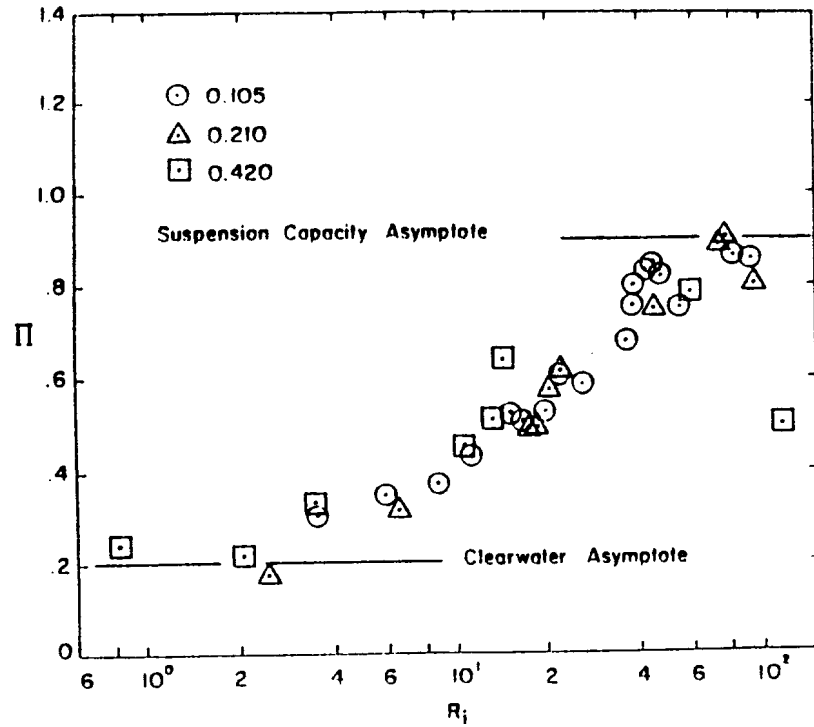


FIG. 2.6: Effect of suspended sediment on the wake strength coefficient

concentration is usually not uniform in the vertical direction. In other words, the von Karman constant κ is not necessarily

constant in sediment-laden flows.

Contrary to Coleman's finding, Lyn (1986, 1988) believed that the effect of sediment suspension mainly occurs near the bed. In other words, the von Karman constant κ may decrease with sediment suspension while the wake strength coefficient Π may be independent of sediment suspension and kept about 0.2, the same as that in clear water.

Recently, Kereselidze and Kutavaia (1995), from their own experiments, deduced that both κ and Π vary with sediment suspension.

No doubt, the log-wake law can improve the accuracy of the velocity profiles in sediment-laden flows. However, the effects of sediment suspension on κ and Π are still debatable.

2.3.3 Log-linear law and others

The log-linear law was originally proposed in temperature stratified flows (Kundu, 1990, p.463). It is written as

$$\frac{\bar{u}_1}{u_*} = \frac{1}{\kappa} \left[\ln \frac{x_3}{x_{30}} + 5 \frac{x_3}{L_M} \right] \quad (2.21)$$

in which x_{30} is a reference point; and L_M is the Monin-Obukhov length. The above equation can be written as a defect form as follows:

$$\begin{aligned} \frac{\bar{u}_{1\max} - \bar{u}_1}{u_*} &= \frac{1}{\kappa} \left[-\ln \frac{x_3}{\delta} + 5 \frac{\delta - x_3}{L_M} \right] \\ &= -\frac{1}{\kappa} \ln \xi + \frac{5}{\kappa} \frac{\delta}{L_M} (1 - \xi) \end{aligned} \quad (2.22)$$

in which $\xi = x_3/\delta$. From the formula appearance, the log-linear law is another type of the log-wake law, except that the wake function is a linear function rather than a sine function. However, from its derivation (Duo, 1987, p.365), the log-linear law, like the log law, is only valid in the overlap since it is assumed that the shear stress is a constant. In addition, the above log-linear law is derived under the assumption of small values of Richardson number R_i (Roll, 1965, p.147). In other words, one cannot expect that it will prove useful under conditions of great density gradient flows.

Itakura and Kishi (1980) and McCutcheon (1981) applied the log-linear law to sediment-laden flows. However, this extension is not accepted by sediment researchers. As pointed out by Lyn (1986), the foundation of the log-linear law, where the turbulent temperature flux is a constant, is not applicable in sediment-laden flows since the turbulent sediment concentration flux is not a constant in the vertical direction at all. Although the log-linear law is not applicable in sediment-laden flows theoretically, the comparison of the log-linear law with experimental data (Itakura and Kishi, 1980; McCutcheon, 1981) looks very good.

Besides the log-wake law and the log-linear law, some other wake function forms can be found in literature. Ni and Hui (1988) proposed a wake flow function with two terms: one indicates the effect of mean concentration; the other expresses the effect of concentration gradient. Umeyama and Gerritsen (1992) and Zhou and Ni (1995)

suggested a Taylor series to express the wake flow function. In addition, the study of the power law was reported by Chien and Wan (1983), Chen (1984), Karim and Kennedy (1987) and Woo, Julien and Richardson (1988).

2.4 Summary

No existing (outer region) velocity profile laws in clear water are fully satisfactory. The log law is valid only in the overlap. The log-wake law does not satisfy the upper boundary condition. The parabolic law is only valid near the water surface in narrow channels. The log-linear law is good in temperature stratified flows, but the foundation of its assumptions may not be applicable in sediment-laden flows. Consequently, the applications of these laws in sediment-laden flows are not satisfactory.

Chapter 3

SIMILARITY ANALYSIS OF CLEAR WATER VELOCITY PROFILES

3.1 Introduction

Turbulence is complicated. Although the governing Navier-Stokes equations have been established over a century, no solutions for turbulent flows (high Reynolds number flows) are yet available, even for a simple steady uniform 2D turbulence. To find a time-averaged solution of turbulence, the Reynolds averaged equations are usually applied. However, the average process brings new unknowns to the flow system. In other words, the Reynolds equations are not closed and cannot be solved theoretically. Dimensional analysis or similarity analysis is usually helpful in such a case. The new difficulty from the classical dimensional analysis is that it only gives similarity parameters. It cannot give the specific functional relations.

Recently, Barenblatt (1996) has extended the dimensional analysis method. In particular, the concept of the intermediate asymptotics suggested by him is very powerful in a turbulence analysis. Based on previous studies, an improved similarity analysis approach is first presented in Section 3.2. Then its application in the study

of clear water velocity profile is discussed in Section 3.3. An eddy viscosity, based on the new velocity profile law, is discussed in Section 3.4. Section 3.5 briefly summarizes the results of this chapter.

3.2 Four-step similarity analysis method

Suppose there is a physical system including a turbulent flow in a 2D pipe or open-channel. The governing equations of the system are not closed, unknown, or too difficult to solve. One may proceed with a similarity analysis in the following way: dimensional analysis, intermediate asymptotics, wake correction, and boundary correction. These four steps are referred to as the *four-step similarity analysis method*. The following is the discussion of each step.

3.2.1 Dimensional analysis

For simplicity, one assumes an equilibrium physical system. The dimensional analysis includes: (a) specifying governing parameters (independent and dependent parameters) and their dimensions; (b) specifying the boundary conditions; (c) choosing the repeated parameters; and (d) using Buckingham's Π theorem to normalize the governing parameters and the boundary conditions with the repeated parameters and putting the function under study into a dimensionless form, i.e.

The governing parameters

$$\Pi = \Phi(\Pi_1, \Pi_2, \dots, \Pi_m) \quad (3.1)$$

The boundary conditions

$$\lim_{x \rightarrow \Gamma} \Pi = \phi, \quad \lim_{x \rightarrow \Gamma} \frac{\partial \Pi}{\partial \Pi_j} = \phi_1, \quad \lim_{x \rightarrow \Gamma} \frac{\partial^2 \Pi}{\partial \Pi_j^2} = \phi_2, \quad \dots \quad (3.2)$$

in which Π is the dependent similarity parameter; Π_1, Π_2, \dots , and Π_m are independent similarity parameters; $x \rightarrow \Gamma$ denotes the space variable tends to the boundary; ϕ denotes the boundary values; and subscripts 1 and 2 denote the values of the first and the second derivatives; and $j = 1, 2, \dots, m$. (3.1) is equivalent to the governing

equations which may be a vector. The number of the boundary conditions depends on the governing equations (ODE or PDE). However, if the governing equations are unknown, try to write as many conditions as possible. (3.2) are constraints of (3.1).

3.2.2 Intermediate asymptotics

According to Barenblatt (1996, p. xiii), the intermediate asymptotics means that for a certain governing similarity parameter, its value is intermediate, i.e., neither too big nor too small. For a time-dependent problem, the intermediate asymptotics means that the system is independent of the fine details of the initial conditions and also far away from the equilibrium state. For an equilibrium problem, the physical domain considered is far away from the boundary. In other words, the dependent parameters under consideration are independent of the boundary conditions. The intermediate asymptotics usually includes two steps: one is the test of “complete similarity assumption”, and the other is the test of “incomplete similarity assumption.”

Complete similarity: If the system is completely independent of a certain parameter, say, Π_m , one says that the system is complete similarity with respect to Π_m . Then Π_m disappears in (3.1), the number of the independent parameters reduces to $m - 1$.

Incomplete similarity: Suppose that Φ tends to zero or infinity when Π_m goes to zero or infinity. This means that the quantity of Π_m remains essential in the system, and (3.1) may be rewritten as (Barenblatt, 1996, p. 24, p. 145, Chap. 5):

$$\Pi = \Pi_m^{\alpha_1} \Phi \left(\frac{\Pi_1}{\Pi_m^{\alpha_2}}, \frac{\Pi_2}{\Pi_m^{\alpha_3}}, \dots, \frac{\Pi_{m-1}}{\Pi_m^{\alpha_m}} \right) \quad (3.3)$$

in which the exponents $\alpha_1, \alpha_2, \dots$, and α_m must be determined experimentally. This kind of similarity is called incomplete similarity.

3.2.3 Wake correction (or wake function)

From its definition, the intermediate asymptotics is not valid beyond the corresponding intermediate domain. The deviation between the real values of Π and the

intermediate asymptotics beyond the intermediate domain is called the wake correction or wake function W . This is analogous to the Coles wake flow function in turbulent boundary layers (Coles, 1956). Now one has

$$\Pi = \Phi(\Pi_1, \Pi_2, \dots, \Pi_{m-1}) + W(\Pi_1, \Pi_2, \dots, \Pi_m) \quad (3.4)$$

for a complete similarity, and

$$\Pi = \Pi_m^{\alpha_1} \Phi\left(\frac{\Pi_1}{\Pi_m^{\alpha_2}}, \frac{\Pi_2}{\Pi_m^{\alpha_3}}, \dots, \frac{\Pi_{m-1}}{\Pi_m^{\alpha_m}}\right) + W(\Pi_1, \Pi_2, \dots, \Pi_m) \quad (3.5)$$

for an incomplete similarity. Obviously, the wake correction must be very small compared with the first term when Π_m goes to its intermediate values.

3.2.4 Boundary correction

Equation (3.4) or (3.5) has extended the solution near the boundary. However, the boundary conditions are usually not satisfied. To meet the boundary condition, another additional term which is called the boundary correction B may be added to (3.4) and (3.5). Then one has

$$\Pi = \underbrace{\Phi(\Pi_1, \Pi_2, \dots, \Pi_{m-1})}_{\text{Intermediate asymptotics}} + \underbrace{W(\Pi_1, \Pi_2, \dots, \Pi_m)}_{\text{Wake correction}} + \underbrace{B(\Pi_1, \Pi_2, \dots, \Pi_m)}_{\text{Boundary correction}} \quad (3.6)$$

or

$$\Pi = \underbrace{\Pi_m^{\alpha_1} \Phi\left(\frac{\Pi_1}{\Pi_m^{\alpha_2}}, \frac{\Pi_2}{\Pi_m^{\alpha_3}}, \dots, \frac{\Pi_{m-1}}{\Pi_m^{\alpha_m}}\right)}_{\text{Intermediate asymptotics}} + \underbrace{W(\Pi_1, \Pi_2, \dots, \Pi_m)}_{\text{Wake correction}} + \underbrace{B(\Pi_1, \Pi_2, \dots, \Pi_m)}_{\text{Boundary correction}} \quad (3.7)$$

The boundary correction function B is usually a polynomial. The power of the polynomial is equal to the highest order of derivative boundary condition. For example, if the highest order of the derivative boundary condition is a first order, then the boundary correction function B will be a linear function. The function B can be determined by expanding the first two terms at the boundary. The detailed method for determining the boundary correction function B will be illustrated in the following section.

One can see that a similarity solution may consist of three parts: intermediate asymptotics, wake correction, and boundary correction. Take the velocity profile in a pipe flow as an example, the above four steps can be summarized in FIG. 3.1.

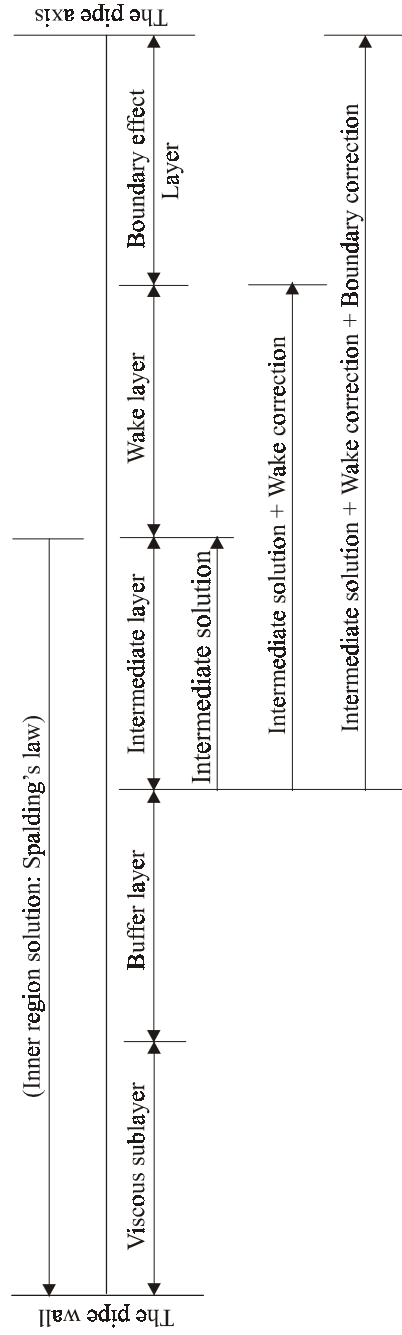


FIG. 3: The four-step similarity analysis scheme for the velocity profile in pipes

3.3 Velocity profile analysis

To give a complete procedure of the four-step similarity analysis method, some previous results are cited in the following analysis.

3.3.1 Dimensional analysis

Like solving a system of partial differential equations, one must consider both the governing parameters (corresponding to governing equations) and the boundary conditions.

Traditionally, the velocity profile in a turbulent boundary shear flow is considered in two different regions separately (White, 1986, p.298). For the inner region, Prandtl deduced in 1930 that \bar{u}_1 must be independent of the shear-layer thickness

$$\bar{u}_1 = f(\mu, \tau_0, \rho_0, x_3) \quad (3.8)$$

By dimensional analysis, this is equivalent to

$$\frac{\bar{u}_1}{u_*} = F\left(\frac{u_* x_3}{\nu}\right) \quad (3.9)$$

or

$$\frac{\bar{u}_1}{u_*} = F(y^+) \quad (3.10)$$

in which $u_* = \sqrt{\tau_0/\rho_0}$ and $\nu = \mu/\rho_0$. (3.9) or (3.10) is called the *law of the wall*. The inner boundary condition corresponding to the law of the wall is the no slip condition. In the literature review (Chapter 2), it has been pointed out that the law of the wall has been well solved by Spalding (White, 1991, p.415). Therefore, this analysis will focus on the outer region velocity profile.

For the outer region, von Karman in 1933 deduced that \bar{u}_1 in the outer region is independent of molecular viscosity but its deviation from the stream velocity $\bar{u}_{1\max}$ (for a 2D open-channel flow, i.e., the water surface velocity) must depend on the shear-layer thickness and the other properties

$$\bar{u}_{1\max} - \bar{u}_1 = g(\delta, \tau_0, \rho_0, x_3) \quad (3.11)$$

Again, by dimensional analysis one writes this as

$$\frac{\bar{u}_{1\max} - \bar{u}_1}{u_*} = G\left(\frac{x_3}{\delta}\right) \quad (3.12)$$

or

$$\frac{\bar{u}_{1\max} - \bar{u}_1}{u_*} = G(\xi) \quad (3.13)$$

in which $\xi = x_3/\delta$. (3.12) or (3.13) is called the *velocity defect law*. The boundary conditions corresponding to the defect law should be (2.9) and (2.12) or (2.13). They will be met by choosing the function G .

3.3.2 Intermediate asymptotics

Assume that the channel bed corresponds to the boundary Γ_1 and the upper boundary (the maximum velocity in a narrow channel or the water surface in a wide channel) corresponds to the boundary Γ_2 in FIG. 3.1. Then the left part corresponds to the inner region in a channel flow while the right part corresponds to the outer region. Obviously, unlike previous studies, the outer region is now divided into three layers: the overlap, the wake layer, and the boundary effect layer. The boundary effect layer is emphasized here.

From FIG. 3.1, the intermediate layer or overlap belongs to both the inner region and the outer region. Then both (3.10) and (3.13) are valid in the overlap. From (3.10) one gets the velocity gradient as (Millikan, 1938; Kundu, 1990, p.452)

$$\frac{d\bar{u}_1}{dx_3} = \frac{u_*^2}{\nu} \frac{dF}{dy^+} \quad (3.14)$$

From (3.13) one has

$$\frac{d\bar{u}_1}{dx_3} = \frac{u_*}{\delta} \frac{dG}{d\xi} \quad (3.15)$$

Equating (3.14) and (3.15) and multiplying by x_3/u_* , one has

$$\xi \frac{dG}{d\xi} = y^+ \frac{dF}{dy^+} = \frac{1}{\kappa_0} \quad (3.16)$$

which is valid for large y^+ and small ξ . Since the left side is only a function of ξ and the right side is only a function of y^+ , both sides must be equal to the same universal

constant, say $1/\kappa_0$, where κ_0 is the von Karman constant in clear water. Integration of (3.16) gives

$$F(y^+) = \frac{1}{\kappa_0} \ln y^+ + C_1 \quad (3.17)$$

and

$$G(\xi) = \frac{1}{\kappa_0} \ln \xi + C_2 \quad (3.18)$$

in which κ_0 , C_1 and C_2 are experimental constants. The above log law is actually derived on the assumption of complete similarity with respect to Reynolds number in the intermediate region.

Barenblatt (1996, p.269) showed that under the assumption of incomplete similarity with Reynolds number, a power law in the intermediate region may be obtained. This study will concentrate on the log law. The brief study of a power law, under the assumption of incomplete similarity, in pipe flows is appended in Appendix A.

3.3.3 Wake correction to the log law

Based on (3.17), Coles (1956, 1969) analyzed a lot of experimental profiles and determined that the wake correction can be well approximated as

$$W(\xi) = \Omega_0 \sin^2 \frac{\pi\xi}{2} \quad (3.19)$$

in which Ω_0 is the wake value at $\xi = 1$. In other words, the log law may be extended to the wake layer by adding the wake function (3.19) to (3.17), i.e.

$$\frac{\bar{u}_1}{u_*} = \frac{1}{\kappa_0} \ln y^+ + C_1 + \Omega_0 \sin^2 \frac{\pi\xi}{2} \quad (3.20)$$

Considering $y^+ = \text{Re}_* \xi$, in which the Reynolds number $\text{Re}_* = u_* \delta / \nu$, the above equation can be rewritten by the outer variable ξ , i.e.

$$\frac{\bar{u}_1}{u_*} = \frac{1}{\kappa_0} \ln \xi + C_3 + \Omega_0 \sin^2 \frac{\pi\xi}{2} \quad (3.21)$$

in which $C_3 = 1/\kappa_0 \ln \text{Re}_* + C_1$. This is just the log-wake law proposed by Coles (1956). As Coles (1969) stated later, this law is not valid near the upper boundary layer since the derivative boundary condition at the boundary edge is not satisfied.

3.3.4 Boundary correction to the log-wake law

According to (3.6), assume a boundary correction function $B(\xi)$, then (3.21) becomes

$$\frac{\bar{u}_1}{u_*} = \frac{1}{\kappa_0} \ln \xi + C_3 + \Omega_0 \sin^2 \frac{\pi \xi}{2} + B(\xi) \quad (3.22)$$

in which $B(\xi)$ is a linear function since the highest derivative boundary condition is a first order derivative.

One can expand the above equation at $\xi = 1$. One has

$$\begin{aligned} \ln \xi &= \ln[1 - (1 - \xi)] = - \sum_{i=1}^{\infty} \frac{(1 - \xi)^i}{i} \\ &= -(1 - \xi) - \frac{(1 - \xi)^2}{2} - \dots \end{aligned} \quad (3.23)$$

$$\begin{aligned} \sin^2 \frac{\pi \xi}{2} &= \frac{1 - \cos \pi \xi}{2} = \frac{1}{2} + \frac{\cos(\pi - \pi \xi)}{2} \\ &= 1 - \frac{1}{2} \sum_{i=1}^{\infty} (-1)^i \frac{[\pi(1 - \xi)]^{2i}}{(2i)!} \\ &= 1 - \frac{\pi^2}{4} (1 - \xi)^2 + \dots \end{aligned} \quad (3.24)$$

and

$$\cos^2 \frac{\pi \xi}{2} = \frac{\pi^2}{4} (1 - \xi)^2 + \dots \quad (3.25)$$

(3.25) will be used later. Now substituting (3.23) and (3.24) into (3.21) and neglecting the 3rd and higher order terms yield that

$$\begin{aligned} \frac{\bar{u}_1}{u_*} &= -\frac{1 - \xi}{\kappa_0} - \frac{(1 - \xi)^2}{2\kappa_0} + C_3 + \Omega_0 \left(1 - \frac{\pi^2}{4} (1 - \xi)^2 \right) + B(\xi) \\ &= (C_3 + \Omega_0) - \frac{1 - \xi}{\kappa_0} - \left(\frac{1}{2\kappa_0} + \frac{\pi^2}{4} \Omega_0 \right) (1 - \xi)^2 + B(\xi) \end{aligned} \quad (3.26)$$

It is assumed that $B(\xi)$ is linear, comparing (3.26) and (2.15), one has

$$C_3 + \Omega_0 = \frac{\bar{u}_{1\max}}{u_*} \quad (3.27)$$

$$B(\xi) = \left[\frac{1}{\kappa_0} - \frac{1}{u_*} \frac{d\bar{u}_1}{d\xi} \Big|_{\xi=1} \right] (1 - \xi) \quad (3.28)$$

Finally, the log-wake law is modified as

$$\frac{\bar{u}_1}{u_*} = \frac{1}{\kappa_0} \ln \xi + \frac{\bar{u}_{1\max}}{u_*} - \Omega_0 \cos^2 \frac{\pi \xi}{2} + \left[\frac{1}{\kappa_0} - \frac{1}{u_*} \frac{d\bar{u}_1}{d\xi} \Big|_{\xi=1} \right] (1 - \xi) \quad (3.29)$$

which can be rewritten as a velocity defect form

$$\boxed{\frac{\bar{u}_{1\max} - \bar{u}_1}{u_*} = -\frac{1}{\kappa_0} \ln \xi + \Omega_0 \cos^2 \frac{\pi \xi}{2} - \left[\frac{1}{\kappa_0} - \frac{1}{u_*} \frac{d\bar{u}_1}{d\xi} \Big|_{\xi=1} \right] (1 - \xi)} \quad (3.30)$$

in which κ_0 and Ω_0 are two experimental constants. This is the final velocity profile equation based on the log law, which is called the *modified log-wake law*. The last term is due to the boundary correction which is a main contribution of this study.

Considering (2.12) and (2.13), (3.30) may further be written as

$$\boxed{\frac{\bar{u}_{1\max} - \bar{u}_1}{u_*} = -\frac{1}{\kappa_0} \ln \xi + \Omega_0 \cos^2 \frac{\pi \xi}{2} - \left[\frac{1}{\kappa_0} - \lambda_0 \left(\frac{V_{\text{wind}} - \bar{u}_{1\max}}{u_*} \right)^2 \right] (1 - \xi)} \quad (3.31)$$

in which $\lambda_0 = 0$ for narrow channels and pipes, and $\lambda_0 > 0$ for wide channels.

3.4 Implication to turbulent eddy viscosity

The eddy viscosity is not a measurable variable. It is usually derived from some assumptions, such as the mixing length hypothesis, or from the mean velocity profiles for simple flows. If (3.30) is correct, an eddy viscosity model can be deduced.

Assume that the shear stress is linearly distributed along the flow depth and the viscous shear stress can be neglected, the distribution of the eddy viscosity ε may be derived from

$$\varepsilon = \frac{\tau_0 (1 - \xi) + \tau|_{\xi=1} / \tau_0}{\rho \frac{1}{\delta} \frac{d\bar{u}_1}{d\xi}} = \delta u_* \frac{(1 - \xi) + \tau|_{\xi=1} / \tau_0}{\frac{1}{u_*} \frac{d\bar{u}_1}{d\xi}}$$

or

$$\varepsilon^+ \equiv \frac{\varepsilon}{\delta u_*} = \frac{(1 - \xi) + \tau|_{\xi=1} / \tau_0}{\frac{1}{u_*} \frac{d\bar{u}_1}{d\xi}} \quad (3.32)$$

in which $\tau|_{\xi=1}$ is the shear stress on the water surface; and ε^+ is defined as the dimensionless eddy viscosity.

From (3.30), one has

$$\frac{1}{u_*} \frac{d\bar{u}_1}{d\xi} = \frac{1-\xi}{\kappa_0\xi} + \frac{\pi\Omega_0}{2} \sin \pi\xi + \frac{1}{u_*} \frac{d\bar{u}_1}{d\xi} \Big|_{\xi=1}$$

Substituting the above equation into (3.32) gives

$$\varepsilon^+ = \frac{(1-\xi) + \tau|_{\xi=1}/\tau_0}{\frac{1-\xi}{\kappa_0\xi} + \frac{\pi\Omega_0}{2} \sin \pi\xi + \frac{1}{u_*} \frac{d\bar{u}_1}{d\xi} \Big|_{\xi=1}} \quad (3.33)$$

which is the eddy viscosity model corresponding to the modified log-wake law. The shear stress and the velocity gradient at the water surface are boundary conditions.

When $\xi \rightarrow 0$, (3.33) tends to

$$\varepsilon^+ \rightarrow \kappa_0\xi \quad (3.34)$$

which is the classical mixing length model. When $\xi \rightarrow 1$, (3.33) tends to

$$\varepsilon^+ \rightarrow \frac{\tau|_{\xi=1}/\tau_0}{\frac{1}{u_*} \frac{d\bar{u}_1}{d\xi} \Big|_{\xi=1}} = \text{const} \quad (3.35)$$

which corresponds to the constant eddy viscosity model.

(3.33) along with (3.30) will be examined with experimental data later.

3.5 Summary

In this chapter, an improved similarity analysis approach, *the four-step similarity analysis method*, is presented, which includes dimensional analysis, intermediate asymptotics, wake correction, and boundary correction. Based on this approach, the *modified log-wake law* is proposed, which is expressed in (3.30) or (3.31). The modified log-wake law satisfies the upper boundary conditions. Furthermore, an eddy viscosity model is deduced.

Chapter 4

SHEAR VELOCITY IN SMOOTH OPEN-CHANNELS

4.1 Introduction

One may skip this chapter if he simply accepts (4.16) and (4.23) as the equations to estimate the centerline bed shear velocity in a rectangular channel. (4.16) is for the aspect ratio $a/h > 2.5$ while (4.23) is for the aspect ratio $a/h \leq 2.5$. After reading this dissertation, if interested, one may come back to enjoy this mathematical derivation.

The shear velocity u_* , as a boundary condition, is a prerequisite in the study of velocity profiles. Conventionally, four methods for determining u_* can be found in the literature (Muste and Patel, 1997; Nezu, Kadita and Nakagawa, 1997): (1) from the shear stress distribution; (2) from the log law; (3) using a global shear velocity based on the hydraulic radius; and (4) using the shear velocity based on the flow depth. The first two methods must be aided with experimental data and are cumbersome. The third one is just a global value of u_* while the shear velocity in the velocity profile should be the local value. The last one is useful for a wide channel. However, most laboratory flume experiments belong to narrow channel flows. Recently, Yang and Lim (1997) presented a method for calculating the shear velocity in smooth open-channels, based on an energy dissipation assumption. The method is excellent for the estimation of the average bed shear velocity, but the calculation of the local shear

velocity is still open. Besides, the equation is implicit and the calculation requires an iterative process. Obviously, the determination of the shear velocity in an open-channel is very difficult.

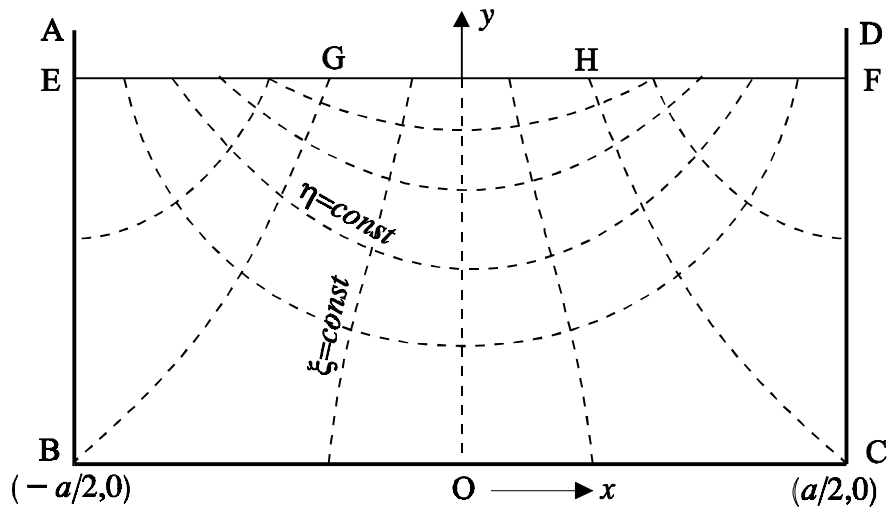
This study will begin with a conformal mapping of a rectangular cross-section into a half-up plane (Section 4.2). Then the bed shear stress distribution (Section 4.3) and the average bed shear stress (Section 4.4) will be derived. Section 4.5 summaries the results of this chapter.

4.2 Conformal mapping from a rectangular cross-section (z -plane) into a half upper plane (w -plane)

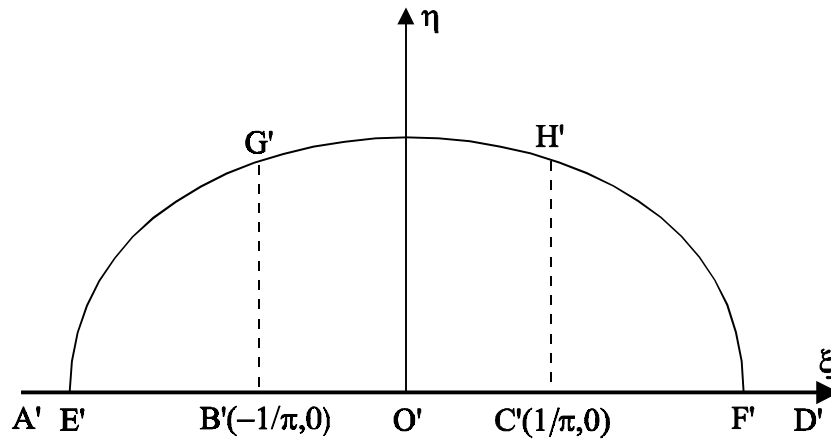
Because of secondary flows and nonuniform roughness distribution around the wetted perimeter, it is impossible to get an exact solution for the boundary shear stress distribution. To obtain an approximate solution, the following assumptions are made: (1) the boundary is smooth; and (2) the velocity contours are parallel to the boundary. That is, the boundary is a velocity contour and there are no secondary flows in the channel. The first assumption can be met in most flume experiments. The second assumption is apparently not true, it will be considered in the solution by introducing a correction factor.

Based on the above assumptions, the Schwartz-Christoffel transformation (Spiegel, 1993, p.206) can be used to find the isovels (velocity contours, which are parallel to the boundary) and the rays (curves which are perpendicular to the isovels and the boundary). Considering a rectangular cross-section with width a and flow depth h and using the Schwartz-Christoffel transformation, one can map the physical flow domain (z -plane) into a half-upper plane (w -plane), shown in FIG. 4.1. The transformation relation between them is

$$w = \frac{a}{\pi} \sin \frac{\pi z}{a} \quad (4.1)$$



(a) Physical flow domain (z - plane)



(b) Mapping flow domain (w - plane)

FIG. 4.1: Scheme of flow domain from a rectangular cross-section to a half upper plane

in which a is the channel width, and

$$z = x + iy \quad (4.2)$$

$$w = \xi + i\eta \quad (4.3)$$

Relation (4.1) can be found in many text books of complex variables (for example, Spiegel, 1993, p.206).

Substituting (4.2) and (4.3) into (4.1), one has

$$\begin{aligned} \xi + i\eta &= \frac{a}{\pi} \sin \frac{\pi}{a}(x + iy) \\ &= \frac{a}{\pi} \left(\sin \frac{\pi x}{a} \cosh \frac{\pi y}{a} + i \cos \frac{\pi x}{a} \sinh \frac{\pi y}{a} \right) \end{aligned}$$

or

$$\xi = \frac{a}{\pi} \sin \frac{\pi x}{a} \cosh \frac{\pi y}{a} \quad (4.4)$$

$$\eta = \frac{a}{\pi} \cos \frac{\pi x}{a} \sinh \frac{\pi y}{a} \quad (4.5)$$

$\xi = \text{const}$ in (4.4) is a ray equation. Similarly, $\eta = \text{const}$ in (4.5) is an isovel equation, shown in FIG. 4.1(a).

Since the water surface in the z -plane is described by the equation $y = h$, where h is the flow depth. Substituting this relation into (4.4) and (4.5) gives the water surface mapping $E'G'H'F'$ in the w -plane, which is a half upper ellipse, as shown in FIG. 4.1(b). The problem is usually solved in the w -plane. In this case, however, one just goes back to the physical plane (z -plane) with the transformations (4.4) and (4.5).

4.3 Bed shear stress distribution and centerline shear velocity

Consider an infinitesimal strip, shown in FIG. 4.2, which is between the curves $x = f(x_1, y)$ and $x = f(x_1 + dx_1, y)$ and dissipates its potential energy to the infinitesimal boundary dx_1 , where x_1 is a point at the bed. If the infinitesimal area is denoted as

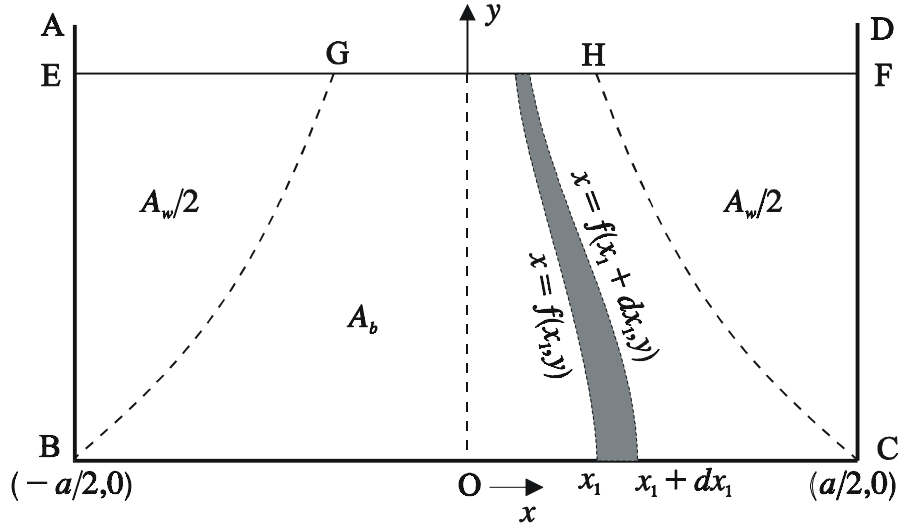


FIG. 4.2: Scheme for computing bed shear stress distribution

dA_b , considering the equilibrium between the gravity component of the strip in the flow direction and the bed shear force in dx_1 gives

$$\rho_0 g S dA_b = \tau_b dx_1 \quad (4.6)$$

in which τ_b is the local bed shear stress. It is noted again that since $x = f(x_1, y)$ is perpendicular to isovels, there is no shear stress between the strip and its neighbor fluid.

Equation (4.6) gives

$$\tau_b = \rho_0 g S \frac{dA_b}{dx_1} \quad (4.7)$$

From FIG. 4.2, one has

$$dA_b = \int_0^h [f(x_1 + dx_1, y) - f(x_1, y)] dy \quad (4.8)$$

Let $dx_1 \rightarrow 0$, one obtains

$$\frac{dA_b}{dx_1} = \int_0^h \frac{df(x_1, y)}{dx_1} dy \quad (4.9)$$

Since the point $(x_1, 0)$ is in the curve: $x = f(x_1, y)$, substituting it into (4.4), one gets

$$\sin \frac{\pi x}{a} \cosh \frac{\pi y}{a} = \sin \frac{\pi x_1}{a} \quad (4.10)$$

That is,

$$x = f(x_1, y) = \frac{a}{\pi} \sin^{-1} \left(\frac{\sin \frac{\pi x_1}{a}}{\cosh \frac{\pi y}{a}} \right) \quad (4.11)$$

Differentiating the above equation with respect to x_1 gives

$$\frac{df(x_1, y)}{dx_1} = \frac{\cos \frac{\pi x_1}{a}}{\sqrt{\cosh^2 \frac{\pi y}{a} - \sin^2 \frac{\pi x_1}{a}}} \quad (4.12)$$

Substituting (4.12) into (4.9) then into (4.7) gives the bed shear stress distribution as

$$\tau_b = \rho_0 g h S \cos \frac{\pi x_1}{a} \int_0^h \frac{dy}{\sqrt{\cosh^2 \frac{\pi y}{a} - \sin^2 \frac{\pi x_1}{a}}} \quad (4.13)$$

or

$$\frac{\tau_b}{\rho_0 g h S} = \cos \frac{\pi x_1}{a} \int_0^1 \frac{dt}{\sqrt{\cosh^2 \left(\frac{\pi h}{a} t \right) - \sin^2 \left(\frac{\pi h}{a} \frac{x_1}{h} \right)}} \quad (4.14)$$

The above equation can not be integrated. A numerical plot of (4.14) is shown in FIG. 4.3. It can be seen that a two-dimensional zone may be found if $a/h = 5$, where the bed shear stress is about $0.94\rho_0 g h S$. When $a/h \geq 10$, the bed shear stress can be approximated as $\rho_0 g h S$ in practice.

This study only concerns the centerline shear stress, i.e., τ_b at $x_1 = 0$. Substituting $x_1 = 0$ into (4.14) gives the centerline shear stress τ_{bc} as

$$\begin{aligned} \frac{\tau_{bc}}{\rho_0 g h S} &= \int_0^1 \frac{dt}{\cosh \left(\frac{\pi h}{a} t \right)} = \int_0^1 \operatorname{sech} \left(\frac{\pi h}{a} t \right) dt \\ &= \frac{a}{\pi h} \int_0^{\pi h/a} \operatorname{sech} x dx \\ &= \frac{a}{\pi h} \sin^{-1} \left(\tanh \frac{\pi h}{a} \right) \end{aligned}$$

i.e.

$$\boxed{\phi_c \equiv \frac{\tau_{bc}}{\rho_0 g h S} = \frac{a}{\pi h} \sin^{-1} \left(\tanh \frac{\pi h}{a} \right)} \quad (4.15)$$

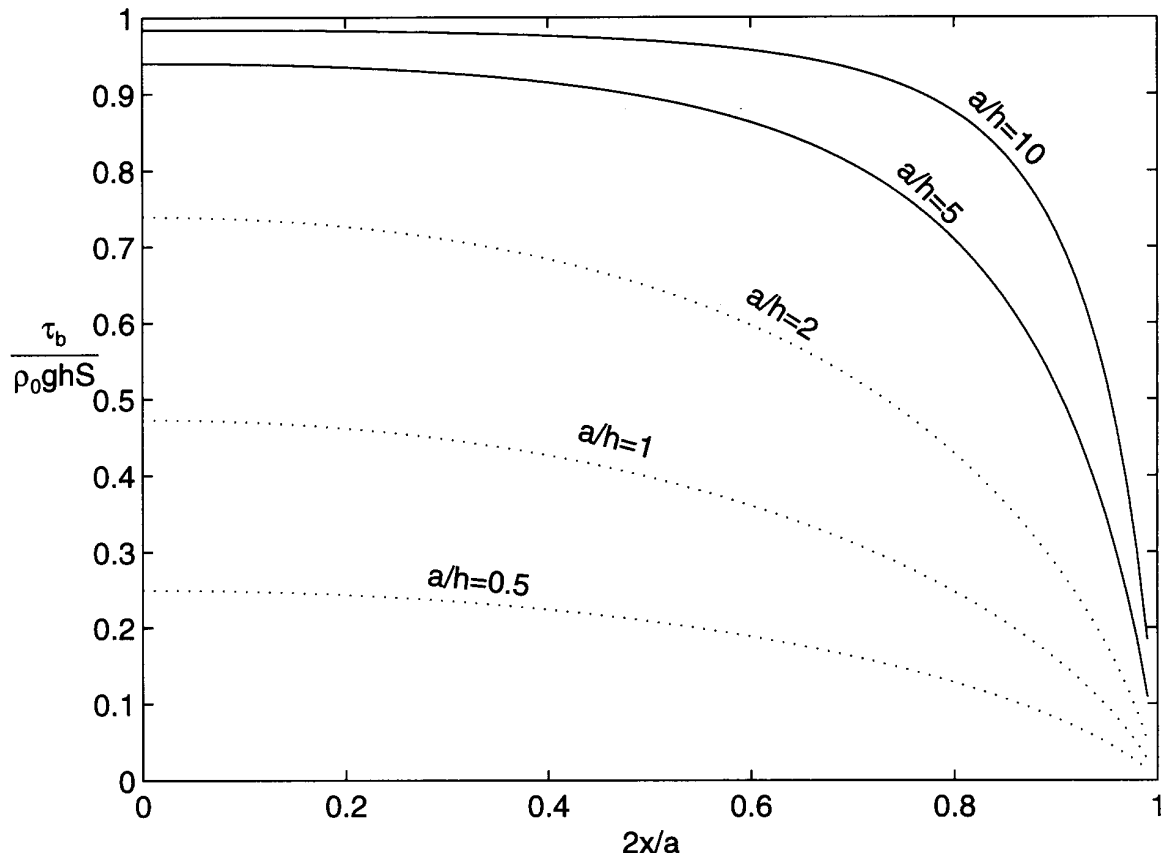


FIG. 4.3: Bed shear stress distribution versus aspect ratio

in which ϕ_c is defined as the side-wall correction factor for the centerline shear stress. The corresponding shear velocity is obviously that

$$\boxed{u_* = \sqrt{\phi_c g h S} = \sqrt{\frac{g a S}{\pi} \sin^{-1} \left(\tanh \frac{\pi h}{a} \right)}} \quad (4.16)$$

According to Yang and Lim (1997), when the aspect ratio $a/h > 2$, the effect of secondary currents on the channel centerline may be neglected. This implies that (4.15) and (4.16) may be valid when $a/h > 2$. To be safe, say $a/h > 2.5$ in this dissertation. (4.15) and (4.16) will be examined using Wang and Qian's experimental data where $a/h = 3 - 3.75$ and Muste's data where $a/h = 7$.

4.4 Average bed shear stress and average bed shear velocity

Although the above mapping model may not be valid for very narrow channels where secondary currents are strong, the average bed shear stress is still based on it. The result will be calibrated by introducing a secondary flow correction factor. Theoretically, the integration of (4.14) can give the average bed shear stress. However, this is very complicated.

Consider the right half of the cross-section, shown in FIG. 4.1(a). The delimitation CH in the z -plane corresponds to $C'H'$ in the w -plane, which is $\xi = const$. Since $(x, y) = (\frac{a}{2}, 0)$ in the z -plane is a point in the delimitation CH , substituting this point into (4.4) gives $\xi = const = \frac{a}{\pi}$, so the equation of the curve CH in the z -plane from (4.4) is

$$\sin \frac{\pi x}{a} \cosh \frac{\pi y}{a} = 1$$

i.e.

$$\frac{\pi y}{a} = \cosh^{-1} \left(\frac{1}{\sin \frac{\pi x}{a}} \right) = \ln \left(\frac{1}{\sin \frac{\pi x}{a}} + \sqrt{\frac{1}{\sin^2 \frac{\pi x}{a}} - 1} \right)$$

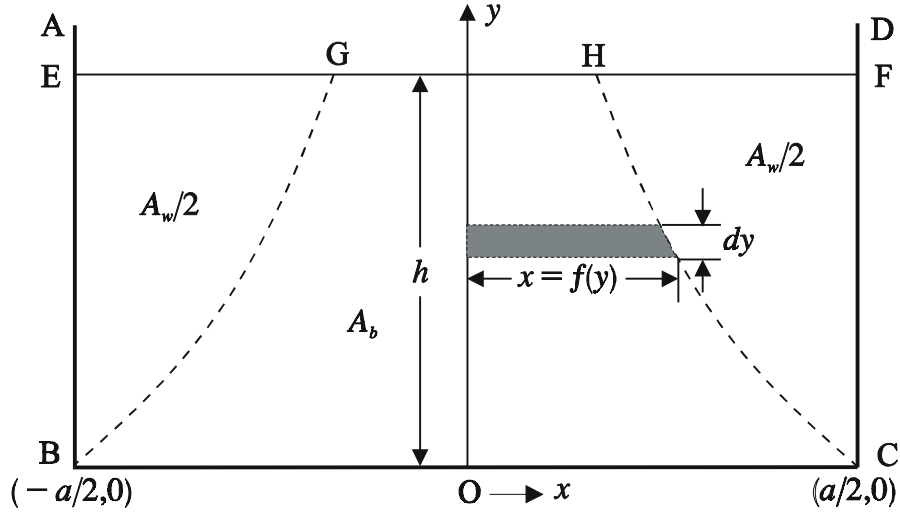


FIG. 4.4: Scheme for computing average bed shear stress

$$\begin{aligned}
 &= \ln \frac{1 + \cos \frac{\pi x}{a}}{\sin \frac{\pi x}{a}} = \ln \frac{2 \cos^2 \frac{\pi x}{2a}}{2 \sin \frac{\pi x}{2a} \cos \frac{\pi x}{2a}} \\
 &= -\ln \tan \frac{\pi x}{2a}
 \end{aligned}$$

or

$$\frac{\pi x}{2a} = \tan^{-1} e^{-\frac{\pi y}{a}} \quad (4.17)$$

For a steady uniform flow, considering the equilibrium between the gravity component of the fluid of the subarea A_b , shown in FIG. 4.4, and the bed shear force in the flow direction, one has the following relation

$$\rho_0 g S A_b = a \bar{\tau}_b \quad (4.18)$$

in which ρ_0 is the water density; g is the gravitational acceleration; S is the bed slope; a is the channel width; and $\bar{\tau}_b$ is the average bed shear stress. Note that the delimitations are perpendicular to isovels, so there is no shear stress between the subareas A_b and A_w . Solving for $\bar{\tau}_b$ in (4.18) gives

$$\bar{\tau}_b = \frac{\rho_0 g S}{a} A_b \quad (4.19)$$

Referring to FIG. 4.4 and considering (4.17), one gets the subarea A_b as

$$A_b = 2 \int_0^h x dy = \frac{4a}{\pi} \int_0^h \tan^{-1} e^{-\frac{\pi y}{a}} dy$$

The integration of the above equation by parts yields

$$A_b = \frac{4ah}{\pi} \tan^{-1} e^{-\frac{\pi y}{a}} + 4 \int_0^h \frac{ye^{-\frac{\pi y}{a}}}{1 + e^{-\frac{2\pi y}{a}}} dy \quad (4.20)$$

Numerical experiments show that the first term on the right-hand side is the leading term. The second term is only a small fraction of the first one. Therefore, one may approximate the second one as

$$\int_0^h \frac{ye^{-\frac{\pi y}{a}}}{1 + e^{-\frac{2\pi y}{a}}} dy \approx \int_0^{\lambda h} ye^{-\frac{\pi y}{a}} dy = \left(\frac{a}{\pi}\right)^2 \left[1 - \left(1 + \frac{\lambda\pi h}{a}\right) e^{-\frac{\lambda\pi h}{a}}\right] \quad (4.21)$$

Since the integrand has been enlarged, the correction factor λ in the upper limit must be in $0 < \lambda < 1$. This can be considered a secondary flow correction factor. Physically, not all the potential energy in the subarea A_b is dissipated by the bed shear stress. A small fraction of potential energy is used to maintain the secondary flows. Therefore, λ must be less than unit. Now the subarea A_b may be interpreted as the effective flow area where the potential energy is dissipated by the bed shear stress. Obviously, the subarea A_b under study now is less than the area in FIG. 4.4. For convenience, the effective subarea is still denoted by A_b .

Substituting (4.21) into (4.20) gives the effective subarea A_b corresponding to the bed shear stress as

$$A_b = \frac{4ah}{\pi} \tan^{-1} e^{-\frac{\pi y}{a}} + 4 \left(\frac{a}{\pi}\right)^2 \left[1 - \left(1 + \frac{\lambda\pi h}{a}\right) e^{-\frac{\lambda\pi h}{a}}\right]$$

Furthermore, substituting this equation into (4.19) gives

$$\bar{\tau}_b = \frac{\rho_0 g S}{a} \left\{ \frac{4ah}{\pi} \tan^{-1} e^{-\frac{\pi y}{a}} + 4 \left(\frac{a}{\pi}\right)^2 \left[1 - \left(1 + \frac{\lambda\pi h}{a}\right) e^{-\frac{\lambda\pi h}{a}}\right] \right\}$$

or

$$\boxed{\phi_m \equiv \frac{\bar{\tau}_b}{\rho_0 g h S} = \frac{4}{\pi} \tan^{-1} e^{-\frac{\pi y}{a}} + \frac{4a}{\pi^2 h} \left[1 - \left(1 + \frac{\lambda\pi h}{a}\right) e^{-\frac{\lambda\pi h}{a}}\right]} \quad (4.22)$$

in which ϕ_m is defined as the side-wall correction factor for average bed shear stress. The secondary correction factor λ is calibrated as 0.6691 using extensive experimental

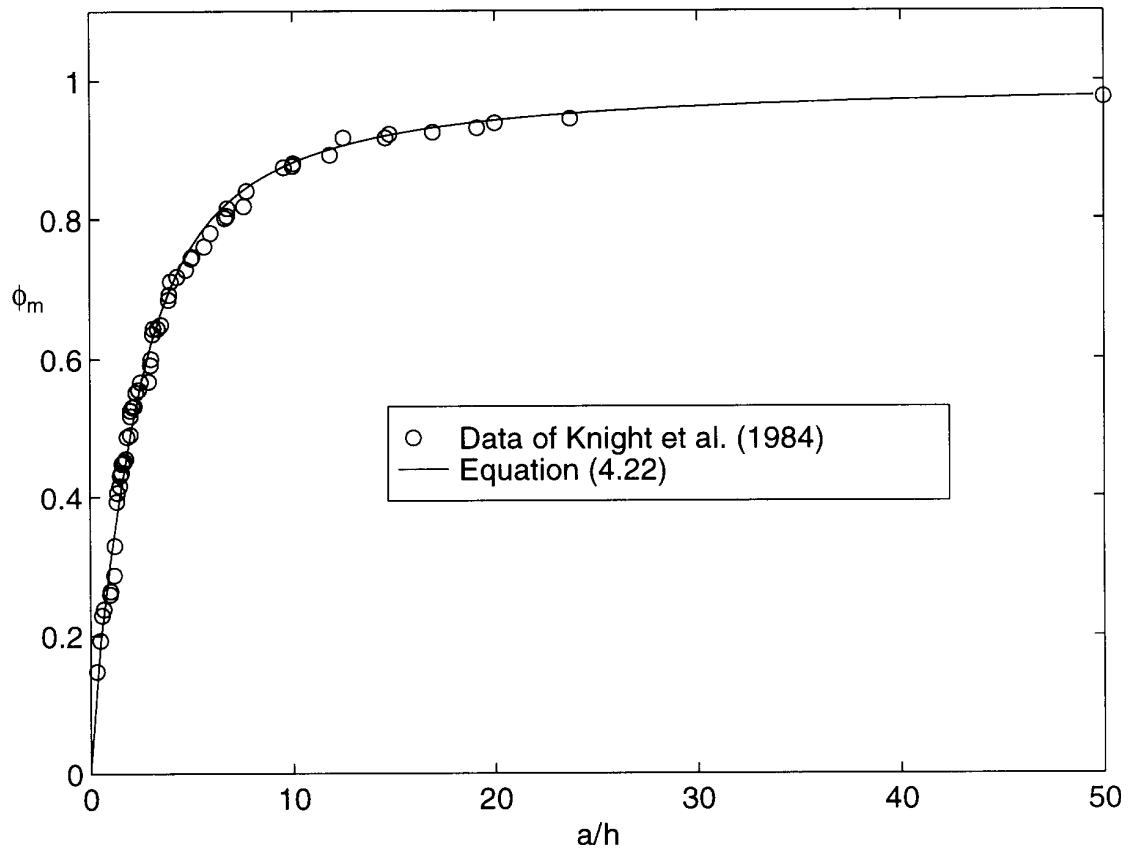


FIG. 4.5: Comparison of the theoretical side-wall correction factor with experimental data

Table 4.1: Comparison of side-wall correction factor with experiments

Measur. ^a		Calcula. ^b		Error		Measur. ^a		Calcula. ^b		Error	
a/h	ϕ_m	ϕ_c	(%)	a/h	ϕ_m	ϕ_c	(%)	a/h	ϕ_m	ϕ_c	(%)
0.310	0.148	0.125	-0.158	3.090	0.636	0.629	-0.012				
0.490	0.193	0.186	-0.035	3.120	0.644	0.632	-0.019				
0.580	0.229	0.212	-0.075	3.350	0.644	0.653	0.014				
0.670	0.238	0.234	-0.015	3.510	0.649	0.667	0.027				
0.990	0.259	0.305	0.176	3.890	0.685	0.696	0.016				
1.000	0.264	0.307	0.161	3.910	0.692	0.697	0.008				
1.190	0.287	0.345	0.202	4.000	0.711	0.704	-0.010				
1.210	0.330	0.349	0.057	4.310	0.718	0.723	0.008				
1.310	0.393	0.368	-0.063	4.740	0.728	0.747	0.026				
1.340	0.406	0.374	-0.078	5.000	0.744	0.760	0.021				
1.470	0.416	0.399	-0.041	5.040	0.746	0.762	0.021				
1.480	0.431	0.401	-0.070	5.650	0.761	0.787	0.034				
1.510	0.433	0.406	-0.062	5.950	0.780	0.798	0.023				
1.560	0.435	0.415	-0.045	6.670	0.801	0.820	0.023				
1.570	0.448	0.417	-0.069	6.760	0.804	0.822	0.023				
1.670	0.450	0.435	-0.033	6.790	0.815	0.823	0.010				
1.700	0.451	0.440	-0.023	7.600	0.818	0.842	0.030				
1.770	0.455	0.453	-0.005	7.730	0.840	0.845	0.006				
1.820	0.487	0.461	-0.053	9.560	0.874	0.875	0.002				
2.000	0.490	0.490	0.001	10.000	0.876	0.881	0.006				
2.000	0.517	0.490	-0.052	10.020	0.880	0.881	0.002				
2.000	0.525	0.490	-0.066	11.840	0.892	0.900	0.009				
2.100	0.530	0.506	-0.046	12.500	0.917	0.906	-0.012				
2.190	0.531	0.519	-0.022	14.590	0.917	0.920	0.003				
2.270	0.551	0.531	-0.037	14.790	0.922	0.921	-0.001				
2.400	0.555	0.549	-0.012	16.940	0.925	0.931	0.007				
2.500	0.566	0.562	-0.008	19.120	0.931	0.939	0.009				
2.910	0.567	0.610	0.076	20.000	0.938	0.942	0.004				
3.000	0.591	0.619	0.048	23.730	0.944	0.952	0.008				
3.020	0.600	0.621	0.036	50.000	0.975	0.977	0.003				

^a Data source: Knight, D. W., Demetriou, J. D. and Hamed M. E. (1984).

“Boundary shear in smooth rectangular channels.” *J. Hydr. Engrg.*, ASCE, 110(4), 405-422.

^b Theoretical formula:

$$\phi_m = \frac{4}{\pi} \tan^{-1} e^{-\frac{\pi h}{a}} + \frac{4}{\pi^2} \frac{a}{h} \left[1 - \left(1 + \lambda \frac{\pi h}{a} \right) e^{-\lambda \frac{\pi h}{a}} \right]$$

in which $\lambda = 0.6691$.

data (Knight et al., 1984). A comparison of (4.22) with experimental data is shown in Table 4.1 and FIG. 4.5, where the correlation coefficient is 0.9961 and the average relative error is 3.7%.

With the side-wall correction factor ϕ_m , the average bed shear velocity u_* can be calculated by the following:

$$u_* = \sqrt{\frac{\bar{\tau}_b}{\rho_0}} = \sqrt{\phi_m g h S} \quad (4.23)$$

The above equation is derived from the model where the maximum velocity always occurs at the water surface, but the parameter λ , determined experimentally, considers the effect of secondary flows. Therefore, it is valid even if the maximum velocity occurs below the water surface.

Empirically, (4.23) can be approximated as the centerline shear velocity when $a/h \leq 2.5$. This will be seen later from Coleman's experimental data in Table 5.3, where the aspect ratio a/h is about 2.

By the way, the side-wall shear stress distribution and its average shear stress can also be calculated in a similar way. They are, however, neglected because of irrelevance to this study.

4.5 Summary

In this chapter, the channel centerline shear velocity equation (4.16) is derived based on the shear stress distribution along the bed. It may be valid for $a/h > 2.5$. The average bed shear velocity, which is calculated from (4.22) and (4.23), may be as a good approximation of the channel centerline shear velocity in narrow channels. A secondary flow correction factor is considered in the average bed shear velocity.

Chapter 5

TEST OF THE MODIFIED LOG-WAKE LAW IN CLEAR WATER

5.1 Introduction

The purposes of this chapter are to examine that: (1) is the structure of the modified log-wake law reasonable? (2) if the structure of the modified log-wake law is correct, how do the model parameters κ_0 , Ω_0 and λ_0 vary with the Reynolds number u_*h/ν or the aspect ratio a/h ? and (3) if the modified log-wake law is correct, does the corresponding eddy viscosity model agree with experimental data?

Since pipe flows are simpler than open-channel flows, the maximum velocity $\bar{u}_{1\max}$ at a pipe axis and the shear velocity u_* in a pipe can be exactly measured or estimated, this test starts with the examination of the modified log-wake law in pipes in Section 5.2. Narrow channel flows are then tested in Section 5.3. Wide channel experiments are tested in Sections 5.4 and 5.5. Note that a wide channel flow is different from that in a narrow channel since their derivative boundary conditions are not the same. This can be easily seen from (2.12) and (2.13) in Chapter 2. Finally, Section 5.6 summarizes the results of this chapter.

5.2 Test of the modified log-wake law in pipes

5.2.1 Modified log-wake law in pipes

Applying the boundary condition (2.13) to (3.30), or $\lambda_0 = 0$ to (3.31), one gets the modified log-wake law in pipes as

$$\boxed{\frac{\bar{u}_{1\max} - \bar{u}_1}{u_*} = -\frac{1}{\kappa_0} \ln \xi + \Omega_0 \cos^2 \frac{\pi \xi}{2} - \frac{1 - \xi}{\kappa_0}} \quad (5.1)$$

in which $\xi = x_3/R$ and R is the radius of the pipe.

5.2.2 Data selection

Since the classical experiments by Nikuradse (1932), many pipe experiments have been reported, a systematic review of these experiments can be found in Zagarola's (1996) dissertation. The latest accurate superpipe measurements by Zagarola (1996) at the Gas Dynamics Lab in Princeton University will be used in this study. Zagarola performed measurements of the mean velocity profiles and static pressure gradients at 26 different Reynolds numbers between 3.1×10^4 and 3.5×10^7 . The complete description of the experimental details and experimental data can be found in his dissertation (Zagarola, 1996) or a Web site in Princeton University: <http://www.princeton.edu/~gasdyn/index.htm>. In this section, only the mean velocity profile data are used to examine the modified log-wake law. By the way, the study of a power-wake law in pipes can be found in Appendix A. However, the power-wake law is not emphasized in this dissertation.

In Zagarola's experimental data, the maximum velocity $\bar{u}_{1\max}$, shear velocity u_* , and sample points (ξ_i, \bar{u}_i) are given. Hence, only the von Karman constant κ_0 and the wake strength coefficient Ω_0 are fitting parameters.

5.2.3 Methods for determining κ_0 and Ω_0

Two methods can be used to determine κ_0 and Ω_0 , one is the asymptotic method, the other is the least-squares method.

Asymptotic method (Graphical method)

For a quick estimation, let $\xi \ll 1$, (5.1) reduces to the classical log law, i.e.

$$\frac{\bar{u}_{1\max} - \bar{u}_1}{u_*} = -\frac{1}{\kappa_0} \ln \xi + \Omega_0 - \frac{1}{\kappa_0} \quad (5.2)$$

Then the von Karman constant κ_0 and the wake strength coefficient Ω_0 can be determined from the slope and intercept at $\xi = 1$ of a semilog plot of $(\bar{u}_{1\max} - \bar{u}_1)/u_*$ versus ξ . This method is similar to that suggested by Coles (1956) and Coleman (1986) in the log-wake law. It is illustrated in FIG. 5.4 (p.51). The asymptotic method is only illustrated herein and not used in this study.

Least-squares method

To accurately estimate κ_0 and Ω_0 , the least-squares method should be used. The least-squares approximation can be represented by

$$\begin{aligned} S &= \sum_i^n \left[\frac{\bar{u}_{1\max} - \bar{u}_{1i}}{u_*} + \frac{1}{\kappa_0} (\ln \xi_i + 1 - \xi_i) - \Omega_0 \cos^2 \frac{\pi \xi_i}{2} \right]^2 \\ &\implies \text{minimum} \end{aligned} \quad (5.3)$$

in which S is the sum of the squares of the residuals; n is the number of sample points (ξ_i, \bar{u}_{1i}) ; and $\bar{u}_{1\max}$ and u_* are given. Then the model parameters κ_0 and Ω_0 can be found by solving the following equations:

$$\frac{\partial S}{\partial \kappa_0} = 0 \quad \text{and} \quad \frac{\partial S}{\partial \Omega_0} = 0 \quad (5.4)$$

That is,

$$\sum_i^n \left[\frac{\bar{u}_{1\max} - \bar{u}_{1i}}{u_*} + \frac{1}{\kappa_0} (\ln \xi_i + 1 - \xi_i) - \Omega_0 \cos^2 \frac{\pi \xi_i}{2} \right] (\ln \xi_i + 1 - \xi_i) = 0 \quad (5.5)$$

and

$$\sum_i^n \left[\frac{\bar{u}_{1\max} - \bar{u}_{1i}}{u_*} + \frac{1}{\kappa_0} (\ln \xi_i + 1 - \xi_i) - \Omega_0 \cos^2 \frac{\pi \xi_i}{2} \right] \cos^2 \frac{\pi \xi_i}{2} = 0 \quad (5.6)$$

The above two equations can be further written as

$$\begin{aligned} &\frac{1}{\kappa_0} \sum_i^n (\ln \xi_i + 1 - \xi_i)^2 - \Omega_0 \sum_i^n (\ln \xi_i + 1 - \xi_i) \cos^2 \frac{\pi \xi_i}{2} \\ &= - \sum_i^n \frac{\bar{u}_{1\max} - \bar{u}_{1i}}{u_*} (\ln \xi_i + 1 - \xi_i) \end{aligned} \quad (5.7)$$

and

$$\begin{aligned} & \frac{1}{\kappa_0} \sum_i^n (\ln \xi_i + 1 - \xi_i) \cos^2 \frac{\pi \xi_i}{2} - \Omega_0 \sum_i^n \cos^4 \frac{\pi \xi_i}{2} \\ = & - \sum_i^n \frac{\bar{u}_{1\max} - \bar{u}_{1i}}{u_*} \cos^2 \frac{\pi \xi_i}{2} \end{aligned} \quad (5.8)$$

(5.7) and (5.8) are linear equations with respect to $1/\kappa_0$ and Ω_0 . A MatLab program has been written to handle this solving process (Appendix B).

5.2.4 Test of the structure of the modified log-wake law

Theoretically, the modified log-wake law is valid in the outer region (overlap + wake layer + boundary effect layer). The lower limit of the overlap is usually taken as $y^+ = 70$. Therefore, the modified log-wake law is valid in $y^+ \geq 70$ and $\xi \leq 1$. FIG. 5.1 is a test of the structure of the modified log-wake law. To emphasize the velocity profile near the bed, a semilog plot is shown in FIG. 5.1a, where the modified log-wake law, the asymptotic log law and the asymptotic parabolic law are compared with Zagarola's (1996) experimental data. The same things are plotted in a rectangular coordinate system in FIG. 5.1b to emphasize the velocity profile near the axis. It can be seen that the modified log-wake law agrees fairly well with experimental data. The correlation coefficient $r = 0.9999$, shown in FIG. 5.1b. Besides, the asymptotic log law can be considered valid until about $\xi = 0.1$; and the asymptotic parabolic law can be considered valid above $\xi = 0.6$. All other profiles are very similar to those in FIG. 5.1. No doubt, *the structure of the modified log-wake law is reasonable.*

5.2.5 Test of κ_0 and Ω_0 with Reynolds number

The structure of the modified log-wake law has been checked to be correct. Are the model parameters κ_0 and Ω_0 universal or Reynolds number dependable constants? FIG. 5.2 is a test of κ_0 and Ω_0 with Reynolds number. It shows that an excellent agreement is obtained for each run. The individual values of κ_0 and Ω_0 are tabulated in Table 5.1, where κ_0 varies between 0.38 and 0.41 and can be approximated by

$$\kappa_0 = 0.3527 + 0.0049 \ln \text{Re}_* \quad (5.9)$$

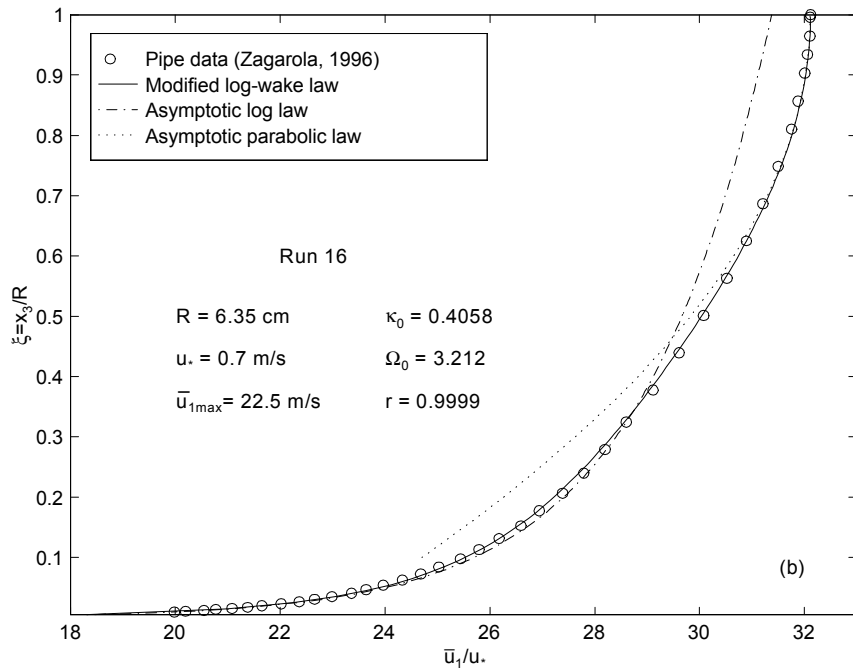
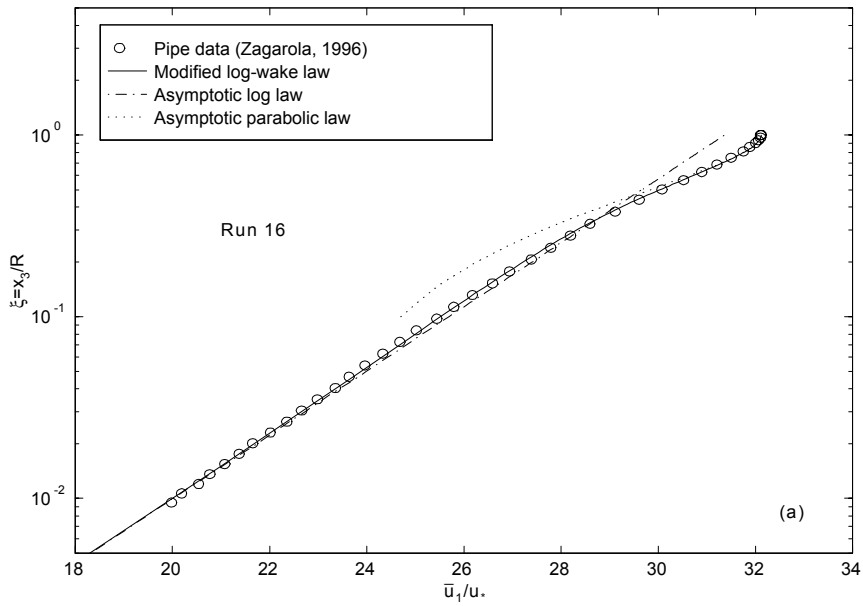


FIG. 5.1: Test of the structure of the modified log-wake law [(a) in a semilog coordinate system; (b) in a rectangular coordinate system.]

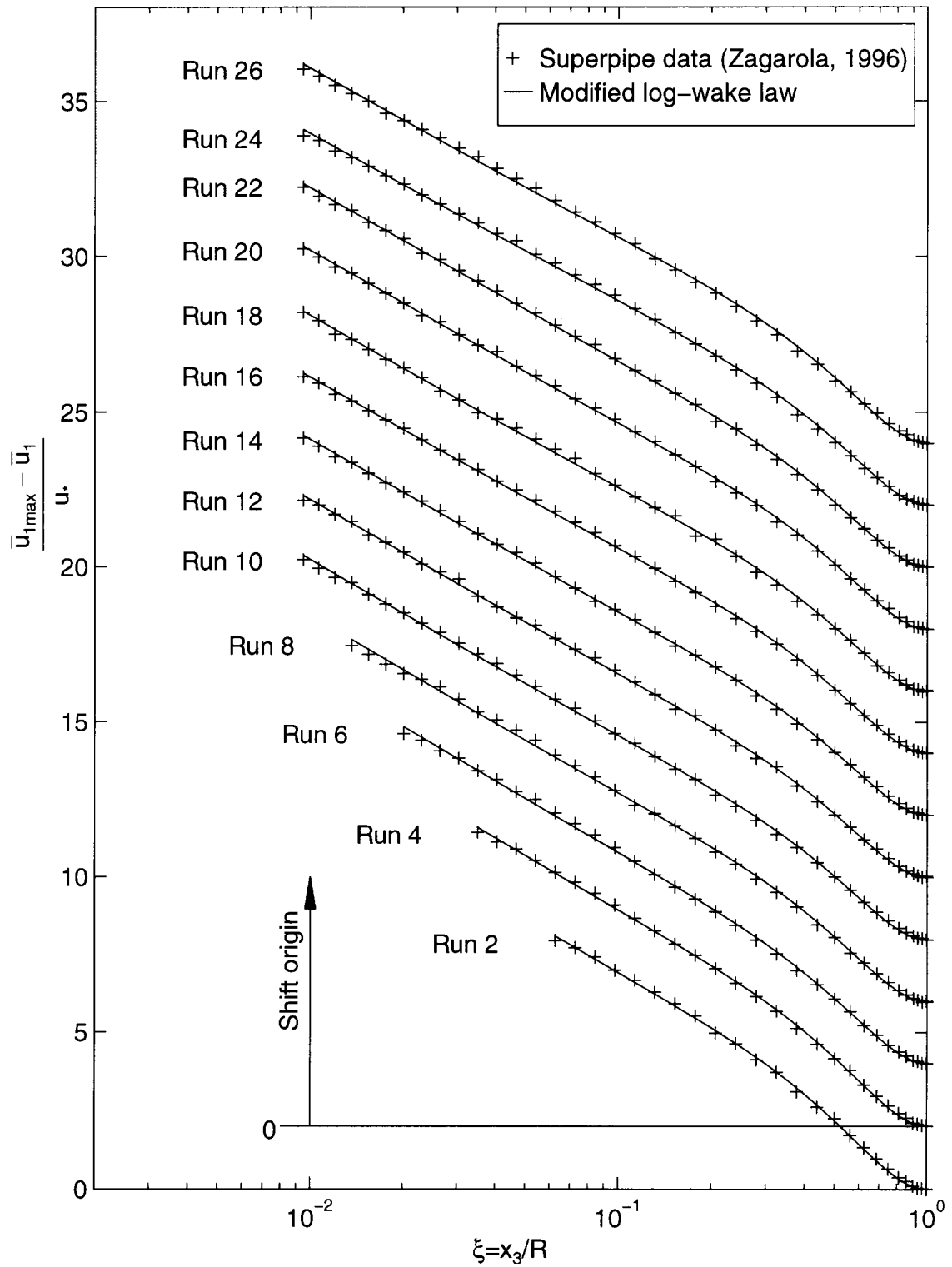


FIG. 5.2: Comparison of the modified log-wake law and Zagarola's superpipe experimental profiles with $y^+ \geq 70$

Table 5.1: The model parameters in the modified log-wake law for individual velocity profiles (Velocity profile data source: Zagarola, 1996)

Run	Reynolds Number Re (10^4)	Reynolds Number Re _* (10^3)	Karman Constant κ_0	Wake Strength Ω_0	Correlation Coefficient r
1	3.16	0.85	0.387	3.286	0.9998
2	4.17	1.09	0.382	3.342	0.9998
3	5.67	1.43	0.379	3.347	0.9998
4	7.43	1.93	0.382	3.361	0.9998
5	9.88	2.34	0.384	3.336	0.9997
6	14.58	3.32	0.383	3.197	0.9998
7	18.54	4.12	0.388	3.205	0.9997
8	23.05	5.02	0.391	3.199	0.9997
9	30.95	6.59	0.401	3.191	0.9997
10	40.93	8.49	0.395	3.086	0.9999
11	53.91	10.94	0.395	3.041	0.9999
12	75.18	14.83	0.399	3.110	0.9999
13	102.38	19.68	0.398	3.075	0.9999
14	134.04	25.23	0.403	3.132	0.9999
15	178.75	32.88	0.400	3.155	0.9999
16	234.50	42.16	0.406	3.212	0.9999
17	309.81	54.65	0.409	3.227	0.9999
18	442.03	76.10	0.405	3.164	0.9998
19	607.27	102.19	0.404	3.187	0.9999
20	771.47	127.32	0.404	3.242	0.9999
21	1024.90	165.56	0.402	3.213	0.9998
22	1359.80	216.04	0.401	3.203	0.9999
23	1819.60	283.32	0.411	3.199	0.9998
24	2397.70	367.00	0.416	3.272	0.9998
25	2992.70	452.40	0.411	3.223	0.9998
26	3525.90	528.57	0.412	3.292	0.9998

in which $Re_* = Ru_*/\nu$. (5.9) is shown in FIG. 5.3a. The wake strength coefficient Ω_0 is about a constant of 3.21 which is shown in FIG. 5.3b.

Obviously, a universal constant of κ_0 does not exist for $y^+ \geq 70$. Motivated by the suggestion of Zagarola (1996), i.e., the lower limit of the validation of the log law is $y^+ = 500$ instead of $y^+ = 70$, one may try a plot of all experimental data with $y^+ \geq 500$, shown in FIG. 5.4. This time an excellent complete similarity is obviously obtained. The least-squares method gives the universal constants κ_0 and Ω_0 as

$$\kappa_0 = 0.4056 \approx 0.406 \quad \text{and} \quad \Omega_0 = 3.201 \approx 3.2 \quad (5.10)$$

with an overall correlation coefficient $r = 0.9998$.

One can now conclude that: (1) *For large Reynolds number $y^+ \geq 500$, a complete similarity velocity defect law exists. The universal constants κ_0 and Ω_0 are 0.406 and 3.2, respectively.* (2) *If the near bed data, $70 \leq y^+ < 500$, are included, κ_0 slightly increases with the Reynolds number Re_* and can be estimated by (5.9). In practice, κ_0 may still be taken as 0.406 as a good approximation. The wake strength coefficient Ω_0 can be approximated as a constant 3.2.*

5.2.6 Test of the eddy viscosity model

The test of eddy viscosity model involves estimating the velocity gradient from a set of data points. However, numerical differentiation is often an unreliable process which can be highly sensitive to small fluctuations in data. In particular, the velocity gradient near the pipe axis is very small and, hence, very difficult to estimate accurately. Therefore, this study does not try to differentiate the aforementioned velocity profile data and get the eddy viscosity. Simply, the authoritative eddy viscosity data calculated by Hinze (1975, p.730) from Laufer's and Nunner's data are examined.

Since the shear stress at a pipe axis $\tau|_{\xi=1} = 0$ and $\frac{d\bar{u}}{d\xi}|_{\xi=1} = 0$, (3.33) in pipes reduces to

$$\boxed{\varepsilon^+ = \frac{\xi}{\frac{1}{\kappa_0} + \frac{\pi\Omega_0}{2} \frac{\xi \sin \pi\xi}{1-\xi}}} \quad (5.11)$$

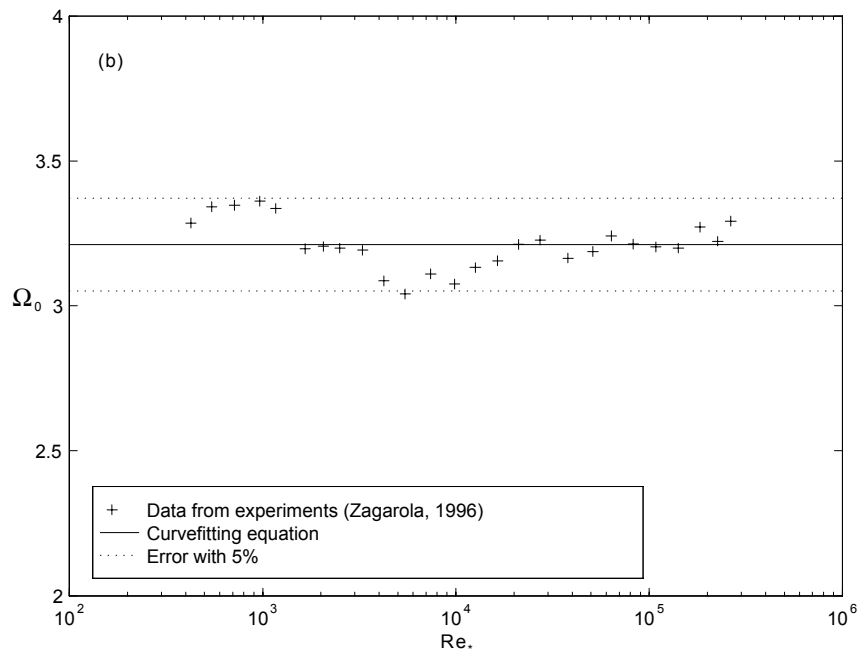
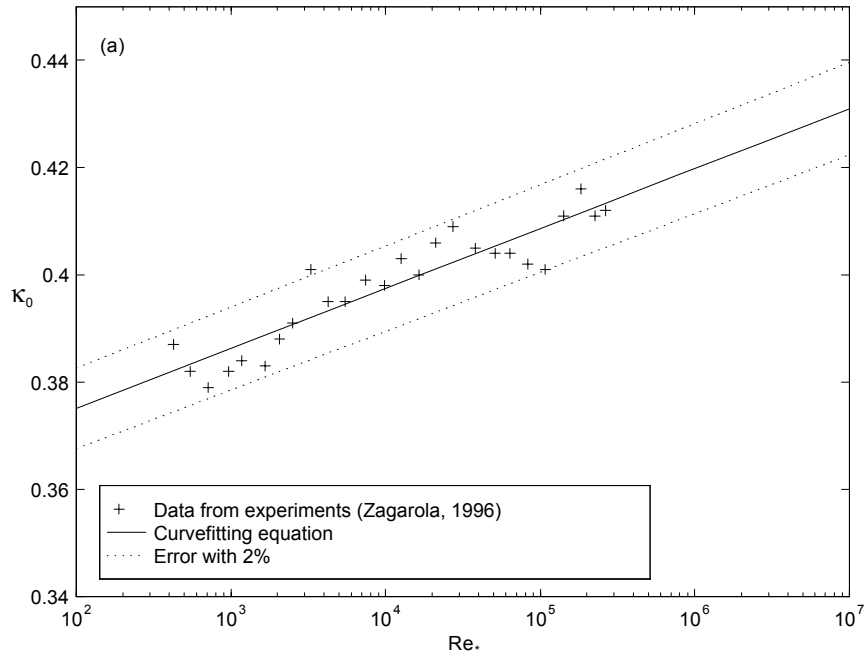


FIG. 5.3: (a) Variation of κ_0 versus Re_* ; (b) Variation of Ω_0 versus Re_*

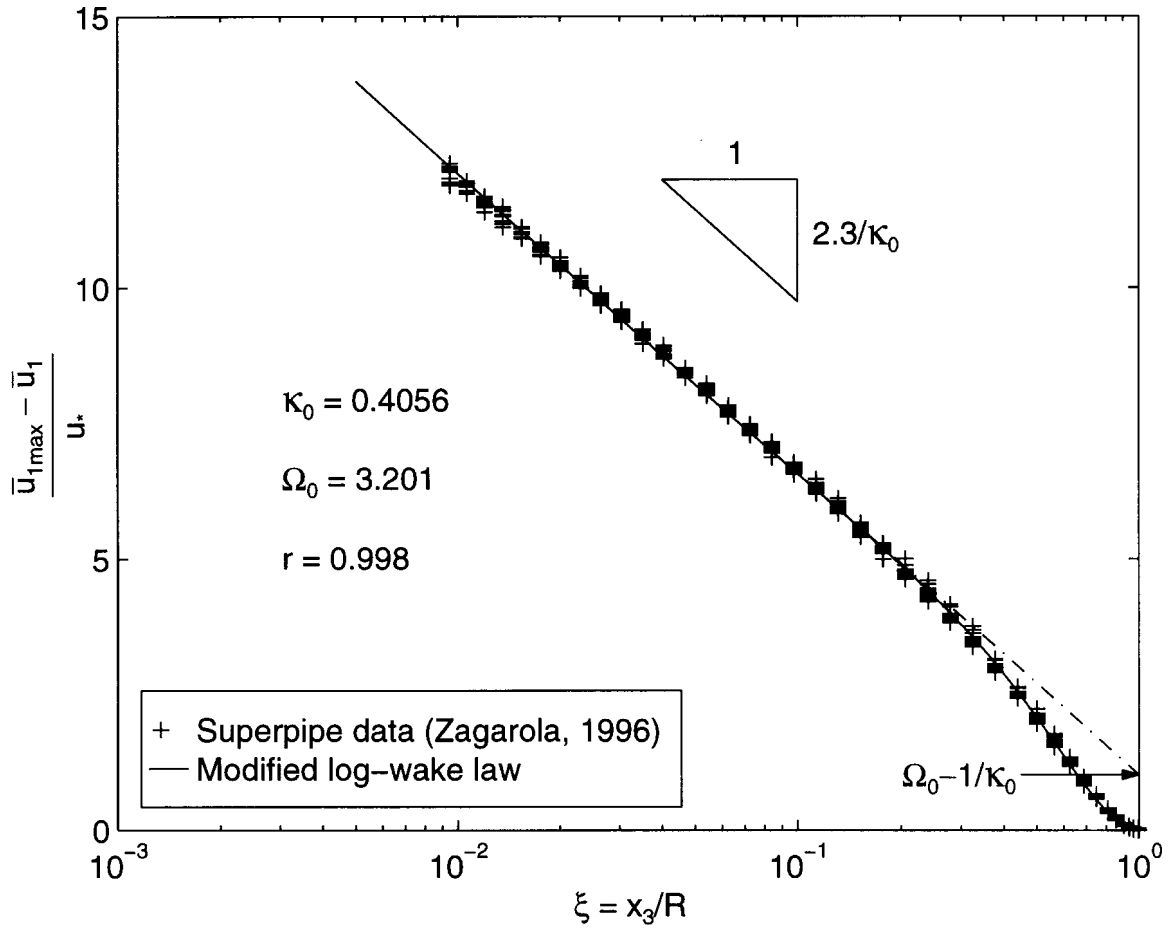


FIG. 5.4: Complete similarity: Comparison of the modified log-wake law with Zagarola's (1996) superpipe experimental data with $y^+ \geq 500$

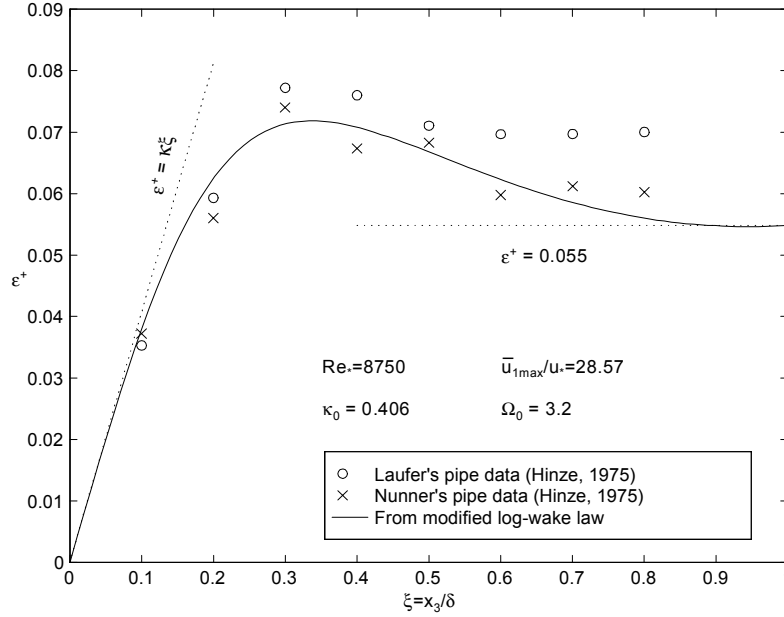


FIG. 5.5: Test of the eddy viscosity model from the modified log-wake law

Near the pipe wall, $\xi \rightarrow 0$, the above equation reduces to

$$\varepsilon^+ \rightarrow \kappa_0 \xi \quad (5.12)$$

which is consistent with the mixing length model. Near the pipe axis, $\xi \rightarrow 1$, one has

$$\frac{\sin \pi \xi}{1 - \xi} = \frac{\sin \pi(1 - \xi)}{1 - \xi} \rightarrow \pi$$

Thus,

$$\varepsilon^+ \rightarrow \frac{1}{\frac{1}{\kappa_0} + \frac{\pi^2 \Omega_0}{2}} = \text{const} \quad (5.13)$$

which is the same as the result of the parabolic law (Hinze, 1975, p.730).

Substituting the universal constants $\kappa_0 = 0.406$ and $\Omega_0 = 3.2$ into (5.11), one can get the eddy viscosity expression corresponding to the modified log-wake law which is drawn in FIG. 5.5.

FIG. 5.5 shows that the predicted eddy viscosity is compatible to Laufer's and Nunner's experimental data. In addition, the present eddy viscosity model is physically reasonable. Since the eddy viscosity ε in the vertical direction is proportional

to u'_3 , the plot of the viscosity model is very similar to that of the measurements of the turbulence intensity in the x_3 -direction (Hinze, 1975, p.725).

5.3 Test of the modified log-wake law in narrow open-channels

As stated earlier, the boundary layer thickness δ is the distance from the bed to the maximum velocity $\bar{u}_{1\max}$ in narrow channels. The derivative boundary condition, as it in pipes, is expressed by (2.13). Thus, the modified log-wake law in narrow channels is the same as that in pipes, i.e., (5.1), here $\xi = x_3/\delta$ in narrow channels.

5.3.1 Data selection

Although many experiments in narrow flumes are reported (Hu and Hui, 1995; Sarma, Lakshminarayana and Rao, 1983), the original data can be found only in a few papers. Three data sources are used here: Wang and Qian (1989), Coleman (1986), and Kironoto (1993).

In Wang and Qian's (1989) data, the experiments were run in a smooth flume (both side-walls and bed) with a bed slope $S = 0.01$, the aspect ratios are 3, 3.33 and 3.75. Therefore, the centerline shear velocity can be estimated from (4.16). The detailed information can be found in Appendix C.

Coleman's (1986) experiments are very similar to Wang and Qian's (1989), except that the bed slope $S = 0.002$ and the aspect ratios are about 2. Therefore, the centerline shear velocity may be estimated from (4.23). Some information about Coleman's experiments is shown in Appendix D.

In both Wang and Qian's (1989) and Coleman's (1986) experiments, given the shear velocity u_* , the fitting parameters include δ , $\bar{u}_{1\max}$, κ_0 , and Ω_0 . If κ_0 is fitted as about 0.406 in these two data sets, it may be proved that the proposed equations for determining the shear velocity u_* in Chapter 4 are reasonable.

Kironoto (1993) did experiments over a rough bed ($k_s = 23$ mm) flume with the

aspect ratio $a/h \approx 2$. So, the centerline shear velocity u_* can be estimated from neither (4.16) nor (4.23). In this case, one assumes that $\kappa_0 = 0.406$, then the fitting parameters are u_* , δ , $\bar{u}_{1\max}$, and Ω_0 . Some information about Kironoto's (1993) experiments can be found in Appendix E.

5.3.2 Method for determining δ and $\bar{u}_{1\max}$

For a narrow channel where the maximum velocity occurs below the water surface, one can assume that the velocity profile near the boundary layer margin (approximately $\xi \geq 0.6$ from the pipe results) obeys the parabolic law, fitting the experimental data (x_{3i}, \bar{u}_{1i}) near the boundary layer margin as a quadratic equation can give the maximum velocity $\bar{u}_{1\max}$ and its corresponding boundary layer thickness δ .

Specifically, let the velocity profile near the boundary layer margin has the following functional form:

$$\bar{u}_1 = a_1 x_3^2 + a_2 x_3 + a_3 \quad (5.14)$$

in which a_1 , a_2 , and a_3 are curve-fitting constants. Using the experimental data (x_{3i}, \bar{u}_{1i}) near the boundary layer margin with the least-squares method, three constants a_1 , a_2 , and a_3 can be determined. Then, the boundary layer thickness δ and the maximum velocity $\bar{u}_{1\max}$ can be easily estimated by setting the velocity gradient $d\bar{u}_1/dx_3 = 0$, which gives

$$\delta = -\frac{a_2}{2a_1} \quad (5.15)$$

$$\bar{u}_{1\max} = a_1 \delta^2 + a_2 \delta + a_3 \quad (5.16)$$

With δ , $\bar{u}_{1\max}$ and u_* or κ_0 available, the exact same procedure as that in pipes is used for determining Ω_0 and κ_0 or u_* .

5.3.3 Test of the modified log-wake law

Wang and Qian's (1989) experiments

As stated earlier, the centerline shear velocities can be calculated from (4.16). After determining the values of δ and $\bar{u}_{1\max}$ from (5.15) and (5.16), respectively, κ_0

and Ω_0 are estimated from (5.7) and (5.8). The calculated results are shown in Table 5.2. A representative velocity profile of Wang and Qian’s clear water experiments is shown in FIG. 5.6, where the bed slope $S = 0.01$. Other profile analyses can be found in Appendix C (Section: Clear water and salt water measurements).

Table 5.2: Calculated results of Wang-Qian’s clear and salt water experiments

RUN	h (cm)	a/h	u_* (cm/s)	δ (cm)	δ/h	$\bar{u}_{1\max}$ (m/s)	Re_*	κ_0	Ω_0	r^a
CW1	10	3.00	9.16	6.36	0.636	2.11	5826	0.419	1.32	0.9992
CW2	10	3.00	9.16	6.25	0.625	2.10	5725	0.412	1.49	0.9994
CW3	10	3.00	9.16	6.71	0.671	2.11	6146	0.390	1.20	0.9996
SW1	9	3.33	8.81	6.19	0.688	2.07	4957	0.385	1.45	0.9987
SW2	9	3.33	8.81	6.51	0.723	2.09	5213	0.424	1.91	0.9993
CW4	8	3.75	8.40	6.06	0.758	1.99	5544	0.412	1.70	0.9993
MEAN								0.407	1.51	

^a Fitting correlation coefficient

Coleman’s (1986) experiments

Since the aspect ratios in Coleman’s experiments are about 2.0, the secondary flows in the corners strongly affect the bed shear stress at the centerline, as an approximation, the average bed shear velocity u_* is used herein. Using the same procedure as before, the values of δ , $\bar{u}_{1\max}$, κ_0 and Ω_0 are calculated, shown in Table 5.3, where the bed slope $S = 0.002$. A representative velocity profile of Coleman’s clear water experiments is shown in FIG. 5.7. Other profiles can be found in Appendix D.

Table 5.3: Calculated results of Coleman’s clear water experiments

RUN	h (cm)	a/h	u_* (cm/s)	δ (cm)	δ/h	$\bar{u}_{1\max}$ (m/s)	Re_*	κ_0	Ω_0	r^a
RUN1	17.2	2.07	4.11	13.26	0.771	1.054	5463	0.370	2.707	0.9997
RUN21	16.9	2.11	4.10	12.61	0.746	1.048	5542	0.400	2.598	0.9992
RUN32	17.3	2.06	4.12	12.88	0.745	1.025	5397	0.432	3.356	0.9997
MEAN								0.401		

^a Fitting correlation coefficient

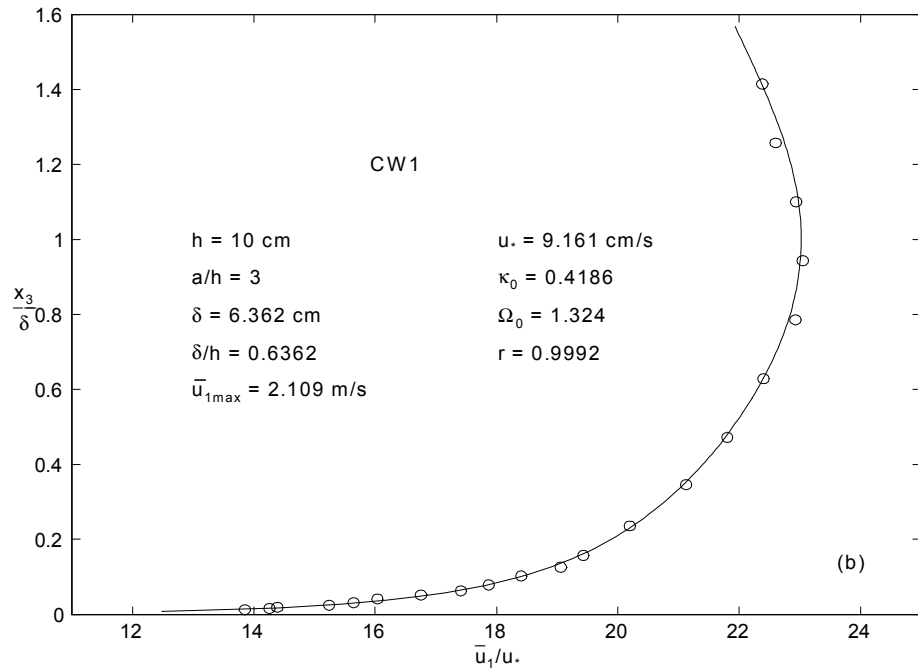
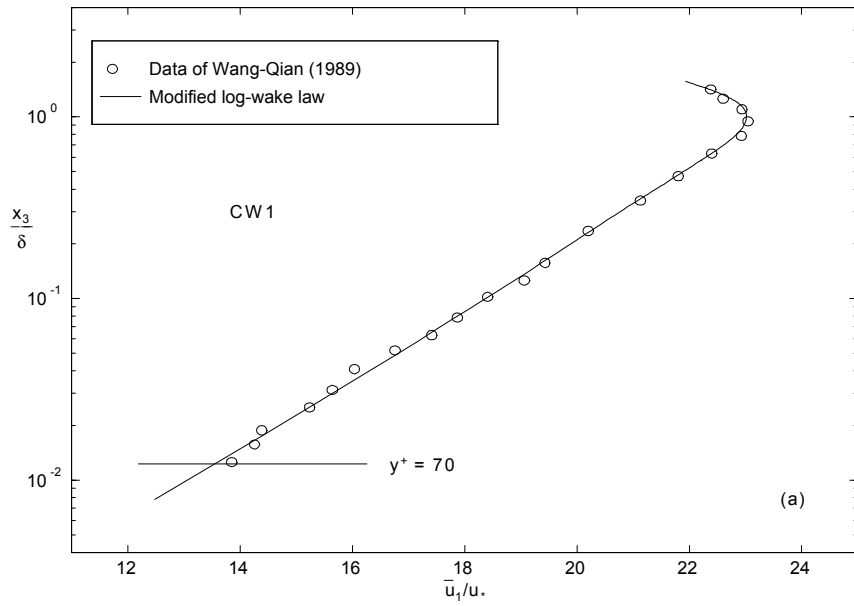


FIG. 5.6: Comparison of the modified log-lake law with Wang-Qian's experiments [(a) in a semilog coordinate system, (b) in a rectangular coordinate system]

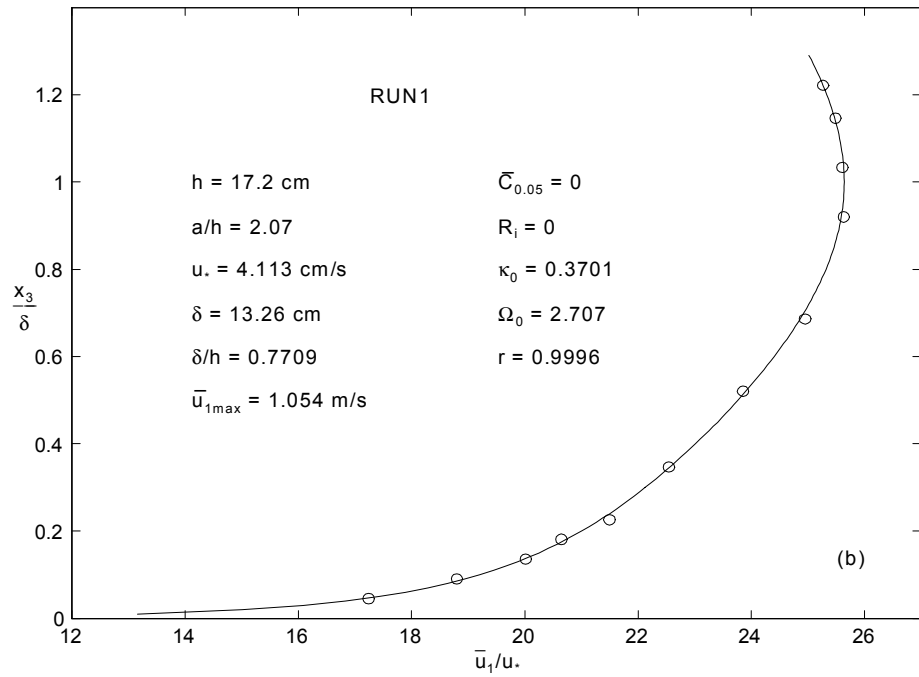
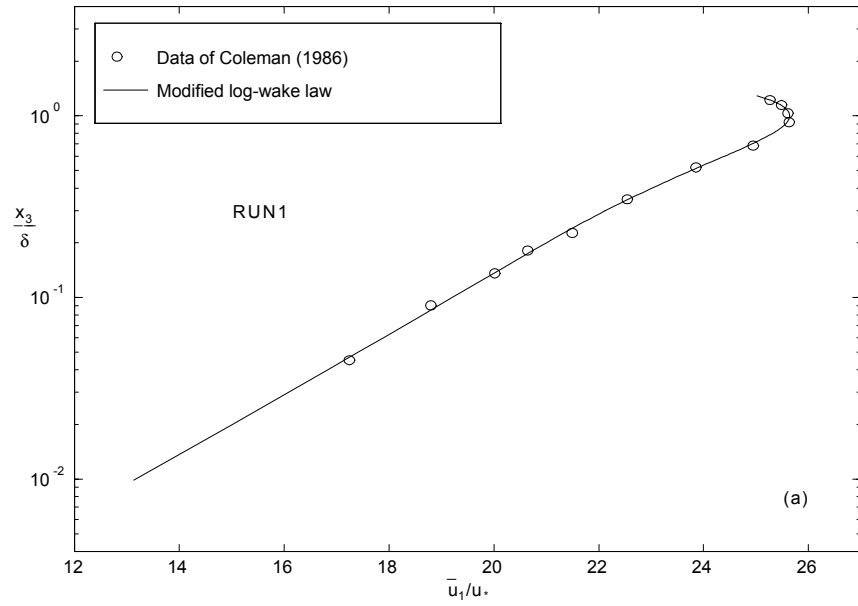


FIG. 5.7: Comparison between the modified log-lake law and Coleman's experimental data [(a) in a semilog coordinate system , (b) in a rectangular coordinate system]

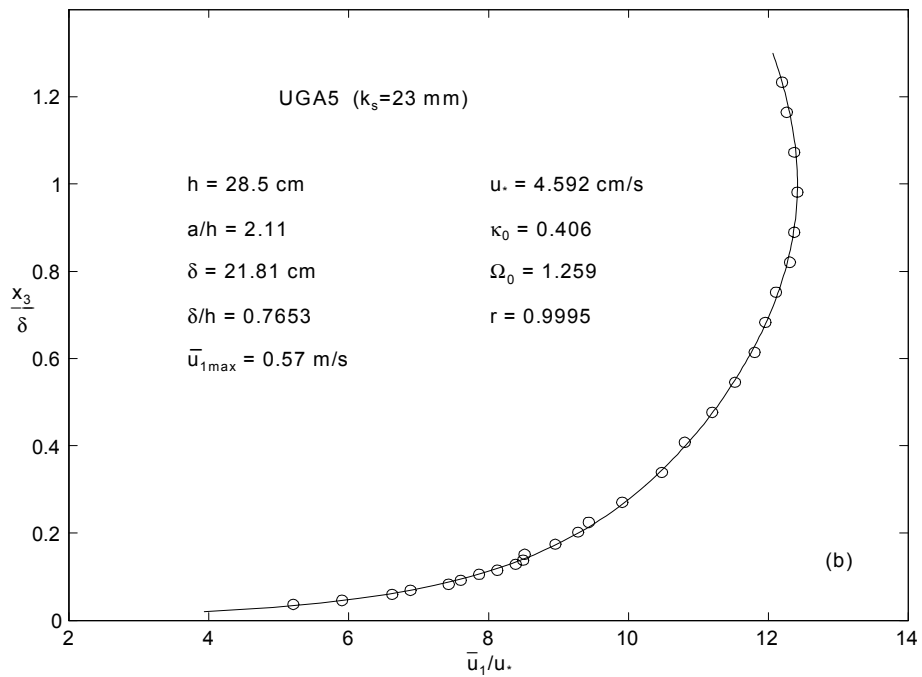
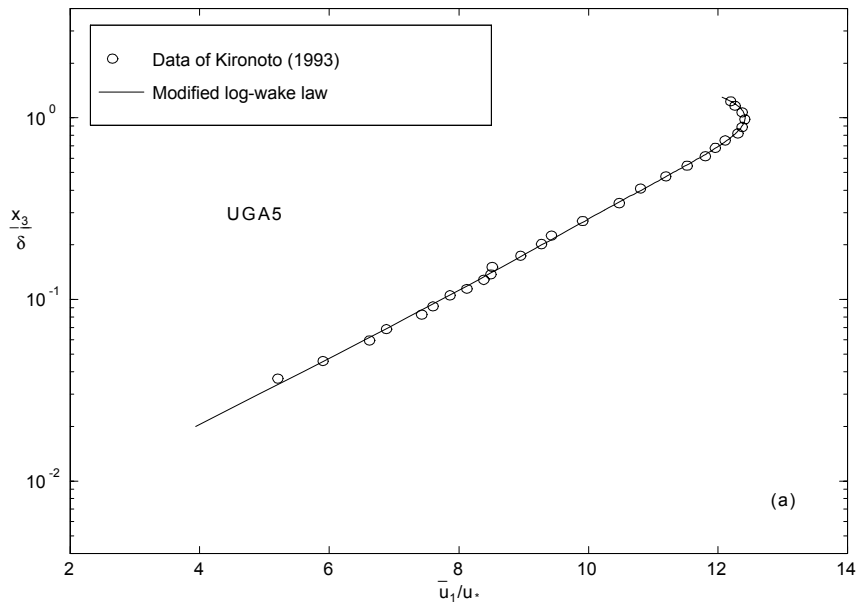


FIG. 5.8: Comparison between the modified log-lake law and Kironoto's narrow flume data [(a) in a semilog coordinate system, (b) in a rectangular coordinate system]

Table 5.4: Calculated results of Kironoto's clear water experiments

RUN	h (cm)	a/h	S	u_* (cm/s)	δ (cm)	δ/h	$\bar{u}_{1\max}$ (m/s)	Re_*	Ω_0	r
UGA3	28.5	2.11	1.0E-3	4.16	21.75	0.763	0.571	9048	1.637	0.9992
UGA5	28.5	2.11	1.0E-3	4.59	21.81	0.765	0.570	10011	1.259	0.9995
UGB3	29.0	2.07	7.5E-4	3.35	21.41	0.738	0.465	7172	2.119	0.9990
UGB5	29.0	2.07	7.5E-4	3.65	24.98	0.860	0.463	9118	1.695	0.9977

Notes: Assume that $\kappa_0 = 0.406$. r = Fitting correlation coefficient.

Kironoto's (1993) experiments

As stated in Section 5.3.1, the shear velocity u_* cannot be estimated from (4.16) or (4.23). Since κ_0 is independent of roughness and should be the same as that in pipe flows (based on previous knowledge), one may assume that $\kappa_0 = 0.406$ in Kironoto's experiments. Then u_* can be evaluated from a curve-fitting. That is, rewrite (5.1) as

$$\bar{u}_{1\max} - \bar{u}_1 = -\frac{u_*}{\kappa_0} [\ln \xi + (1 - \xi)] + u_* \Omega_0 \cos^2 \frac{\pi \xi}{2} \quad (5.17)$$

Let

$$p_1 = \frac{u_*}{\kappa_0} \quad \text{and} \quad p_2 = u_* \Omega_0 \quad (5.18)$$

in (5.17), then p_1 and p_2 can be found using the least-squares method. Furthermore, u_* and Ω_0 can be estimated (5.18), shown in Table 5.4. A representative velocity profile is shown in FIG. 5.8 (p.58). Other profiles can be found in Appendix E.

Results of narrow channel experiments

From Tables 5.2-5.4, and FIGS. 5.6-5.8, one can see that: (1) The modified log-wake law has a very high correlation with measurement data. (2) κ_0 varies within 0.385 and 0.432, its average value is 0.405 which is compatible to both that in pipe flows in Section 5.2.5 and previous studies 0.40-0.41 (Kironoto and Graf, 1994; Muste and Patel, 1997; Nezu, Kadota and Nakagawa, 1997). On the other hand, the values of κ_0 here show that the shear velocity equations (4.16) and (4.23) are reasonable. (3) Ω_0 may vary with the aspect ratio a/h and the relative roughness k_s/h . This will further be discussed in Subsection 5.4.4. (4) The modified log-wake law can

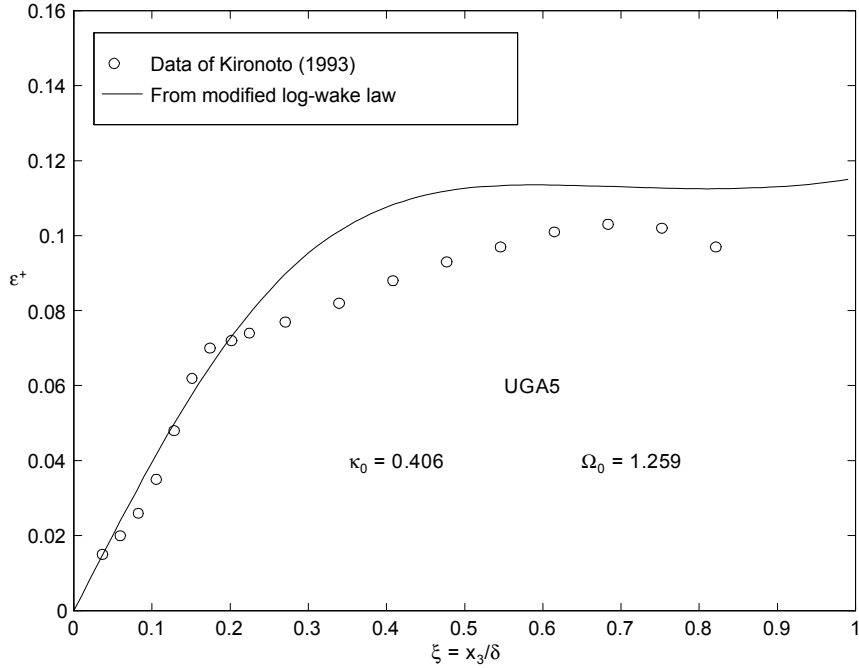


FIG. 5.9: Test of the eddy viscosity model from the modified log-wake law

reproduce even the measurement data beyond the boundary layer thickness. This is an important aspect of the modified log-wake law.

5.3.4 Test of the eddy viscosity model

The eddy viscosity model in a narrow channel is the same as that in pipes, i.e., (5.11). From Table 5.4 or FIG. 5.8, one has $\kappa_0 = 0.406$ and $\Omega_0 = 1.259$ for UGA5 of Kironoto's data sets (see Appendix E). Substituting these values into (5.11) gives the corresponding eddy viscosity. FIG. 5.9 shows the comparison of the proposed model with one of Kironoto's (1993) data. Following Hinze (1975, p.730), the data beyond $\xi = 0.9$ are omitted since the numerical estimation of the velocity gradient near the boundary layer margin is very sensitive to small data fluctuation. It can be seen from the figure that the proposed model is compatible to the measurements. However, the agreement is not as good as the corresponding velocity profile (FIG. 5.8). Again this is because the velocity gradient is difficult to estimate numerically.

5.4 Test of the modified log-wake law in wide open-channels

5.4.1 Data selection

In the test of the modified log-wake law in wide channels, if one assumes $\kappa_0 = 0.406$, there are still four fitting parameters, u_* , Ω_0 , λ_0 and $\bar{u}_{1\max}$. More fitting parameters will reduce the reliability of the fitting results. Therefore, this test will only use the experimental data reported by Kironoto (1993), where the maximum velocity $\bar{u}_{1\max}$ is measured. Only three parameters, u_* , Ω_0 , and λ_0 , need to be fitted. In addition, the channel side-walls are smooth and the bed is rough with $k_s = 4.8$ mm. The aspect ratios a/h are between 5 and 7.

5.4.2 Method for determining u_* , Ω_0 , and λ_0

The modified log-wake law is described by (3.31) in wide open-channels, where the water surface shear effect factor $\lambda_0 \neq 0$. Rewrite (5.23) as

$$\begin{aligned} \bar{u}_{1\max} - \bar{u}_1 &= -\frac{u_*}{\kappa_0} [\ln \xi + (1 - \xi)] + \Omega_0 u_* \cos^2 \frac{\pi \xi}{2} \\ &\quad + \lambda_0 \left(\frac{V_{\text{wind}} - \bar{u}_{1\max}}{u_*} \right)^2 u_* (1 - \xi) \end{aligned} \quad (5.19)$$

Let

$$p_1 = \frac{u_*}{\kappa_0} \quad , \quad p_2 = \Omega_0 u_* \quad , \quad p_3 = \lambda_0 \left(\frac{V_{\text{wind}} - \bar{u}_{1\max}}{u_*} \right)^2 u_* \quad (5.20)$$

then p_1 , p_2 and p_3 can be estimated by the least-squares method (linear regression).

A MatLab program to handle the above process is appended in Appendix B.

With p_1 , p_2 and p_3 available, one has

$$u_* = \kappa_0 p_1 \quad , \quad \Omega_0 = p_2 / u_* \quad , \quad \lambda_0 = \frac{p_3}{u_*} \left(\frac{V_{\text{wind}} - \bar{u}_{1\max}}{u_*} \right)^{-2}$$

5.4.3 Test of the modified log-wake law

The calculated results of Kironoto's (1993) data in a wide flume are shown in Table 5.5. A representative velocity profile, along with the modified log-wake law,

Table 5.5: Results of Kironoto’s wide channel experiments from the modified log-wake law

RUN	h	a/h	u_*	Re_*	k_s/h	Ω_0	λ_0	r
	(cm)		(cm/s)					
UPA3	11.50	5.22	3.37	3636	0.042	-0.1642	0.0107	0.9992
UPA5	11.50	5.22	3.20	3445	0.042	-0.2831	0.0118	0.9996
UPB3	10.10	5.94	3.54	3355	0.048	-0.6431	0.0143	0.9993
UPB5	10.10	5.94	3.53	3339	0.048	-0.5015	0.0129	0.9993
UPC3	11.90	5.04	2.31	2576	0.040	1.0642	0.0063	0.9994
UPC5	11.90	5.04	2.26	2516	0.040	0.4360	0.0088	0.9994
UPD3	8.70	6.90	3.37	2752	0.055	-0.3178	0.0146	0.9992
UPD5	8.70	6.90	3.67	2995	0.055	-0.0845	0.0142	0.9996

Notes: Rough bed $k_s = 4.8$ mm; assume $\kappa_0 = 0.406$;
 r = correlation coefficient.

is shown in FIG. 5.10. One can see that the modified log-wake law compares the data fairly well. However, the wake strength seems very small compared with that in narrow channels.

5.4.4 Wake strength coefficient Ω_0 in open-channels

A plot of the wake strength coefficient Ω_0 against the aspect ratio a/h is shown in FIG. 5.11. The data are from Tables 5.2, 5.3, 5.4 and 5.5. One can see that the wake strength coefficient Ω_0 decreases with the aspect ratio a/h in narrow channels. However, when $a/h \geq 5$, the wake strength coefficient Ω_0 is about 0. This shows that: (1) the wake strength coefficient Ω_0 is, in essence, a factor to reflect the effect of the side-walls; and (2) when the aspect ratio $a/h \geq 5$, the side-wall effect may be neglected and the wake strength coefficient Ω_0 then tends to zero. Physically, the wake function reflects large-scale turbulent mixing. In open-channels, secondary flows in the channel corners can be regarded as a kind of large scale eddies. For a wide channels, secondary flows may only be limited to near the corners and have little effect on the centerline velocity profiles. Hence, the wake function in a wide channel is relatively small. On the other hand, the free surface suppresses the vertical turbulent mixing and then further weaken the wake function. Finally, the wake strength Ω_0 is

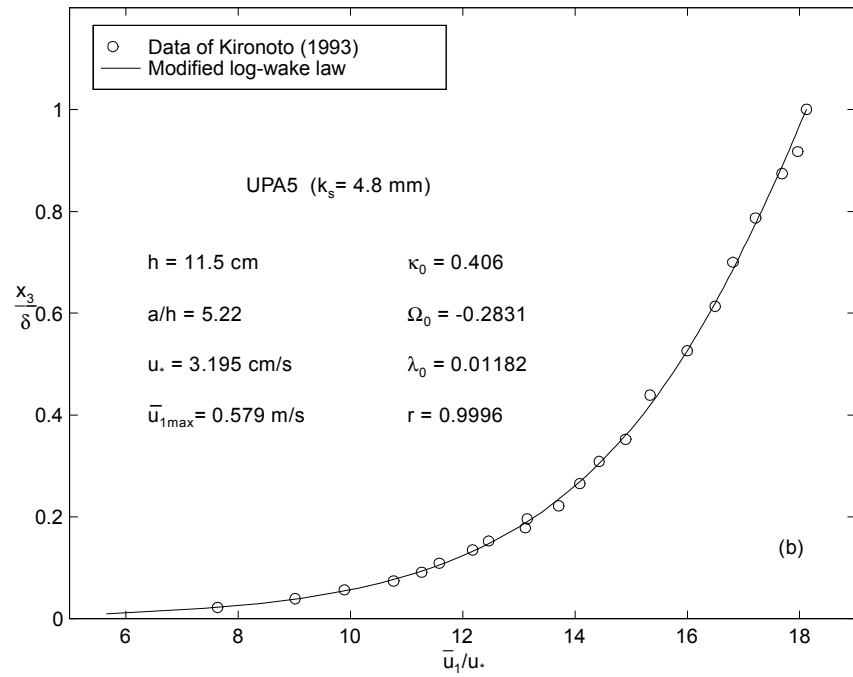
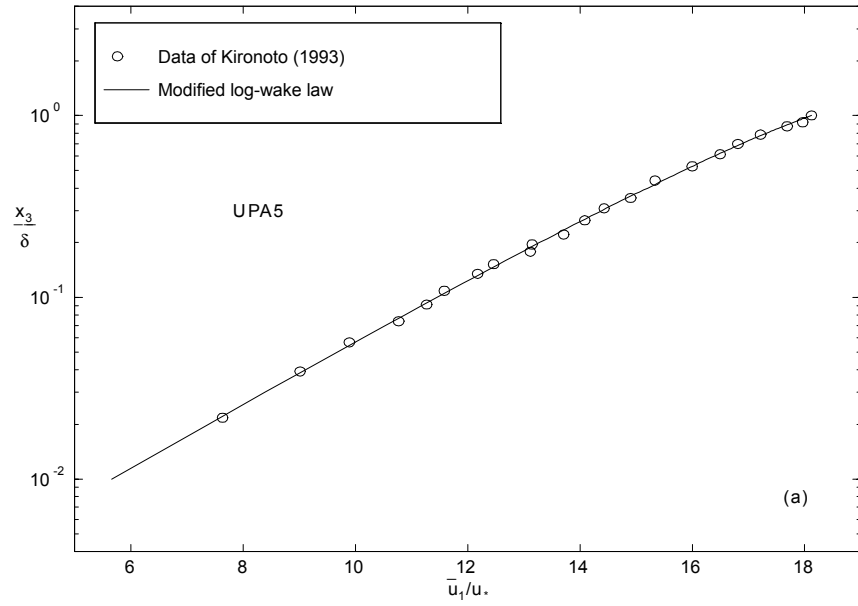


FIG. 5.10: Comparison of the modified log-wake law with Kironoto's wide channel data [(a) in a rectangular coordinate, (b) in a semilog coordinate]

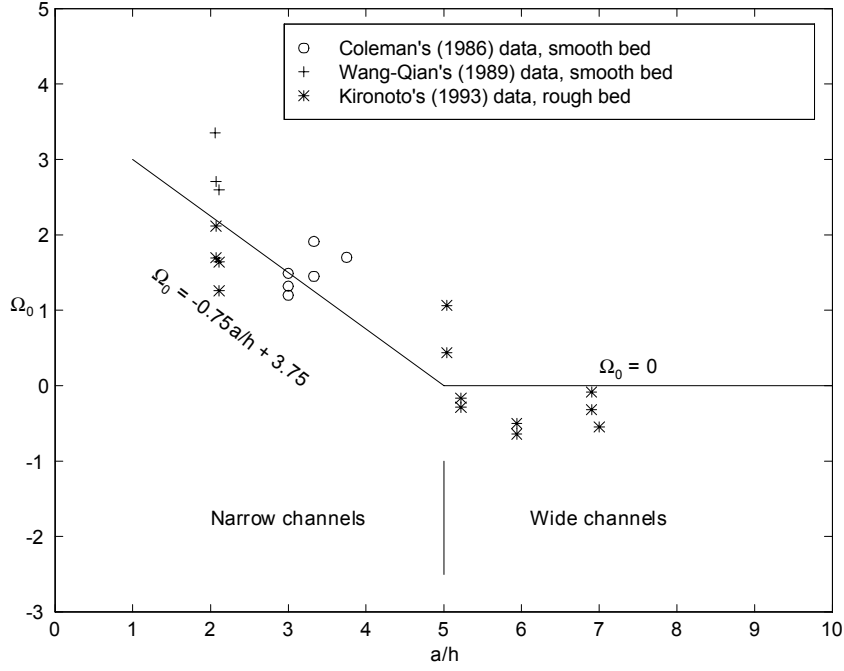


FIG. 5.11: The wake strength coefficient Ω_0 versus the aspect ratio a/h

very small or tends to zero in wide channels. An empirical equation for the estimation of Ω_0 is suggested as follows:

$$\Omega_0 = \begin{cases} -0.75\frac{a}{h} + 3.75 & \text{if } a/h < 5 \\ 0 & \text{if } a/h \geq 5 \end{cases} \quad (5.21)$$

5.5 Simplification of the modified log-wake law and its test in wide open-channels

5.5.1 Simplification of the modified log-wake law (the log-linear law) in wide open-channels

One may draw inspiration from FIG. 5.11, i.e., the wake component may be neglected in wide channels. Thus, the modified log-wake law reduces to a log-linear law. This may also be proved mathematically. Referring to (3.23) and (3.25), one

can expand the modified log-wake law at the water surface, i.e.

$$\frac{\bar{u}_{1\max} - \bar{u}_1}{u_*} = -\frac{1}{u_*} \left. \frac{d\bar{u}_1}{d\xi} \right|_{\xi=1} (1 - \xi) + \left(\frac{1}{2\kappa_0} + \Omega_0 \right) (1 - \xi)^2 + \dots \quad (5.22)$$

In pipes and narrow channels, $\left. \frac{d\bar{u}_1}{d\xi} \right|_{\xi=1} = 0$, the leading term is a second order term $\left(\frac{1}{2\kappa_0} + \Omega_0 \right) (1 - \xi)^2$ near the water surface, which relates to the wake strength coefficient Ω_0 . Therefore, the wake component is certainly important. In wide channels, however, $\left. \frac{d\bar{u}_1}{d\xi} \right|_{\xi=1} \neq 0$, the leading term is obviously a first order term $-\frac{1}{u_*} \left. \frac{d\bar{u}_1}{d\xi} \right|_{\xi=1} (1 - \xi)$, which is irrelevant to the wake strength coefficient Ω_0 . As a first approximation, i.e., neglecting the second and higher order terms, one can see that the wake strength coefficient Ω_0 just has little effect on the flow near the water surface. That is, the wake component may be neglected in wide channels, i.e.,

$$\frac{\bar{u}_{1\max} - \bar{u}_1}{u_*} = -\frac{1}{\kappa_0} \ln \xi - \left[\frac{1}{\kappa_0} - \frac{1}{u_*} \left. \frac{d\bar{u}_1}{d\xi} \right|_{\xi=1} \right] (1 - \xi)$$

or

$$\boxed{\frac{\bar{u}_{1\max} - \bar{u}_1}{u_*} = -\frac{1}{\kappa_0} \ln \xi - \left[\frac{1}{\kappa_0} - \lambda_0 \left(\frac{V_{\text{wind}} - \bar{u}_{1\max}}{u_*} \right)^2 \right] (1 - \xi)} \quad (5.23)$$

in which λ_0 is the water surface shear effect factor and will be determined experimentally. The above equation is the simplification of the modified log-wake law in wide open-channels. For simplicity, it is referred to as the *log-linear law*. Note that this log-linear law is different from (2.22) where it is only valid for sediment-laden flows.

Let $\kappa_0 = 0.406$, the fitting parameters in the log-linear law are $\bar{u}_{1\max}$, u_* , and λ_0 .

5.5.2 Data selection

Besides the data of Kironoto (1993) in Subsection 5.4.1, experiments by Muste (1995), McQuivey (1971), and Guy, Simons and Richardson (1966) will also be used in this section. Muste (1995) recorded 3 clear water experiments (Appendix F) in a smooth flume in his dissertation. The aspect ratios are about 7. McQuivey (1971) collected a huge data set in the CSU Hydraulics Laboratory. Only the 12 runs of his

first table (Appendix G) are used here, where the first 6 runs were over a smooth bed while last 6 runs over a rough bed. The aspect ratios are about 6. In addition, several clear water velocity profile measurements in a wide flume (8 ft wide) by Guy, Simons and Richardson (1966) are tested, see Appendix H.

5.5.3 Method for determining u_* , λ_0 and $\bar{u}_{1\max}$

Rewrite (5.23) as

$$\bar{u}_1 = \frac{u_*}{\kappa_0} [\ln \xi + (1 - \xi)] - \lambda_0 \left(\frac{V_{\text{wind}} - \bar{u}_{1\max}}{u_*} \right)^2 u_* (1 - \xi) - \bar{u}_{1\max} \quad (5.24)$$

Let

$$p_1 = \frac{u_*}{\kappa_0}, \quad p_2 = \lambda_0 \left(\frac{V_{\text{wind}} - \bar{u}_{1\max}}{u_*} \right)^2 u_*, \quad \text{and} \quad p_3 = \bar{u}_{1\max} \quad (5.25)$$

then p_1 , p_2 and p_3 can be estimated by the least-squares method (linear regression).

A MatLab program to handle the above process is appended in Appendix B.

With p_1 , p_2 and p_3 available, one has

$$u_* = \kappa_0 p_1 \quad (5.26)$$

$$\bar{u}_{1\max} = p_3 \quad (5.27)$$

$$\lambda_0 = \frac{p_2}{u_*} \left(\frac{V_{\text{wind}} - \bar{u}_{1\max}}{u_*} \right)^{-2} \quad (5.28)$$

In Kironoto's (1993) experiments, the maximum velocity $\bar{u}_{1\max}$ is measured, then only u_* and λ_0 are determined.

5.5.4 Test of the log-linear law

The calculated results of Kironoto's (1993) wide flume data over a rough bed, Muste's (1995) experiments over a smooth bed, McQuivey's (1971) experiments over a smooth bed and a rough bed, and Guy, Simons and Richardson's (1966) experiments over transition and rough beds are listed in Tables 5.6, 5.7, 5.8, and 5.9, respectively. Four representative velocity profiles, along with the log-linear law, from the experiments of Kironoto, Muste, McQuivey, Guy et al. are shown in FIGS. 5.12, 5.13, 5.14,

Table 5.6: Results of Kironoto’s wide channel experiments

RUN	h	a/h	u_*	Re_*	k_s/h	λ_0	r
	(cm)		(cm/s)				
UPA3	11.50	5.22	3.37	3548	0.042	0.0101	0.9992
UPA5	11.50	5.22	3.20	3363	0.042	0.0109	0.9996
UPB3	10.10	5.94	3.55	3282	0.048	0.0115	0.9992
UPB5	10.10	5.94	3.54	3265	0.048	0.0108	0.9993
UPC3	11.90	5.04	2.30	2500	0.040	0.0101	0.9992
UPC5	11.90	5.04	2.25	2448	0.040	0.0102	0.9994
UPD3	8.70	6.90	3.38	2686	0.055	0.0133	0.9992
UPD5	8.70	6.90	3.67	2921	0.055	0.0137	0.9996

Notes: Rough bed $k_s = 4.8$ mm; assume $\kappa_0 = 0.406$;
 r = correlation coefficient.

Table 5.7: Results of Muste’s wide channel experiments

RUN	h	a/h	$\bar{u}_{1\max}$	u_*	Re_*	λ_0	r
	(cm)		(m/s)	(cm/s)			
CW01	13.00	7.00	0.715	2.87	3502	0.00531	0.9995
CW02	12.80	7.11	0.729	2.89	3359	0.00584	0.9997
CW03	12.70	7.17	0.750	2.48	2885	0.00614	0.9993

Note: Smooth bed; assume $\kappa_0 = 0.406$.

and 5.15, respectively. Other profiles can be found in Appendixes E, F, G, and H. In particular, comparing Tables 5.5 and 5.6, one sees that the log-linear law is very close to the modified log-wake law. However, the log-linear law is simpler and contains only two model parameters.

In the above experiments, it is assumed that V_{wind} is zero in laboratories and the von Karman constant $\kappa_0 = 0.406$. It is evident, from Tables 5.6-5.9 and FIGS. 5.12-5.15, that the neglect of the wake term in the modified log-wake law is reasonable in wide channels; and the log-linear law fits the data quite well in the entire outer region. The water surface shear effect factor λ_0 is discussed next subsection.

5.5.5 The water surface shear effect factor λ_0

It is assumed that the water surface shear effect factor λ_0 relates to the water viscosity ν , the velocity at the water surface $\bar{u}_{1\max}$, and the gravitational acceleration

Table 5.8: Results of McQuivey’s wide channel experiments

RUN	h	a/h	$\bar{u}_{1\max}$	u_*	Re_*	λ_0	r	Remark
	(cm)		(m/s)	(cm/s)				
1	2.93	6.58	0.318	2.08	703	0.00715	0.9993	Smooth
2	3.08	6.26	0.462	2.57	915	0.00766	0.9999	Smooth
3	2.87	6.72	0.701	3.13	1051	0.00887	0.9976	Smooth
4	2.96	6.52	0.318	2.03	633	0.00888	0.9963	Smooth
5	3.02	6.38	0.462	2.25	718	0.00682	0.9996	Smooth
6	3.08	6.26	0.666	3.66	1191	0.00778	1.0000	Smooth
7	3.11	6.20	0.351	2.42	808	0.0163	0.9986	Rough ^a
8	3.02	6.38	0.591	4.72	1515	0.0148	1.0000	Rough
9	3.08	6.26	0.828	6.20	2017	0.0139	0.9999	Rough
10	3.26	5.91	0.346	2.58	912	0.0147	0.9989	Rough
11	3.20	6.02	0.631	4.55	1580	0.0128	0.9988	Rough
12	3.08	6.26	0.787	5.27	1761	0.0123	0.9991	Rough

^a Only “shot rough” is given, the value of k_s is not found.

Table 5.9: Results of Guy et al.’s wide channel experiments

RUN	d_{50}	h	a/h	u_*	$\bar{u}_{1\max}$	Re_*	k_s/h ^a	λ_0	r
	(mm)	(cm)		(cm/s)	(m/s)				
22C ^b	0.19	12.2	20.0	0.902	0.342	1023	1.55e-3	0.00648	0.9961
24	0.19	28.5	8.5	1.036	0.371	2786	6.66e-4	0.00470	0.9925
26	0.19	8.4	29.2	0.946	0.324	756	2.28e-3	0.00496	0.9983
19	0.93	29.7	8.2	2.344	0.492	6758	3.13e-3	0.00666	0.9941
20	0.93	29.9	8.2	3.477	0.617	10034	3.11e-3	0.00559	0.9990
25	0.93	29.9	8.1	2.441	0.558	7006	3.11e-3	0.00555	0.9968
26A	0.93	30.7	7.9	2.737	0.610	8005	3.03e-3	0.00601	0.9965
27	0.93	30.6	8.0	3.312	0.615	10571	3.04e-3	0.00563	0.9953

^a According to Engelund (Chien and Wan, 1983, p.206), it is assumed that $k_s = 2.5d_{50}$.

^b RUNS 22C, 26, and 19 are transition beds, the rest are rough beds.

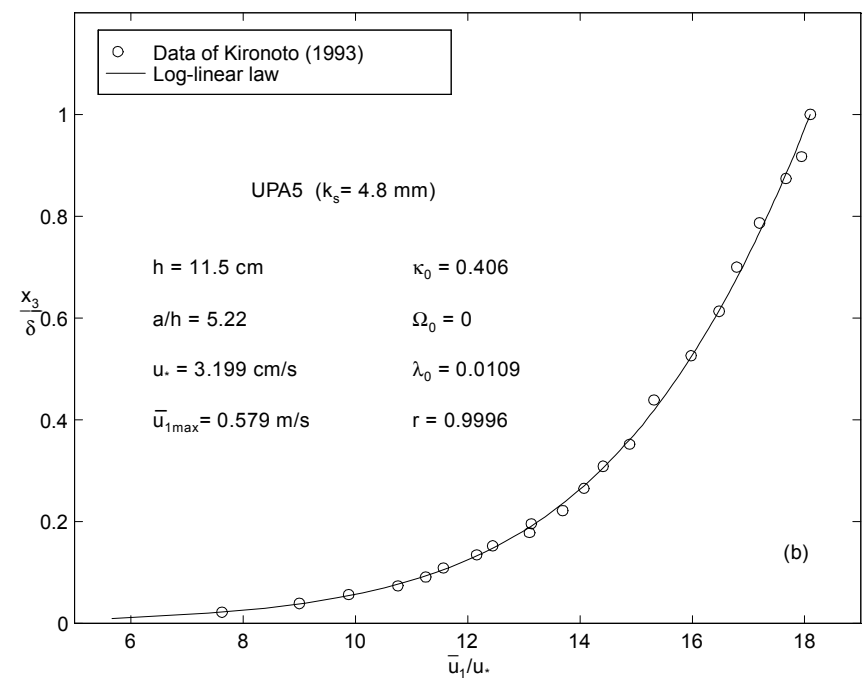
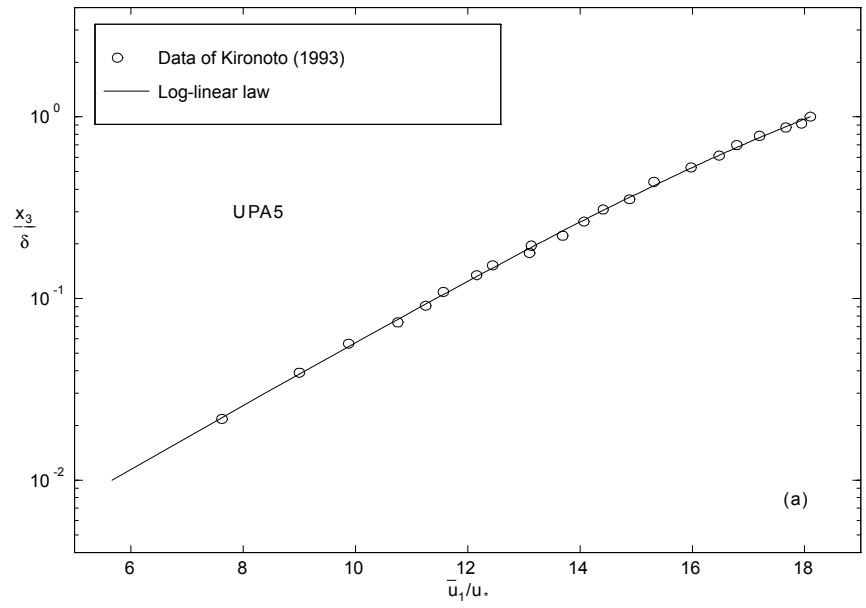


FIG. 5.12: Comparison of the log-linear law with Kironoto's experimental data [(a) in a rectangular coordinate, (b) in a semilog coordinate]

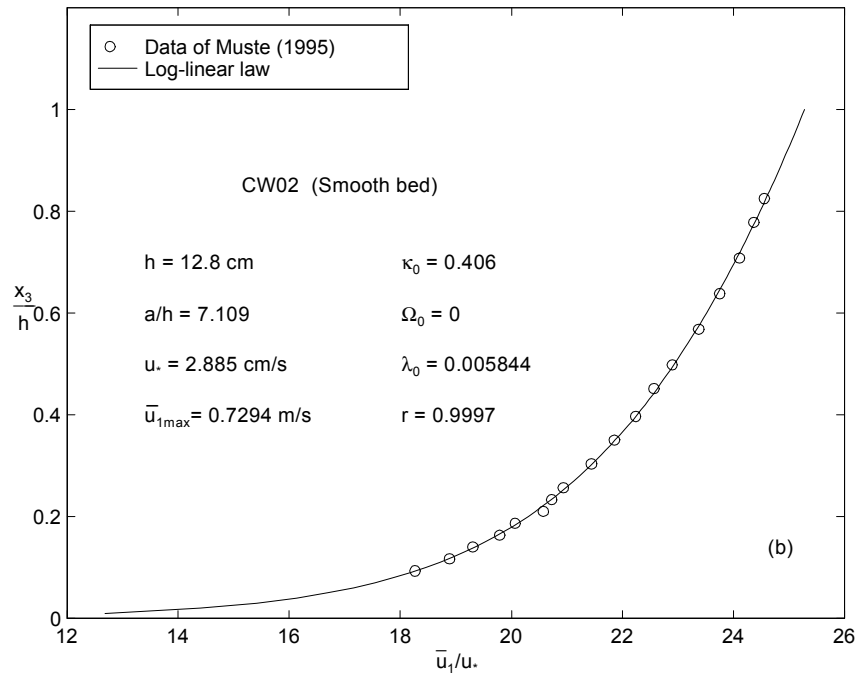
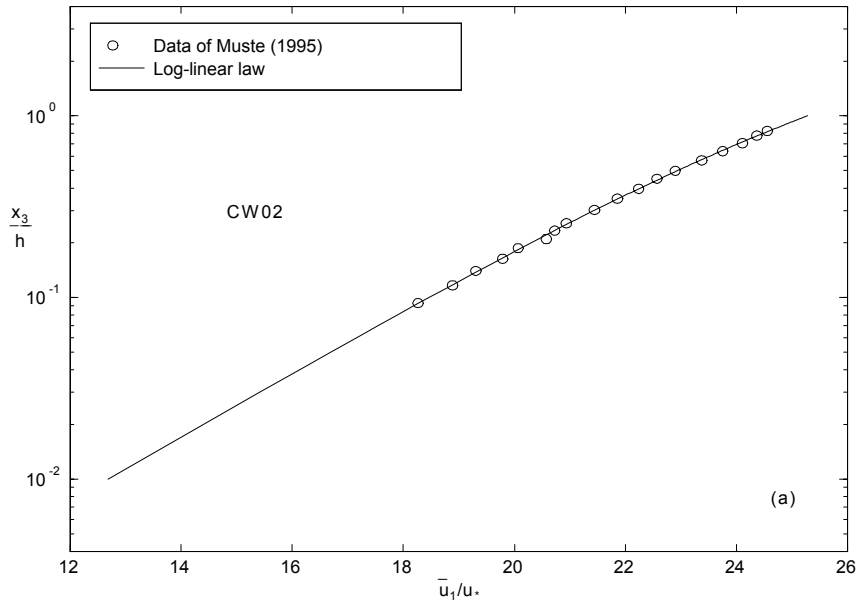


FIG. 5.13: Comparison between the log-linear law and Muste's experimental data [(a) in a rectangular coordinate, (b) in a semilog coordinate]

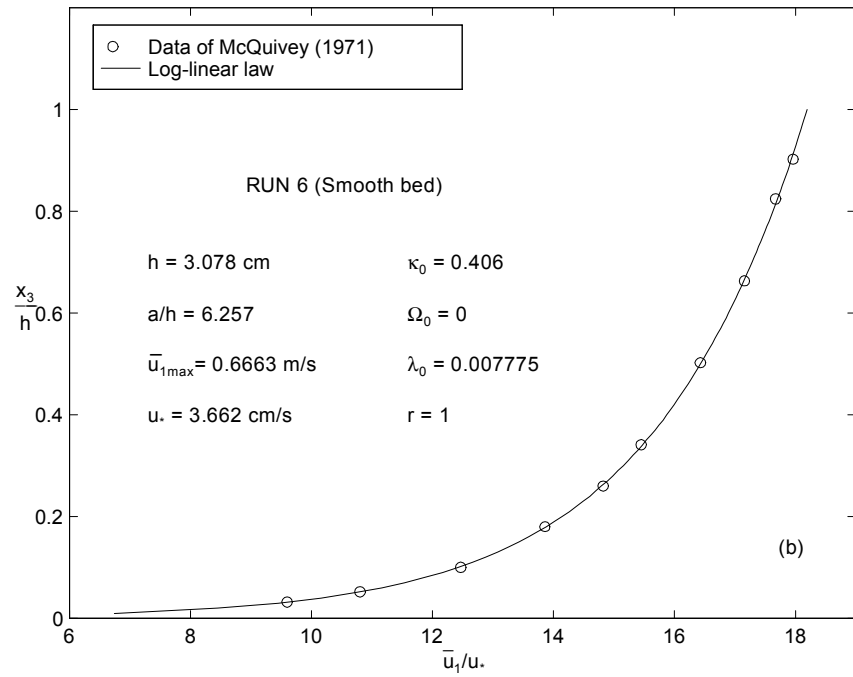
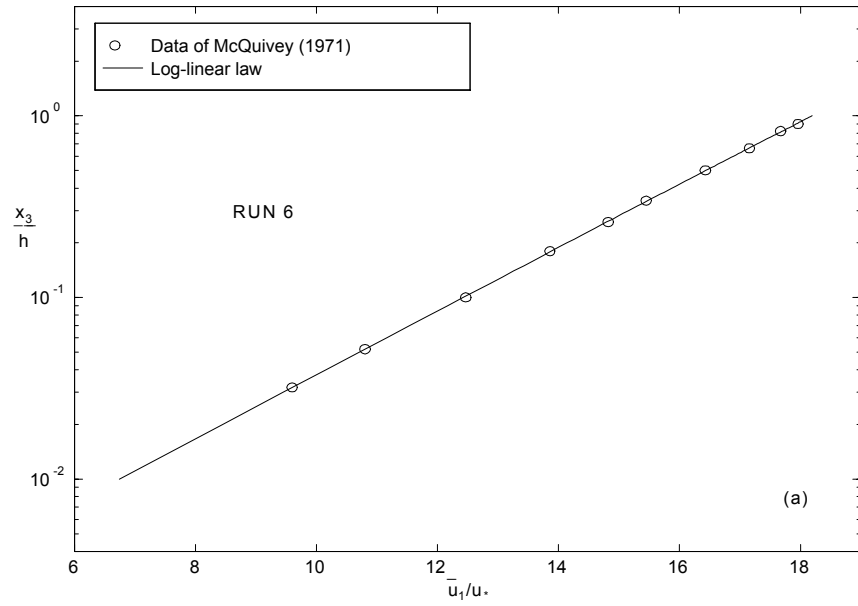


FIG. 5.14: Comparison between the log-linear law and McQuivey's experimental data [(a) in a rectangular coordinate, (b) in a semilog coordinate]

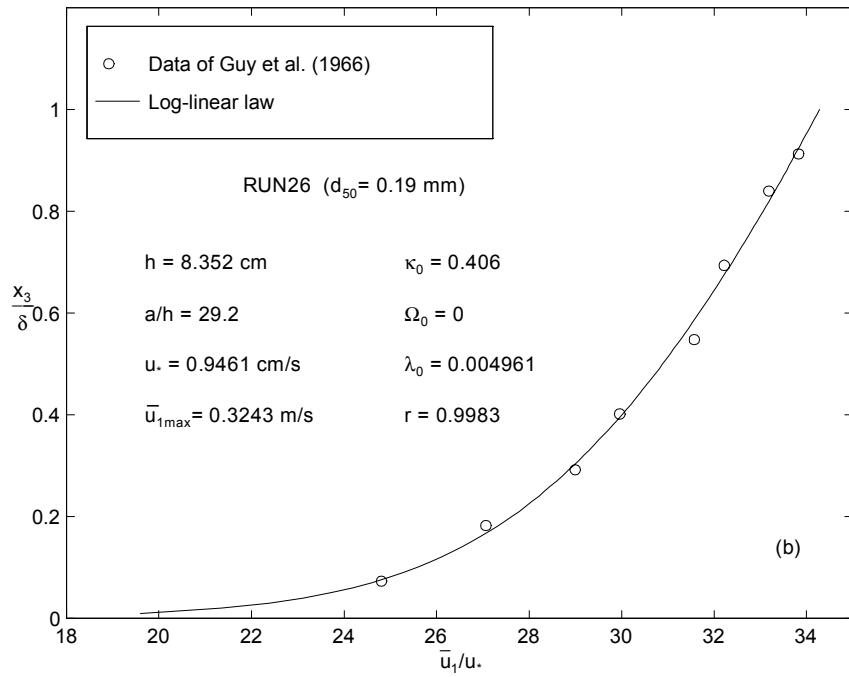
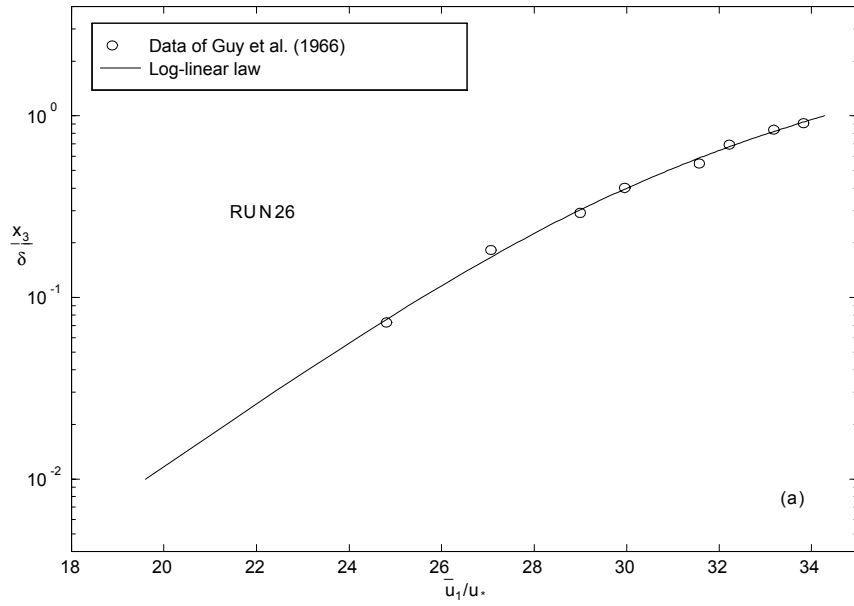


FIG. 5.15: Comparison between the log-linear law and Guy et al.'s experimental data [(a) in a rectangular coordinate system, (b) in a semilog coordinate system]

g which is a main factor of the surface wave, i.e.

$$\lambda_0 = f(\nu, \bar{u}_{1\max}, g) \quad (5.29)$$

Since $\bar{u}_{1\max} \propto U = F(u_*, u_*h/\nu, k_s/h)$, in which U = the vertical average velocity, f is a functional sign, the above equation may be written as

$$\lambda_0 = f\left(\nu, g, u_*, \frac{u_*h}{\nu}, \frac{k_s}{h}\right) \quad (5.30)$$

which may further be written as a dimensionless form

$$\lambda_0 = f\left(\frac{u_*^3}{g\nu}, \frac{u_*h}{\nu}, \frac{k_s}{h}\right) \quad (5.31)$$

If the water surface wave can be neglected and the momentum mixing between water and air on the water surface is turbulent mixing, i.e., the effects of $\frac{u_*^3}{g\nu}$ and $\frac{u_*h}{\nu}$ may be neglected. Then one has

$$\lambda_0 = f\left(\frac{k_s}{h}\right) \quad (5.32)$$

A plot of λ_0 versus k_s/h , from Table 5.6 to Table 5.9 except the rough bed experiments of McQuivey (where the roughness is not given), is shown in FIG. 5.16. It can be seen that the water surface effect factor λ_0 can be approximated as

$$\lambda_0 \approx \begin{cases} 0.065 & \text{for } k_s/h < 0.024 \\ 0.2163 \frac{k_s}{h} + 0.0013 & \text{for } k_s/h \geq 0.024 \end{cases} \quad (5.33)$$

In most fluvial channels, $k_s/h < 0.024$, thus λ_0 can be taken as 0.065 in practice.

5.5.6 Test of the eddy viscosity model

Neglecting the wake component, substituting (2.10) and (2.12) into (3.33) and considering $V_{\text{wind}} = 0$ and $\tau_0 = \rho_0 u_*^2$, one gets

$$\varepsilon^+ = \frac{(1 - \xi) + C_d \frac{\rho_{\text{air}}}{\rho_0} \left(\frac{\bar{u}_{1\max}}{u_*}\right)^2}{\frac{1 - \xi}{\kappa_0 \xi} + \lambda_0 \left(\frac{\bar{u}_{1\max}}{u_*}\right)^2} \quad (5.34)$$

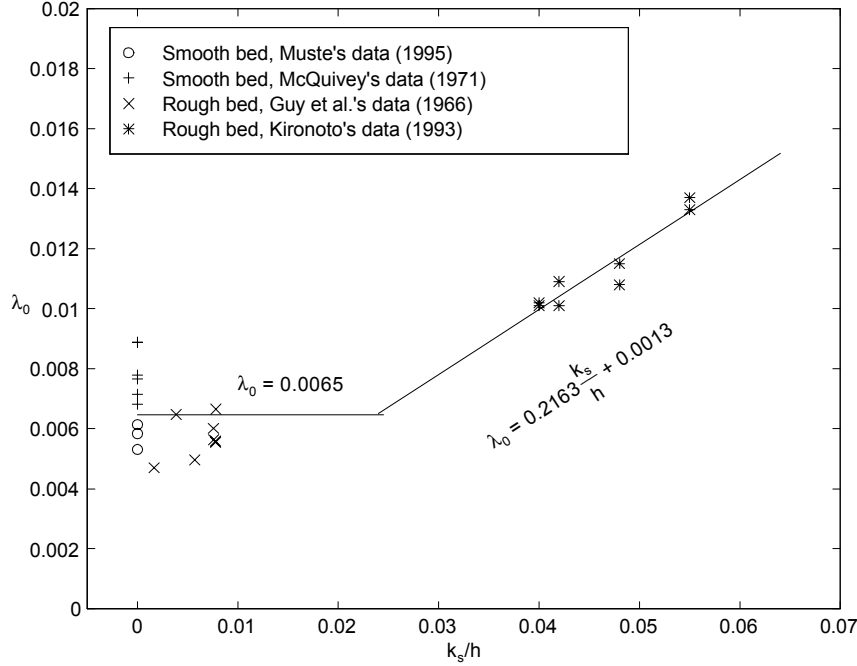


FIG. 5.16: The water surface effect factor λ_0

in which $C_d \approx 0.001$ (Roll, 1965, p.160).

Near the water surface, i.e., $\xi \rightarrow 1$, one has

$$\varepsilon^+ = \frac{C_d \rho_{\text{air}}}{\lambda_0 \rho_0} \quad (5.35)$$

Assuming $C_d = 0.001$, $\lambda_0 = 0.0065$, $\rho_{\text{air}} = 1.21 \text{ kg/m}^3$, and $\rho_0 = 1000 \text{ kg/m}^3$, one has

$$\varepsilon^+ = 1.86 \times 10^{-4} \quad (5.36)$$

which is negligibly small in practice.

A comparison of the above equation with Kironoto's (1993) experimental data (UPA5) is shown in FIG. 5.17, where it is assumed that $\rho_{\text{air}} = 1.21 \text{ kg/m}^3$ and $\rho_0 = 1000 \text{ kg/m}^3$, the other parameters are shown in the figure. It is seen that the proposed model is compatible to the measurement data. The scatter of the data is ordinary because of the numerical differentiation of the velocity profile. Note that the shear stress and the eddy viscosity are not zero at the water surface although they may be very small.

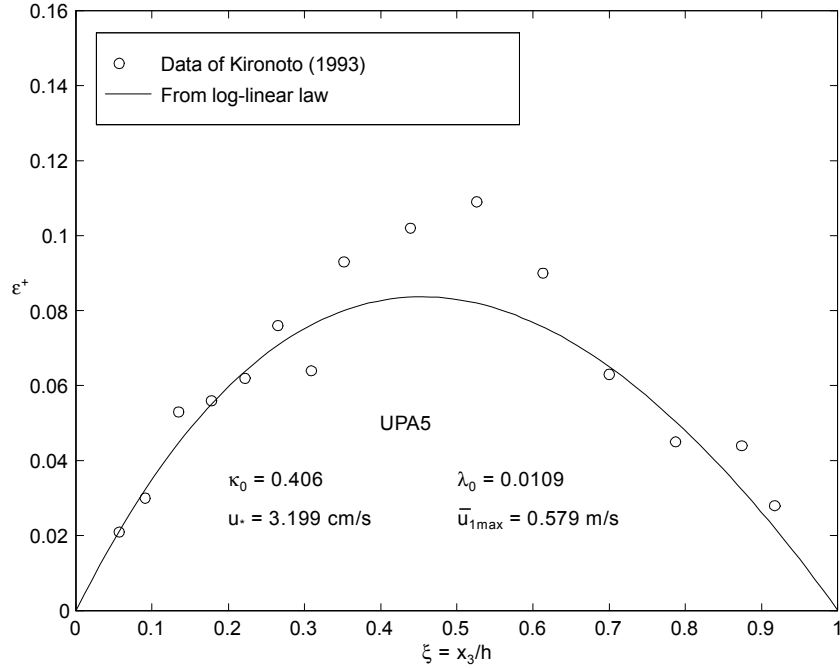


FIG. 5.17: Test of the eddy viscosity model from the log-linear law

5.6 Summary

The modified log-wake law contains three model parameters: the von Karman constant κ_0 , the wake strength coefficient Ω_0 , and the water surface shear effect factor λ_0 . The examinations in pipes, narrow channels and wide channels show that:

(1) The von Karman constant κ_0 expresses the effect of the pipe wall or the channel bed. It is a universal constant 0.406 in pipes, narrow channels and wide channels.

(2) The wake strength coefficient Ω_0 expresses the effect of the side-walls in open-channels. It is a universal constant 3.2 in pipes. However, it decreases with the aspect ratio a/h in narrow channels, shown in FIG. 5.11. In wide channels, $a/h \geq 5$, it can be approximated as zero. Therefore, the modified log-wake law reduces to the log-linear law in wide channels.

(3) The water surface shear effect factor λ_0 expresses the effect of the shear stress between the air and the water surface. The value of λ_0 is 0 in pipes and narrow channels since a free surface does not exist in a pipe axis or the boundary layer margin

in a narrow channel. The value of λ_0 is almost a constant 0.065 for smooth beds and small roughness but increases with the relative roughness k_s/h when $k_s/h \geq 0.024$, see FIG. 5.16.

(4) The modified log-wake law compares very well with experiments in pipes, narrow channels and wide channels.

(5) The log-linear law, which is the reduction of the modified log-wake law, compares quite well with experiments in wide channels.

(6) The eddy viscosity models (5.11) and (5.34) from the modified log-wake law and the log-linear law are compatible to experimental data in pipes, narrow channels and wide channels.

Chapter 6

THEORETICAL ANALYSIS OF SEDIMENT-LADEN FLOWS

6.1 Introduction

In the study of clear water flow, the governing equations are not used at all. The modified log-wake law is simply based on a similarity analysis. However, a similarity analysis may not be very helpful in the study of sediment-laden flows since more variables are involved. To study the velocity profiles in sediment-laden flows, one may start with the governing equations.

Section 6.2 treats of the governing equations in sediment-laden flows. Section 6.3 discusses the applications of the governing equations in steady uniform 2D flows. Sections 6.4 and 6.5 discuss the effects of sediment suspension. Section 6.6 discusses sediment-laden velocity profiles. Section 6.7 summarizes the results of this chapter.

6.2 Governing equations

6.2.1 Navier-Stokes equations in sediment-laden flows

This study aims at the mean velocity profiles in steady uniform 2D sediment-laden flows. However, the turbulent shear stress is significantly affected by turbulence

intensity. To emphasize the effects of sediment suspension on turbulence intensity, this study starts with unsteady 3D governing equations. To simplify the analysis, the **Boussinesq approximation** (Spiegel and Veronis, 1960; Kundu, 1990, p.113) on stratified flows is introduced, i.e., the effect of sediment concentration on the fluid density may be neglected in the continuity and the momentum equations, except in the gravity term. The viscosity is also assumed constant in this assumption.

Continuity equation

Based on the Boussinesq assumption, the continuity equation in sediment-laden flows is the same as that in clear water, i.e.

$$\frac{\partial u_i}{\partial x_i} = 0 \quad (6.1)$$

in which u_i is the velocity component in the x_i direction and $i = 1, 2,$ and 3 .

Momentum equation

Similarly, the momentum equation in sediment-laden flows is written as

$$\frac{\partial u_i}{\partial t} + u_j \frac{\partial u_i}{\partial x_j} = \frac{\rho}{\rho_m} g_i - \frac{1}{\rho_m} \frac{\partial p}{\partial x_i} + \nu_m \frac{\partial^2 u_i}{\partial x_j \partial x_j} \quad (6.2)$$

in which t is time; j is a dummy subscript; ρ is local density and varies with sediment concentration; ρ_m is the (constant) space average of density ρ , i.e. $\rho_m = \frac{1}{V} \int_V \rho dV$; g_i is the component of the gravitational acceleration in the x_i direction; p is pressure; and ν_m is the (constant) kinematic viscosity corresponding to ρ_m .

Sediment concentration equation

Applying the mass conservation law to sediment phase, one has the sediment concentration equation as

$$\frac{\partial C}{\partial t} + u_j \frac{\partial C}{\partial x_j} = \frac{\partial}{\partial x_j} \left(D \frac{\partial C}{\partial x_j} \right) \quad (6.3)$$

in which C is the sediment volumetric concentration; the first term on the left-hand side is the concentration change with time; u_j , which is not necessary to be the

same as that in (6.2), is the convective velocity of sediment; the second term on the left-hand side is the transport by convection; D is the (constant) molecular diffusion coefficient; and the right-hand side is the transport by molecular diffusion.

State equation or density equation

The density equation can be easily written as

$$\rho = \rho_0 + (\rho_s - \rho_0)C \quad (6.4)$$

in which ρ_0 is the clear water density; and ρ_s is the sediment density.

The above equation set (6.1-6.4) is closed since one has 6 equations (1 continuity, 3 momentum, 1 concentration and 1 density equation) with 6 unknowns (3 velocity components u_i , 1 pressure p , 1 density ρ , and 1 concentration C). However, like any other turbulence, the above equations are very difficult to solve for large Reynolds number flows, i.e., turbulent flows. To study the mean velocity field of a turbulent flow, the Reynolds average method may be applied.

6.2.2 Reynolds mean equations and turbulent equations in sediment-laden flows

Following Reynolds, one must decompose a variable into its (time) mean part denoted with an overbar, and a turbulent part denoted with a prime, i.e.

$$\begin{aligned} u_i &= \bar{u}_i + u'_i & p &= \bar{p} + p' \\ \rho &= \bar{\rho} + \rho' & C &= \bar{C} + C' \end{aligned} \quad (6.5)$$

Substituting (6.5) into (6.1-6.4) and introducing the Reynolds average method, one can get the motion equations for the mean flow and the turbulent flow, respectively.

Continuity equation

Substituting the expressions (6.5) into (6.1) and taking the Reynolds average, one has

$$\frac{\partial \bar{u}_i}{\partial x_i} = 0 \quad (6.6)$$

for the mean motion, and

$$\frac{\partial u'_i}{\partial x_i} = 0 \quad (6.7)$$

for the turbulent motion.

From the above two continuity equations, one can get the following two identities:

$$\bar{u}_j \frac{\partial f}{\partial x_j} = \frac{\partial(\bar{u}_j f)}{\partial x_j} \quad u'_j \frac{\partial f}{\partial x_j} = \frac{\partial(u'_j f)}{\partial x_j} \quad (6.8)$$

in which f can be any variable. These two identities will be frequently used in the derivations later.

Momentum equation

Substituting (6.5) into (6.2), one gets

$$\frac{\partial(\bar{u}_i + u'_i)}{\partial t} + (\bar{u}_k + u'_k) \frac{\partial(\bar{u}_i + u'_i)}{\partial x_k} = \frac{\bar{\rho} + \rho'}{\rho_m} g_i - \frac{1}{\rho_m} \frac{\partial(\bar{p} + p')}{\partial x_i} + \nu_m \frac{\partial^2}{\partial x_k \partial x_k} (\bar{u}_i + u'_i)$$

in which $\rho_m = \frac{1}{V} \int_V \bar{\rho} dV$. Applying the identities (6.8) to the convective term and expanding it, one obtains

$$\begin{aligned} & \frac{\partial(\bar{u}_i + u'_i)}{\partial t} + \frac{\partial(\bar{u}_i \bar{u}_k + \bar{u}_i u'_k + u'_i \bar{u}_k + u'_i u'_k)}{\partial x_k} \\ &= \frac{\bar{\rho} + \rho'}{\rho_m} g_i - \frac{1}{\rho_m} \frac{\partial(\bar{p} + p')}{\partial x_i} + \nu_m \frac{\partial^2}{\partial x_k \partial x_k} (\bar{u}_i + u'_i) \end{aligned} \quad (6.9)$$

Taking the average over this equation and considering that the average of a fluctuating variable is zero, one has the following mean motion equation for sediment-laden flow:

$$\frac{\partial \bar{u}_i}{\partial t} + \frac{\partial(\bar{u}_i \bar{u}_k + \overline{u'_i u'_k})}{\partial x_k} = \frac{\bar{\rho}}{\rho_m} g_i - \frac{1}{\rho_m} \frac{\partial \bar{p}}{\partial x_i} + \nu_m \frac{\partial^2 \bar{u}_i}{\partial x_k \partial x_k} \quad (6.10)$$

or

$$\frac{\partial \bar{u}_i}{\partial t} + \bar{u}_k \frac{\partial \bar{u}_i}{\partial x_k} = \frac{\bar{\rho}}{\rho_m} g_i - \frac{1}{\rho_m} \frac{\partial \bar{p}}{\partial x_i} + \nu_m \frac{\partial^2 \bar{u}_i}{\partial x_k \partial x_k} - \frac{\partial \overline{u'_i u'_k}}{\partial x_k} \quad (6.11)$$

in which $\overline{u'_i u'_k}$ is the one-point turbulent velocity correlation. The product of ρ_m and $-\overline{u'_i u'_k}$ is the so-called turbulent stress or Reynolds stress. (6.11) will be used to study the mean velocity profiles in sediment-laden flows.

The subtraction of the mean motion equation (6.10) from the total motion equation (6.9) gives the turbulent motion equation, i.e.

$$\frac{\partial u'_i}{\partial t} + \frac{\partial(\bar{u}_i u'_k + u'_i \bar{u}_k + u'_i u'_k - \overline{u'_i u'_k})}{\partial x_k} = \frac{\rho'}{\rho_m} g_i - \frac{1}{\rho_m} \frac{\partial p'}{\partial x_i} + \nu_m \frac{\partial^2 u'_i}{\partial x_k \partial x_k}$$

or

$$\frac{\partial u'_i}{\partial t} + u'_k \frac{\partial \bar{u}_i}{\partial x_k} + \bar{u}_k \frac{\partial u'_i}{\partial x_k} + \frac{\partial u'_i u'_k}{\partial x_k} - \frac{\partial \overline{u'_i u'_k}}{\partial x_k} = \frac{\rho'}{\rho_m} g_i - \frac{1}{\rho_m} \frac{\partial p'}{\partial x_i} + \nu_m \frac{\partial^2 u'_i}{\partial x_k \partial x_k} \quad (6.12)$$

This equation will serve to analyze the effects of sediment suspension on turbulence intensity.

Sediment concentration equation

Applying (6.5) to (6.3) yields

$$\frac{\partial (\bar{C} + C')}{\partial t} + (\bar{u}_j + u'_j) \frac{\partial (\bar{C} + C')}{\partial x_j} = \frac{\partial}{\partial x_j} \left(D \frac{\partial (\bar{C} + C')}{\partial x_j} \right)$$

or

$$\frac{\partial \bar{C}}{\partial t} + \frac{\partial C'}{\partial t} + \bar{u}_j \frac{\partial \bar{C}}{\partial x_j} + \bar{u}_j \frac{\partial C'}{\partial x_j} + u'_j \frac{\partial \bar{C}}{\partial x_j} + \frac{\partial u'_j C'}{\partial x_j} = \frac{\partial}{\partial x_j} \left(D \frac{\partial (\bar{C} + C')}{\partial x_j} \right) \quad (6.13)$$

Taking the average over this equation gives the mean concentration equation:

$$\frac{\partial \bar{C}}{\partial t} + \bar{u}_j \frac{\partial \bar{C}}{\partial x_j} = \frac{\partial}{\partial x_j} \left(D \frac{\partial \bar{C}}{\partial x_j} - \overline{u'_j C'} \right) \quad (6.14)$$

Similarly, the subtraction of (6.14) from (6.13) gives the turbulent concentration equation:

$$\frac{\partial C'}{\partial t} + \bar{u}_j \frac{\partial C'}{\partial x_j} + u'_j \frac{\partial \bar{C}}{\partial x_j} + \frac{\partial u'_j C'}{\partial x_j} - \frac{\partial \overline{u'_j C'}}{\partial x_j} = \frac{\partial}{\partial x_j} \left(D \frac{\partial C'}{\partial x_j} \right) \quad (6.15)$$

State equation or density equation

Applying (6.5) to (6.4) results in

$$\bar{\rho} + \rho' = \rho_0 + (\rho_s - \rho_0) (\bar{C} + C') \quad (6.16)$$

Taking the average over this equation gives the (time) mean density equation:

$$\bar{\rho} = \rho_0 + (\rho_s - \rho_0) \bar{C} \quad (6.17)$$

Note that this mean density varies with space and has the relation with the space mean ρ_m as: $\rho_m = \int_V \bar{\rho} dV$.

Similarly, one can obtain the turbulent density equation:

$$\rho' = (\rho_s - \rho_0) C' \quad (6.18)$$

Summary

In brief, the mean motion equations for sediment-laden flows can be summarized as follows:

$$\frac{\partial \bar{u}_i}{\partial x_i} = 0 \quad (6.6)$$

$$\frac{\partial \bar{u}_i}{\partial t} + \bar{u}_k \frac{\partial \bar{u}_i}{\partial x_k} = \frac{\bar{p}}{\rho_m} g_i - \frac{1}{\rho_m} \frac{\partial \bar{p}}{\partial x_i} + \nu_m \frac{\partial^2 \bar{u}_i}{\partial x_k \partial x_k} - \frac{\partial \overline{u'_i u'_k}}{\partial x_k} \quad (6.11)$$

$$\frac{\partial \bar{C}}{\partial t} + \bar{u}_j \frac{\partial \bar{C}}{\partial x_j} = \frac{\partial}{\partial x_j} \left(D \frac{\partial \bar{C}}{\partial x_j} - \overline{u'_j C'} \right) \quad (6.14)$$

$$\bar{\rho} = \rho_0 + (\rho_s - \rho_0) \bar{C} \quad (6.17)$$

To solve this set of equations, one must make some assumptions about $\overline{u'_i u'_k}$ and $\overline{u'_j C'}$. This is known as the closure problem.

The turbulent motion equations are summarized as

$$\frac{\partial u'_i}{\partial x_i} = 0 \quad (6.7)$$

$$\frac{\partial u'_i}{\partial t} + u'_k \frac{\partial \bar{u}_i}{\partial x_k} + \bar{u}_k \frac{\partial u'_i}{\partial x_k} + \frac{\partial u'_i u'_k}{\partial x_k} - \frac{\partial \overline{u'_i u'_k}}{\partial x_k} = \frac{\rho'}{\rho_m} g_i - \frac{1}{\rho_m} \frac{\partial p'}{\partial x_i} + \nu_m \frac{\partial^2 u'_i}{\partial x_k \partial x_k} \quad (6.12)$$

$$\frac{\partial C'}{\partial t} + \bar{u}_j \frac{\partial C'}{\partial x_j} + u'_j \frac{\partial \bar{C}}{\partial x_j} + \frac{\partial u'_j C'}{\partial x_j} - \frac{\partial \overline{u'_j C'}}{\partial x_j} = \frac{\partial}{\partial x_j} \left(D \frac{\partial C'}{\partial x_j} \right) \quad (6.15)$$

$$\rho' = (\rho_s - \rho_0) C' \quad (6.18)$$

Only (6.12) of this set will be used to study the effects of sediment suspension on turbulence intensity.

6.3 Simplifications of governing equations in steady uniform 2D flows

To simplify the analysis, this study assumes that the *mean flow* is 2D steady uniform, shown in FIG. 6.1. That is,

$$\text{steady} : \quad \frac{\partial (\overline{\quad})}{\partial t} = 0 \quad (6.19)$$

$$\text{uniform} : \quad \frac{\partial (\overline{\quad})}{\partial x_1} = 0, \quad \frac{\partial (\overline{\quad})}{\partial x_2} = 0 \quad (6.20)$$

$$\text{2D flow} : \quad \bar{u}_1 = \bar{u}_1(x_3), \quad \bar{u}_2 = \bar{u}_3 = 0, \quad \bar{C} = \bar{C}(x_3) \quad (6.21)$$

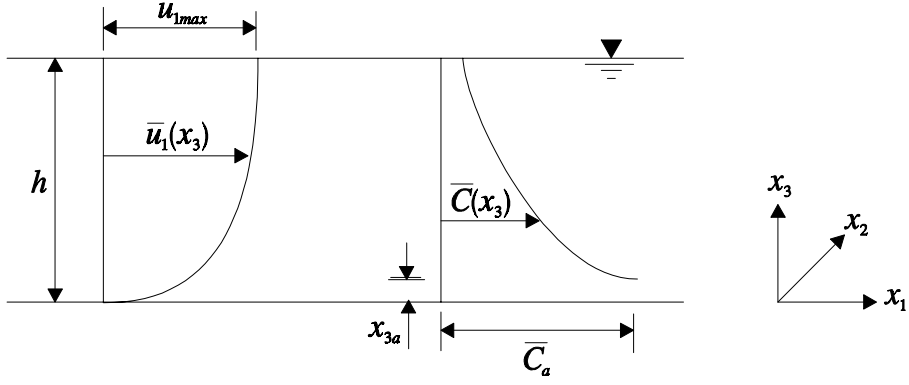


FIG. 6.1: Scheme of steady uniform 2D sediment-laden flows

in which $t = \text{time}$; $\overline{(\quad)}$ means any (time) mean variable; $\overline{u}_1 = (\text{time})$ mean velocity in the flow direction x_1 ; $\overline{u}_2 = (\text{time})$ mean velocity in the lateral direction x_2 , $\overline{u}_3 = (\text{time})$ mean velocity in the vertical (normal) direction x_3 ; and $\overline{C} = (\text{time})$ mean sediment concentration.

Based on the above assumptions, the mean continuity equation is automatically satisfied. The momentum equations reduce to

$$x_1 - \text{direction:} \quad \overline{\rho}g_1 + \mu_m \frac{\partial^2 \overline{u}_1}{\partial x_3^2} - \rho_m \frac{\partial \overline{u'_1 u'_3}}{\partial x_3} = 0 \quad (6.22)$$

$$x_2 - \text{direction:} \quad \frac{\partial \overline{u'_2 u'_3}}{\partial x_3} = 0 \quad (6.23)$$

$$x_3 - \text{direction:} \quad \overline{\rho}g_3 - \frac{\partial \overline{p}}{\partial x_3} - \overline{\rho}_m \frac{\partial \overline{u_3'^2}}{\partial x_3} = 0 \quad (6.24)$$

Fortunately, (6.23) and (6.24) are not coupled with (6.22), then only (6.22) is used to find the velocity profile $\overline{u}_1(x_3)$. (6.22) can be further written as

$$-\frac{\partial}{\partial x_3} \left(\mu_m \frac{\partial \overline{u}_1}{\partial x_3} - \rho_m \overline{u'_1 u'_3} \right) = \overline{\rho}g_1 \quad (6.25)$$

in which $\mu_m = \rho_m \nu_m$ is the mean kinetic viscosity of the mixture water. Considering that the shear stress at the water surface is $\tau|_{\xi=1}$, i.e., $(\mu_m \partial \overline{u}_1 / \partial x_3 - \rho_m \overline{u'_1 u'_3})_{x_3=h} = \tau|_{\xi=1}$, and substituting (6.17) into (6.25) and integrating yields

$$-\left(\mu_m \frac{\partial \overline{u}_1}{\partial x_3} - \rho_m \overline{u'_1 u'_3} \right) \Big|_{x_3}^h = \int_{x_3}^h (\rho_0 + (\rho_s - \rho_0) \overline{C}) g_1 dx_3$$

or

$$\mu_m \frac{\partial \bar{u}_1}{\partial x_3} - \rho_m \overline{u'_1 u'_3} - \tau|_{\xi=1} = \rho_0 g_1 (h - x_3) + (\rho_s - \rho_0) g_1 \int_{x_3}^h \bar{C} dx_3 \quad (6.26)$$

Now one can see that the effects of sediment suspension on velocity profiles may be in three ways: (1) changing the fluid viscosity μ_m and then changing the viscous shear stress (1st term on the left-hand side); (2) changing the fluid density and turbulence intensity and consequently changing the turbulent shear stress (2nd term on the left-hand side); and (3) producing density gradient and then increasing the gravity component in the flow direction (2nd term on the right-hand side). To further simplify (6.26), a magnitude order for each term in (6.26) is analyzed as follows:

By experience, one may assume

$$\bar{u}_1 \sim U, \quad x_3 \sim h, \quad \overline{u'_1 u'_3} \sim u_*^2, \quad \bar{C} \sim \bar{C}_a, \quad \rho_m \sim \rho_0$$

in which U is the vertical average velocity; u_* is the shear velocity; and \bar{C}_a is a near bed concentration, then one has:

$$\begin{array}{ccccccc} \mu_m \frac{\partial \bar{u}_1}{\partial x_3} & - \rho_m \overline{u'_1 u'_3} & - \tau|_{\xi=1} & = & \rho_0 g_1 h & - \rho_0 g_1 x_3 & + (\rho_s - \rho_0) g_1 \int_{x_3}^h \bar{C} dx_3 \\ \frac{\mu_m U}{h} & \rho_m u_*^2 & \text{Keep} & & \rho_0 g_1 h & \rho_0 g_1 h & (\rho_s - \rho_0) g_1 h \bar{C}_a \end{array}$$

Divided by $\rho_m U^2$

$$\begin{array}{ccccccc} \frac{\mu_m}{\rho_m U h} & \left(\frac{u_*}{U}\right)^2 & \text{Keep} & & \frac{\rho_0}{\rho_m} \frac{g_1 h}{U^2} & \frac{\rho_0}{\rho_m} \frac{g_1 h}{U^2} & \frac{\rho_s - \rho_0}{\rho_m} \frac{g_1 h}{U^2} \bar{C}_a \end{array}$$

Since $u_* = \sqrt{ghS} = \sqrt{g_1 h}$, and $\rho_m \sim \rho_0$, one has

$$\begin{array}{ccccccc} \frac{1}{\text{Re}} & \left(\frac{u_*}{U}\right)^2 & \text{Keep} & & \left(\frac{u_*}{U}\right)^2 & \left(\frac{u_*}{U}\right)^2 & \frac{\rho_s - \rho_0}{\rho_m} \left(\frac{u_*}{U}\right)^2 \bar{C}_a \end{array}$$

Multiplying $(U/u_*)^2$:

$$\begin{array}{ccccccc} \frac{1}{\text{Re}} \left(\frac{U}{u_*}\right)^2 & 1 & \text{Keep} & & 1 & 1 & \frac{\rho_s - \rho_0}{\rho_m} \bar{C}_a \end{array}$$

In practice, $\text{Re} > 10^4$, $\frac{U}{u_*} \sim 10$, and let $\frac{\rho_s - \rho_0}{\rho_m} \bar{C}_a < 0.1$

$$\begin{array}{ccccccc} < 0.01 & 1 & \text{Keep} & & 1 & 1 & < 0.1 \end{array}$$

The above magnitude order analysis shows that the main effects of sediment suspension on the mean velocity profiles are by the turbulent shear stress. In other words, the momentum equation in steady uniform 2D sediment-laden flows can be further simplified as

$$-\rho_m \overline{u'_1 u'_3} - \tau|_{\xi=1} = \rho_0 g_1 (h - x_3) \quad (6.27)$$

Note that $\tau|_{\xi=1}$ is kept in the above equation since it is the derivative boundary condition at the water surface although it may be very small. The above equation is similar to that in clear water, but the turbulent shear stress must be modified by sediment suspension. Introducing the eddy viscosity concept, i.e., $-\overline{u'_1 u'_3} = \varepsilon^+ u_* h d\bar{u}_1/dx_3$, in which ε^+ is the dimensionless eddy viscosity, the above equation becomes

$$\rho_m \varepsilon^+ u_* h \frac{d\bar{u}_1}{dx_3} - \tau|_{\xi=1} = \rho_0 g_1 (h - x_3) \quad (6.28)$$

Furthermore, if one defines $\varepsilon_m^+ = (\rho_m/\rho_0)\varepsilon^+$ as the dimensionless eddy viscosity in sediment-laden flows, then one obtains

$$\boxed{\rho_0 \varepsilon_m^+ u_* h \frac{d\bar{u}_1}{dx_3} - \tau|_{\xi=1} = \rho_0 g_1 (h - x_3)} \quad (6.29)$$

The above equation is exactly the same as that in clear water except that the eddy viscosity is modified by sediment suspension.

Note that the assumption of $(\rho_s - \rho_0)/\rho_m \bar{C}_a < 0.1$ means that for plastic sediments (specific gravity $G = 1.05$), \bar{C}_a can be very large; for natural sediments ($G = 2.65$), $\bar{C}_a < 0.1$. When $\bar{C}_a \geq 0.1$ in natural sediment-laden flows, the effect of sediment suspension on the gravity must be included.

Similarly, for steady uniform 2D flows, the sediment concentration equation (6.14) reduces to

$$-\omega \frac{\partial \bar{C}}{\partial x_3} = \frac{\partial}{\partial x_3} \left(D \frac{\partial \bar{C}}{\partial x_3} - \overline{u'_3 C'} \right) \quad (6.30)$$

in which $\bar{u}_3 = -\omega$, where ω is sediment settling velocity. Integrating (6.30) gives that

$$D \frac{\partial \bar{C}}{\partial x_3} - \overline{u'_3 C'} + \omega \bar{C} = \text{const}$$

Considering that no sediments enter into flow from the water surface, one has

$$D \frac{\partial \bar{C}}{\partial x_3} - \overline{u'_3 C'} + \omega \bar{C} = 0$$

Usually the molecular diffusion flux of sediment is much smaller than the turbulent flux, i.e., the above equation may be simplified as

$$-\overline{u'_3 C'} + \omega \bar{C} = 0 \quad (6.31)$$

According to Reynolds analogy, introducing $-\overline{u'_3 C'} = \varepsilon_s^+ u_* h d\bar{C}/dx_3$, in which ε_s^+ is the turbulent sediment diffusion coefficient, the above equation becomes

$$\boxed{\varepsilon_s^+ u_* h \frac{d\bar{C}}{dx_3} + \omega \bar{C} = 0} \quad (6.32)$$

Equations (6.29) and (6.32) constitute the governing equations in steady uniform 2D sediment-laden flows. The eddy viscosity models from clear water, i.e., (5.11) for narrow channels and (5.34) for wide channels, may be used for the problem closure. Again, the effects of the sediment suspension on the eddy viscosity models must be considered.

6.4 Effects of sediment suspension on turbulence intensities

Sediment suspension is due to turbulent kinetic energy. The eddy viscosity ε in the vertical direction relates to a characteristic length scale and the vertical turbulence intensity u'_3 . The larger the turbulence intensity u'_3 , the stronger the turbulent diffusion or mixing, i.e.

$$\varepsilon \sim \delta u'_3 \quad (6.33)$$

in which δ is the boundary layer thickness (characteristic length scale). For wide channels, $\delta = h$. Hence, the study of the effects of sediment suspension on the turbulence intensities (the kinetic energy budget and the eddy viscosity) is important.

6.4.1 Turbulence intensity $\overline{u'_i u'_j}$ in sediment-laden flows

One may start with (6.12), the equation for the turbulent velocity component u'_i . One can also write the same equation for the velocity component u'_j . Multiplying the equation for u'_i by u'_j and the equation for u'_j by u'_i , one gets

$$u'_j \frac{\partial u'_i}{\partial t} + u'_j u'_k \frac{\partial \bar{u}_i}{\partial x_k} + u'_j \bar{u}_k \frac{\partial u'_i}{\partial x_k} + u'_j \frac{\partial (u'_i u'_k - \overline{u'_i u'_k})}{\partial x_k} = \frac{u'_j \rho'}{\rho_m} g_i - \frac{u'_j}{\rho_m} \frac{\partial p'}{\partial x_i} + \nu_m u'_j \frac{\partial^2 u'_i}{\partial x_k \partial x_k}$$

and

$$u'_i \frac{\partial u'_j}{\partial t} + u'_i u'_k \frac{\partial \bar{u}_j}{\partial x_k} + u'_i \bar{u}_k \frac{\partial u'_j}{\partial x_k} + u'_i \frac{\partial (u'_j u'_k - \overline{u'_j u'_k})}{\partial x_k} = \frac{u'_i \rho'}{\rho_m} g_j - \frac{u'_i}{\rho_m} \frac{\partial p'}{\partial x_j} + \nu_m u'_i \frac{\partial^2 u'_j}{\partial x_k \partial x_k}$$

Adding the above two equations gives

$$\begin{aligned} & \frac{\partial u'_i u'_j}{\partial t} + u'_j u'_k \frac{\partial \bar{u}_i}{\partial x_k} + u'_i u'_k \frac{\partial \bar{u}_j}{\partial x_k} + \bar{u}_k \frac{\partial u'_i u'_j}{\partial x_k} + u'_j \frac{\partial (u'_i u'_k - \overline{u'_i u'_k})}{\partial x_k} + u'_i \frac{\partial (u'_j u'_k - \overline{u'_j u'_k})}{\partial x_k} \\ &= \frac{u'_j \rho'}{\rho_m} g_i + \frac{u'_i \rho'}{\rho_m} g_j - \frac{u'_j}{\rho_m} \frac{\partial p'}{\partial x_i} - \frac{u'_i}{\rho_m} \frac{\partial p'}{\partial x_j} + \nu_m \left(u'_j \frac{\partial^2 u'_i}{\partial x_k \partial x_k} + u'_i \frac{\partial^2 u'_j}{\partial x_k \partial x_k} \right) \end{aligned}$$

The average over this equation yields the correlation equation of $\overline{u'_i u'_j}$, i.e.

$$\begin{aligned} & \frac{\partial \overline{u'_i u'_j}}{\partial t} + \overline{u'_j u'_k} \frac{\partial \bar{u}_i}{\partial x_k} + \overline{u'_i u'_k} \frac{\partial \bar{u}_j}{\partial x_k} + \bar{u}_k \frac{\partial \overline{u'_i u'_j}}{\partial x_k} \\ &= - \left(\overline{u'_j \frac{\partial u'_i u'_k}{\partial x_k}} + \overline{u'_i \frac{\partial u'_j u'_k}{\partial x_k}} \right) + \frac{1}{\rho_m} (\overline{u'_j \rho' g_i} + \overline{u'_i \rho' g_j}) \\ & \quad - \frac{1}{\rho_m} \left(\overline{u'_j \frac{\partial p'}{\partial x_i}} + \overline{u'_i \frac{\partial p'}{\partial x_j}} \right) + \nu_m \left(\overline{u'_j \frac{\partial^2 u'_i}{\partial x_k \partial x_k}} + \overline{u'_i \frac{\partial^2 u'_j}{\partial x_k \partial x_k}} \right) \end{aligned} \quad (6.34)$$

The terms on the right-hand side of this equation may be transformed to measurable forms.

Applying the identities (6.8), the stuff within the bracket of the first term on the right-hand side becomes

$$\overline{u'_j \frac{\partial u'_i u'_k}{\partial x_k}} + \overline{u'_i \frac{\partial u'_j u'_k}{\partial x_k}} = \overline{u'_j u'_k \frac{\partial u'_i}{\partial x_k}} + \overline{u'_i \frac{\partial u'_j u'_k}{\partial x_k}} = \frac{\partial \overline{u'_i u'_j u'_k}}{\partial x_k} \quad (6.35)$$

Considering (6.18), the stuff within the bracket of the second term on the right-hand side becomes

$$\overline{u'_j \rho' g_i} + \overline{u'_i \rho' g_j} = (\rho_s - \rho_0) (\overline{u'_j C' g_i} + \overline{u'_i C' g_j}) \quad (6.36)$$

The stuff within the bracket of the third term on the right-hand side may be written as

$$\begin{aligned}\overline{u'_j \frac{\partial p'}{\partial x_i}} + \overline{u'_i \frac{\partial p'}{\partial x_j}} &= \overline{\frac{\partial p' u'_j}{\partial x_i}} - \overline{p' \frac{\partial u'_j}{\partial x_i}} + \overline{\frac{\partial p' u'_i}{\partial x_j}} - \overline{p' \frac{\partial u'_i}{\partial x_j}} \\ &= \left(\overline{\frac{\partial p' u'_j}{\partial x_i}} + \overline{\frac{\partial p' u'_i}{\partial x_j}} \right) - \overline{p' \left(\frac{\partial u'_j}{\partial x_i} + \frac{\partial u'_i}{\partial x_j} \right)}\end{aligned}\quad (6.37)$$

Since

$$\begin{aligned}\frac{\partial^2}{\partial x_k \partial x_k} \overline{u'_i u'_j} &= \frac{\partial}{\partial x_k} \overline{\left(u'_i \frac{\partial u'_j}{\partial x_k} + u'_j \frac{\partial u'_i}{\partial x_k} \right)} \\ &= \overline{\frac{\partial u'_i}{\partial x_k} \frac{\partial u'_j}{\partial x_k}} + \overline{u'_i \frac{\partial^2 u'_j}{\partial x_k \partial x_k}} + \overline{\frac{\partial u'_j}{\partial x_k} \frac{\partial u'_i}{\partial x_k}} + \overline{u'_j \frac{\partial^2 u'_i}{\partial x_k \partial x_k}} \\ &= \overline{u'_i \frac{\partial^2 u'_j}{\partial x_k \partial x_k}} + \overline{u'_j \frac{\partial^2 u'_i}{\partial x_k \partial x_k}} + 2 \overline{\frac{\partial u'_i}{\partial x_k} \frac{\partial u'_j}{\partial x_k}}\end{aligned}$$

one can get the fourth term on the right-hand side as

$$\overline{u'_i \frac{\partial^2 u'_j}{\partial x_k \partial x_k}} + \overline{u'_j \frac{\partial^2 u'_i}{\partial x_k \partial x_k}} = \frac{\partial^2}{\partial x_k \partial x_k} \overline{u'_i u'_j} - 2 \overline{\frac{\partial u'_i}{\partial x_k} \frac{\partial u'_j}{\partial x_k}}\quad (6.38)$$

Substituting (6.35-6.38) into (6.34) yields the one-point velocity correlation equation:

$$\begin{aligned}\frac{\partial \overline{u'_i u'_j}}{\partial t} + \overline{u_k} \frac{\partial \overline{u'_i u'_j}}{\partial x_k} &= - \left(\overline{u'_j u'_k} \frac{\partial \overline{u}_i}{\partial x_k} + \overline{u'_i u'_k} \frac{\partial \overline{u}_j}{\partial x_k} \right) + \frac{\rho_s - \rho_0}{\rho_m} \left(\overline{u'_j C' g_i} + \overline{u'_i C' g_j} \right) \\ &\quad - \frac{\partial \overline{u'_i u'_j u'_k}}{\partial x_k} - \frac{1}{\rho_m} \left(\overline{\frac{\partial p' u'_j}{\partial x_i}} + \overline{\frac{\partial p' u'_i}{\partial x_j}} \right) + \frac{1}{\rho_m} \overline{p' \left(\frac{\partial u'_j}{\partial x_i} + \frac{\partial u'_i}{\partial x_j} \right)} \\ &\quad + \nu_m \frac{\partial^2 \overline{u'_i u'_j}}{\partial x_k \partial x_k} - 2 \nu_m \overline{\frac{\partial u'_i}{\partial x_k} \frac{\partial u'_j}{\partial x_k}}\end{aligned}\quad (6.39)$$

This equation is the same as that in clear water (Hinze, 1975, p.324) except an extra term which relates to sediment suspension. The above equation is the general one-point velocity correlation equation. It can be used to study any second order velocity correlations, such as $\overline{u_1^2}$, $\overline{u_1 u_2}$, $\overline{u_1 u_3}$, $\overline{u_2^2}$, $\overline{u_2 u_3}$, $\overline{u_3^2}$, and turbulent kinetic energy $\frac{1}{2} \overline{u'_i u'_i}$. In this section, only the turbulent kinetic energy $\frac{1}{2} \overline{u'_i u'_i}$ and the vertical turbulence intensity $\overline{u_3^2}$ are concerned since they relate to the Richardson number and the eddy viscosity in sediment-laden flows.

6.4.2 Turbulent kinetic energy budget and Richardson number in sediment-laden flows

To study the turbulent kinetic energy budget, let $i = j$ in (6.39), then one has

$$\frac{\partial \overline{u'_i u'_i}}{\partial t} = -2 \overline{u'_i u'_3} \frac{\partial \overline{u}_i}{\partial x_3} + 2 \frac{\rho_s - \rho_0}{\rho_m} \overline{u'_i C'} g_i - \frac{\partial \overline{u'_i u'_i u'_3}}{\partial x_3} - \frac{2}{\rho_m} \frac{\partial \overline{p' u'_3}}{\partial x_3} + \nu_m \frac{\partial^2 \overline{u'_i u'_i}}{\partial x_3 \partial x_3} - 2 \nu_m \frac{\partial \overline{u'_i}}{\partial x_k} \frac{\partial \overline{u'_i}}{\partial x_k}$$

or

$$\begin{aligned} \frac{\partial \overline{q^2}}{\partial t} \frac{1}{2} = & \underbrace{-\overline{u'_1 u'_3} \frac{\partial \overline{u}_1}{\partial x_3}}_{\text{turb. production}} + \underbrace{\frac{\rho_s - \rho_0}{\rho_m} \overline{u'_i C'} g_i}_{\text{sediment suspension}} - \underbrace{\frac{\partial}{\partial x_3} \left(\frac{q^2}{2} + \frac{p'}{\rho_m} \right) u'_3}_{\text{turbulent transport}} \\ & + \underbrace{\nu_m \frac{\partial^2}{\partial x_3^2} \left(\frac{q^2}{2} \right)}_{\text{viscous transport}} - \underbrace{\nu_m \frac{\partial \overline{u'_i}}{\partial x_k} \frac{\partial \overline{u'_i}}{\partial x_k}}_{\text{energy dissipation}} \end{aligned} \quad (6.40)$$

in which $q^2 = u'_i u'_i$. The transport by viscous diffusion is usually neglected. The turbulent transport may also be neglected if the turbulence intensity is not very strong. This is because $p' \propto q^2 > 0$, $\overline{p' u'_3} \propto \overline{q^2 u'_3} \approx 0$. Thus, (6.40) reduces to

$$\frac{\partial \overline{q^2}}{\partial t} \frac{1}{2} = \underbrace{-\overline{u'_1 u'_3} \frac{\partial \overline{u}_1}{\partial x_3}}_{\text{turb. production}} + \underbrace{\frac{\rho_s - \rho_0}{\rho_m} \overline{u'_i C'} g_i}_{\text{sediment suspension}} - \underbrace{\nu_m \frac{\partial \overline{u'_i}}{\partial x_k} \frac{\partial \overline{u'_i}}{\partial x_k}}_{\text{energy dissipation}} \quad (6.41)$$

Experiments (Vanoni, 1946; Einstein and Chien, 1955; Elata and Ippen, 1961; and others) have shown that both $-\overline{u'_1 u'_3}$ and $\frac{\partial \overline{u}_1}{\partial x_3}$ are positive and increase with sediment suspension. This implies that the effect of sediment suspension on the turbulent production amplifies the turbulent kinetic energy.

Because the concentration field is homogeneous in the x_1 and the x_2 directions, the mean turbulent mixing fluxes in these directions must be zero, i.e.

$$\overline{u'_1 C'} = \overline{u'_2 C'} = 0 \quad (6.42)$$

Thus,

$$\frac{\rho_s - \rho_0}{\rho_m} \overline{u'_i C'} g_i = \frac{\rho_s - \rho_0}{\rho_m} \overline{u'_3 C'} g_3$$

To balance the sediment settling from upward, the turbulent mixing flux $\overline{u'_3 C'}$ in the x_3 direction must be positive, i.e.

$$\overline{u'_3 C'} > 0 \quad (6.43)$$

Considering $g_3 = -g \cos \theta \approx -g$ (in which θ is the angle between the channel bed and the datum), one has

$$\frac{\rho_s - \rho_0}{\rho_m} \overline{u'_3 C'} g_3 < 0 \quad (6.44)$$

which implies that sediment suspension decreases the turbulent kinetic energy. In other words, the energy supported suspended-load comes from the turbulent kinetic energy rather than the mean flow energy.

Since sediment presence increases the viscosity ν_m , it is expected that the energy dissipation increases in sediment-laden flow.

Of all three terms on the right-hand side in (6.41), two of them are negative (sediment suspension + energy dissipation) and one (turbulent production) is positive, the resultant of the right-hand side may increase and may decrease the turbulent kinetic energy. However, in any case, sediment suspension will increase the mean flow energy loss. This is because sediment suspension increases turbulent production which, in turn, comes from the mean flow energy.

The Richardson number R_i is defined as the ratio of the sediment suspension energy to the turbulent production in (6.41), i.e.

$$R_i = \frac{\frac{\rho_s - \rho_0}{\rho_m} \overline{u'_3 C'} g}{-\overline{u'_1 u'_3} \frac{d\bar{u}_1}{dx_3}} \quad (6.45)$$

Introducing

$$\begin{aligned} -\overline{u'_1 u'_3} &= \varepsilon_m \frac{d\bar{u}_1}{dx_3} \\ -\overline{u'_3 C'} &= \varepsilon_s \frac{d\bar{C}}{dx_3} \end{aligned}$$

in which the turbulent sediment diffusion coefficient ε_s is proportional to the momentum eddy viscosity ε_m . Therefore,

$$R_i \propto -\frac{(\rho_s - \rho_0)g}{\rho_m} \frac{\frac{d\bar{C}}{dx_3}}{\left(\frac{d\bar{u}_1}{dx_3}\right)^2}$$

The global Richardson number is defined as

$$R_i \propto -\frac{(\rho_s - \rho_0)g}{\rho_m} \frac{\overline{C}_1 - \overline{C}_{0.05}}{\delta} \frac{1}{\left(\frac{\overline{u}_{1\max}}{\delta}\right)^2}$$

in which \overline{C}_1 is the concentration at $\xi = 1$; and $\overline{C}_{0.05}$ is the concentration at $\xi = 0.05$. Considering $\overline{u}_{1\max} \propto u_*$, and $\rho_m = \rho_0 + (\rho_s - \rho_0)\overline{C}_m$ in which \overline{C}_m is the average vertical concentration, the above equation may be written as an equality,

$$R_i = \frac{g\delta}{u_*^2} \frac{\rho_s - \rho_0}{\rho_0} \frac{\overline{C}_{0.05} - \overline{C}_1}{1 + \frac{\rho_s - \rho_0}{\rho_0}\overline{C}_m} \quad (6.46)$$

This Richardson number is very important. It expresses the density gradient intensity in a sediment-laden flow. In a neutral sediment-laden flow, $\overline{C}_{0.05} = \overline{C}_1$, thus $R_i = 0$. In a density sediment-laden flow, $\overline{C}_{0.05} > \overline{C}_1$, thus $R_i > 0$. The stronger the density gradient, the larger the Richardson number. The Richardson number will be used as an indicator of the density gradient effect on the velocity profile model parameters.

To estimate the Richardson number R_i from (6.46), one must know the concentration profile which may be solved from (6.32) and will be discussed in the next chapter.

By the way, considering $\overline{\rho} = \rho_0 + (\rho_s - \rho_0)\overline{C}$, (6.46) can also be written as

$$R_i = \frac{g\delta}{u_*^2} \frac{\overline{\rho}_{0.05} - \overline{\rho}_1}{\overline{\rho}_m} \quad (6.47)$$

which appears in Coleman's (1981, 1986) classical papers.

6.4.3 Effects of sediment suspension on the vertical eddy viscosity

To study the effect of sediment suspension on $\overline{u_3'^2}$, let $i = j = 3$ in (6.39), one gives

$$\frac{\partial \overline{u_3'^2}}{\partial t} + \overline{u_k} \frac{\partial \overline{u_3'^2}}{\partial x_k} = -2\overline{u_3' u_k'} \frac{\partial \overline{u_3}}{\partial x_k} + 2\frac{\rho_s - \rho_0}{\rho_m} \overline{u_3' C'} g_3$$

$$\begin{aligned}
& -\frac{\overline{\partial u'_3 u'_3 u'_k}}{\partial x_k} - \frac{2}{\rho_m} \frac{\overline{\partial p' u'_3}}{\partial x_3} + \frac{2}{\rho_m} \overline{p' \frac{\partial u'_3}{\partial x_3}} \\
& + \nu_m \frac{\overline{\partial^2 u_3'^2}}{\partial x_3^2} - 2\nu_m \overline{\frac{\partial u'_3}{\partial x_k} \frac{\partial u'_3}{\partial x_k}}
\end{aligned} \tag{6.48}$$

Considering (6.20) and (6.21) gives that

$$\overline{u_k \frac{\partial u_3'^2}{\partial x_k}} = 0 \tag{6.49}$$

Considering $\overline{u_3} = 0$ gives that

$$\overline{u'_3 u'_k \frac{\partial \overline{u_3}}{\partial x_k}} = 0 \tag{6.50}$$

Considering (6.20) gives that

$$\frac{\overline{\partial u'_3 u'_3 u'_k}}{\partial x_k} = \frac{\overline{\partial u_3'^3}}{\partial x_3} \tag{6.51}$$

Then (6.48) becomes

$$\begin{aligned}
\frac{\overline{\partial u_3'^2}}{\partial t} &= \underbrace{2 \frac{\rho_s - \rho_0}{\rho_m} \overline{u'_3 C' g_3}}_{\text{sediment suspension}} - \underbrace{\frac{\overline{\partial u_3'^3}}{\partial x_3} - \frac{2}{\rho_m} \frac{\overline{\partial p' u'_3}}{\partial x_3} + \frac{2}{\rho_m} \overline{p' \frac{\partial u'_3}{\partial x_3}}}_{\text{turbulent transport}} \\
&+ \underbrace{\nu_m \frac{\overline{\partial^2 u_3'^2}}{\partial x_3^2}}_{\text{vis. transp.}} - \underbrace{2\nu_m \overline{\frac{\partial u'_3}{\partial x_k} \frac{\partial u'_3}{\partial x_k}}}_{\text{energy dissipation}}
\end{aligned} \tag{6.52}$$

In the following, one will assume a clear water running in a flume, then add some sediments to the flow to see how $\overline{u_3'^2}$ adjusts according to the right-hand side terms.

Assume that the viscous and the turbulent transport terms are neglected or secondary. Then the effects of sediment suspension on $\overline{u_3'^2}$ are mainly through two terms: *sediment suspension and energy dissipation*.

As those in (6.41), both the sediment suspension term and the energy dissipation term are negative. They will damp the turbulence intensity u'_3 . Consequently, sediment suspension damps the eddy viscosity in the vertical direction. The decrease of the eddy viscosity weakens turbulent mixing compared with a clear water flow. In other words, the outer region (overlap + wake layer + boundary effect layer) velocity gradient in a sediment-laden flow increases compared with a clear water flow.

6.5 Modification of the eddy viscosity model in sediment-laden flows

Assume that the structure of the eddy viscosity model (3.33) obtained in clear water flows is still valid in sediment-laden flows. Then the incorporation of the effect of sediment concentration may be four alternatives:

Alternative 1: To consider the sediment damping effect, following Monin and Obukhov (Duo, 1987, p.365), a concentration factor Φ_s may be introduced to the eddy viscosity expression, i.e.

$$\varepsilon_m^+ = \frac{1}{\Phi_s} \frac{(1 - \xi) + \tau|_{\xi=1} / \tau_w}{\frac{1 - \xi}{\kappa_0 \xi} + \frac{\pi \Omega_0}{2} \sin \pi \xi + \frac{1}{u_*} \left. \frac{d\bar{u}_1}{d\xi} \right|_{\xi=1}} \quad (6.53)$$

in which Φ_s is a function of concentration \bar{C} , i.e.

$$\Phi_s = 1 + \alpha_1 \bar{C} + \alpha_2 \bar{C}^2 + \dots \quad (6.54)$$

where α_1 and α_2 are experimental constants. In this case, the concentration equation (6.32) must be coupled with (6.29). Besides, if \bar{C} is replaced by a characteristic concentration \bar{C}_a and if \bar{C}_a is very small, then sediment concentration will not affect the von Karman constant κ_0 and the wake strength coefficient Ω_0 . Only an additional term is added in the clear water velocity profile equation, like the Monin-Obukhov equation in an atmosphere flow (Kundu, 1990, p.463). Note that the subscript “0” denotes values in clear water.

Alternative 2: Both the von Karman constant κ and the wake strength coefficient Ω in sediment-laden flows vary with a characteristic concentration, i.e., the sediment damping may be considered by decreasing κ and increasing Ω . That is, $\kappa < \kappa_0$, and $\Omega > \Omega_0$.

Alternative 3: κ may become smaller with a characteristic concentration, i.e., $\kappa < \kappa_0$, while Ω may keep the same as that in clear water, i.e., $\Omega = \Omega_0$.

Alternative 4: κ may keep the same as that in clear water, i.e., $\kappa = \kappa_0 = 0.406$, while Ω may increase with a characteristic concentration, i.e., $\Omega > \Omega_0$.

Alternative 1 is cumbersome. Alternatives 2, 3 and 4 are relative simple since one can choose a near bed concentration or the vertical mean concentration to reflect the effect of sediment suspension. In this dissertation, only last three alternatives are examined.

6.6 Velocity profiles in sediment-laden flows

Of course, for the last three alternatives, the velocity profile equations are similar to those in clear water except that the von Karman constant κ , the wake strength coefficient Ω , and the water surface shear effect factor λ may vary with sediment suspension. That is, the velocity profiles in narrow channels can still be described by (5.1), and the velocity profiles in wide channels can still be expressed by (5.23). However, one has

$$\begin{aligned}\kappa, \Omega, \lambda &= F(\text{characteristic concentration, density gradient}) \\ &= F(\bar{C}_a, R_i)\end{aligned}\tag{6.55}$$

in which $\bar{C}_a = \bar{C}_{0.05}$ for κ and $\bar{C}_a = \bar{C}_1$ for Ω and λ . This is because the von Karman constant is determined by the near bed flow while the wake strength coefficient Ω and the water surface shear effect factor λ are determined by the flow near the boundary layer margin or the water surface.

6.7 Summary

In this chapter, one starts with the full governing equations in sediment-laden flows and obtains the steady uniform 2D governing equations. Based on the turbulent kinetic energy equation, the global Richardson number R_i is derived. Based on the equation of the turbulence intensity $\overline{u_3^2}$, it is shown that sediment suspension affects the eddy viscosity in two ways: *increasing the molecular viscosity and then increasing energy dissipation, and losing turbulent energy to support sediment suspension*. Both ways will damp the vertical eddy viscosity. Using a magnitude order

analysis method, it is shown that the velocity profile equation in a sediment-laden flow takes the same form as that in clear water, except the model parameters may vary with a characteristic concentration and density gradient.

Chapter 7

TEST OF THE MODIFIED LOG-WAKE LAW IN SEDIMENT-LADEN FLOWS

7.1 Introduction

The modified log-wake law has been tested to be true in clear water in Chapter 5. Chapter 6 shows that it may be true for sediment-laden flows. However, sediment suspension may modify the parameters κ , Ω and λ . This chapter will test the modified log-wake law in sediment-laden flows and study the variations of κ , Ω and λ with sediment suspension.

Section 7.2 presents a test strategy, i.e., using two extreme experiments to test the effects of molecular viscosity and density gradient. Sections 7.3 and 7.4 discuss the effects of sediment suspension on the model parameters in narrow and wide channels. Section 7.5 summarizes the results of this chapter.

7.2 Preliminary analysis of the model parameters

In Chapter 6, one sees that sediment suspension affects the velocity profiles of sediment-laden flows in two ways: one is that sediment concentration increases mole-

cular viscosity and then increases energy dissipation and consequently damps turbulence intensity; the other is that to balance sediment settling due to the gravity, suspended sediments obtain energy from turbulent kinetic energy and then damp turbulence intensity. These two effects can be examined in two kinds of extreme experiments: one is neutral sediment-laden experiments where the concentration can be very high, the effect of viscosity is emphasized, but sediment suspension does not cost turbulent energy at all; the other is density (stratified) sediment-laden experiments where the concentration keeps so small that the effect of molecular viscosity may be neglected but the effect of the density gradient is emphasized.

For neutral sediment-laden flows, $\overline{C} = \overline{C}_{0.05} = \overline{C}_1$, $R_i = 0$, then (6.55) reduces to

$$\kappa, \Omega, \lambda = F_1(\overline{C}) \quad (7.1)$$

For density sediment-laden flows with dilute concentration, the effect of viscosity may be neglected. Then (6.55) reduces to

$$\kappa, \Omega, \lambda = F_2(R_i) \quad (7.2)$$

(7.1) and (7.2) are two asymptotic expressions. A composite expression for (6.55) may be expressed as

$$\kappa, \Omega, \lambda = F_1(\overline{C}_a) + F_2(R_i) - (\kappa, \Omega, \lambda)|_{\text{clear water}} \quad (7.3)$$

In the following, one will find the functional forms of F_1 and F_2 for each parameter κ , Ω and λ .

7.3 Test of the modified log-wake law in narrow open-channels

The model parameters in narrow channels include κ and Ω . The plastic particle experiments by Wang and Qian (1989) will serve to test the effect of molecular viscosity. The sediment experiments by Coleman (1986) will serve to study the effect of density gradient.

7.3.1 Effect of molecular viscosity

Wang and Qian (1989) did three types of experiments: clear water and pure salt water (see Section 5.3.3), neutral sediment-laden flows (salt water + plastic particles), and density sediment-laden flows (clear water + plastic particles, clear water + natural sands). The specific gravity of plastic particles $G = 1.05$, the particle concentration distribution in clear water is close to uniform, so the clear water + plastic particle experiments can be regarded as quasi-neutral sediment-laden flows, i.e., the effect of density gradient may be neglected herein. In the experiments, three sediment sizes (fine, middle and coarse) were used, see Appendix C. The flume perimeters were kept the same (smooth boundary, flow depth $h = 9$ cm, flume width $a = 30$ cm, and bed slope $S = 0.01$), the differences among individual runs are only attributed to different concentrations. The maximum volumetric concentration was 20%.

In the following tests, the shear velocity u_* , as it in clear water, is determined by (4.16) since it is a kinematic variable. The kinematic molecular viscosity ν_m due to volumetric sediment concentration is calculated by (Coleman, 1986)

$$\nu_m = \frac{\mu(1 + 2.5\bar{C} + 6.25\bar{C}^2 + 15.62\bar{C}^3)}{\rho_0 + (\rho_s - \rho_0)\bar{C}} \quad (7.4)$$

in which μ is the kinetic molecular viscosity of water; and \bar{C} is the volumetric sediment concentration. The velocity profile analysis procedure is the exact same as that in clear water.

Velocity profiles

A representative velocity profile, along with the modified log-wake law, of neutrally-buoyant sediment-laden flows is shown in FIG. 7.1. All other profiles can be found in Appendix C. Four velocity profiles of the fine particle (medium size $d_{50} = 0.268$ mm) experiments with different concentrations are plotted in FIG. 7.2. From the above two figures, one sees that: (1) The sediment concentration amplifies the thickness of the viscous layer (the viscous sublayer + the buffer layer). The higher the concentration, the thicker the viscous layer. (2) As the concentration increases, the position of

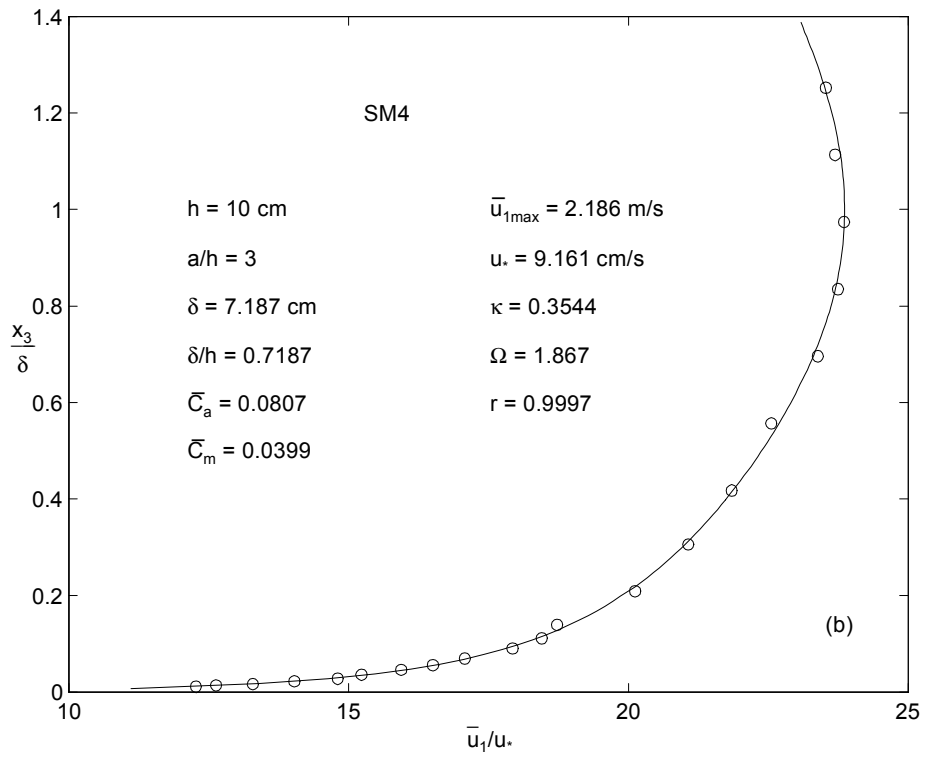
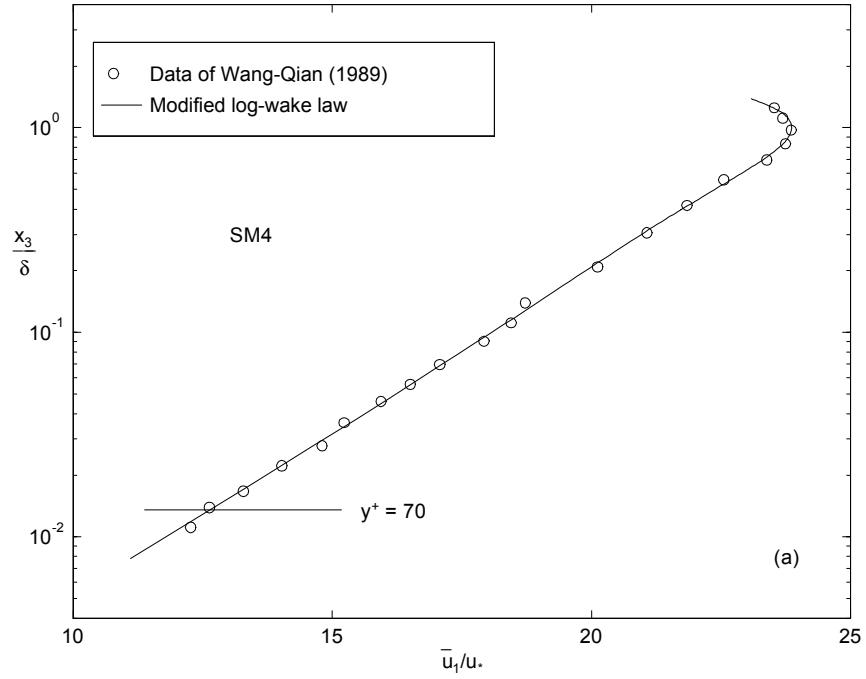


FIG. 7.1: A representative velocity profile of neutral sediment-laden flows in narrow channels [(a) in a semilog coordinate; (b) in a rectangular coordinate]

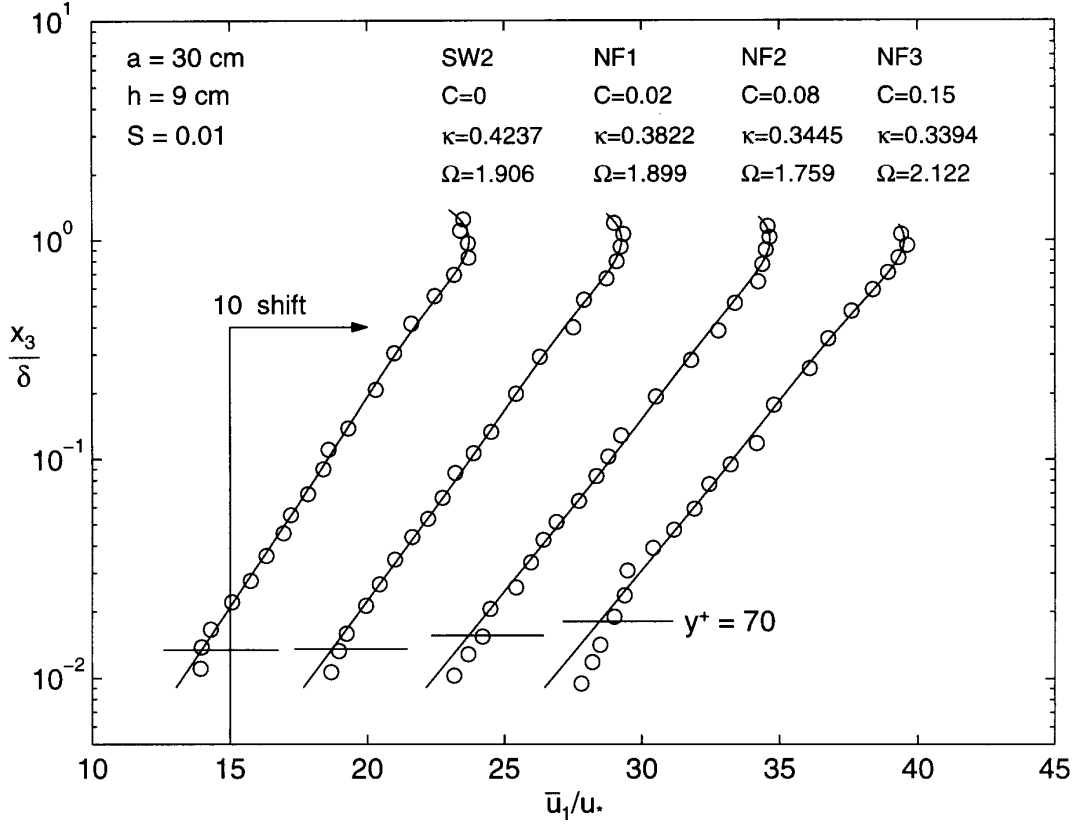


FIG. 7.2: The effect of molecular viscosity on the velocity profiles [o: Wang and Qian’s data (1989); —: The modified log-wake law]

the maximum velocity moves up and closes to the water surface. (3) The modified log-wake law (solid line) is still valid in the outer region ($y^+ \geq 70$) of sediment-laden flows. (4) The von Karman constant κ decreases with sediment concentration. (5) The variation of the wake strength coefficient Ω with sediment concentration is not clear at this moment. The quantitative study of κ and Ω is followed in the next subsection.

The von Karman constant κ and the wake strength coefficient Ω

The calculated results of all neutral and quasi-neutral particle experiments are shown in Tables 7.1 and 7.2, respectively. Except SF3 and SF4 (which may be

Table 7.1: Calculated results of Wang-Qian's neutral particle experiments

RUN	h (cm)	a/h	S	u_* (cm/s)	δ (cm)	$\bar{u}_{1\max}$ (m/s)	\bar{C}	κ	Ω	r
NF1	9	3.33	0.01	8.81	6.77	2.14	0.02	0.389	1.96	0.9994
NF2	9	3.33	0.01	8.81	7.00	2.17	0.08	0.355	1.88	0.9987
NF3	9	3.33	0.01	8.81	7.61	2.16	0.15	0.339	2.12	0.9984
NM1	10	3.00	0.01	9.16	6.79	2.08	0.02	0.419	2.01	0.9987
NM2	10	3.00	0.01	9.16	7.04	2.12	0.07	0.365	2.10	0.9990
NM3	10	3.00	0.01	9.16	7.65	2.13	0.13	0.374	2.29	0.9975
NM4	10	3.00	0.01	9.16	7.94	2.12	0.20	0.327	2.09	0.9989
NC1	10	3.00	0.01	9.16	6.33	2.10	0.02	0.400	2.02	0.9985
NC2	10	3.00	0.01	9.16	7.44	2.10	0.07	0.409	2.11	0.9968
NC3	10	3.00	0.01	9.16	6.94	2.11	0.13	0.353	2.09	0.9984
NC4	10	3.00	0.01	9.16	7.16	2.12	0.20	0.340	2.42	0.9982

outliers) in Table 7.2, a plot between \bar{C} and κ , including clear water and pure salt water experiments in Table 5.2, is shown in FIG. 7.3, where the MIT neutral particle result in pipes (Chien and Wan, 1983, p.410) is also plotted. It is clear that the present results from narrow channels are compatible to those from pipes at MIT. The data scatter may be due to the slight density gradient in the quasi-neutral sediment-laden experiments. The von Karman constant κ decreases with sediment concentration \bar{C} . A linear relation between \bar{C} and κ exists, i.e., the function F_1 in (7.3) for κ may be written as

$$\kappa = F_1(\bar{C}) = \kappa_0 - \alpha\bar{C} \quad (7.5)$$

in which the experimental constant κ_0 is determined to be 0.406, the value in clear water. The constant α is determined to be 0.372. (7.5) can be rewritten as

$$\boxed{\frac{\kappa}{\kappa_0} = 1 - 0.92\bar{C}} \quad (7.6)$$

A plot of the volumetric sediment concentration \bar{C} (the average values are taken for quasi-neutral particle experiments) versus the wake strength coefficient Ω is plotted in FIG. 7.4. It is shown that the wake strength coefficient Ω increases with sediment

Table 7.2: Calculated results of Wang-Qian's quasi-neutral particle experiments

RUN	h (cm)	a/h	u_*	δ (cm)	$\bar{u}_{1\max}$ (m/s)	$\bar{C}_{0.05}$ (%)	\bar{C}_m (%)	κ	Ω	r
SF1	10	3.00	9.16	6.66	2.12	0.53	0.41	0.435	1.83	0.9987
SF2	10	3.00	9.16	6.60	2.09	1.39	1.02	0.396	1.44	0.9991
SF3	10	3.00	9.16	6.57	2.07	2.86	2.28	0.465	1.94	0.9982
SF4	10	3.00	9.16	7.44	2.08	5.55	4.60	0.449	2.12	0.9987
SF5	8	3.75	8.40	5.29	1.96	10.08	9.06	0.360	1.85	0.9980
SF6	9	3.49	8.65	9.01	2.16	14.73	13.26	0.356	2.51	0.9980
SM1	10	3.00	9.16	7.06	2.11	0.74	0.42	0.421	1.46	0.9992
SM2	10	3.00	9.16	6.55	2.15	2.74	1.20	0.416	1.71	0.9989
SM3	10	3.00	9.16	7.07	2.16	5.07	2.38	0.398	2.00	0.9997
SM4	10	3.00	9.16	7.19	2.19	7.99	3.99	0.354	1.87	0.9997
SM5	10	3.00	9.16	8.83	2.20	11.56	6.23	0.375	1.90	0.9991
SM6	10	3.00	9.16	9.40	2.21	14.40	7.54	0.348	1.70	0.9953
SM7	10	3.00	9.16	8.68	2.23	21.72	13.72	0.355	2.68	0.9995
SC1	10	3.00	9.16	6.43	2.12	1.04	0.43	0.402	1.81	0.9993
SC2	10	3.00	9.16	6.79	2.10	2.06	0.85	0.380	1.29	0.9995
SC3	10	3.00	9.16	6.64	2.11	4.18	1.98	0.378	1.86	0.9997
SC4	10	3.00	9.16	7.19	2.13	7.31	3.40	0.378	2.02	0.9992
SC5	10	3.00	9.16	7.35	2.15	11.72	6.51	0.357	2.42	0.9992
SC6	10	3.00	9.16	7.54	2.17	17.10	9.37	0.337	2.46	0.9990
SC7	10	3.00	9.16	7.73	2.16	21.00	12.25	0.317	2.15	0.9985

concentration (molecular viscosity). For Wang and Qian's (1989) experiments where $a/h \approx 3$, the following regression equation can be obtained:

$$\Omega = 1.65 + 3.71\bar{C} \quad (7.7)$$

When $\bar{C} = 0$, $\Omega = 1.65$ which is compatible to FIG. 5.11. In density sediment-laden flows, \bar{C} in the above equation should be replaced by the water surface concentration \bar{C}_1 . Fortunately, all sediment-laden flows in practice are density flows. In such a flow, \bar{C}_1 is usually very small. Therefore, the effect of the concentration on the wake strength coefficient Ω may be neglected. In other words, in density sediment-laden flows, one has $\Omega \approx \Omega_0$, which can be estimated from (5.21) or FIG. 5.11.

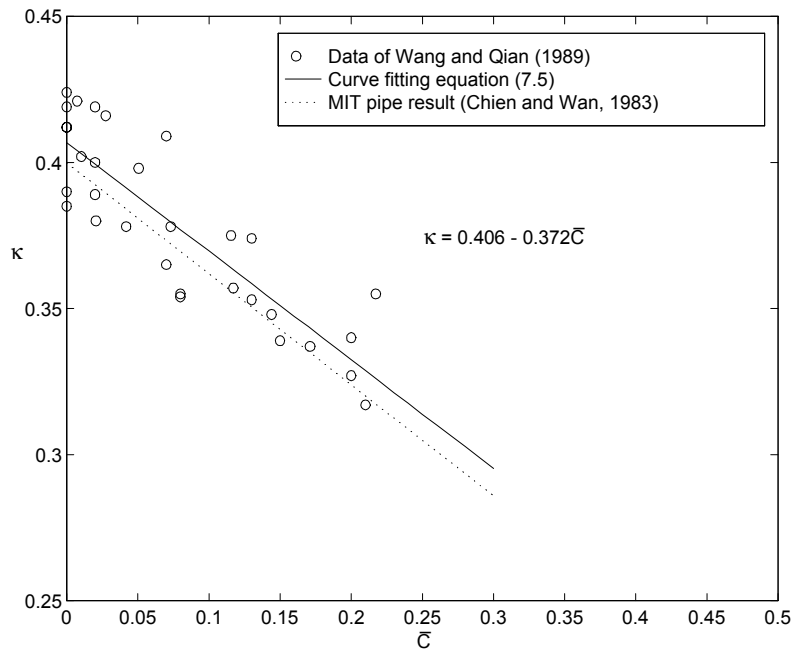


FIG. 7.3: The effect of molecular viscosity on the von Karman constant

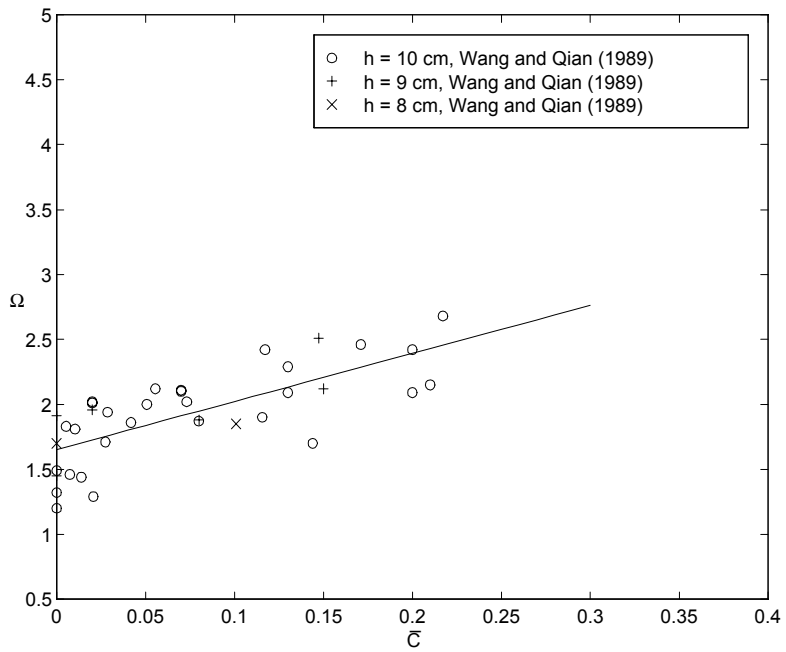


FIG. 7.4: The effect of molecular viscosity on the wake strength coefficient

7.3.2 Effect of density gradient

The experimental studies of the effect of density gradient on velocity profiles in sediment-laden flows were reported by Vanoni (1946), Einstein and Chien (1955), and Coleman (1986). Vanoni (1946) did not publish the experimental data. Einstein and Chien's (1955) data were widely cited, however, they just measured the velocity profile near the bed (about $x_3/h < 0.4$). The velocity profile data near the water surface are necessary in the test of the modified log-wake law. Hence, Einstein and Chien's data cannot be used here. Coleman's (1986) data set is a valuable source. It includes all necessary information to test the modified log-wake law in sediment-laden flows.

Like Wang and Qian's (1989) experiments, the flow conditions (smooth boundary, $h \approx 170$ mm, $a = 356$ mm, $S = 0.002$) were kept the same in all runs. The maximum local volumetric concentration is 2.3%. Hence, the effect due to molecular viscosity may be neglected. The differences of the velocity profiles among individual runs are just attributed to the density gradient.

Velocity profiles

FIGS. 7.5 shows a representative velocity profile of Coleman's (1986) measurements with the modified log-wake law. FIG. 7.6 shows a comparison of 5 velocity profiles with different Richardson number R_i . Other profiles can be found in Appendix D. Again, the modified log-wake law agrees fairly well with experimental data. The von Karman constant κ decreases with R_i while the variation of the wake strength coefficient Ω is not clear at this moment.

The von Karman constant κ and the wake strength coefficient Ω

As stated in Chapter 5, the density gradient effect on the model parameters κ and Ω may be expressed by the Richardson number R_i . From (6.46), one sees that the estimation of R_i requires the values of $\overline{C}_{0.05}$, \overline{C}_1 and \overline{C}_m . Fortunately, in Coleman's (1986) experiments, the sediment concentration profiles are all measured. Therefore,

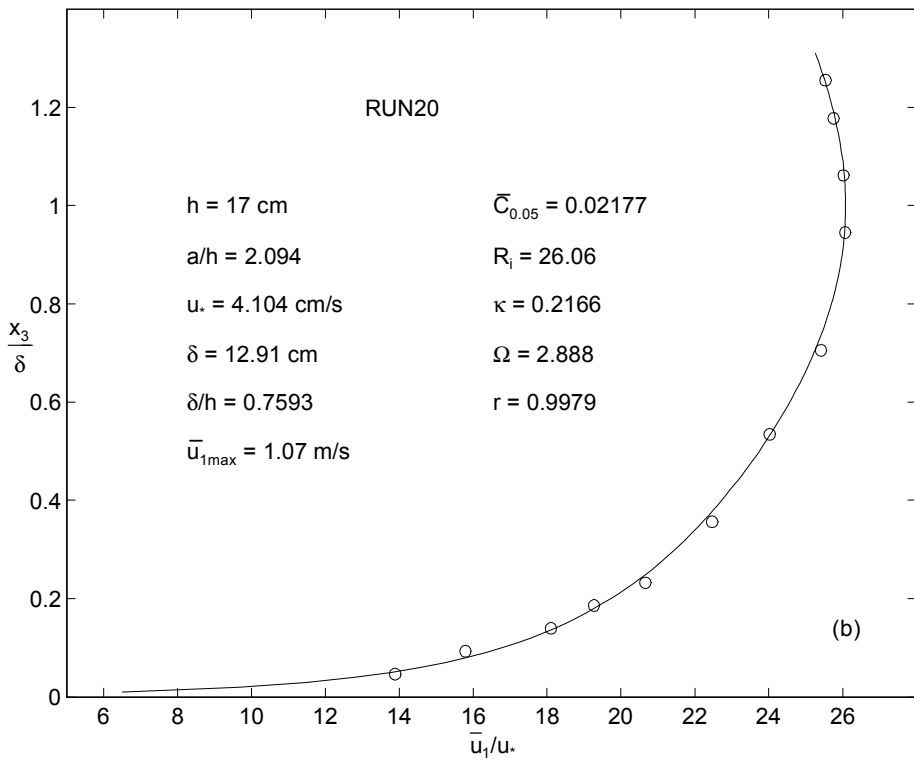
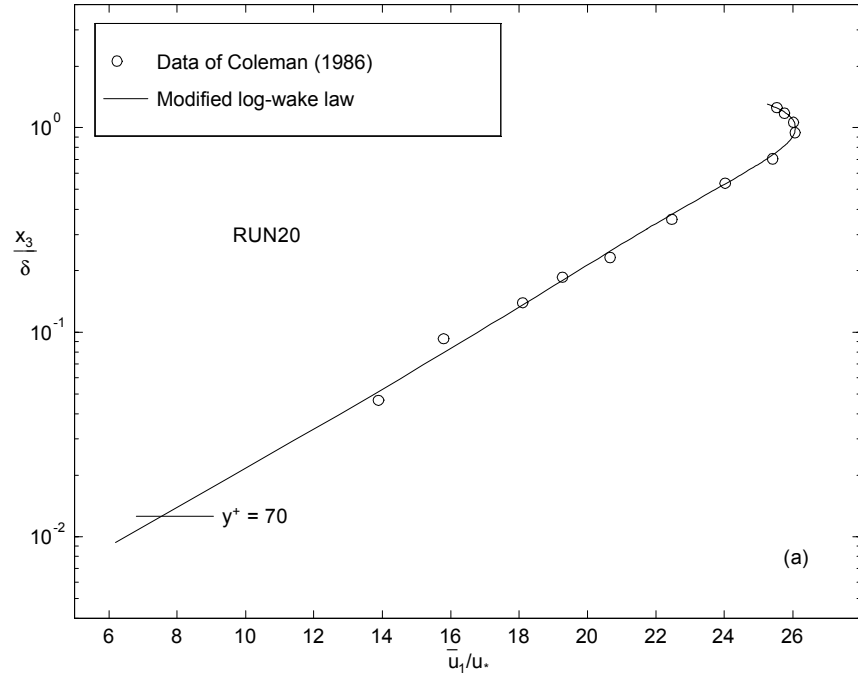


FIG. 7.5: A representative velocity profile of sediment-laden flows in narrow channels [(a) in a semilog coordinate; (b) in a rectangular coordinate]

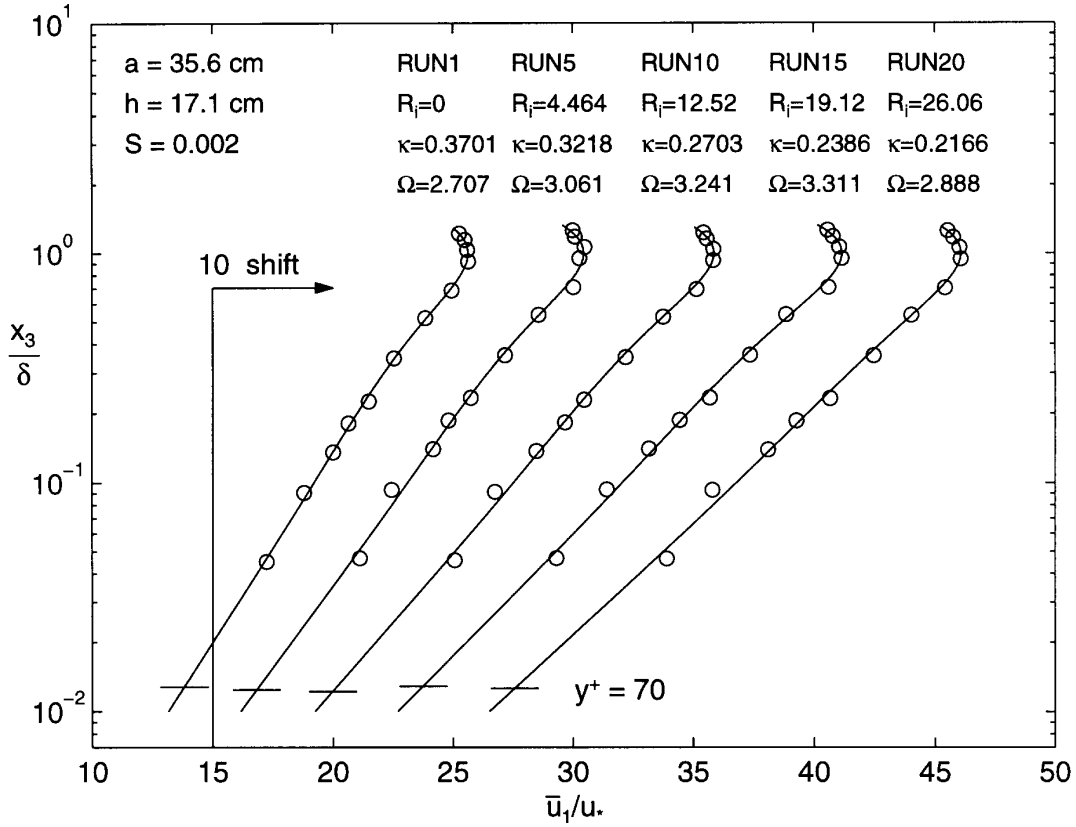


FIG. 7.6: The effect of density gradient on velocity profiles [o: Coleman's data (1986); —: The modified log-wake law]

R_i can be easily calculated without a concentration profile equation. The calculated results of all Coleman's (1986) experimental profiles are shown in Table 7.3 . A plot of the von Karman constant κ versus the Richardson number R_i is shown in FIG. 7.7. It can be seen that the density gradient (the Richardson number R_i) has a significant effect on the von Karman constant κ . The stronger the density gradient, the smaller the von Karman constant. An exponential relation between κ and R_i may exist, i.e., the function F_2 for κ in (7.2) may be written as

$$\frac{\kappa}{\kappa_0} = \exp \{-\beta R_i^m\} \quad (7.8)$$

Table 7.3: Calculated results of Coleman's experimental data

RUN	h (cm)	a/h	δ (cm)	u_* (cm/s)	\bar{u}_1^{\max} (m/s)	$C_{0.05}$ (10^{-3})	C_1 (10^{-3})	C_m (10^{-3})	R_i	κ	Ω	r
1	17.2	2.07	13.26	4.113	1.054	0.00	0.00	0.00	0.0	0.370	2.71	0.9996
2	17.1	2.08	12.59	4.108	1.045	0.84	0.09	0.25	0.90	0.351	2.48	0.9988
3	17.2	2.07	12.70	4.113	1.043	1.65	0.16	0.45	1.81	0.334	2.76	0.9980
4	17.1	2.08	12.88	4.108	1.046	2.70	0.23	0.67	3.04	0.319	2.72	0.9991
5	17.1	2.08	12.86	4.108	1.046	3.82	0.34	0.92	4.28	0.322	3.06	0.9980
6	17.0	2.09	12.73	4.104	1.052	4.89	0.42	1.12	5.47	0.341	3.7	0.9975
7	17.1	2.08	12.81	4.108	1.053	5.95	0.48	1.40	6.71	0.295	3.19	0.9980
8	17.1	2.08	13.29	4.108	1.044	7.21	0.53	1.58	8.49	0.299	3.21	0.9988
9	17.2	2.07	13.22	4.113	1.051	8.53	0.52	1.79	10.10	0.289	3.34	0.9973
10	17.1	2.08	13.12	4.108	1.063	10.31	0.64	2.06	12.13	0.270	3.24	0.9988
11	16.9	2.11	13.16	4.099	1.081	11.35	0.62	2.25	13.55	0.261	3.41	0.9979
12	17.3	2.06	13.74	4.117	1.049	11.86	0.58	2.24	14.75	0.253	2.79	0.9974
13	17.1	2.08	12.74	4.108	1.065	13.53	0.79	2.71	15.50	0.252	3.37	0.9977
14	17.1	2.08	13.09	4.108	1.065	14.26	0.77	2.84	16.85	0.245	3.10	0.9976
15	17.1	2.08	12.82	4.108	1.075	16.18	0.99	3.04	18.58	0.239	3.31	0.9986
16	17.1	2.08	12.76	4.108	1.073	17.27	0.94	3.18	19.89	0.228	3.11	0.9977
17	17.1	2.08	14.02	4.108	1.065	16.68	0.77	2.77	21.29	0.222	2.30	0.9963
18	17.2	2.07	12.91	4.113	1.053	17.95	0.93	3.12	20.92	0.244	3.00	0.9985
19	17.0	2.09	12.92	4.104	1.072	19.79	0.95	3.27	23.28	0.228	3.21	0.9979
20	17.0	2.09	12.91	4.104	1.07	21.48	1.05	3.37	25.21	0.217	2.89	0.9979

(Continued)

(Continued)

RUN	h (cm)	a/h	δ (cm)	u_* (cm/s)	$\bar{u}_{1\max}$ (m/s)	$\bar{C}_{0.05}$ (10^{-3})	\bar{C}_1 (10^{-3})	\bar{C}_m (10^{-3})	R_i	κ	Ω	r
21	16.9	2.11	12.61	4.099	1.048	0.00	0.00	0.00	0.00	0.400	2.60	0.9992
22	17.0	2.09	12.72	4.104	1.027	0.95	0.07	0.20	1.07	0.508	3.10	0.9976
23	17.0	2.09	12.46	4.104	1.047	2.04	0.13	0.39	2.28	0.431	3.38	0.9988
24	16.9	2.11	12.74	4.099	1.050	3.21	0.21	0.58	3.68	0.345	3.01	0.9972
25	16.7	2.13	12.49	4.09	1.069	4.63	0.26	0.78	5.27	0.295	3.09	0.9987
26	17.1	2.08	13.01	4.108	1.045	5.08	0.31	0.96	5.95	0.324	3.29	0.9991
27	16.8	2.12	12.74	4.095	1.069	6.33	0.33	1.15	7.36	0.319	3.72	0.9974
28	17.0	2.09	12.91	4.104	1.063	7.59	0.34	1.29	8.98	0.304	3.55	0.9989
29	16.8	2.12	13.01	4.095	1.083	8.84	0.46	1.46	10.51	0.287	3.65	0.9978
30	16.8	2.12	13.06	4.095	1.092	10.15	0.49	1.58	12.15	0.295	3.79	0.9970
31	17.2	2.07	13.25	4.113	1.060	10.93	0.47	1.62	13.22	0.27	3.53	0.9993
32	17.3	2.06	12.88	4.117	1.025	0.00	0.00	0.00	0.00	0.432	3.36	0.9997
33	17.4	2.05	13.08	4.121	1.036	0.25	0.02	0.04	0.28	0.389	3.07	0.9964
34	17.2	2.07	12.7	4.113	1.044	0.48	0.03	0.07	0.54	0.457	3.83	0.9974
35	17.2	2.07	13.06	4.113	1.055	0.84	0.05	0.11	0.98	0.375	3.52	0.9975
36	17.1	2.08	13.02	4.108	1.082	1.52	0.08	0.18	1.80	0.342	3.54	0.9971
37	16.7	2.13	12.96	4.090	1.081	1.72	0.11	0.22	2.02	0.328	3.77	0.9981
38	16.7	2.13	13.05	4.290	1.114	1.70	0.11	0.22	1.83	0.385	4.27	0.9948
39	17.1	2.08	13.15	4.309	1.096	2.39	0.15	0.30	2.57	0.358	3.91	0.9983
40	17.1	2.08	13.21	4.108	1.101	2.30	0.16	0.31	2.71	0.318	4.06	0.9955

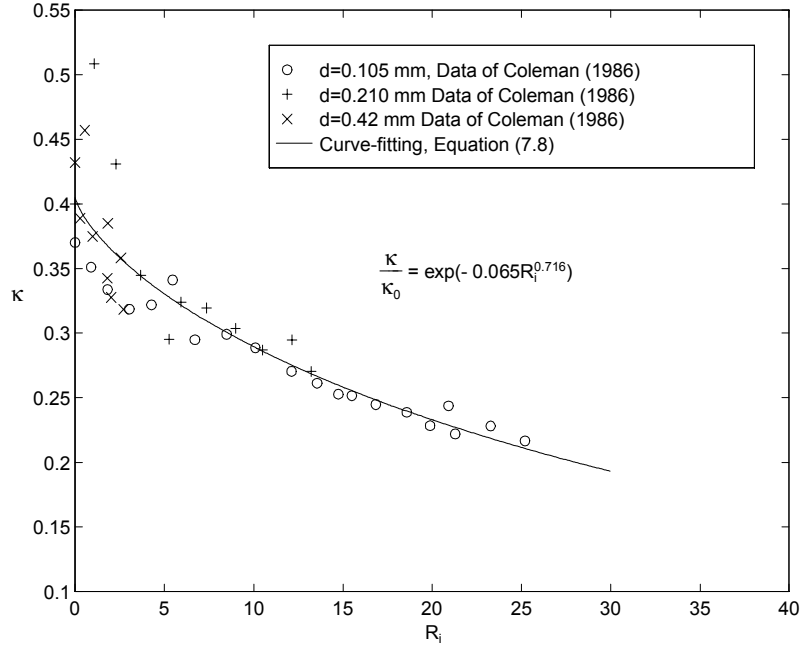


FIG. 7.7: The effect of density gradient on the von Karman constant

in which κ_0 is the von Karman constant, 0.406, in clear water flows. β and m are determined to be 0.065 and 0.716, respectively, using experimental data. The general correlation coefficient is 0.89. The very small concentration is usually difficult to measure accurately, so the data scatters when $R_i < 5$.

The relation between the wake strength coefficient Ω and the Richardson number R_i is plotted in FIG. 7.8, which shows that the effect of density gradient on the wake strength coefficient Ω is trivial. This again shows that the wake strength coefficient Ω , in essence, expresses the effect of the side-wall.

7.3.3 Combination of the effects of molecular viscosity and density gradient

Substituting (7.6) and (7.8) into (7.3) for the composite expression of κ , one gets

$$\frac{\kappa}{\kappa_0} = \exp \{ -\beta R_i^m \} - \alpha \bar{C}_{0.05} \quad (7.9)$$

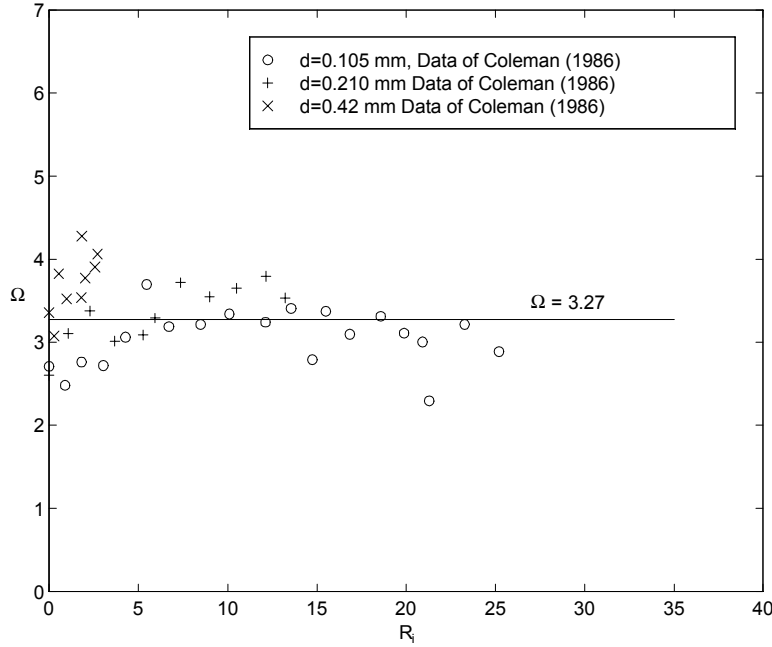


FIG. 7.8: The effect of density gradient on the wake strength coefficient

in which $\kappa_0 = 0.406$, $\beta = 0.0636$, $m = 0.716$, and $\alpha = 0.92$. Considering the value of κ is determined by the near bed flow, $\bar{C}_{0.05}$ is used herein for density gradient flows. The further accurate values of α , β and m may be obtained if a two dimensional curve-fitting method is applied to (7.9).

As stated earlier, the effects of both concentration and density gradient in practice are so small that they may be neglected. That is, the wake strength coefficient Ω is only affected by the side-walls (the aspect ratio a/h), i.e., $\Omega \approx \Omega_0$.

7.4 Test of the log-linear law in natural rivers

7.4.1 Test of the log-linear law in natural rivers

As stated earlier, the modified log-wake law reduces to the log-linear law in wide open-channels. Vanoni's (1946) experiments, Elata and Ippen's experiments (1961), Guy, Simons and Richardson's (1966) experiments, and Muste's (1995) experiments

can be regarded as wide channel experiments. However, both Vanoni (1946) and Elata and Ippen (1961) did not publish their experimental data. Guy, Simons and Richardson (1966) collected a huge data set of sediment transport. Most of their runs have bed forms which create difficulty in determining the shear velocity u_* . Therefore, their experiments are not very suitable to this study. Muste's (1995) recorded four sediment-laden experiments. He concluded that sediment suspension has little effect on fluid velocity profile. This is because both concentration ($\bar{C} \approx 10^{-5}$) and density gradient in his experiments are very small.

The end of this study is to predict the velocity profiles in natural rivers. Thus, the test of the log-linear law in rivers is necessary. However, bedforms in natural streams create difficulty for determining the shear velocity (corresponding to the skin friction). The study of bedform resistance is beyond the scope of this dissertation. To avoid the error due to the determination of the shear velocity, only dimensional velocity profiles in natural rivers are compared with the log-linear law in this subsection.

To build the Xiao-Lang-Di Reservoir and the Three Gorges Reservoir, Chinese engineers collected many velocity and concentration profiles in the Yellow River and the Yangtze River. Appendix I tabulates some measurement data in the Yellow River and the Yangtze River¹. FIGS. 7.9 and 7.10 show the comparisons of the log-linear law with some measurement velocity profiles. One can see that the log-linear law agrees fairly well with the field measurements. This reveals that the structure of the log-linear law in wide open-channels is correct.

7.4.2 Conjecture of the effects of sediment suspension in wide open-channels

Fortunately, the von Karman constant κ only relates to the near bed flow. The near bed velocity profiles in narrow and wide channels are similar, one naturally reaches that (7.9) may also be valid in wide open-channels.

The water surface shear effect factor λ in a wide channel, like the wake strength

¹Provided by Prof. Yu-Jia Hui, Tsinghua University, Beijing, China

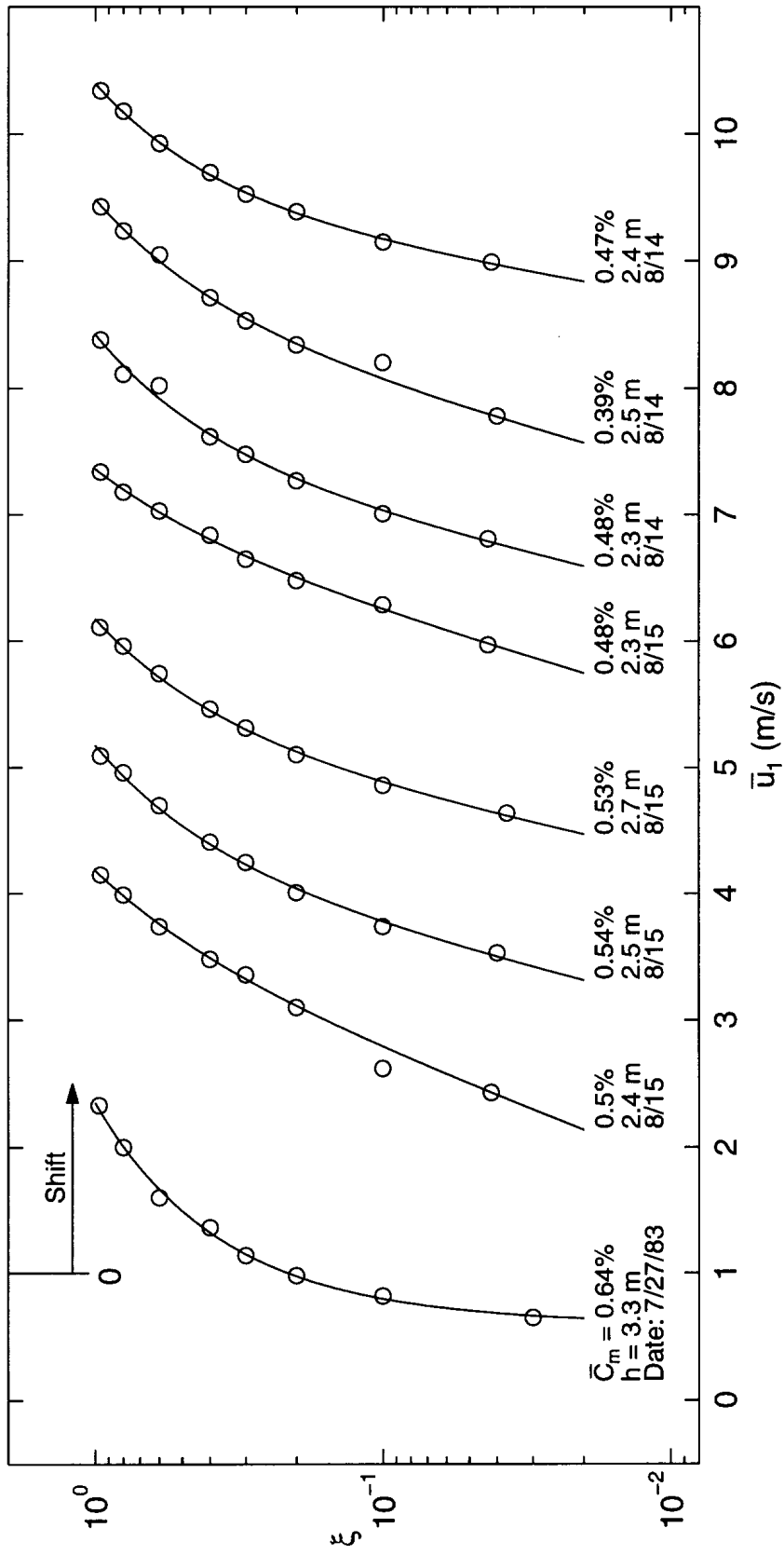


FIG. 7.11: Comparison of the log-linear law with the Yellow River measurement velocity profiles

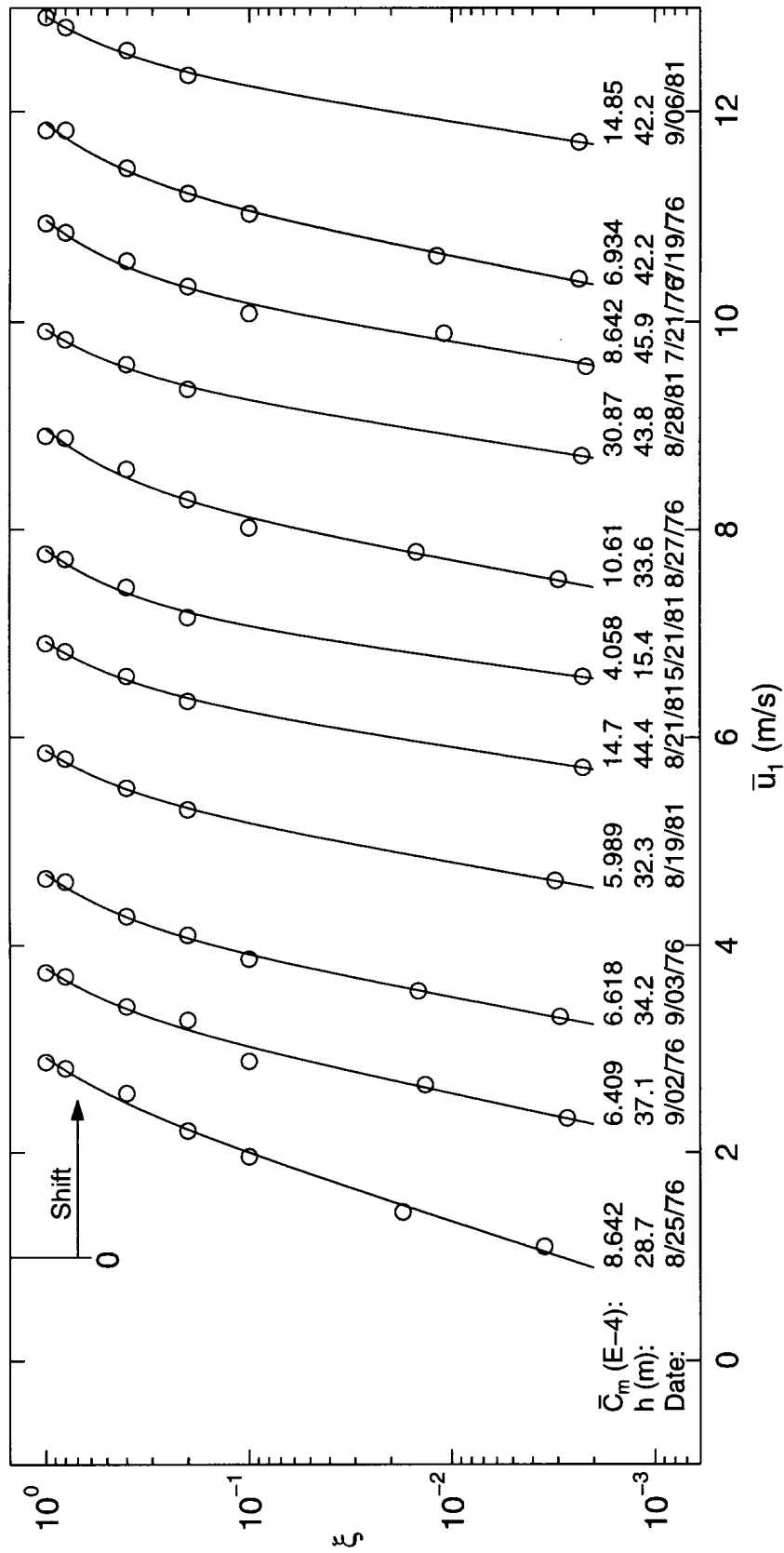


FIG. 7.12: Comparison of the log-linear law with the Yangtze River measurement velocity profiles

coefficient Ω in narrow channels, only relates to the near surface flow. Since both concentration and density gradient at the water surface are usually very small, their effects on λ may be neglected. Thus, (5.33), from clear water, may also be valid in sediment-laden flows.

7.5 Summary

In this chapter, the modified log-wake law first compares with neutral particle-laden experiments in narrow channels. It shows that the von Karman constant κ decreases with volumetric sediment concentration and can be estimated from (7.6). This is because sediment concentration increases molecular viscosity and then increases energy dissipation. The wake strength coefficient Ω slightly increases with sediment concentration, but its effect may, in practice, be neglected in density sediment-laden flows. Note that a neutral particle-laden flow belongs to a two-phase flow, which is different from a one-phase thick fluid. Given the same boundary condition, a two-phase flow dissipates more energy than a one-phase thick flow. This is because in a two-phase (liquid + solid particles) flow, solid particles increase the effective surface between fluid and solid boundaries.

The modified log-wake is then tested with density sediment-laden experiments in narrow channels. It shows that the von Karman constant κ also decreases with the Richardson number R_i (density gradient) and can be estimated from (7.8). Unlike κ , the wake strength coefficient Ω has little to do with the Richardson number R_i . It may still be estimated from (5.21).

The log-linear law, which is the reduction of the log-wake law in wide channels, compares quite well with measurement velocity profiles in the Yellow River and the Yangtze River. It is conjectured that like the wake strength coefficient Ω , sediment suspension may have little effect on the water surface shear correction factor λ .

The combination of the effects of concentration and density gradient on the von Karman constant κ may be expressed by (7.9). It may be valid in both narrow and wide channels.

Chapter 8

APPLICATIONS OF THE MODIFIED LOG-WAKE LAW

8.1 Applications of the modified log-wake law in pipes

8.1.1 Relation between the maximum velocity $\bar{u}_{1\max}$ and the average velocity U

Neglecting the viscous sublayer and the buffer layer and integrating (5.1) over the cross-sectional area, one obtains that

$$\begin{aligned}\frac{\bar{u}_{1\max} - U}{u_*} &= 2 \int_0^1 \left[-\frac{1}{\kappa_0} \ln \xi + \Omega_0 \cos^2 \frac{\pi \xi}{2} - \frac{1 - \xi}{\kappa_0} \right] (1 - \xi) d\xi \\ &= -\frac{2}{\kappa_0} \int_0^1 (1 - \xi) \ln \xi + 2\Omega_0 \int_0^1 (1 - \xi) \cos^2 \frac{\pi \xi}{2} d\xi - \frac{2}{\kappa_0} \int_0^1 (1 - \xi)^2 d\xi\end{aligned}$$

Since

$$\begin{aligned}\int_0^1 (1 - \xi) \ln \xi &= \int_0^1 \ln \xi d\xi - \int_0^1 \xi \ln \xi d\xi \\ &= -1 - \left[\frac{\xi^2}{2} \ln \xi - \frac{\xi^2}{4} \right]_0^1 \\ &= -1 + \frac{1}{4} = -\frac{3}{4}\end{aligned}$$

$$\begin{aligned}
& \int_0^1 (1 - \xi) \cos^2 \frac{\pi \xi}{2} d\xi \\
&= \int_0^1 \cos^2 \frac{\pi \xi}{2} d\xi - \int_0^1 \xi \cos^2 \frac{\pi \xi}{2} d\xi \\
&= \frac{2}{\pi} \int_0^{\pi/2} \cos^2 \xi d\xi - \int_0^1 \frac{1 + \cos \pi \xi}{2} \xi d\xi \\
&= \frac{1}{2} - \left(\frac{1}{4} + \frac{1}{2} \int_0^1 \xi \cos \pi \xi d\xi \right) \\
&= \frac{1}{4} - \frac{1}{2} \left(\frac{1}{\pi^2} \cos \pi \xi + \frac{\xi}{\pi} \sin \pi \xi \right)_0^1 \\
&= \frac{1}{4} + \frac{1}{\pi^2}
\end{aligned}$$

and

$$\int_0^1 (1 - \xi)^2 d\xi = \frac{1}{3}$$

one has

$$\begin{aligned}
\frac{\bar{u}_{1 \max} - U}{u_*} &= -\frac{2}{\kappa_0} \left[-\frac{3}{4} \right] + 2\Omega_0 \left[\frac{1}{4} + \frac{1}{\pi^2} \right] - \frac{2}{\kappa_0} \left(\frac{1}{3} \right) \\
&= \frac{5}{6\kappa_0} + \left(\frac{1}{2} + \frac{2}{\pi^2} \right) \Omega_0
\end{aligned}$$

Taking $\kappa_0 = 0.406$ and $\Omega_0 = 3.2$, one obtains

$$\boxed{\frac{\bar{u}_{1 \max} - U}{u_*} = 4.3} \quad (8.1)$$

8.1.2 Position of the average velocity U

Equating the right-hand side of (5.1) to the right-hand side of (8.1) and solving the resultant equation, one obtains the position of the average velocity U , which is

$$\boxed{\bar{\xi} = 0.25} \quad (8.2)$$

This equation can be used to measure the pipe average velocity at one point.

8.1.3 Procedures for applying the modified log-wake law

Provided that the pipe diameter d , the shear velocity u_* (or the pipe length L and the pressure drop Δp), one can calculate the pipe velocity profile as follows:

Step 1: Estimate the friction factor f , which is defined as $f = 8(u_*/U)^2$, and the average velocity U . The study of the friction factor is beyond this dissertation. Prandtl's classical equation (Schlichting, 1979, p.611, p.624) or Zagarola's (1996) resistance formula may be used.

Prandtl's formula (Schlichting, 1979, p.611, p.624):

$$\frac{1}{\sqrt{f}} = 2 \log \left(\text{Re} \sqrt{f} \right) - 0.8 \quad (\text{hydraulically smooth}) \quad (8.3)$$

in which $\text{Re} = Ud/\nu$. The above equation is valid up to $\text{Re} = 3.4 \times 10^6$.

$$f = \frac{1}{\left(2 \log \frac{R}{k_s} + 1.74 \right)^2} \quad (\text{completely rough}) \quad (8.4)$$

in which R is the pipe radius; and k_s is roughness.

Zagarola's (1996, p.204) formula (hydraulically smooth):

$$\frac{1}{\sqrt{f}} = 1.872 \log \left(\text{Re} \sqrt{f} \right) - 0.2555 - \frac{228}{(\text{Re} \sqrt{f})^{0.89}} \quad (8.5)$$

which is valid for $\text{Re} = 3.1 \times 10^4 - 3.5 \times 10^7$.

Step 2: With the average velocity U available, the maximum velocity $\bar{u}_{1\max}$ can be estimated using (8.1).

Step 3: Given the maximum velocity $\bar{u}_{1\max}$, the shear velocity u_* , $\kappa_0 = 0.406$, and $\Omega_0 = 3.2$, the velocity profile can be estimated using (5.1), i.e.

$$\frac{\bar{u}_{1\max} - \bar{u}_1}{u_*} = -\frac{1}{\kappa_0} \ln \xi + \Omega_0 \cos^2 \frac{\pi \xi}{2} - \frac{1 - \xi}{\kappa_0}$$

8.2 Applications of the modified log-wake law in open-channels

The flow in a narrow open-channel is three-dimensional and much more complicated than that in a wide open-channel. The velocity profile over the whole cross-section in a narrow channel is not studied in this dissertation. So, a full application of the modified log-wake law in narrow channels cannot be recommended at this moment. However, the log-linear law, which is the reduction of the modified log-wake law in wide channels, has been ready to apply in wide open-channel flows.

8.2.1 Magnitude of the linear term in the log-linear law

From (5.23), the linear term in the log-linear law is

$$-\left[\frac{1}{\kappa} - \lambda_0 \left(\frac{V_{\text{wind}} - \bar{u}_{1\text{max}}}{u_*}\right)^2\right] (1 - \xi)$$

in which κ is the von Karman constant in sediment-laden flows and varies between 0.2 and 0.406, $\lambda_0 \approx 0.0065$. Usually, $\bar{u}_{1\text{max}}/u_* = 10 - 30$. If $V_{\text{wind}} = 0$, one has

$$-5 < -\left[\frac{1}{\kappa} - \lambda_0 \left(\frac{V_{\text{wind}} - \bar{u}_{1\text{max}}}{u_*}\right)^2\right] < 4 \quad (8.6)$$

One can see that the coefficient of the linear term may be positive and may be negative. In some cases, the coefficient may be close to zero, the linear term may be neglected and the classical log law is restored. However, this cannot be generalized. In particular, the linear term cannot be neglected in a sediment-laden flow. This can be easily seen from FIGS. 7.9 and 7.10, where the velocity profiles are not straight lines in a semilog coordinate system.

8.2.2 Relation between the maximum velocity $\bar{u}_{1\text{max}}$ and the average velocity U

For a wide open-channel (2D), neglecting the viscous sublayer and the buffer layer and integrating the log-linear law (5.23) over the entire flow depth, one has

$$\begin{aligned} \frac{\bar{u}_{1\text{max}} - U}{u_*} &= \int_0^1 \left\{ -\frac{1}{\kappa} \ln \xi - \left[\frac{1}{\kappa} - \lambda_0 \left(\frac{V_{\text{wind}} - \bar{u}_{1\text{max}}}{u_*} \right)^2 \right] (1 - \xi) \right\} d\xi \\ &= -\frac{1}{\kappa} \int_0^1 \ln \xi d\xi - \left[\frac{1}{\kappa} - \lambda_0 \left(\frac{V_{\text{wind}} - \bar{u}_{1\text{max}}}{u_*} \right)^2 \right] \int_0^1 (1 - \xi) d\xi \\ &= \frac{1}{\kappa} - \frac{1}{2} \left[\frac{1}{\kappa} - \lambda_0 \left(\frac{V_{\text{wind}} - \bar{u}_{1\text{max}}}{u_*} \right)^2 \right] \\ &= \frac{1}{2\kappa} + \frac{\lambda_0}{2} \left(\frac{V_{\text{wind}} - \bar{u}_{1\text{max}}}{u_*} \right)^2 \end{aligned} \quad (8.7)$$

i.e.

$$\frac{\lambda_0}{2} \left(\frac{V_{\text{wind}} - \bar{u}_{1\text{max}}}{u_*} \right)^2 - \frac{\bar{u}_{1\text{max}} - U}{u_*} + \frac{1}{2\kappa} = 0 \quad (8.8)$$

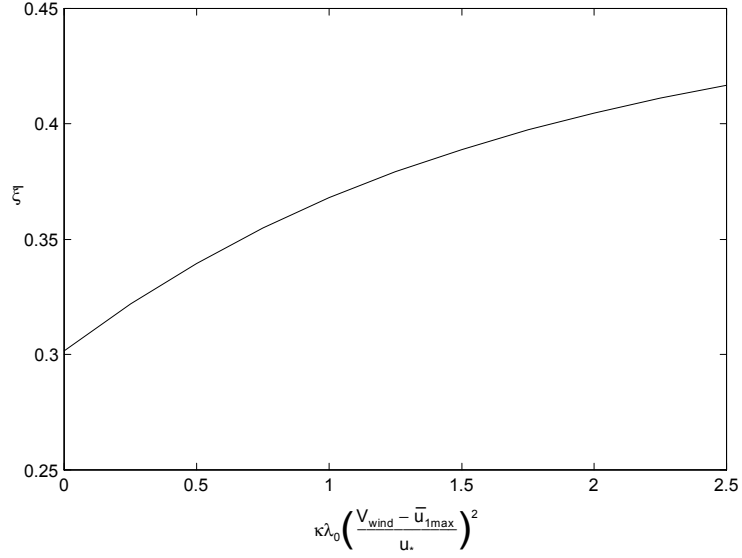


FIG. 8.1: Position of the average velocity versus the water surface shear correction in which κ is the von Karman constant in sediment-laden flows.

Given V_{wind} , U , κ , and λ_0 , one can solve for the maximum velocity $\bar{u}_{1\text{max}}$.

8.2.3 Position of the average velocity U

Equating the right-hand side of (5.23) and the right-hand side of (8.7) and rearranging them, one gets

$$1 + \ln \xi + \left[1 - \kappa \lambda_0 \left(\frac{V_{\text{wind}} - \bar{u}_{1\text{max}}}{u_*} \right)^2 \right] \left(\frac{1}{2} - \xi \right) = 0 \quad (8.9)$$

Again, it is assumed that $\kappa = 0.2 - 0.406$, $\lambda_0 \approx 0.0065$, $V_{\text{wind}} = 0$, $\bar{u}_{1\text{max}}/u_* = 10 - 30$. Then one has

$$0 < \kappa \lambda_0 \left(\frac{V_{\text{wind}} - \bar{u}_{1\text{max}}}{u_*} \right)^2 < 2.5 \quad (8.10)$$

Solving (8.9) for ξ under the condition of (8.10), one obtains the position of the average velocity, which is shown in FIG. 8.1. It can be seen that after the water surface shear correction, the position of the average velocity varies between 0.3 and 0.42.

8.2.4 Procedures for applying the log-linear law

Assume a uniform flow in a wide channel with a plane bed. Provided that the flow depth h , the bed slope S , the sediment size d_s , and the volumetric sediment concentration $\bar{C}_{0.05}$, one may estimate the velocity profile in the following way:

Step 1: Estimate the shear velocity u_* , i.e., $u_* = \sqrt{ghS}$, where g is the gravitational acceleration. Note that for bedform channels, the skin shear velocity u'_* should be used.

Step 2: Estimate the average velocity U . The classical resistance equation by Keulegan (Chien and Wan, 1983, p.205) may be used, i.e.

$$\frac{U}{u_*} = 5.75 \log \left(\frac{hu_*}{\nu} \right) + 3.25 \quad (\text{hydraulically smooth}) \quad (8.11)$$

$$\frac{U}{u_*} = 5.75 \log \left(\frac{h}{k_s} \right) + 6.25 \quad (\text{completely rough}) \quad (8.12)$$

in which ν is the water kinematic viscosity; and the roughness k_s is usually taken as $(2 - 7)d_{50}$ (Chien and Wan, 1983, p.206; Julien, 1995, p.96). For sand bed channels, $k_s = 2.5d_{50}$ may be used.

Step 3: Estimate the Richardson number from (6.46), i.e.

$$R_i = \frac{g\delta}{u_*^2} \frac{\rho_s - \rho_0}{\rho_0} \frac{\bar{C}_{0.05} - \bar{C}_1}{1 + \frac{\rho_s - \rho_0}{\rho_0} \bar{C}_m}$$

in which $\delta = h$ for wide open-channels. For density sediment-laden flows, usually $\bar{C}_1 \ll \bar{C}_{0.05}$, and $\bar{C}_m \ll 1$. Then the above expression reduces to

$$R_i = \frac{g\delta}{u_*^2} \frac{\rho_s - \rho_0}{\rho_0} \bar{C}_{0.05} \quad (8.13)$$

Step 4: Estimate the von Karman constant κ from (7.9), i.e.

$$\frac{\kappa}{\kappa_0} = \exp\{-\beta R_i^m\} - \alpha \bar{C}_{0.05}$$

in which $\kappa_0 = 0.406$, $\beta = 0.0636$, $m = 0.716$, and $\alpha = 0.92$.

Step 5: Assume $\lambda_0 = 0.0065$ for sand channels or calculate λ_0 from (5.33) for gravel channels. With κ , u_* and U , estimate the maximum velocity $\bar{u}_{1\max}$ from (8.8).

Step 6: Estimate the velocity profile with the log-linear law, i.e.

$$\frac{\bar{u}_{1 \max} - \bar{u}_1}{u_*} = -\frac{1}{\kappa} \ln \xi - \left[\frac{1}{\kappa} - \lambda_0 \left(\frac{V_{\text{wind}} - \bar{u}_{1 \max}}{u_*} \right)^2 \right] (1 - \xi)$$

in which V_{wind} may be assumed to be zero in laboratory or measured in field cases.

Chapter 9

SUMMARY AND CONCLUSIONS

9.1 Summary

Turbulent velocity profiles in pipes and open-channels with clear water and sediment-laden flows are investigated. A new similarity analysis method, *the four-step similarity analysis method*, is first presented, which includes dimensional analysis, intermediate asymptotics, wake correction, and boundary correction. Based on the four-step similarity analysis method, a clear water velocity profile model, *the modified log-wake law*, is proposed. The modified log-wake law consists of three components: a log term, a wake term, and a linear term. Physically, the log term expresses the inertia effect; the wake term expresses the large-scale turbulent mixing; and the linear term expresses the boundary condition effect. In open-channels, the wake term reflects the side-wall effect. A theoretical analysis and a magnitude order analysis show that the modified log-wake law is also valid in sediment-laden flows. In particular, the modified log-wake law considers the derivative boundary condition at the boundary layer margin, which is not satisfied in previous studies.

The modified log-wake law has compared quite well with experiments in pipes, narrow open-channels and wide open-channels, including both clear water flows and sediment-laden flows.

In wide channels, the wake component may be neglected. The reduction of the log-wake law is called the *log-linear law*. The log-linear law agrees excellently with both laboratory experiments and field measurements.

Theoretical and experimental analyses show that sediment suspension affects the velocity profile in two ways: changing the fluid viscosity, and obtaining energy from the turbulent energy. Both ways will damp the turbulence intensity and increase the velocity gradient.

As a prerequisite of the velocity profiles in open-channels, an equation for determining the bed shear velocity, based on a conformal mapping method, in smooth rectangular channels is also presented. In addition, an eddy viscosity model is derived from the log-wake law.

9.2 Conclusions

9.2.1 Clear water flows

1. Clear water velocity profiles in pipes and open-channels can be described by the modified log-wake law, i.e.

$$\frac{\bar{u}_{1\max} - \bar{u}_1}{u_*} = -\frac{1}{\kappa_0} \ln \xi + \Omega_0 \cos^2 \frac{\pi \xi}{2} - \left[\frac{1}{\kappa_0} - \lambda_0 \left(\frac{V_{\text{wind}} - \bar{u}_{1\max}}{u_*} \right)^2 \right] (1 - \xi) \quad (3.31)$$

in which $\bar{u}_{1\max}$ = the maximum velocity; u_* = the shear velocity; \bar{u}_1 = the velocity at normalized distance $\xi = x_3/\delta$ ($\delta = R$ for pipes and $\delta = h$ for wide channels) from the bed; κ_0 = the von Karman constant in clear water; Ω_0 = the wake strength coefficient in clear water; λ_0 = the water surface shear effect factor; and V_{wind} = the wind velocity over the water surface. The first term on the right-hand side is the so-called intermediate asymptotics which is the classical log law and reflects the effect of the channel bed; the second term is the so-called wake correction which is the Coles wake function and reflects the effect of the side-walls; and the third term is the so-called boundary correction and reflects the effect of the boundary condition at the boundary layer margin.

2. For pipe flows, $\lambda_0 = 0$. This is because there does not exist a free surface along a pipe axis. Therefore, the modified log-wake law reduces to

$$\frac{\bar{u}_{1\max} - \bar{u}_1}{u_*} = -\frac{1}{\kappa_0} \ln \xi + \Omega_0 \cos^2 \frac{\pi \xi}{2} - \frac{1 - \xi}{\kappa_0} \quad (5.1)$$

Superpipe experiments show that κ_0 and Ω_0 are two universal constants 0.406 and 3.2 for $y^+ \geq 500$, respectively. However, κ_0 may slightly increases with the Reynolds number $\text{Re}_* = u_* R / \nu$, where $R =$ radius of pipe, and $\nu =$ water kinematic viscosity, if the data of $70 < y^+ < 500$ are included.

3. For narrow channels ($a/h < 5$), where the boundary layer thickness is defined as the distance from the bed to the maximum velocity position, as it in pipes, a free surface at the boundary layer margin does not exist. In other words, the velocity gradient and the shear stress are zero at $\xi = 1$. Therefore, the velocity profile equation is the same as that in pipes. Narrow flume experiments show that κ_0 is the same as that in pipes, 0.406 (the average value is 0.405 in narrow channel tests) while Ω_0 decreases with the aspect ratio a/h , see FIG. 5.11. Ω_0 can be estimated by

$$\Omega_0 = \begin{cases} -0.75 \frac{a}{h} + 3.75 & \text{if } a/h < 5 \\ 0 & \text{if } a/h \geq 5 \end{cases} \quad (5.18)$$

4. For wide channels ($a/h \geq 5$), the wake component is very small and negligible, see FIG. 5.11. The modified log-wake law is, then, reduces to the log-linear law as follows:

$$\frac{\bar{u}_{1\max} - \bar{u}_1}{u_*} = -\frac{1}{\kappa_0} \ln \xi - \left[\frac{1}{\kappa_0} - \lambda_0 \left(\frac{V_{\text{wind}} - \bar{u}_{1\max}}{u_*} \right)^2 \right] (1 - \xi) \quad (5.20)$$

in which the water surface shear effect factor can be estimated by the following empirical relation:

$$\lambda \approx \begin{cases} 0.065 & \text{for } k_s/h < 0.024 \\ 0.2163 \frac{k_s}{h} + 0.013 & \text{for } k_s/h \geq 0.024 \end{cases} \quad (5.30)$$

in which $h =$ the flow depth; $k_s = 2.5d_s$; and $d_s =$ sediment diameter. The above equation is valid for both smooth and rough beds. The log-linear law has compared well with 47 laboratory experiments and field measurements, the correlation coefficient r is always greater than 0.99.

9.2.2 Sediment-laden flows

1. The theoretical analysis and experimental data show that the structure of the modified log-wake law is also valid in sediment-laden flows. However, sediment suspension modifies the velocity profile in two factors: sediment concentration and density gradient (the global Richardson number R_i). Since both concentration and density gradient are large near the bed, the effects of sediment suspension mainly occur near the bed.
2. The von Karman constant κ decreases with both concentration and density gradient in a sediment-laden flow. It can be estimated by

$$\frac{\kappa}{\kappa_0} = \exp \{-\beta R_i^m\} - \alpha \bar{C}_{0.05} \quad (7.15)$$

in which κ_0 is the von Karman constant in clear water, 0.406; $\beta = 0.062$ and $m = 0.716$. The Richardson number R_i is defined as

$$R_i = \frac{g\delta}{u_*^2} \frac{\rho_s - \rho_0}{\rho_0} \frac{\bar{C}_{0.05} - \bar{C}_1}{1 + \frac{\rho_s - \rho_0}{\rho_0} \bar{C}_m} \quad (6.46)$$

in which ρ_0 = water density; and ρ_s = sediment density. Given a reference concentration \bar{C}_a at ξ_a . Usually, in sediment-laden flows, $\bar{C}_1 \ll \bar{C}_{0.05}$, and $\bar{C}_m \ll 1$. Then, the Richardson number may reduce to

$$R_i = \frac{g\delta}{u_*^2} \frac{\rho_s - \rho_0}{\rho_0} \bar{C}_{0.05}$$

3. The wake strength coefficient Ω may slightly increase with the concentration. However, in practice, the concentration \bar{C}_1 is usually very small in a density sediment-laden flow. Its effect may be neglected. In addition, like the concentration near the water surface, the density gradient is also very small near the water surface. Therefore, the effect of the density gradient may also be neglected. In other words, the wake strength coefficient Ω in sediment-laden flows can be approximated as $\Omega \approx \Omega_0$, which is estimated from (5.21).
4. Like the wake strength coefficient Ω , both concentration and density gradient have little effect on the water surface shear effect factor λ , i.e., $\lambda \approx \lambda_0$, which is estimated from (5.33).

5. A procedure for applying the modified log-wake law is presented in Chapter 8. However, several parameters, such as the boundary layer thickness δ and the maximum velocity $\bar{u}_{1\max}$ in narrow open-channels, are needed to fully describe velocity profiles in sediment-laden flows.
6. An eddy viscosity model from the modified log-wake law is derived as

$$\varepsilon^+ = \frac{(1 - \xi) + \tau|_{\xi=1} / \tau_0}{\frac{1 - \xi}{\kappa\xi} + \frac{\pi\Omega}{2} \sin \pi\xi + \frac{1}{u_*} \left. \frac{d\bar{u}_1}{d\xi} \right|_{\xi=1}} \quad (3.33)$$

in which $\varepsilon^+ = \varepsilon / (u_*\delta)$ is the dimensionless eddy viscosity. The above model is compatible to experiments in pipes, narrow channels and wide channels.

9.3 Recommendations

Except those questions raised in the above section, an immediate recommendation is to apply the modified log-wake over a dune-bed flow and to correlate the pressure gradient to the wake strength coefficient Ω_0 . Then a reasonable velocity profile model for dune-bed flows may be derived. This is very helpful to study the skin friction in a bedform channel.

Another immediate recommendation is to try a three-dimensional velocity profile law over the whole cross-section in narrow channels, based on the modified log-wake law.

In addition, based on the power law in the overlap, a power-wake law in open-channels, as it in pipes (Appendix A), may be worthy to try in the future.

REFERENCES

- Barenblatt, G. I. (1953). "On the motion of suspended particles in a turbulent flow." *Prikl. Mat. Mekh.*, 17(3), 261-274.
- Barenblatt, G. I. (1996). "Scaling, self-similarity, and intermediate asymptotics." Cambridge University Press.
- Barton, J. K. and Lin, P. N. (1955). "A study of sediment transport in alluvial channels." Report No. 55JRB2, Civil Engineering Department, Colorado State University, Fort Collins, CO.
- Chen, Y. (1984). "Vertical distribution of suspended sediment in open channel." *J. Sediment Research*, Beijing, China, (1), 31-40 (in Chinese).
- Chien, N. and Wan, Z. H. (1983). *Sediment Transport Mechanics*. China Science Press, Beijing, China (in Chinese).
- Cioffi F. and Gallerano, F. (1991). "Velocity and concentration profiles of solid particles in a channel with movable and erodible bed." *J. Hydr. Engrg.*, ASCE, 29(3), 387-401.
- Coleman, N. L. (1970). "Flume studies of the sediment transport coefficient." *Water Resources Research*, AGU, 6(3), 801-809.
- Coleman, N. L. (1981). "Velocity profiles with suspended sediment." *J. Hydr. Res.*, 19(3), 211-229.
- Coleman, N. L. (1986). "Effects of suspended sediment on the open-channel distribution." *Water Resources Research*, AGU, 22(10), 1377-1384.

- Coles, D. E. (1956). "The law of the wake in the turbulent boundary layer." *J. Fluid Mechanics*, 1, 191-226.
- Coles, D. (1969). "The young person's guide to the data." *Proceedings Computation of Turbulent Boundary Layers — 1968 AFOSR-IFP-STANFORD CONFERENCE*, 2, 1-19.
- Dou, Guoren (1987). *Turbulence*, Vol. 2, Higher Education Press, Beijing, China (in Chinese).
- Einstein, H. A. and Chien, N. (1955). "Effects of heavy sediment concentration near the bed on velocity and sediment distribution." U. S. Army Corps of Engineers, Missouri River Division Rep. No. 8.
- Elata, C. and Ippen, A. T. (1961). "The dynamics of open channel flow with suspensions of neutrally buoyant particles." Technical Report No. 45, Hydrodynamics Lab, MIT.
- Guy, H. P., Simons, D. B. and Richardson, E. V. (1966). *Summary of alluvial channel data from flume experiments, 1956-1961*. USGS Professional Paper 462-I.
- Hinze, J. O. (1975). *Turbulence*. 2nd Ed., McGraw-Hill, New York.
- Hu, C. H. and Hui, Y. J. (1995). *Mechanical and Statistical Laws in Open-Channel Flows*. China Science Press, Beijing, China (in Chinese).
- Ippen, A. T. (1971). "A new look at sedimentation in turbulent streams." *J. Boston Civil Engineers*, 58(3), 131-163.
- Itakura, T. and Kishi, T. (1980). "Open channel flow with suspended sediments." *J. Hydr. Div.*, ASCE, 106(8), 1325-1343.
- Janin, L. F. (1986). "Sediment-laden velocity profiles developed in a large boundary-layer wind tunnel.." PhD dissertation, Colorado State University, Fort Collins, CO.

- Julien, P. Y. (1995). *Erosion and Sedimentation*. Cambridge University Press.
- Karim, M. F. and Kennedy, J. F. (1987). "velocity and sediment-concentration profiles in river flows." *J. Hydr. Engrg.*, ASCE, 113(2), 159-178.
- Kereselidze, N. B. and Kutavaia, V. I. (1995). "Experimental research on kinematics of flows with high suspended solid concentration." *J. Hydr. Res.*, 33(1), 65-75.
- Keulegan, G. H. (1938). "Laws of turbulent flow in open channels." *J. Research.*, Nat. Bureau of Standards, 21(6), 707-741.
- Kironoto, B. A. (1993). *Turbulence characteristics of uniform and non-uniform, rough open-channel flow*. PhD Dissertation, Swiss Federal Institute of Technology at Lausanne, Switzerland.
- Kironoto, B. A. and Graf, W. H. (1994). "Turbulence characteristics in rough uniform open-channel flow." *Proc. Instn Civ. Engrs Wat. Marit. & Energy*, 106(12), 333-344.
- Knight, D. W., Demetriou, J. D. and Hamed M. E. (1984). "Boundary shear in smooth rectangular channels." *J. Hydr. Engrg.*, ASCE, 110(4), 405-422.
- Kolmogorov, A. N. (1954). "On a new variant of the gravitational theory of motion of suspended sediment." *Vestn. MGU*, 3, 41-45.
- Kundu, P. K. (1990). *Fluid Mechanics*. Academic Press, Inc., New York.
- Laufer, J. (1954). The structure of turbulence in fully developed pipe flow. Report 1174, National Advisory Committee for Aeronautics, Washington, D. C.
- Lyn, D. A. (1986). *Turbulence and turbulent transport in sediment-laden open-channel flows*. W. M. Keck Laboratory of Hydraulics and Water Resources, California Institute of Technology, Pasadena, California.
- Lyn, D. A. (1988). "A similarity approach to turbulent sediment-laden flows in open channels." *J. Fluid Mechanics*, 193, 1-26.

- McCutcheon, S. C. (1981). "Vertical velocity profiles in stratified flows." *J. Hydr. Div.*, ASCE, 107(8), 973-988.
- McQivey, R. S. (1971). *Summary of turbulent data from rivers, conveyance channels, and laboratory flumes*. USGS Professional Paper 802-B.
- McTigue, D. F. (1981). "Mixture theory for suspended sediment transport." *J. Hydr. Engrg.*, ASCE, 107(6), 659-673.
- Millikan, C. B. A. (1938). *Proc. of 5th international congress on applied mechanics*. John Wiley, 386-392.
- Muste, M. (1995). *Particle and liquid velocity measurements in sediment-laden flows with a discriminator laser-doppler velocimeter*. PhD Dissertation, University of Iowa, Iowa City, Iowa.
- Muste, M. and Patel, V. C. (1997). "Velocity profiles for particles and liquid in open-channel flow with suspended sediment." *J. Hydr. Engrg.*, ASCE, 123(9), 742-751.
- Nezu, I. and Nakagawa, H. (1993). *Turbulence in open-channel flows*. IAHR Monograph Series, A.A. Balkema Publishers, Old Post Road, Brookfield, VT, USA.
- Nezu, I., Kadoto, A., and Nakagawa, H. (1997). "Turbulent structure in unsteady depth-varying open-channel flows." *J. Hydr. Engrg.*, ASCE, 123(9), 764-773.
- Ni, J. and Hui, Y. (1988). "The relation between the velocity distribution and the suspended concentration distribution." *J. Sediment Research*, Beijing, China, (2), 17-27 (in Chinese).
- Nikuradse, J. (1932). *Gesetzmässigkeiten der turbulenten strömung in glatten röhren*. VDI Forschungscheft No. 356.
- Parker, G. and Coleman, N. L. (1986). "Simple model of sediment-laden flows." *J. Hydr. Engrg.*, ASCE, 112(5), 356-375.

- Patel, V. C. and Head, M. R. (1969). "Some observations on skin friction and velocity profiles in fully developed pipe and channel flows." *J. Fluid Mechanics*, 38(1), 181-201.
- Roll, H. U. (1965). *Physics of the Marine Atmosphere*. Academic Press, New York and London.
- Sarma, K. V. N., Lakshminarayana, P., and Rao, N. S. L. (1983). "Velocity distribution in smooth rectangular open channels." *J. Hydr. Engrg.*, ASCE, 109(2), 271-289.
- Schlichting, H. (1979). *Boundary-layer Theory*. McGraw-Hill Book Company, New York.
- Spiegel, E. A. and Veronis, G. (1960). "On the Boussinesq approximation for a compressible fluid." *Astrophysical Journal*, 131, 442-447.
- Spiegel, M. R. (1993). *Complex Variables*. McGraw-Hill, Inc., New York.
- Umeyama, M. and Gerritsen, F. (1992). "Velocity distribution in uniform sediment-laden flow." *J. Hydr. Engrg.*, ASCE, 118(2), 229-245.
- van Rijn, L. C. (1984). "Sediment transport, Part II: Suspended load transport." *J. Hydr. Engrg.*, ASCE, 110(11), 1613-1641.
- Vanoni, V. A. (1946). "Transportation of suspended sediment by running water." *Trans.*, ASCE, 111, 67-133.
- Vanoni, V. A. (1975). *Sedimentation Engineering*. ASCE Manual, Washington D. C.
- Vanoni, V. A. and Nomicos, G. N. (1960). "Resistance properties in sediment-laden streams." *Trans.*, ASCE, 125, Paper No. 3055, 1140-1175.
- Wang, X. and Qian, N. (1989). "Turbulence characteristics of sediment-laden flows." *J. Hydr. Engrg.*, ASCE, 115(6), 781-799.

- White, F. M. (1986). *Fluid Mechanics*. 2nd ed., McGraw-Hill Book Company, New York.
- White, F. M. (1991). *Viscous fluid flow*. McGraw-Hill Book Company, New York.
- Woo, H. S., Julien, P. Y. and Richardson, E. V. (1988). "Suspension of large concentration of sands." *J. Hydr. Engrg.*, ASCE, 114(8), 888-889.
- Yang, Shu-Qing and Lim, Siow-Yong (1997). "Mechanism of energy transportation and turbulent flow in a 3D channel." *J. Hydr. Engrg.*, ASCE, 123(8), 684-692.
- Zagarola, M. V. (1996). "Mean-flow scaling of turbulent pipe flow." PhD Dissertation, Princeton University, Princeton, NJ.
- Zhou, D. and Ni, J. R. (1995). "Effects of dynamic interaction on sediment-laden turbulent flows." *J. Geophy. Res.*, AGU, 100(C1), 981-996.

Appendix A

POWER-WAKE LAW IN TURBULENT PIPE FLOWS

Development of the power-wake law

Similar to the development of the modified log-wake law in Chapter 3, a power-wake law can be derived based on the four-step similarity analysis method and the assumption of incomplete similarity.

Dimensional analysis

Considering the velocity gradient in a turbulent shear flow, one has (Barenblatt, 1996, p.269):

$$\frac{\partial \bar{u}_1}{\partial x_3} = f(\tau_0, \rho_0, x_3, \nu, \delta) \quad (\text{A.1})$$

in which \bar{u}_1 is the velocity in the flow direction x_1 , x_3 is the distance from the wall; τ_0 is the wall shear stress; ρ_0 is the fluid density; ν is the fluid kinematic viscosity; and δ is the boundary layer thickness or the pipe radius.

The above equation can be rewritten as a dimensionless form, i.e.

$$\frac{x_3}{u_*} \frac{\partial \bar{u}_1}{\partial x_3} = \Phi_1 \left(\frac{u_* x_3}{\nu}, \frac{u_* \delta}{\nu} \right) \quad (\text{A.2})$$

Intermediate asymptotics

Following Barenblatt (1996, p.271), one assumes that the flow is incomplete similarity with respect to the local Reynolds number u_*x_3/ν and lack of self-similarity with respect to the global Reynolds number $u_*\delta/\nu$. According to (3.3), (A.2) may be written as follows:

$$\frac{x_3}{u_*} \frac{\partial \bar{u}_1}{\partial x_3} = \left(\frac{u_*x_3}{\nu} \right)^\alpha \Phi \left(\frac{u_*\delta}{\nu} \right) \quad (\text{A.3})$$

in which α is an experimental parameter.

The integration of the above equation gives that

$$\frac{\bar{u}_1}{u_*} = C_i \left(\frac{u_*x_3}{\nu} \right)^\alpha + C_4 \quad (\text{A.4})$$

in which $C_i = (1/\alpha)\Phi(u_*\delta/\nu)$; and C_4 is usually taken as zero experimentally. This equation is the so-called power law in the intermediate subregion.

If one writes the above power law in terms of the outer variable $\xi = x_3/\delta$, then one has

$$\frac{\bar{u}_1}{u_*} = C_o \xi^\alpha \quad (\text{A.5})$$

in which $C_o = C_i(u_*\delta/\nu)^\alpha$.

Wake correction

Similar to the modified log-wake law, the Coles wake function is regarded as a good approximation of the wake correction function. Then the above power law may be extended to the wake layer by adding the Coles wake function, i.e.

$$\frac{\bar{u}_1}{u_*} = C_o \xi^\alpha + \Omega_0 \sin^2 \frac{\pi \xi}{2} \quad (\text{A.6})$$

Boundary correction

The above equation does not satisfy the derivative boundary condition at the axis, i.e. $d\bar{u}_1/d\xi = 0$ is not satisfied at $\xi = 1$. To force it to satisfy the derivative boundary condition, one must add a linear term $\alpha C_o(1 - \xi)$, i.e.

$$\frac{\bar{u}_1}{u_*} = C_o \xi^\alpha + \Omega_0 \sin^2 \frac{\pi \xi}{2} + \alpha C_o(1 - \xi) \quad (\text{A.7})$$

Considering the relation

$$\frac{\bar{u}_{1\max}}{u_*} = C_0 + \Omega_0 \quad (\text{A.8})$$

the above equation may be written as a defect form, i.e.

$$\boxed{\frac{\bar{u}_{1\max} - \bar{u}_1}{u_*} = C_0(1 - \xi^\alpha) + \Omega_0 \cos^2 \frac{\pi\xi}{2} - \alpha C_o(1 - \xi)} \quad (\text{A.9})$$

This equation is referred to as the *power-wake law*. It is similar to the modified log-wake law, except the intermediate asymptotics is different. Like the modified log-wake law, it is a two parameter model since given $\bar{u}_{1\max}$, C_o and Ω_0 must satisfy (A.8).

Determinations of α and C_o in the power-wake law

The least-squares method is also used to find α and C_o . The least-squares approximation is written as

$$S = \sum_i^n \left[\frac{\bar{u}_{1i}}{u_*} - C_o \xi_i^\alpha - \left(\frac{\bar{u}_{1\max}}{u_*} - C_o \right) \sin^2 \frac{\pi\xi_i}{2} - \alpha C_o(1 - \xi_i) \right]^2$$

$$\Rightarrow \text{minimum} \quad (\text{A.10})$$

in which (A.8) has been used; α and C_o are solving parameters; and all others are the same as those in (5.3). The parameters α and C_o are solved by setting

$$\frac{\partial S}{\partial \alpha} = 0 \quad \text{and} \quad \frac{\partial S}{\partial C_o} = 0 \quad (\text{A.11})$$

i.e.,

$$\sum_i^n \left[\frac{\bar{u}_{1i}}{u_*} - C_o \xi_i^\alpha - \left(\frac{\bar{u}_{1\max}}{u_*} - C_o \right) \sin^2 \frac{\pi\xi_i}{2} - \alpha C_o(1 - \xi_i) \right] [\xi_i^\alpha \ln \xi_i + (1 - \xi_i)]$$

$$= 0 \quad (\text{A.12})$$

$$\sum_i^n \left[\frac{\bar{u}_{1i}}{u_*} - C_o \xi_i^\alpha - \left(\frac{\bar{u}_{1\max}}{u_*} - C_o \right) \sin^2 \frac{\pi\xi_i}{2} - \alpha C_o(1 - \xi_i) \right] \left[\xi_i^\alpha - \sin^2 \frac{\pi\xi_i}{2} + \alpha(1 - \xi_i) \right]$$

$$= 0 \quad (\text{A.13})$$

Unlike (5.7) and (5.8), the above two equations are complicated nonlinear equations. Fortunately, the least-squares function in MATLAB can ease this process.

Test of the power-wake law

The power-wake law is based on the assumption of incomplete similarity, hence the parameters α and C_o certainly vary with Reynolds number Re_* . According to Zagarola (1996), the lower limit of the power law is $y^+ = 50$. A comparison of the power-wake law with some experimental profiles is shown in FIG. A.1 (dashed line). An excellent agreement is again obtained for each run. The individual values of α and C_o , computed by the least-squares method, are listed in Table A.1. Following the suggestion of Barenblatt (1993), α and C_o may be series in terms of $1/\ln Re_*$. Using the data of Table A.1, α and C_o may be approximated by

$$\alpha = \frac{3.605}{\ln Re_*} - \frac{81.5}{\ln^2 Re_*} + \frac{890.1}{\ln^3 Re_*} - \frac{2962.3}{\ln^4 Re_*} + \dots \quad (\text{A.14})$$

and

$$C_o = 1.8125 \ln Re_* + 14.11 - \frac{42.39}{\ln Re_*} + \dots \quad (\text{A.15})$$

The above two equations along with experimental data are shown in FIG. A.2a and FIG. A.2b. Apparently, this analysis shows that the structure of the power-wake law is also correct, the parameters α and C_o vary systematically with Reynolds number Re_* .

The comparison of the power-wake law and the modified log-wake law in FIG. A.1 shows that both the modified log-wake law and the power wake law are excellent approximations for turbulent flows in pipes.

Table A.1: The model parameters in the power-wake law for individual velocity profiles (Velocity profile data source: Zagarola, 1996)

Run	Reynolds Number Re (10^4)	Reynolds Number Re _* (10^3)	α	C_o	Correlation Coefficient r
1	3.16	0.85	0.211	20.08	0.9998
2	4.17	1.09	0.213	20.69	0.9998
3	5.67	1.43	0.209	21.40	0.9999
4	7.43	1.93	0.203	22.07	0.9999
5	9.88	2.34	0.196	22.70	0.9999
6	14.58	3.32	0.189	23.66	0.9999
7	18.54	4.12	0.183	24.21	0.9999
8	23.05	5.02	0.177	24.70	0.9999
9	30.95	6.59	0.169	25.25	0.9998
10	40.93	8.49	0.164	25.93	0.9998
11	53.91	10.94	0.157	26.47	0.9997
12	75.18	14.83	0.147	27.09	0.9997
13	102.38	19.68	0.141	27.74	0.9997
14	134.04	25.23	0.134	28.24	0.9998
15	178.75	32.88	0.131	28.86	0.9998
16	234.50	42.16	0.124	29.40	0.9999
17	309.81	54.65	0.120	29.89	0.9999
18	442.03	76.10	0.117	30.62	0.9998
19	607.27	102.19	0.113	31.28	0.9999
20	771.47	127.32	0.110	31.83	0.9999
21	1024.90	165.56	0.108	32.49	0.9999
22	1359.80	216.04	0.106	33.01	0.9999
23	1819.60	283.32	0.100	33.53	1.0000
24	2397.70	367.00	0.096	34.00	1.0000
25	2992.70	452.40	0.096	34.48	0.9999
26	3525.90	528.57	0.094	34.73	0.9999

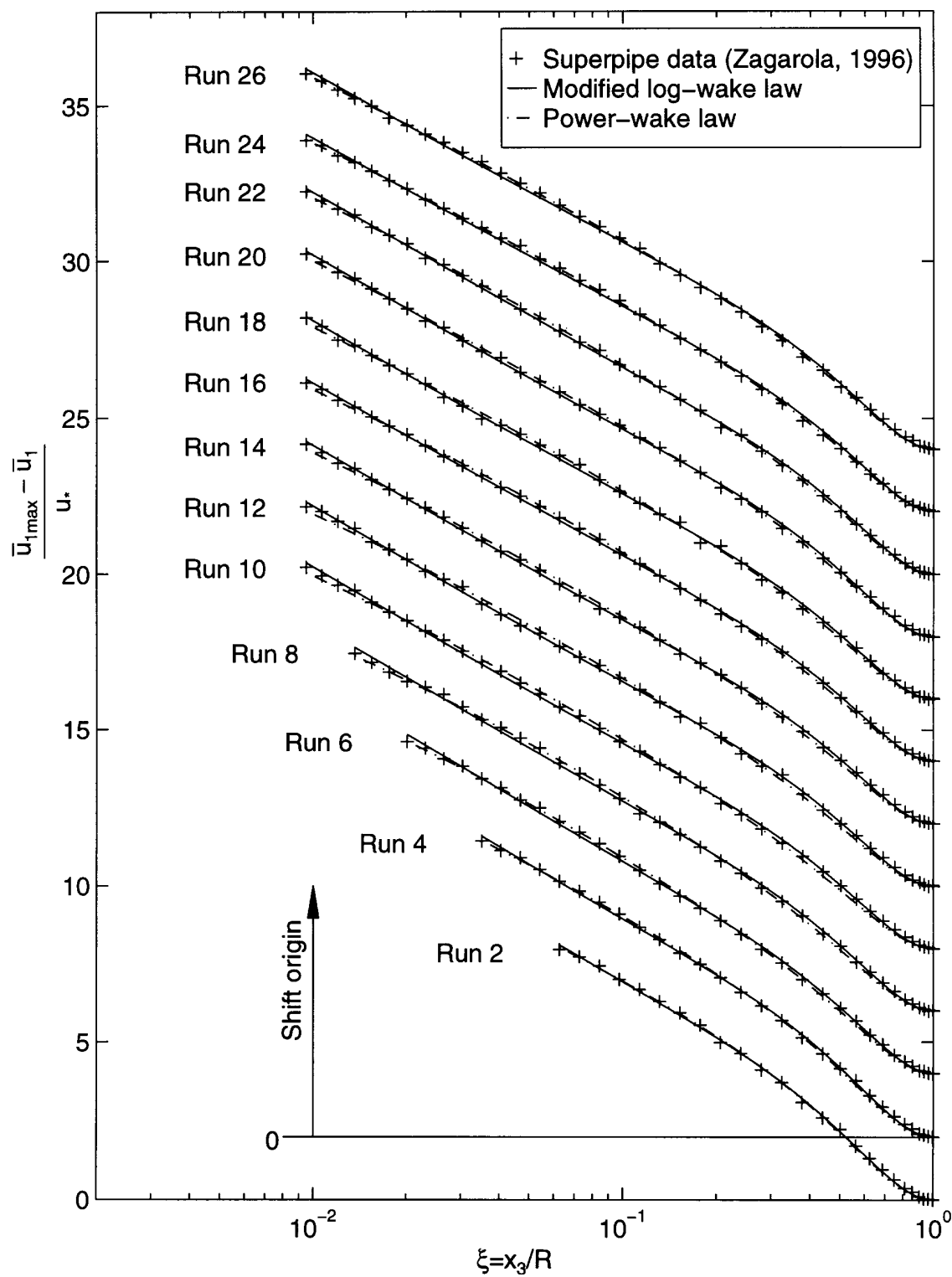


FIG. A.1: Comparison among the power-wake law, the modified log-wake law and Zagarola's superpipe experimental data ($y^+ \geq 50$)

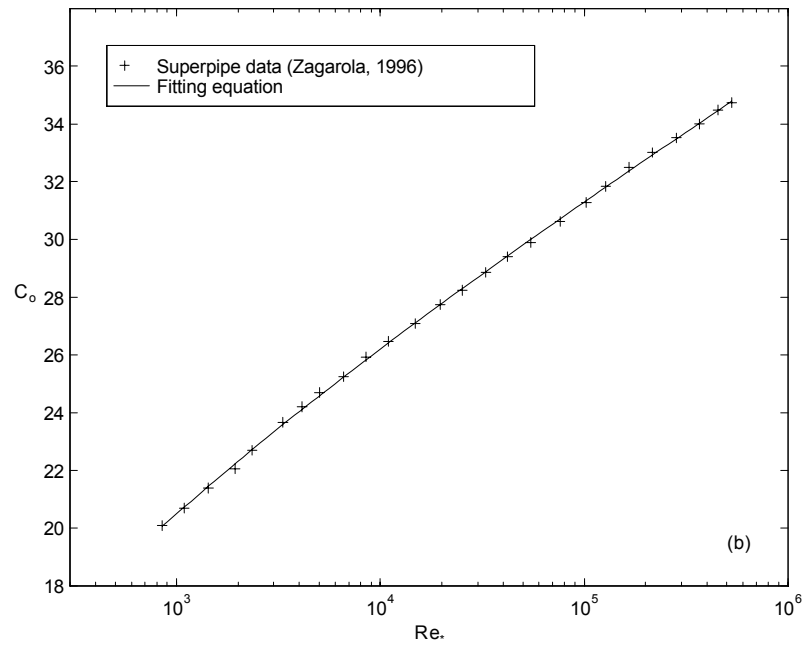
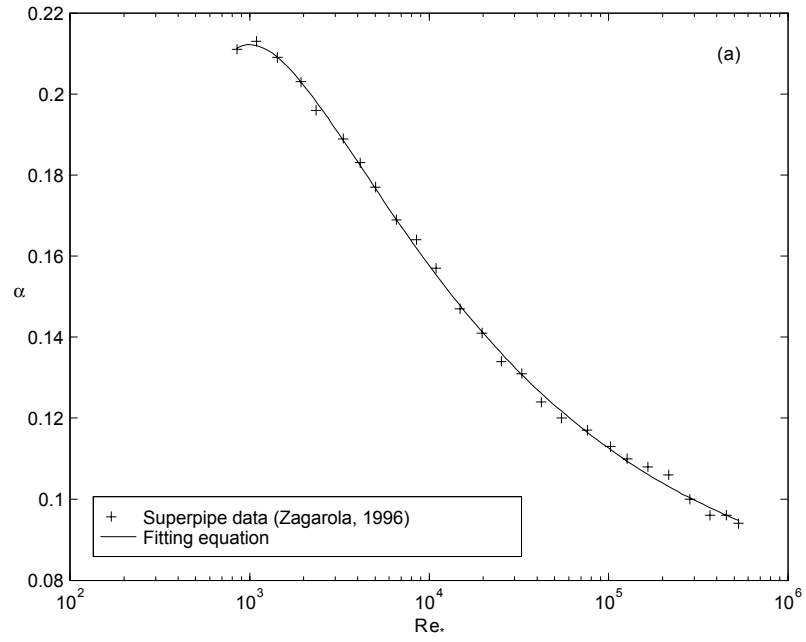


FIG. A.2: The variations of the model parameters with Reynolds number: (a) α versus Re_* , (b) C_o versus Re_*

Appendix B

MATLAB PROGRAMS

Program for solving κ and Ω in the modified log-wake law

```
%%%%%%%%%%%%%%%%%%%%%%%%%%%%%%%%%%%%%%%%%%%%%%%%%%%%%%%%%%%%%%%%%%%%%%%%%
% MATLAB PROGRAM FOR SOLVING THE VON KARMAN CONSTANT kappa AND
% THE WAKE STRENGTH COEFFICIENT W_0
%
% GIVEN:
% u_1max: MAXIMUM VELOCITY;
% u_*: SHEAR VELOCITY; and
% (xi_i, u_1i): SAMPLE POINTS.
%
% FIND: kappa AND Omega
%
% Written by Junke Guo, Mar. 20, 1997
%%%%%%%%%%%%%%%%%%%%%%%%%%%%%%%%%%%%%%%%%%%%%%%%%%%%%%%%%%%%%%%%%%%%%%%%%

% Replace the following question marks with right numbers
u1max = ?; % maximum velocity
ustar = ?; % shear velocity
x = [?]; % normalized distance by flow depth, x = xi
u1 = [?]; % sampling velocity

% Define the velocity defect phi
phi = (u1max - u1)./ustar;

% Plot sample data
semilogx(x,phi,'+'), hold on

% Find kappa, Omega and correlation coefficient r
p = curvefit(x,phi,'[-log(x)-(1-x) cos(pi./2.*x).^2]',[1 1 0 '+']); %Function
kappa = 1./p(1); Omega = p(2); r = p(3); % Correlation coefficient

% Plot fitting equation
```

```

x = logspace(log10(0.005),0,100);
y = p(1).*(-log(x)-(1-x)) + p(2).*cos(pi./2.*x).^2;
semilogx(x,y,'r'), hold off
legend('Measured data','Modified log-wake law')
xlabel('\xi = x_3/R')
ylabel('\frac{u{\left{6.7}\up{5}\-}_{1max} \- u{\left{6.7}\up{5}\-}_1}{u_*}')

```

%%%

```

function pr=curvefit(x,y,arg3,options)
%%%%%%%%%%%%%%%%%%%%%%%%%%%%%%%%%%%%%%%%%%%%%%%%%%%%%%%%%%%%%%%%%%%%%%%%%
% CURVEFIT Curve fitting and plotting routine
% pr = [parameters_fitted; corrcoef].
%
% CURVEFIT(X,Y) plots the points specified by the vectors
% X and Y using the symbol '*', and simultaneously plots a
% straight line that represents the best linear fit to
% the data.
%
% CURVEFIT(X,Y,N) for integer N fits an Nth order polynomial
% to the data.
%
% CURVEFIT(X,Y,'[F1(x) F2(x) ...]') fits Y to the closest
% linear combinations of the vectors F1(x), F2(x), etc.
% This is useful for fitting arbitrary functions of X to Y.
% (Ie. curvefit(X,Y,'[exp(X) cos(2*X)]')
%
% P=CURVEFIT(X,Y,...) returns the estimated fitting
% coefficients in the vector P. In the polynomial fitting case,
% the P coefficients are ordered highest order first (slope,
% then y-intercept in the 1st order case).
%
% CURVEFIT(X,Y,N,OPTIONS) allow the caller to specify certain
% options. If OPTIONS(1)=1, then no plot is generated. This
% useful if the caller is only interested in the returned
% values. If OPTIONS(2)=1, then the X-axis is plotted on
% a log scale. If OPTIONS(3)=1, then the Y-axis is plotted on
% a log scale. If OPTIONS(4) is specified, it's value is
% assumed to be a character representing the symbol to use
% to plot the original data, which has a default value of '*'.
% This element can be set to the character 'i' for invisible if
% only the best-fit curve is desired in the plot.
%
% Written by Junke Guo, Dec. 29, 1996
%%%%%%%%%%%%%%%%%%%%%%%%%%%%%%%%%%%%%%%%%%%%%%%%%%%%%%%%%%%%%%%%%%%%%%%%%

```

```

if nargin<2, error('too few arguments'); end
f = [];
if nargin<4,
options=[0 0 0 '*'];
else
options=options(:)'; %Forces options to be a row vector

% This zeros all non-existent terms.

```

```

    if length(options)<4, options(4)='*'; end
end

% Regulate input data to columns
x = x(:); y = y(:);

if nargin<3,
    N=1; % Fit a straight line
else
    % if arg3 is a scalar, set N to it.
    [r,c]=size(arg3);
    if max([r,c])==1, N=arg3;
        else
            f=eval(arg3);
        end
    end
end

if isempty(f),
    P = polyfit(x,y,N);
    yfitted = polyval(P,x);
else
    % Determine the size of f
    [r c] = size(f);
    N = c;

    % Determine the matrix of linear system equations
    for j=1:N
        for k=1:N, a = f(:,j).*f(:,k); A(j,k) = sum(a); end
        b = f(:,j).*y; B(j) = sum(b);
    end
    B = B(:);

    % Determine the fitted coefficients
    P = A\B;

    % Determine the fitted values of y
    yfitted = f*P;
end

% Calculate correlation coefficient
R = corrcoef(y,yfitted); R = R(1,2);

if options(1)~=1, % If we are plotting...

    % Determine which plot command to use.
    if options(2)==0,
        if options(3)==0,
            plotcmd = 'plot';
        else
            plotcmd = 'semilogy';
        end
    else
        if options(3)==0,
            plotcmd = 'semilogx';
        end
    end
end

```

```

else
    plotcmd = 'loglog';
end
end

% Plot data
eval([plotcmd '(x,y,options(4))']); hold on

% Plot fitted equation
x = linspace(min(x),max(x),100); x=x(:);
if isempty(f)
    y1 = polyval(P,x);
else
    f = eval(arg3);
    y1 = f*P;
end
plot(x,y1); hold off
end

if isempty(f)
    pr = [P R];
else
    pr = [P' R];
end
end

```

Program for solving κ , $\bar{u}_{1\max}$ and λ in the log-linear law

```

%%%%%%%%%%%%%%%%%%%%%%%%%%%%%%%%%%%%%%%%%%%%%%%%%%%%%%%%%%%%%%%%%%%%%%%%
% Program for solving kappa or u_star, u_1max and epsilon_0
% in the log-linear law
%
% Given:
% kappa: the vonKarman constant; and
% (xi_i, u_1i): sample data.
%
% Find:
% u_star: shear velocity;
% u_1max: water surface velocity; and
% lambda: dimensionless eddy viscosity at the water surface.
%
% Written by Junke Guo, Mar. 23, 1997
%%%%%%%%%%%%%%%%%%%%%%%%%%%%%%%%%%%%%%%%%%%%%%%%%%%%%%%%%%%%%%%%%%%%%%%%

% Replace the following question marks with right values
x = [?]; %x = xi; normalized distance from the bed
u = [?]; %measured velocity with dimension.

% Find u_star, u_1max and epsilon_0
p = curvefit(x,u,'[(log(x)+1-x) -(1-x) ones(size(x))]',[1 1 0 '+']);

```

```

k = 0.406;
ustar = 0.406.*p(1);
lambda = p(2)./ustar./(max(u)./ustar).^2;

x1 = 0.01:0.01:1;
y1 = -1./k.*(log(x1)+1-x1) + p(2)./ustar.*(1-x1);

figure(1)
semilogy(u./ustar,x,'o',max(u)./ustar-y1,x1)
xlabel('u{\left{7}\up{7}\-}_1/u_*')
ylabel('\down{-30}\frac{x_3}{\delta}', 'Rot', 0)

xmin = floor(min(max(u)./ustar-y1)-0.5);
xmax = ceil(max(max(u)./ustar-y1)+0.5);
axis([xmin xmax 0.004 4])

leg = legend('Data of Kironoto (1993)', 'Log-linear law');
set(leg, 'position', [0.15 0.75 0.4 0.15])

t3 = xmin + 0.2.*(xmax - xmin);
stext(t3, 0.3, 'run')

t4 = xmin + 0.9.*(xmax - xmin);
stext(t4, 0.008, '(a)')

eval(['printsto ', run, 'a'])

figure(2)
plot(u./ustar,x,'o',max(u)./ustar-y1,x1)
axis([xmin xmax 0 1.2])
xlabel('u{\left{7}\up{7}\-}_1/u_*')
ylabel('\down{0}\frac{x_3}{\delta}', 'Rot', 0)

legend('Data of Kironoto (1993)', 'Log-linear law')
set(leg, 'position', [0.15 0.75 0.4 0.15])

t0 = xmin + 0.225.*(xmax - xmin);
stext(t0, 0.85, [run, ' (k_s= 4.8 mm)'])

t1 = xmin + 0.1.*(xmax - xmin);
stext(t1, 0.7, ['h = ', num2str(h*100), ' cm'])
stext(t1, 0.6, ['a/h = ', num2str(wh)])
stext(t1, 0.5, ['u_* = ', num2str(ustar*100), ' cm/s'])
stext(t1, 0.4, ['u\bar_{1max}= ', num2str(max(u)), ' m/s'])

t2 = xmin + 0.43.*(xmax - xmin);
stext(t2, 0.7, ['\kappa = ', num2str(k)])
stext(t2, 0.6, ['\lambda = ', num2str(lambda)])
stext(t2, 0.5, ['r = ', num2str(p(3))])

stext(t4, 0.14, '(b)')

eval(['printsto ', run, 'b'])

```

Appendix C

ANALYSIS OF WANG-QIAN'S EXPERIMENTAL DATA

Introduction of the experiments

Xing-Kui Wang, under the guidance of Dr. Ning Qian, did a series of experiments with both plastic particles and natural sediments in the Sedimentation Laboratory, Tsinghua University, Beijing, China (Wang and Qian, 1989). The experiments were conducted in a recirculating, tilting flume 20 m long, 30 cm wide, and 40 cm high. The velocity and concentration profiles were taken at the central vertical of the section 12.3 m downstream from the entrance. The channel bed was lined with concrete plate and analysis of time-average velocity data connected with these data indicated a hydraulic smooth surface. The bed slope $S = 0.01$.

During the experiment, a uniform flow was maintained. As the bases of the study, 6 clear water and pure salt water experiments were measured, i.e., CW1, CW2, CW3, CW4, SW1, and SW2. To study the effects of molecular viscosity, several neutral particle-laden velocity profiles (salt water + plastic particles) were measured, NF1, NF2, NF3, NF4, NF5, NM1, NM2, NM3, NM4, NM5, NM6, NM7, NC1, NC2, NC3, NC4, NC5, NC6, and NC7. To study the effects of density gradient effects, several density experiments (water + plastic particles, $G = 1.05$; water + natural sediments, $G = 2.64$) were measured, i.e., SF1, SF2, SF3, SF4, SF5, SF6, SM1, SM2, SM3, SM4, SM5, SM6, SM7, SC1, SC2, SC3, SC4, SC5, SC6, SC7, SQ1, SQ2, and SQ3.

The flow depth h is shown in the following tables and plots. The sediment sizes

are as follows:

- NF1-3: Salt water + fine plastic particles ($d_m = 0.266$ mm, $d_{50} = 0.268$ mm)
- NM1-4: Salt water + middle plastic particles ($d_m = 0.96$ mm, $d_{50} = 0.96$ mm)
- NC1-4: Salt water + coarse plastic particles ($d_m = 1.42$ mm, $d_{50} = 1.42$ mm)
- SF1-6: Clear water + fine plastic particles ($d_m = 0.266$ mm, $d_{50} = 0.268$ mm)
- SM1-7: Clear water + middle plastic particles ($d_m = 0.96$ mm, $d_{50} = 0.96$ mm)
- SC1-7: Clear water + coarse plastic particles ($d_m = 1.42$ mm, $d_{50} = 1.42$ mm)
- SQ1-3: Clear water + Qin-Huang-Dao beach sands ($d_m = 0.15$ mm, $d_{50} = 0.137$ mm)

Measurements of velocity profile and concentration profile data (Wang and Qian, 1989)

The velocity profile data of clear water and salt water flows are listed in Table C.1. The neutral particle experiment data are listed in Table C.2. The density velocity profile data are tabulated in Table C.3. The concentration profile data of the density flows are shown in Table C.4.

Velocity profile analysis

All velocity profile analyses are attached after the tables. Run numbers are shown in the figures. In each figure, (a) is a semilog plot where the velocity profile near the bed is emphasized; and (b) is a rectangular plot where the velocity profile near the water surface is emphasized.

Table C.1: Wang-Qian's (1989) measurements of elocity profiles in clear water and salt water

x_3/h	CW1		CW2		CW3		CW4		SW1		SW2	
	\bar{u}_1 (m/s)											
0.008	1.269	1.231	1.199	1.166	1.166	1.208	1.227					
0.010	1.306	1.266	1.233	1.158	1.158	1.213	1.231					
0.012	1.318	1.309	1.310	1.217	1.217	1.269	1.259					
0.016	1.396	1.346	1.353	1.249	1.249	1.306	1.327					
0.020	1.433	1.413	1.404	1.315	1.315	1.320	1.387					
0.026	1.469	1.458	1.467	1.368	1.368	1.399	1.437					
0.033	1.535	1.526	1.511	1.404	1.404	1.479	1.492					
0.040	1.595	1.537	1.579	1.442	1.442	1.521	1.515					
0.050	1.637	1.605	1.601	1.484	1.484	1.538	1.571					
0.065	1.686	1.661	1.676	1.527	1.527	1.617	1.620					
0.080	1.746	1.689	1.706	1.572	1.572	1.645	1.636					
0.100	1.780	1.751	1.756	1.610	1.610	1.732	1.700					
0.150	1.850	1.837	1.858	1.701	1.701	1.782	1.788					
0.220	1.935	1.923	1.929	1.792	1.792	1.869	1.848					
0.300	1.997	1.993	1.991	1.830	1.830	1.936	1.903					
0.400	2.052	2.053	2.056	1.906	1.906	2.008	1.978					
0.500	2.100	2.079	2.091	1.924	1.924	2.035	2.041					
0.600	2.111	2.103	2.116	1.966	1.966	2.070	2.087					
0.700	2.101	2.090	2.105	2.003	2.003	2.071	2.085					
0.800	2.070	2.064	2.097	1.999	1.999	2.049	2.060					
0.900	2.050	2.028	2.074	1.969	1.969	2.038	2.070					
h (cm)	10	10	10	8	8	9	9					

Table C.3: Wang-Qian's measurements of velocity profiles in density sediment-laden flows

x_3/h	SF1	SF2	SF3	SF4	SF5	SF6	SM1	SM2	SM3	SM4	SM5	SM6	SM7
	\bar{u}_1 (m/s)												
0.008	1.259	1.196	1.242	1.166	1.067	1.115	1.237	1.259	1.192	1.124	1.156	1.169	1.062
0.010	1.285	1.229	1.279	1.189	1.156	1.090	1.282	1.299	1.223	1.157	1.170	1.206	1.145
0.012	1.315	1.258	1.324	1.285	1.138	1.158	1.271	1.347	1.268	1.217	1.197	1.237	1.183
0.016	1.380	1.347	1.363	1.312	1.158	1.170	1.363	1.381	1.326	1.285	1.288	1.293	1.222
0.020	1.394	1.367	1.374	1.357	1.219	1.256	1.411	1.407	1.383	1.356	1.341	1.296	1.281
0.026	1.452	1.435	1.438	1.393	1.232	1.295	1.480	1.475	1.437	1.395	1.412	1.309	1.316
0.033	1.516	1.493	1.478	1.434	1.345	1.312	1.536	1.523	1.479	1.460	1.453	1.388	1.384
0.040	1.546	1.495	1.487	1.470	1.381	1.362	1.560	1.602	1.526	1.512	1.521	1.427	1.431
0.050	1.593	1.557	1.537	1.512	1.411	1.454	1.609	1.629	1.560	1.564	1.556	1.484	1.468
0.065	1.643	1.648	1.612	1.575	1.488	1.479	1.670	1.681	1.647	1.642	1.623	1.595	1.539
0.080	1.719	1.681	1.656	1.615	1.521	1.512	1.708	1.713	1.688	1.690	1.647	1.618	1.626
0.100	1.747	1.736	1.701	1.652	1.599	1.609	1.749	1.773	1.715	1.715	1.729	1.708	1.669
0.150	1.809	1.816	1.781	1.745	1.626	1.674	1.814	1.838	1.824	1.843	1.812	1.810	1.764
0.220	1.919	1.894	1.862	1.818	1.740	1.762	1.898	1.953	1.918	1.930	1.878	1.922	1.854
0.300	1.971	1.964	1.949	1.908	1.808	1.865	1.960	2.009	1.974	2.001	1.975	1.997	1.952
0.400	2.075	2.038	1.994	1.990	1.872	1.974	2.022	2.088	2.056	2.066	2.044	2.070	2.035
0.500	2.097	2.063	2.052	2.028	1.920	1.985	2.078	2.122	2.108	2.142	2.076	2.092	2.103
0.600	2.106	2.095	2.067	2.075	1.946	2.055	2.114	2.147	2.147	2.175	2.129	2.133	2.169
0.700	2.116	2.086	2.067	2.066	1.964	2.103	2.097	2.137	2.155	2.185	2.207	2.189	2.209
0.800	2.094	2.066	2.039	2.073	2.050	2.133	2.103	2.113	2.144	2.170	2.209	2.217	2.228
0.900	2.074	2.043	2.016	2.067	2.066	2.146	2.082	2.092	2.118	2.155	2.183	2.192	2.224
$h(\text{cm})$	10	10	10	10	8	9	10	10	10	10	10	10	10

Table C.3 (continued)

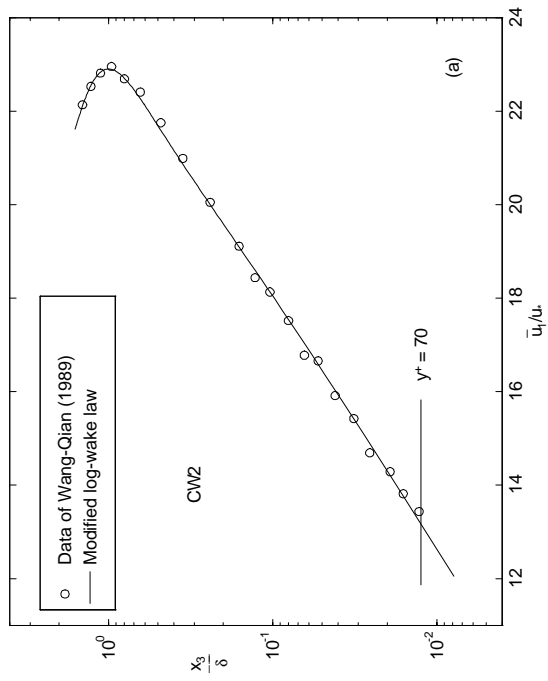
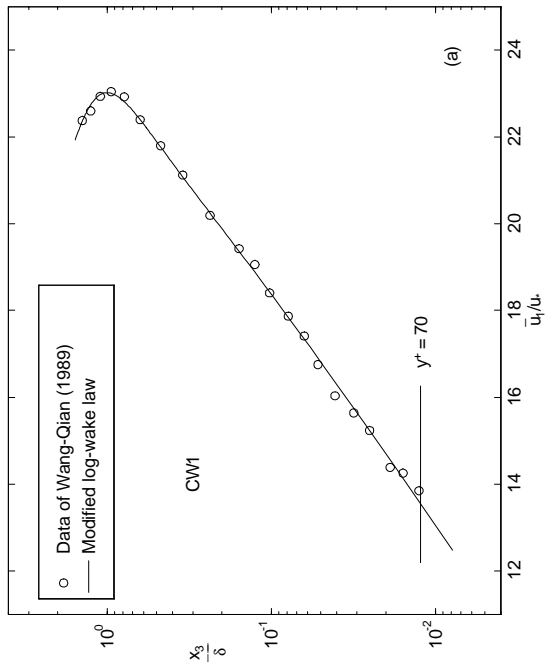
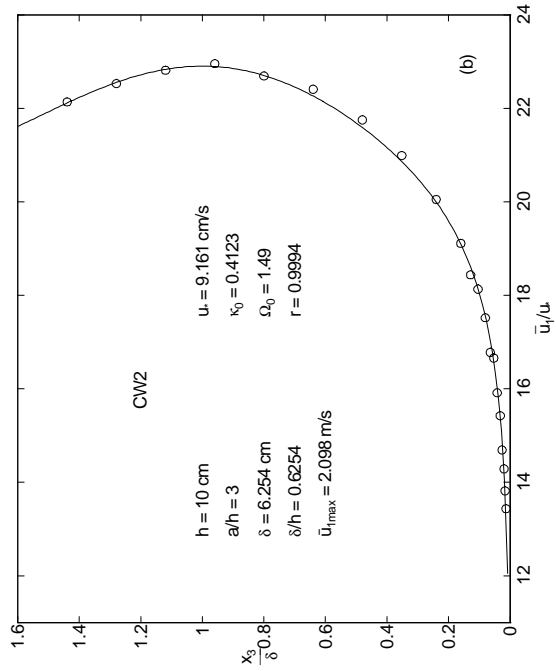
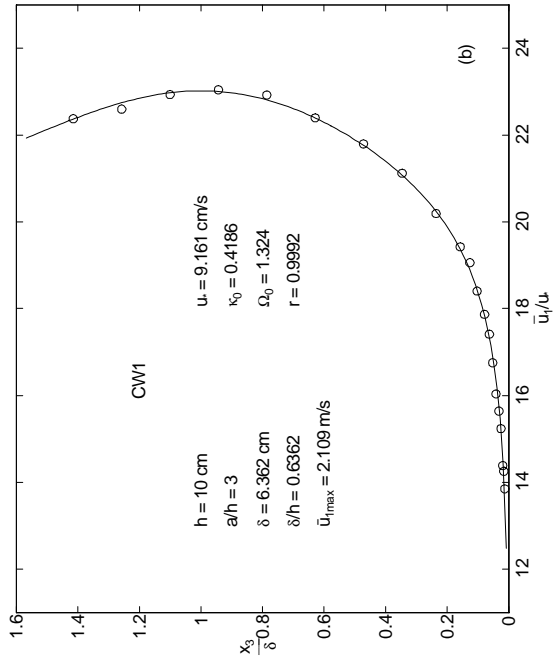
x_3/h	SC1	SC2	SC3	SC4	SC5	SC6	SC7	SQ1	SQ2	SQ3
	\bar{u}_1 (m/s)									
0.008	1.213	1.190	1.125	1.148	1.081	1.086	1.036	1.133	1.105	1.083
0.010	1.248	1.206	1.155	1.145	1.089	1.096	1.063	1.140	1.107	1.088
0.012	1.286	1.261	1.209	1.178	1.139	1.134	1.081	1.177	1.137	1.107
0.016	1.324	1.321	1.260	1.233	1.208	1.182	1.117	1.228	1.209	1.166
0.020	1.389	1.368	1.330	1.331	1.231	1.219	1.219	1.262	1.274	1.199
0.026	1.449	1.419	1.390	1.374	1.295	1.290	1.263	1.350	1.330	1.234
0.033	1.466	1.469	1.429	1.441	1.353	1.336	1.298	1.386	1.345	1.298
0.040	1.521	1.534	1.488	1.480	1.440	1.401	1.351	1.425	1.386	1.330
0.050	1.577	1.584	1.543	1.516	1.507	1.465	1.468	1.468	1.450	1.396
0.065	1.641	1.626	1.600	1.588	1.539	1.565	1.524	1.513	1.482	1.443
0.080	1.673	1.690	1.658	1.634	1.587	1.585	1.599	1.544	1.521	1.489
0.100	1.746	1.752	1.706	1.695	1.654	1.652	1.649	1.604	1.547	1.539
0.150	1.830	1.817	1.785	1.792	1.757	1.775	1.753	1.695	1.659	1.666
0.220	1.907	1.917	1.865	1.831	1.829	1.851	1.835	1.751	1.765	1.764
0.300	1.986	1.970	1.942	1.938	1.935	1.916	1.913	1.794	1.836	1.804
0.400	2.057	2.032	2.008	1.999	1.999	2.011	2.016	1.875	1.885	1.866
0.500	2.098	2.054	2.079	2.073	2.087	2.068	2.054	1.933	1.962	1.936
0.600	2.123	2.110	2.112	2.119	2.128	2.159	2.137	1.991	1.995	2.005
0.700	2.112	2.103	2.104	2.134	2.151	2.180	2.175	2.005	2.013	2.003
0.800	2.087	2.090	2.074	2.111	2.149	2.164	2.145	2.078	2.092	2.038
0.900	2.051	2.054	2.043	2.093	2.112	2.145	2.147	2.069	2.058	2.018
h (cm)	10	10	10	10	10	10	10	8	8	8

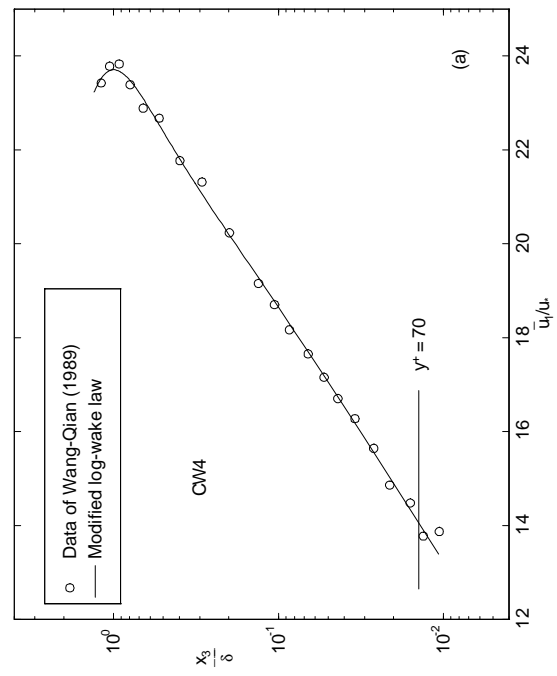
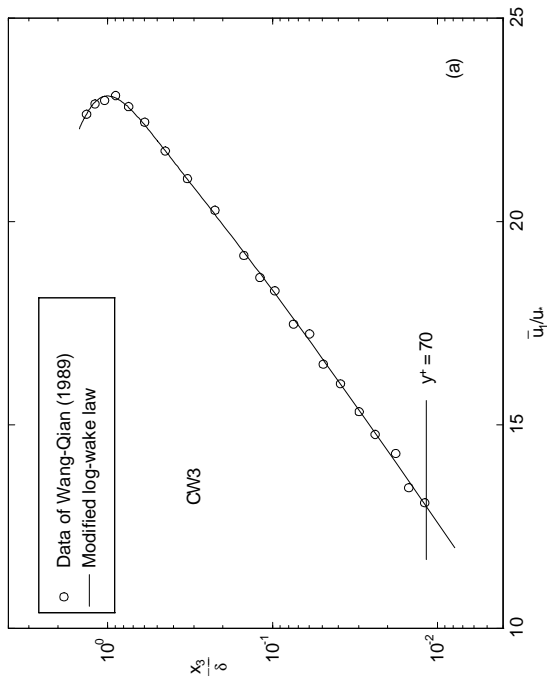
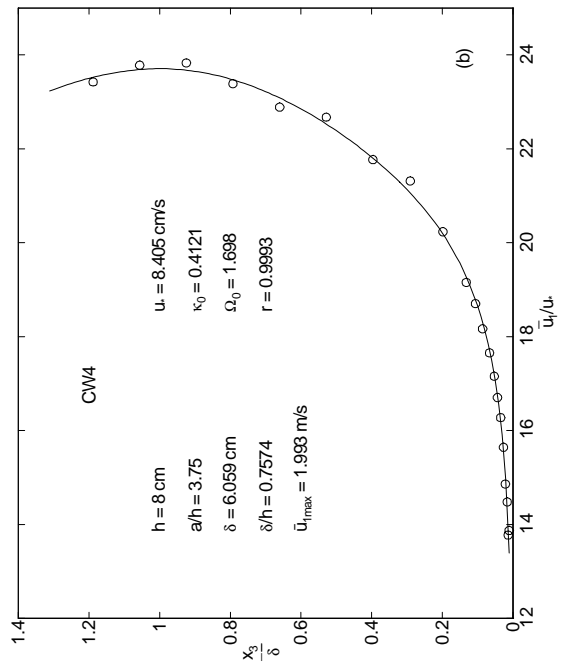
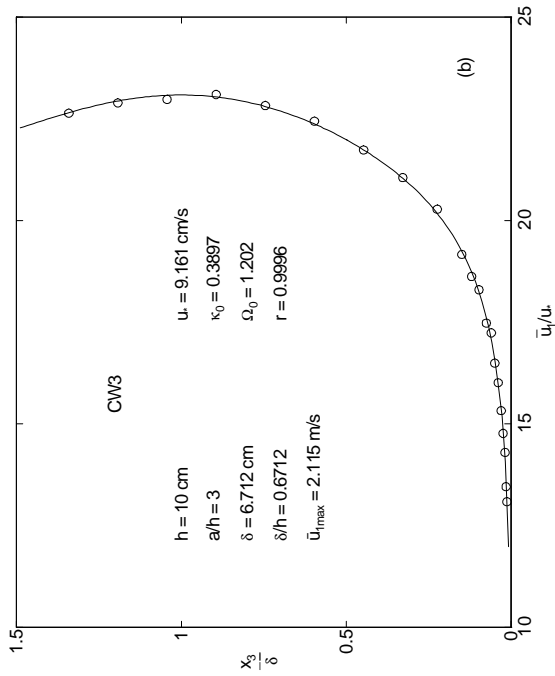
Table C.4: Wang-Qian's (1989) measurements of concentration profiles

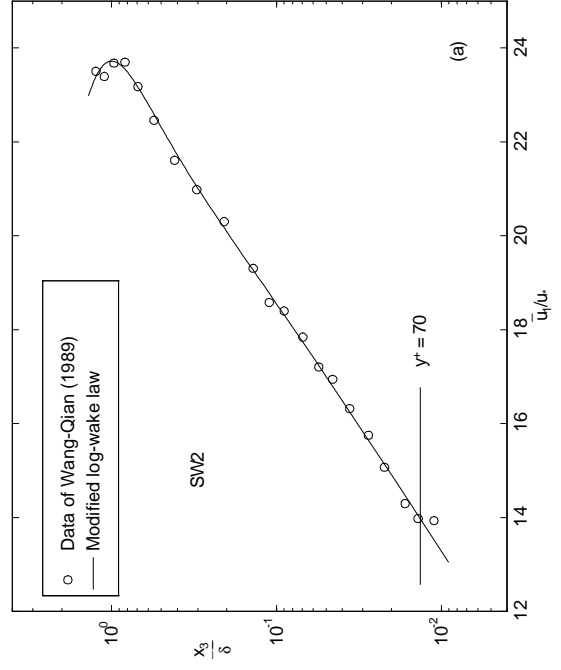
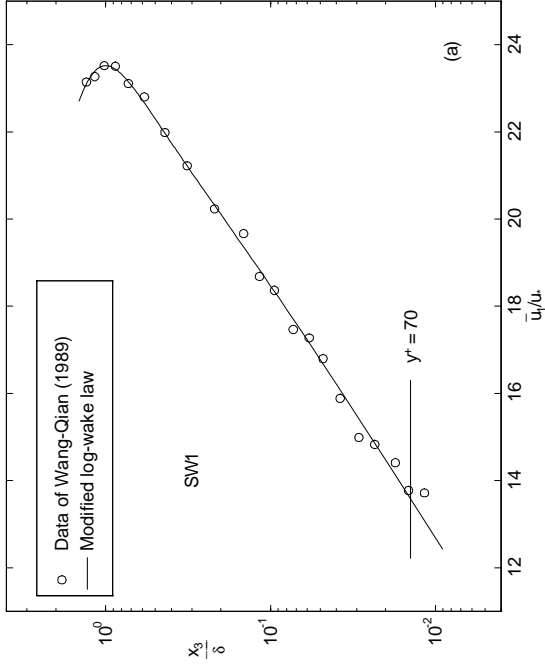
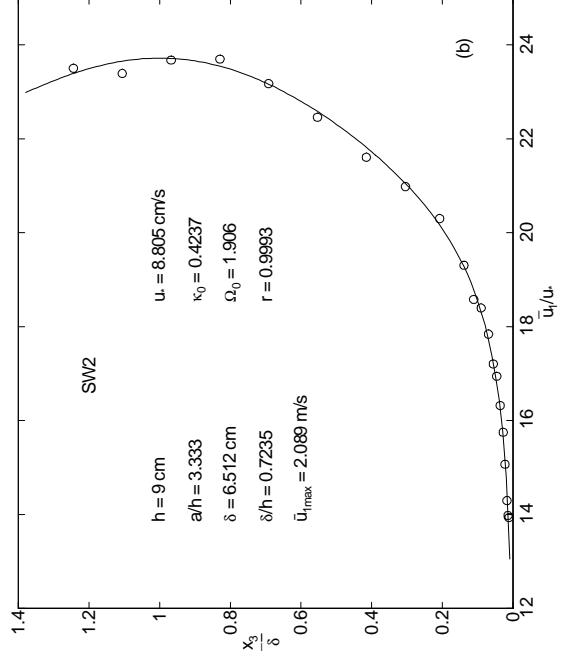
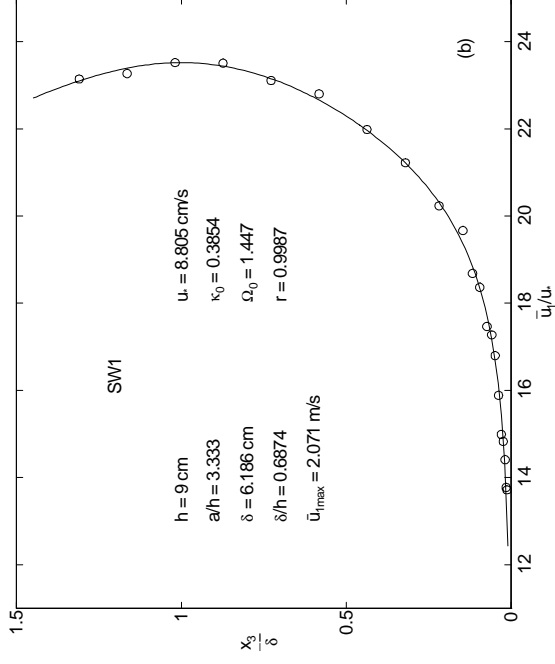
x_3/h	SF1	SF2	SF3	SF4	SF5	SF6	SM1	SM2	SM3	SM4	SM5	SM6	SM7
	\bar{C}												
	(%)	(%)	(%)	(%)	(%)	(%)	(%)	(%)	(%)	(%)	(%)	(%)	(%)
0.016	0.62	1.35	2.90	5.76	10.43	15.51	0.84	2.96	5.36	8.39	12.51	13.89	20.95
0.026	0.53	1.39	2.88	5.64	10.47	15.15	0.80	2.82	5.30	8.44	12.55	13.97	20.67
0.040	0.55	1.38	2.83	5.53	10.50	14.78	0.71	2.65	4.95	7.81	11.67	14.43	21.59
0.065	0.53	1.32	2.73	5.39	10.34	14.81	0.65	2.41	4.70	7.61	11.94	13.77	21.38
0.100	0.47	1.19	2.64	5.24	10.18	14.83	0.59	2.32	4.36	7.12	11.12	13.20	21.21
0.200	0.47	1.15	2.51	5.16	10.05	14.73	0.48	1.88	3.66	6.12	9.80	11.29	19.34
0.300	0.40	1.16	2.53	5.09	9.91	14.63	0.40	1.55	3.02	5.29	8.75	10.49	17.75
0.400	0.47	1.10	2.43	5.01	9.73	14.15	0.34	1.25	2.76	4.66	7.37	9.04	15.75
0.500	0.43	1.06	2.42	4.92	9.56	13.66	0.28	1.07	2.13	3.73	5.97	7.58	14.37
0.600	0.40	0.98	2.19	4.65	9.30	13.59	0.32	0.82	1.75	3.08	4.78	5.78	12.19
0.700	0.41	0.98	2.23	4.39	9.03	13.52	0.18	0.68	1.41	2.27	3.47	4.49	9.75
0.800	0.40	0.93	2.17	4.35	8.85	13.15	0.16	0.57	1.10	1.78	2.51	3.47	7.36
0.900	0.37	0.94	2.17	4.31	8.67	12.77	0.11	0.43	0.90	1.54	2.22	2.83	8.84
$\bar{C}_{0.1}$	0.56	1.36	2.85	5.60	10.44	15.09	1.310	2.740	5.100	8.070	12.150	14.05	21.17
\bar{C}_m	0.41	1.02	2.28	4.6	9.06	13.26	0.420	1.200	2.380	3.990	6.230	7.540	13.720

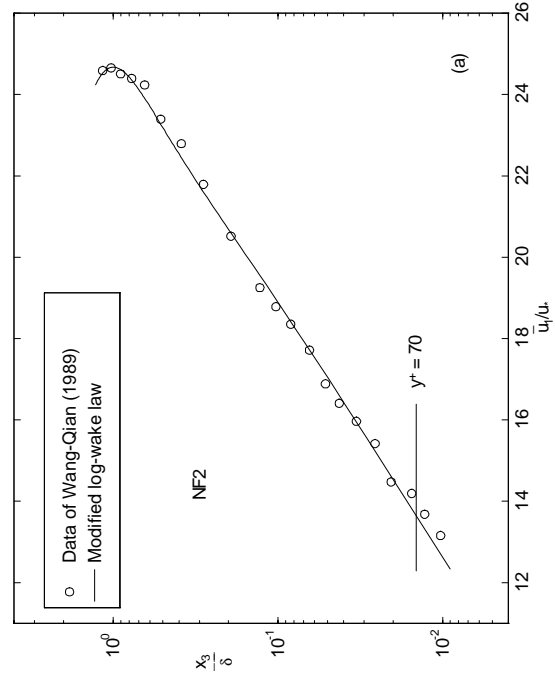
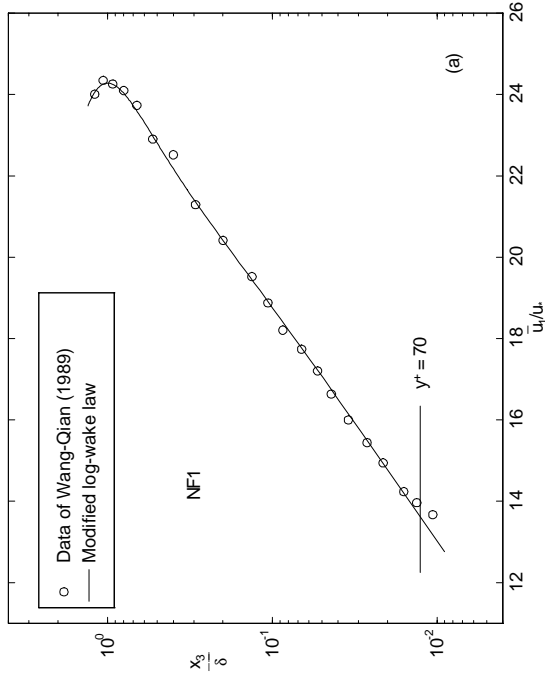
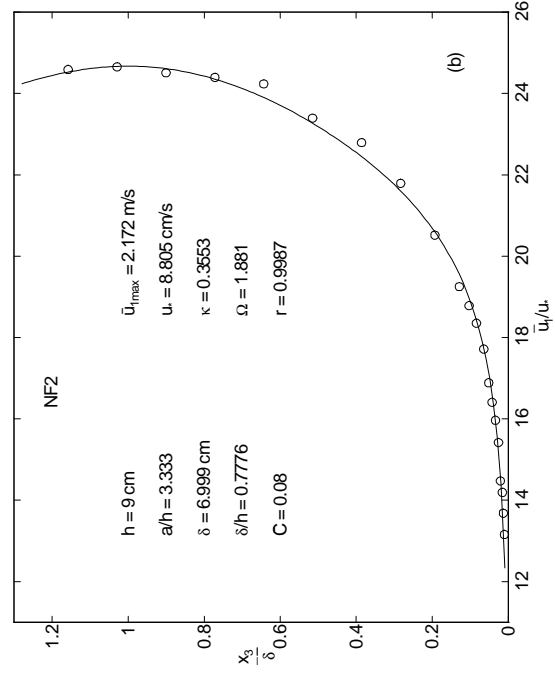
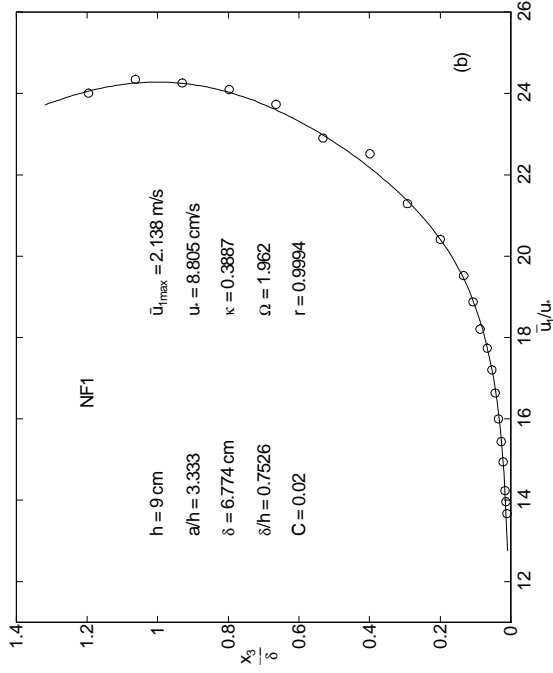
Table C.4 (continued)

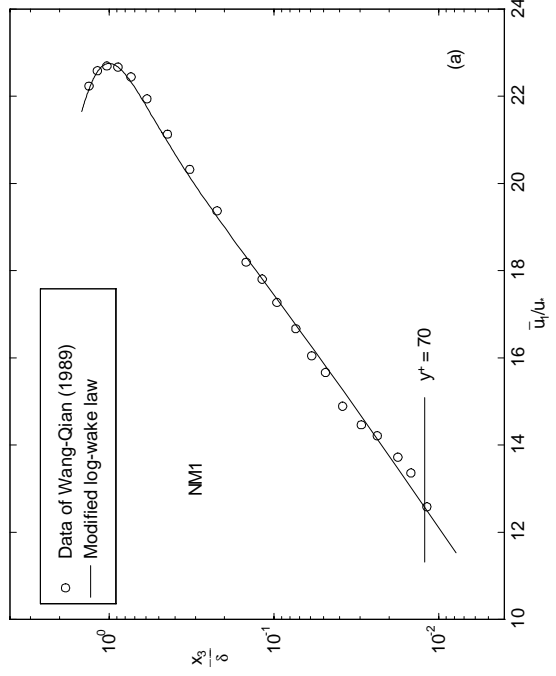
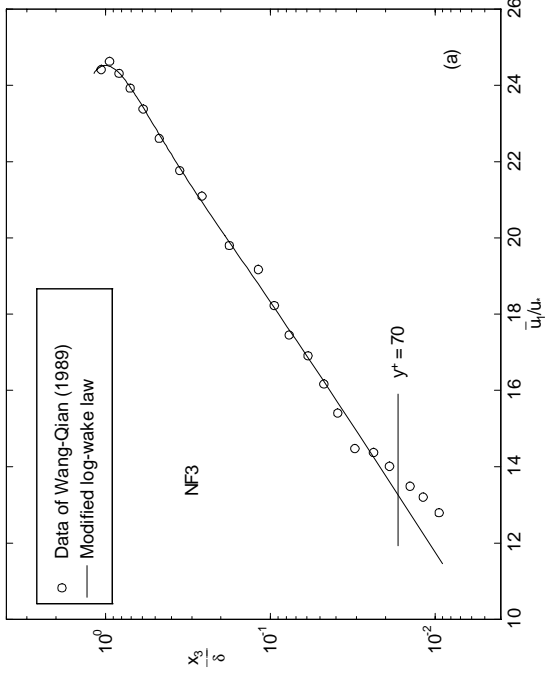
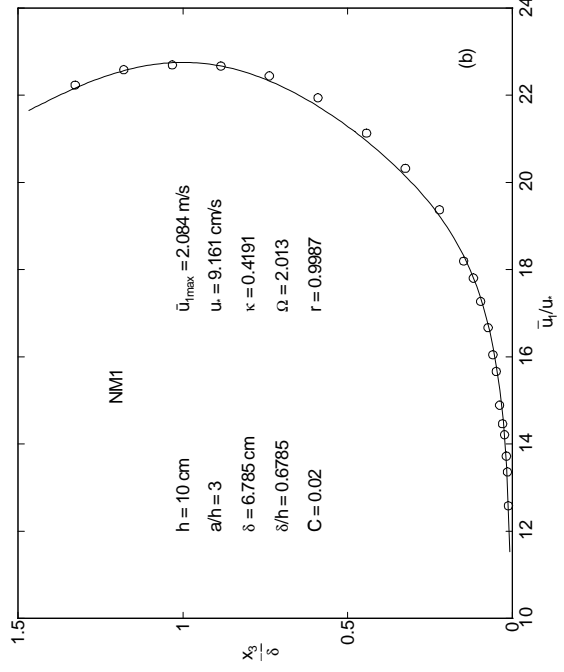
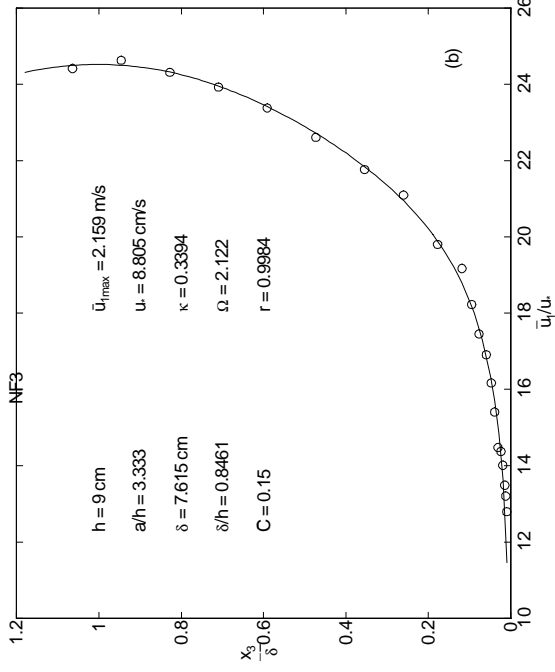
x_3/h	SC1	SC2	SC3	SC4	SC5	SC6	SC7	SQ1	SQ2	SQ3
	\bar{C} (%)									
0.016	1.020	2.200	4.510	7.470	11.170	17.110	21.000	2.170	7.950	9.640
0.026	1.050	2.130	4.350	7.410	12.640	17.090	21.000	2.110	7.630	9.540
0.040	1.020	2.010	4.040	7.250	11.410	17.080	21.000	1.780	6.250	8.320
0.065	0.930	1.780	3.900	6.660	11.720	16.370	21.000	1.420	5.170	6.930
0.100	0.840	1.640	3.600	6.280	11.630	15.980	20.100	1.090	4.440	5.590
0.200	0.690	1.410	2.990	5.260	10.250	14.760	17.740	0.810	2.770	3.550
0.300	0.550	1.130	2.550	4.360	8.960	12.680	17.190	0.600	2.020	2.500
0.400	0.480	0.950	2.190	3.830	7.740	11.200	15.290	0.470	1.450	1.690
0.500	0.390	0.710	1.870	3.240	6.420	9.580	13.120	0.390	1.080	1.080
0.600	0.300	0.590	1.470	2.480	5.060	7.420	10.270	0.290	0.830	0.670
0.700	0.240	0.460	1.150	1.910	3.810	5.600	7.950	0.230	0.540	0.440
0.800	0.210	0.380	0.960	1.550	2.960	4.430	5.660	0.180	0.380	0.270
0.900	0.070	0.090	0.810	1.300	2.460	3.320	4.370	0.140	0.280	0.170
\bar{C}_1	1.010	2.05	4.22	7.24	11.62	16.96	21.000	1.900	6.850	8.720
\bar{C}_m	0.430	0.850	1.980	3.400	6.510	9.370	12.250	0.530	1.770	2.100

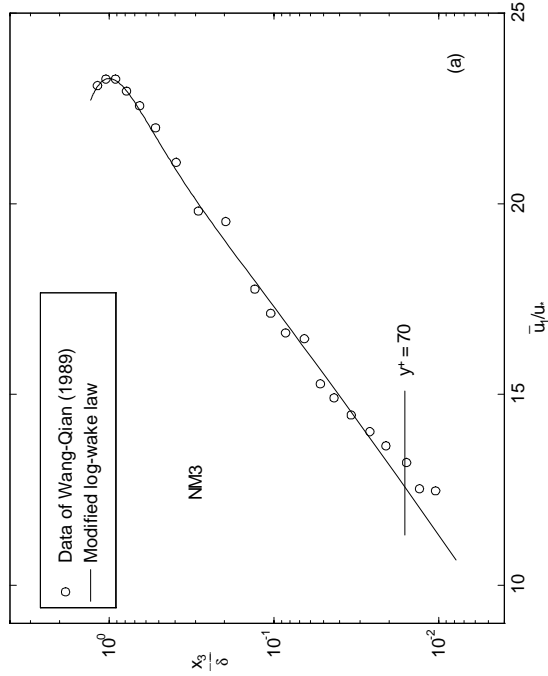
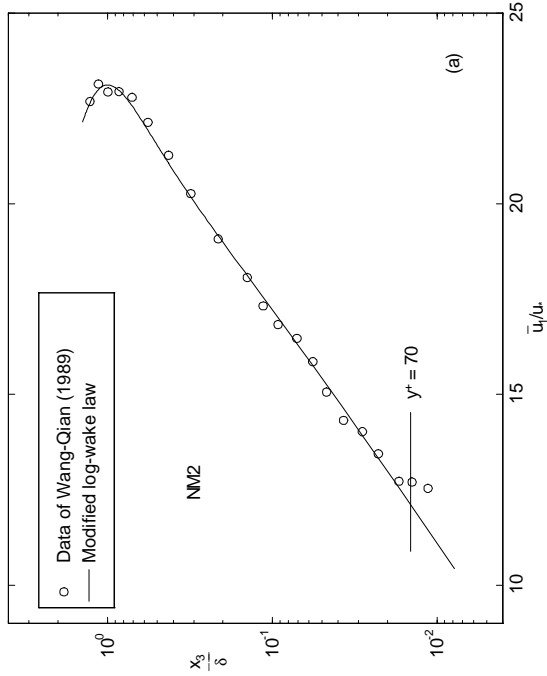
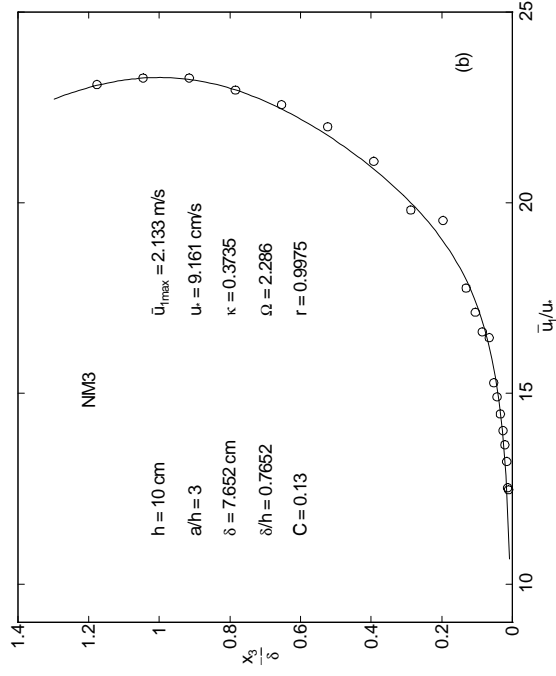
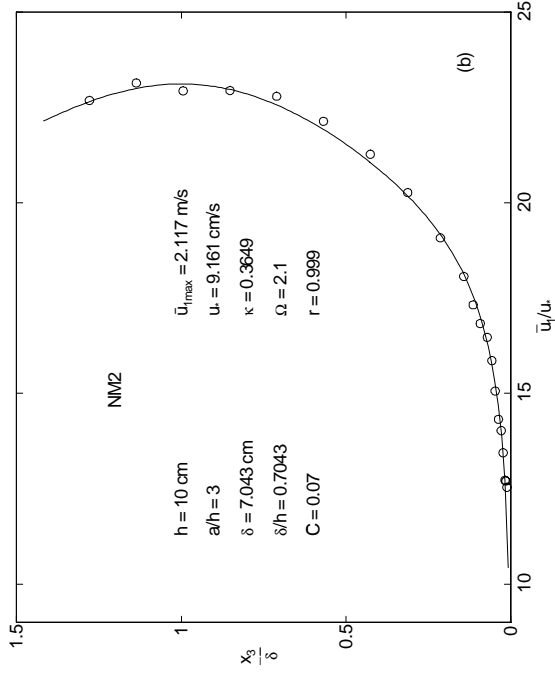


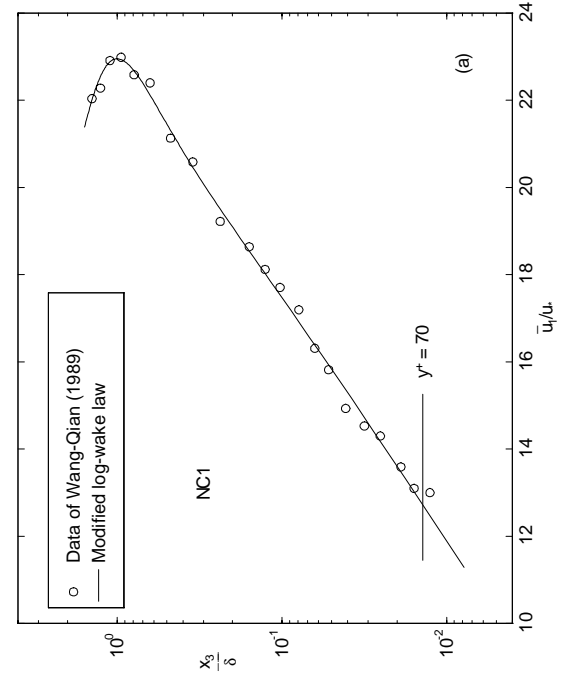
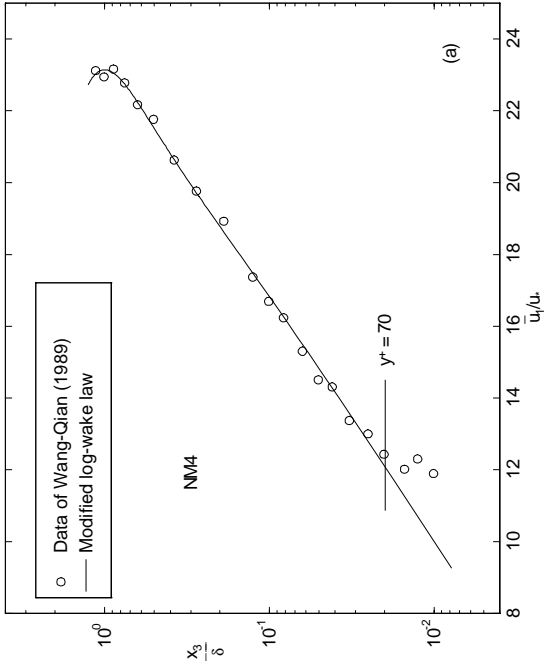
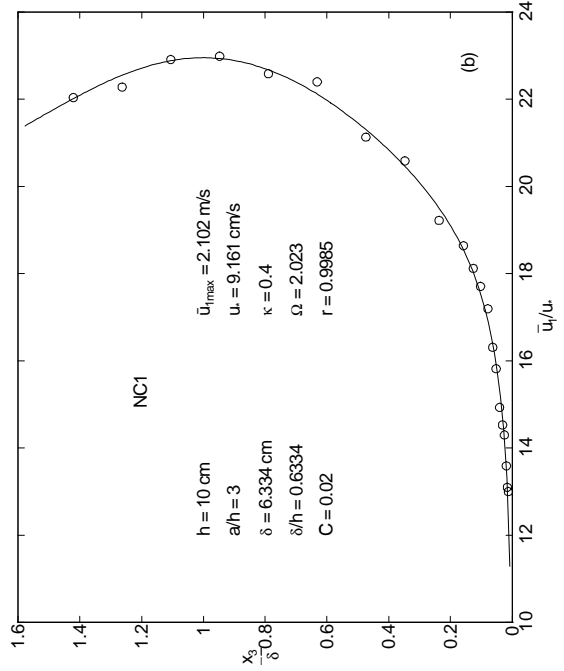
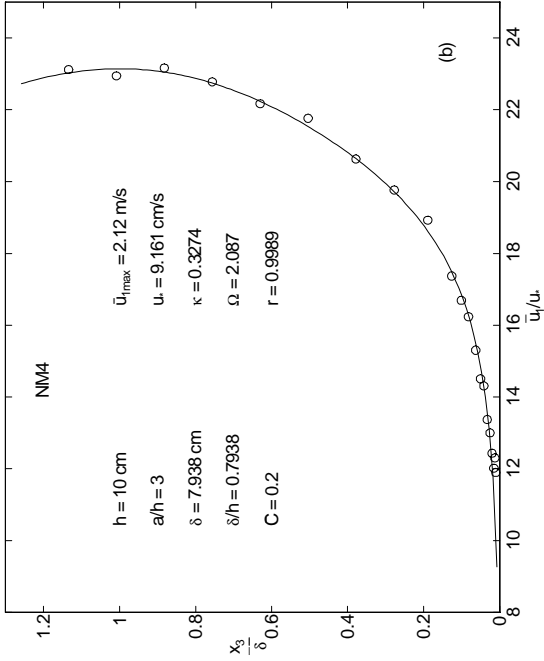


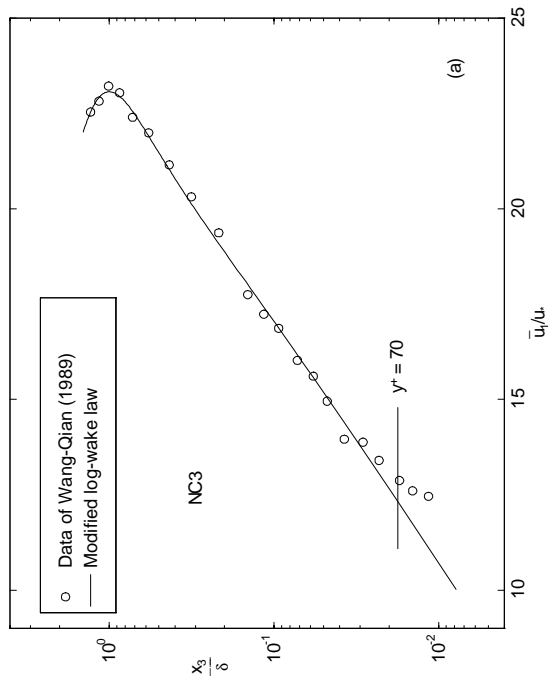
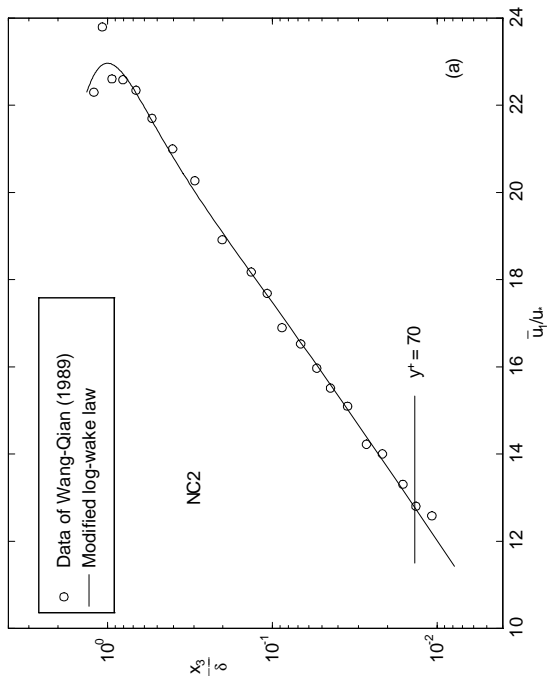
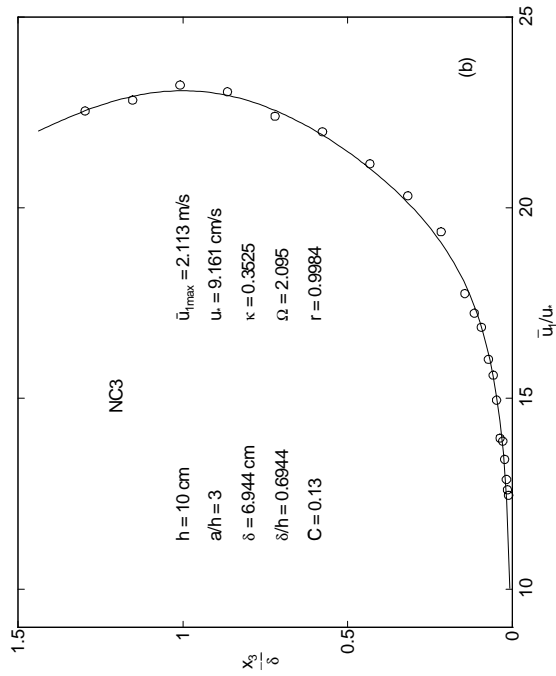
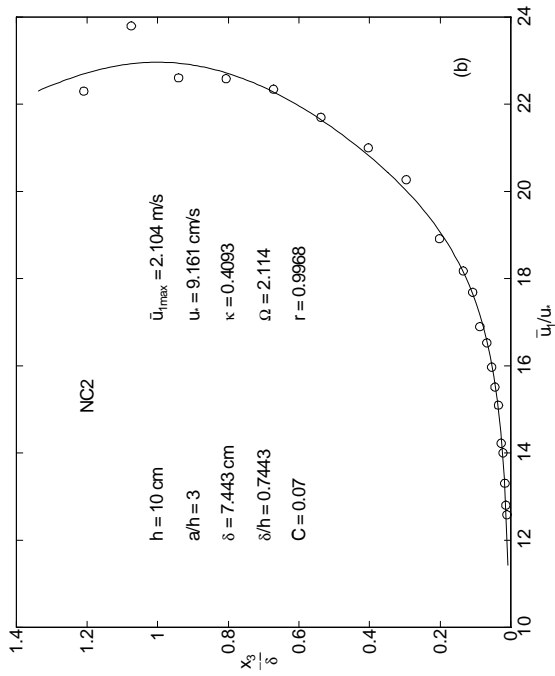


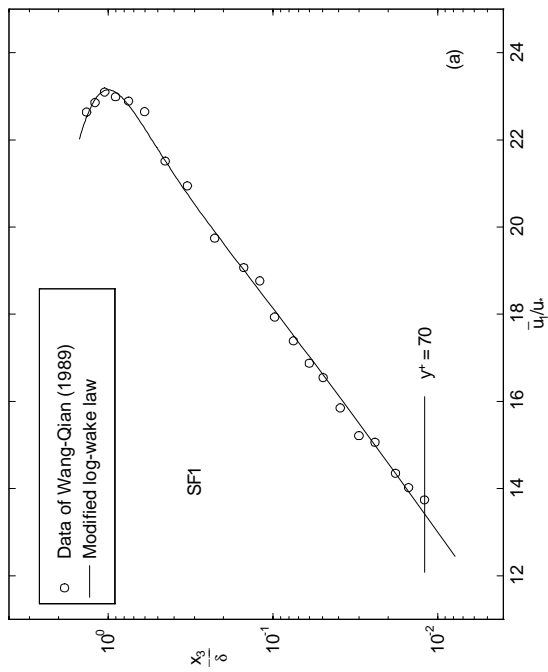
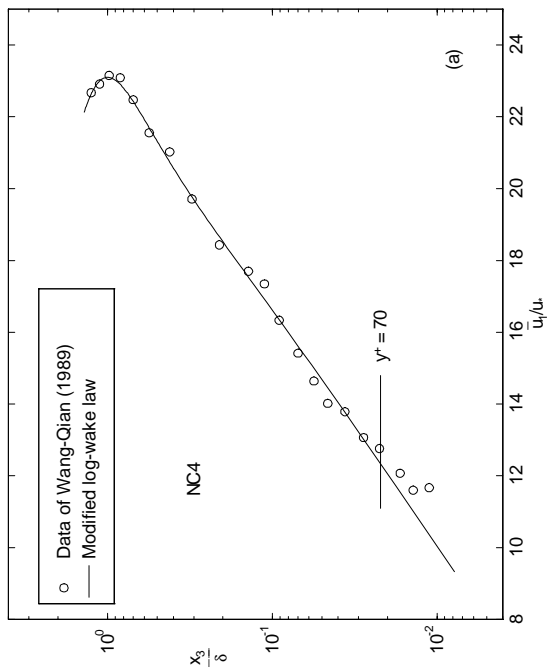
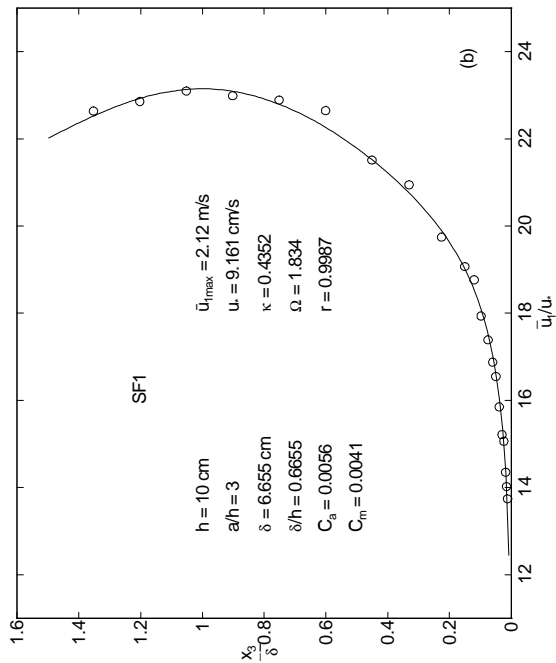
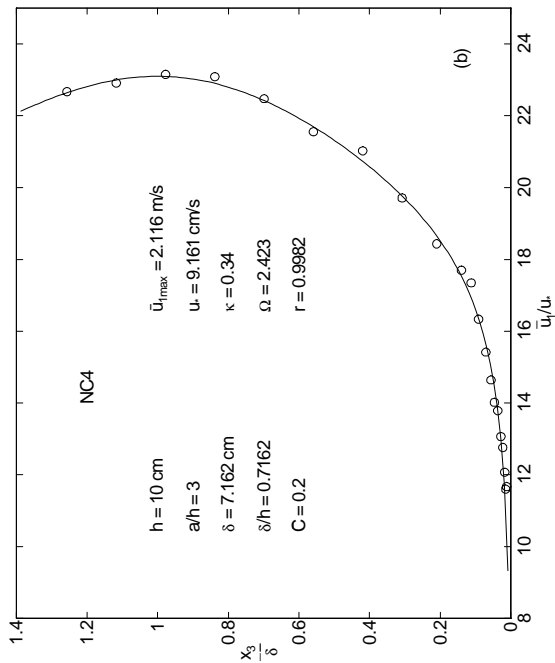


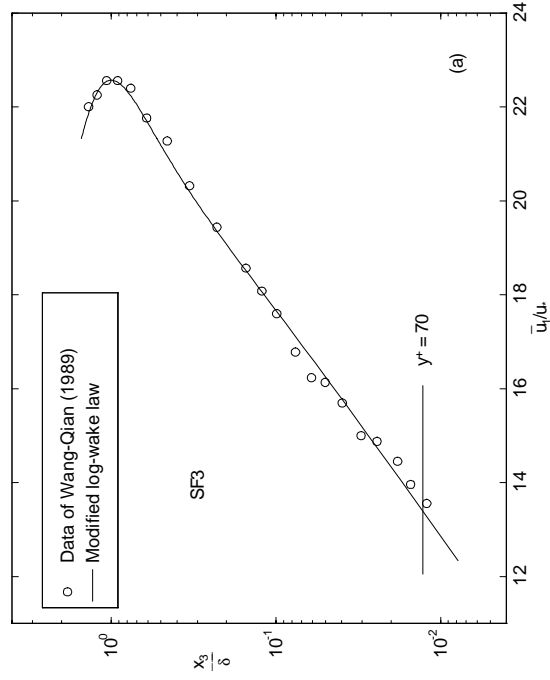
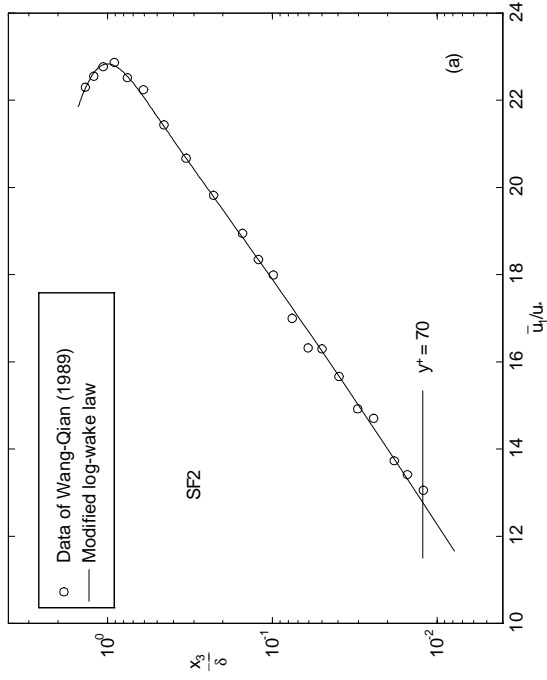
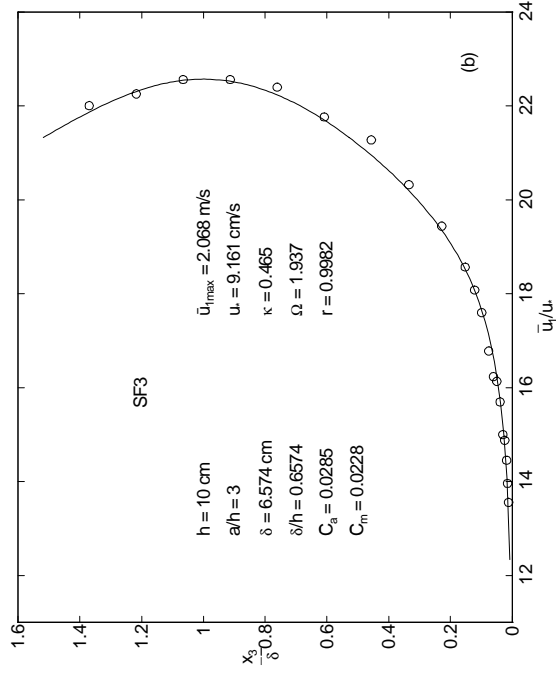
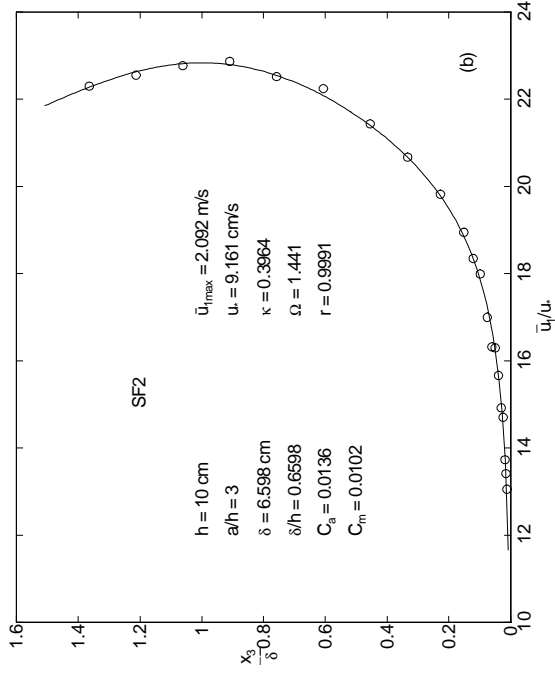


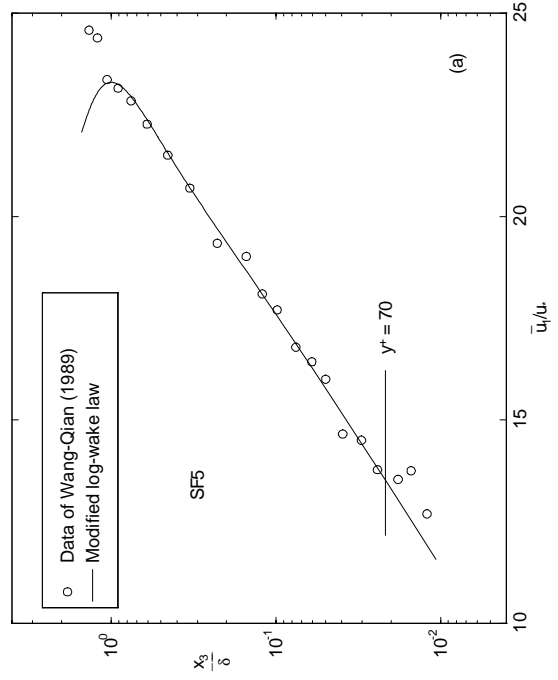
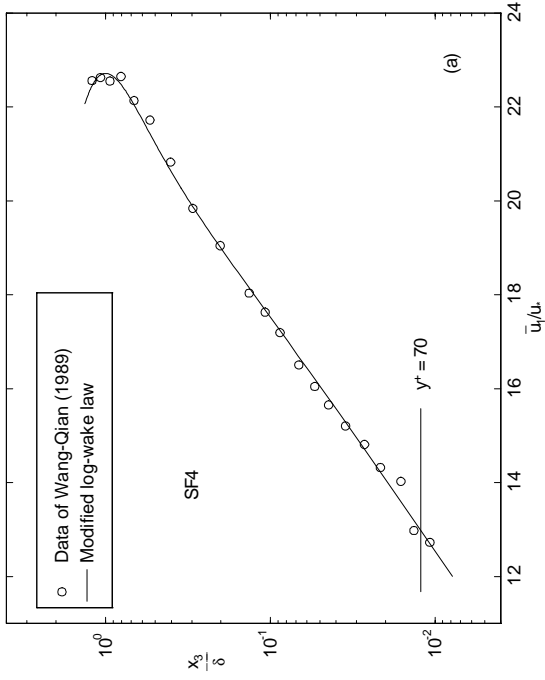
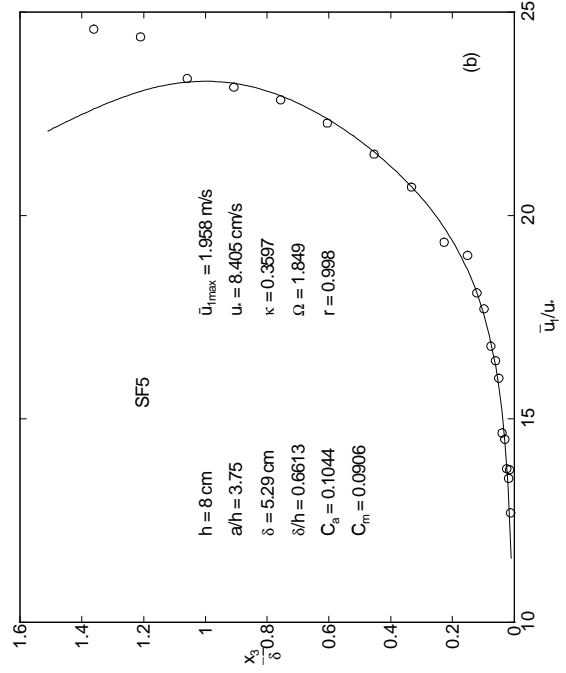
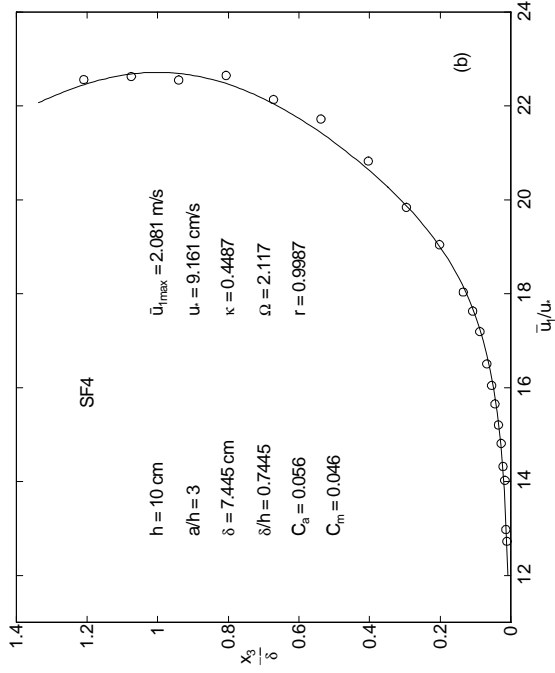


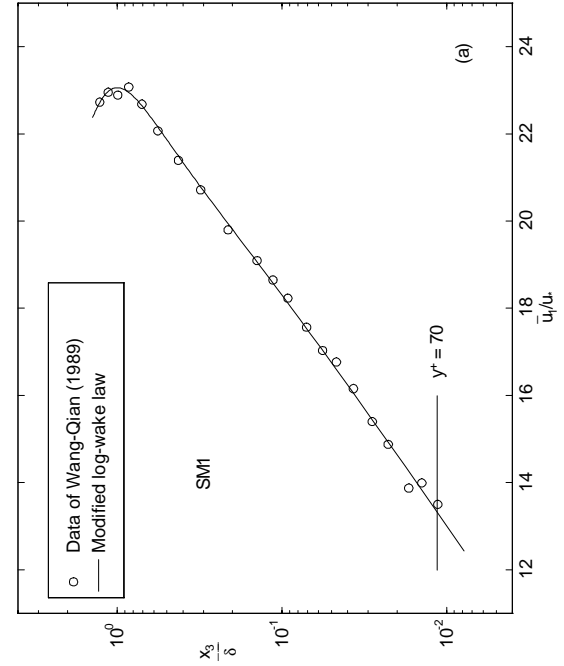
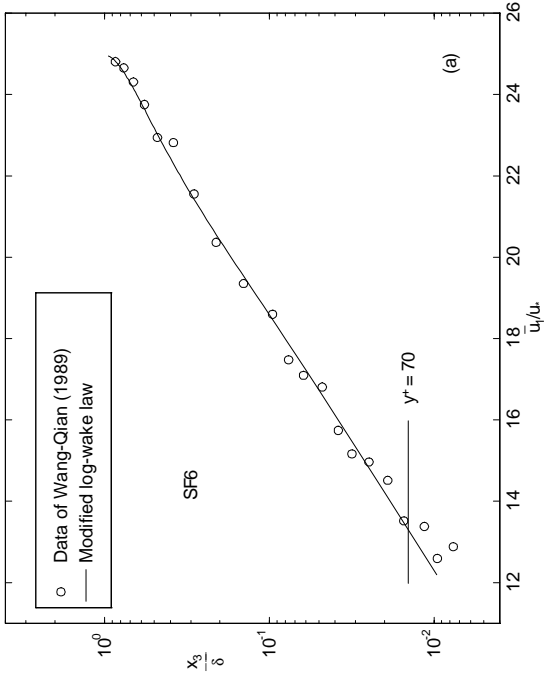
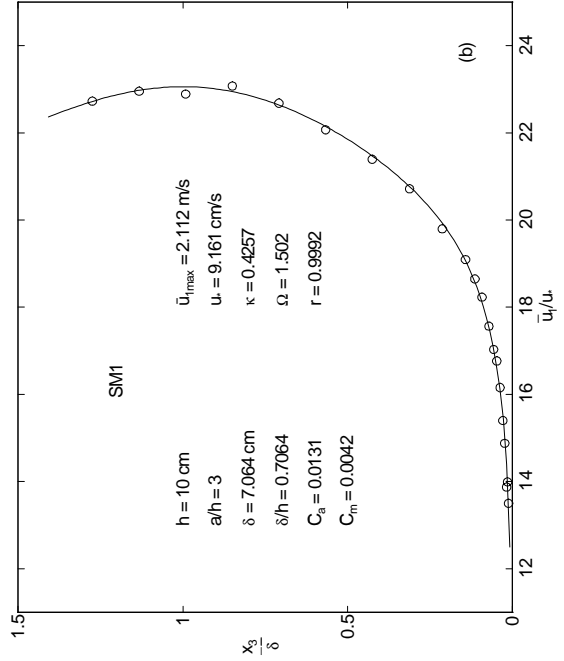
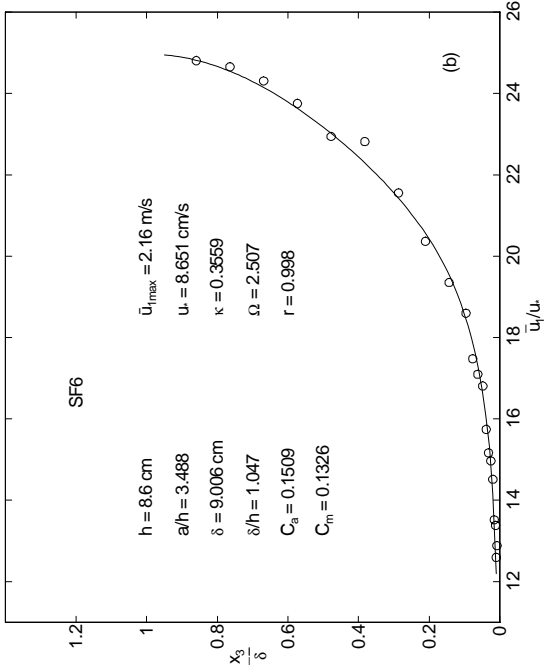


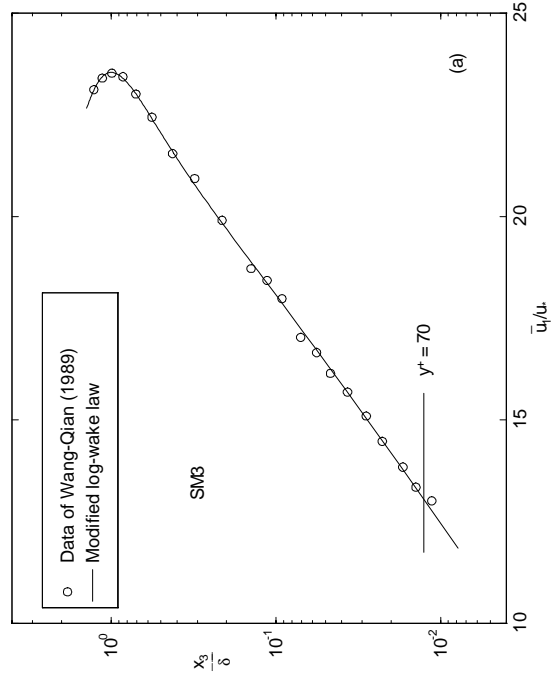
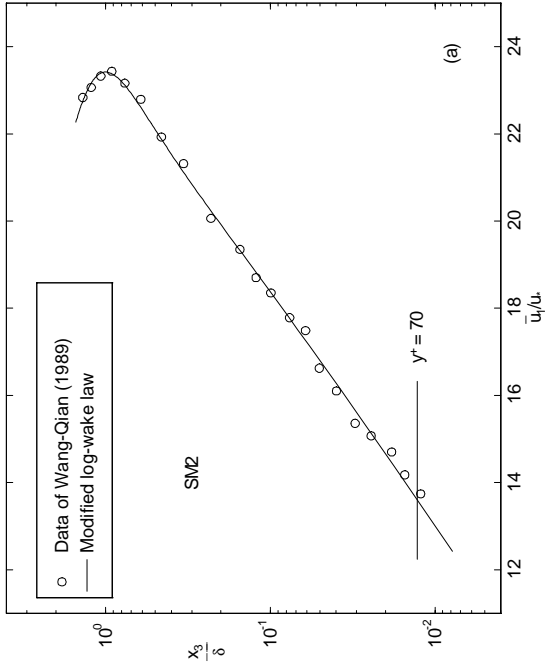
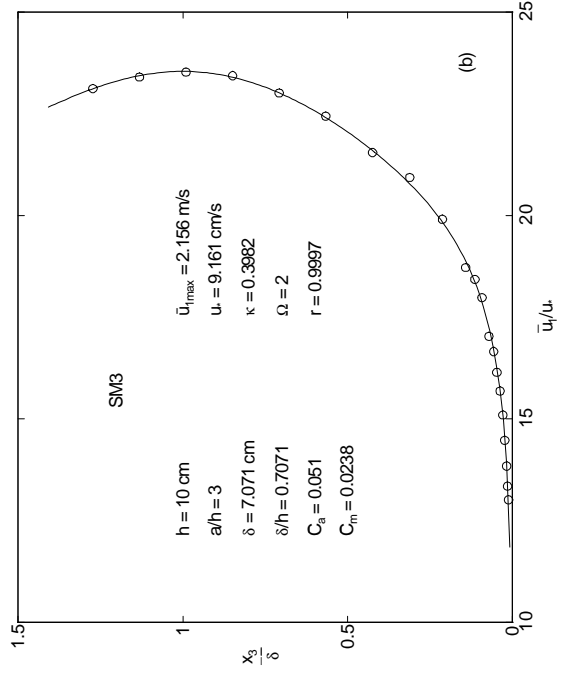
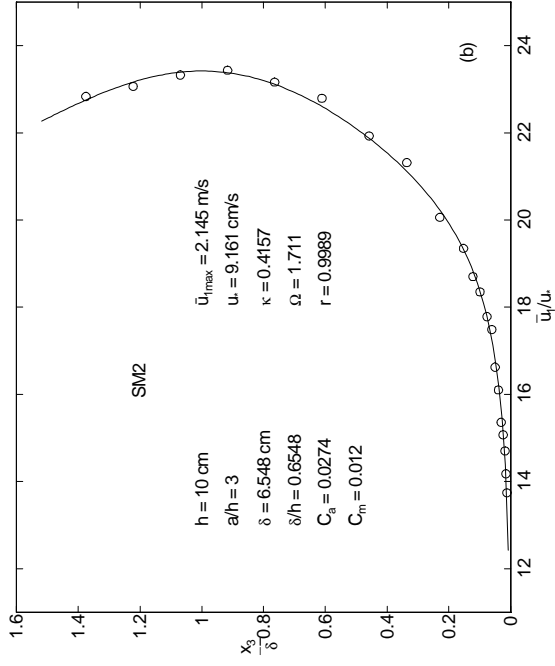


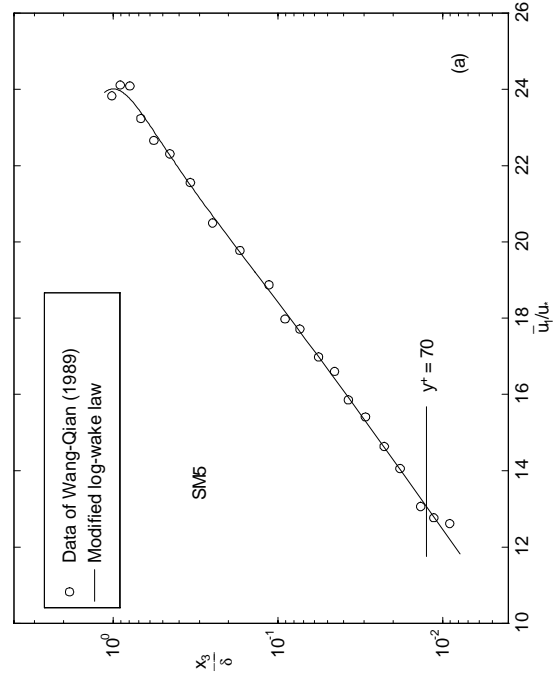
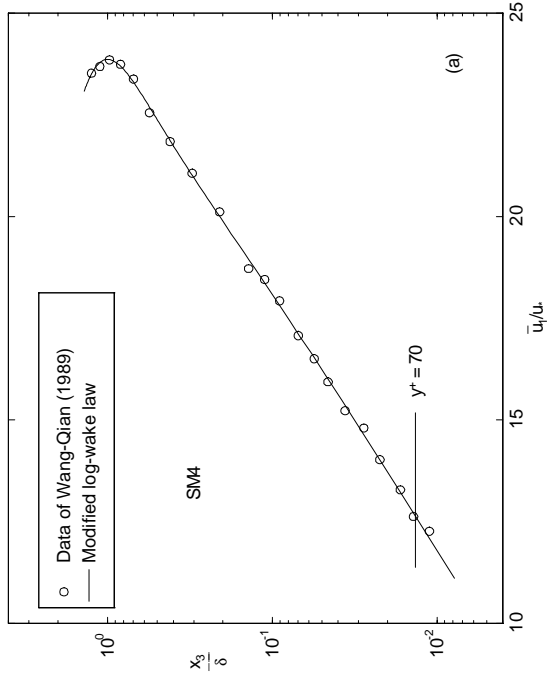
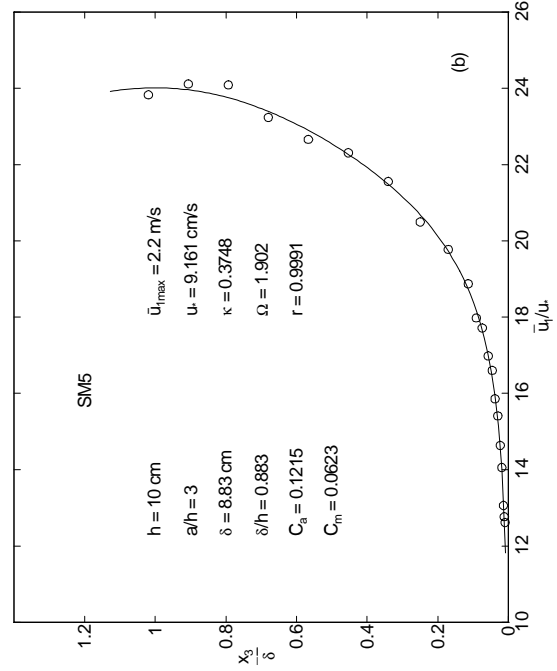
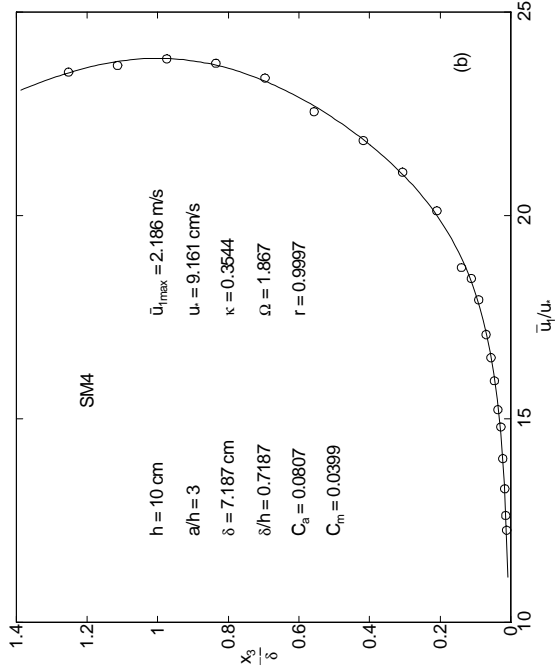


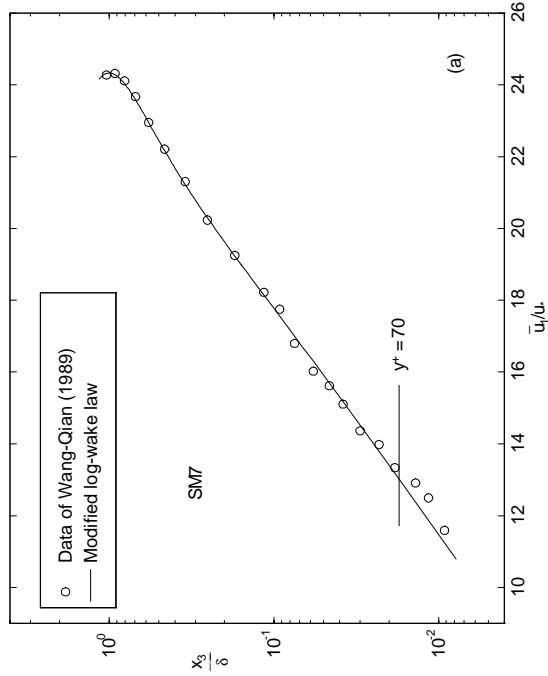
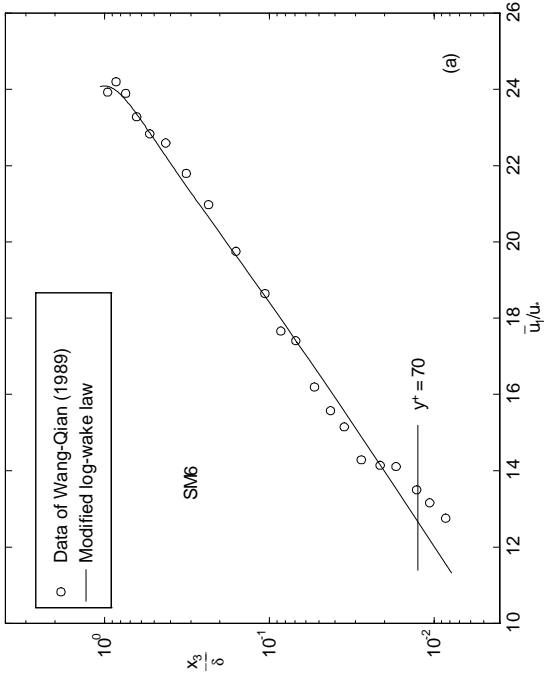
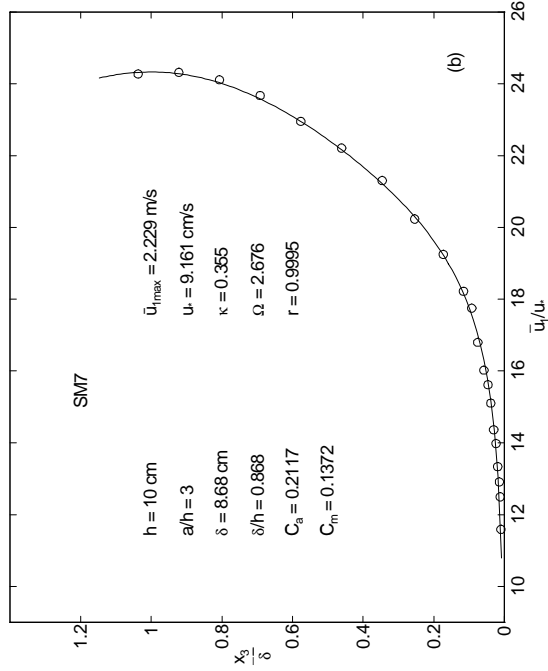
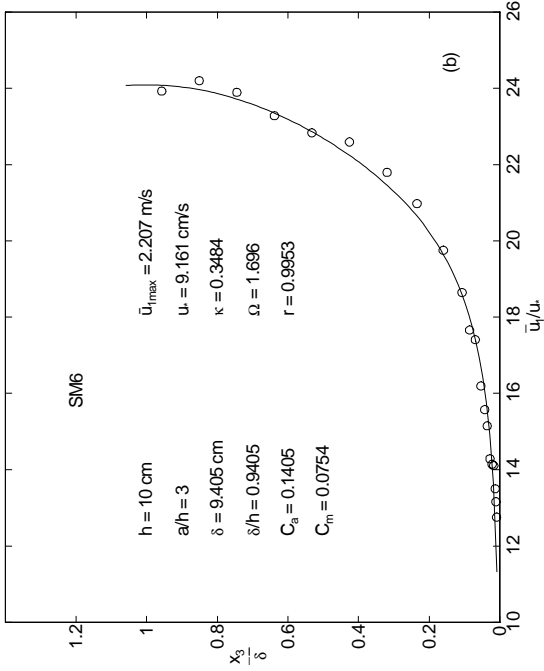


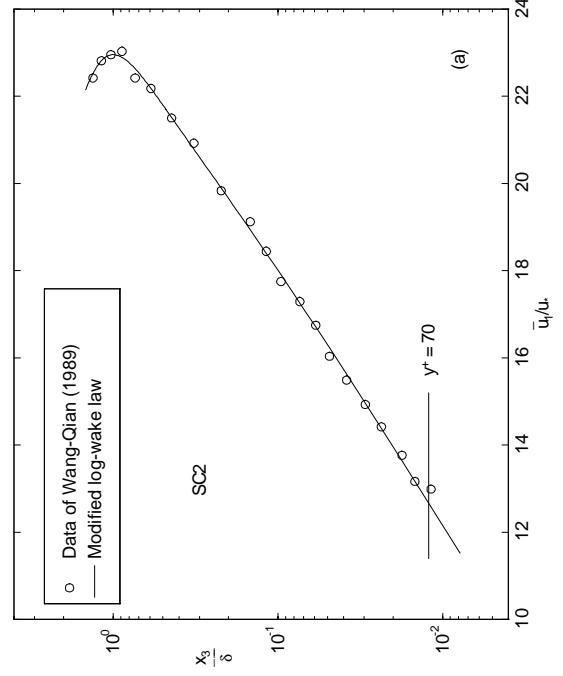
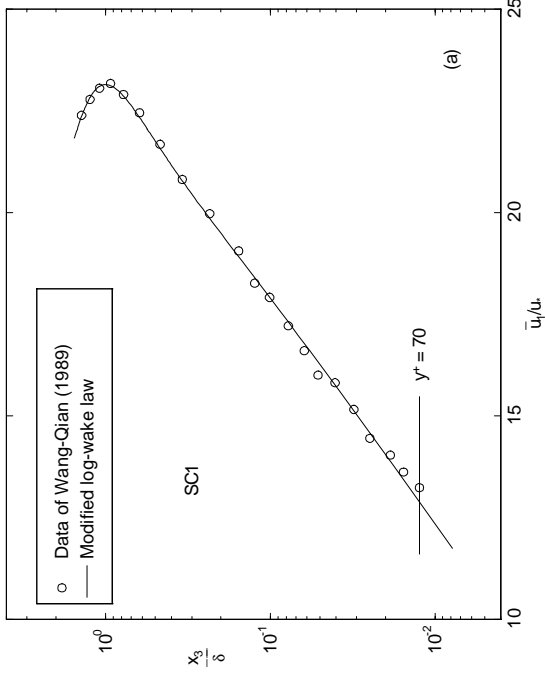
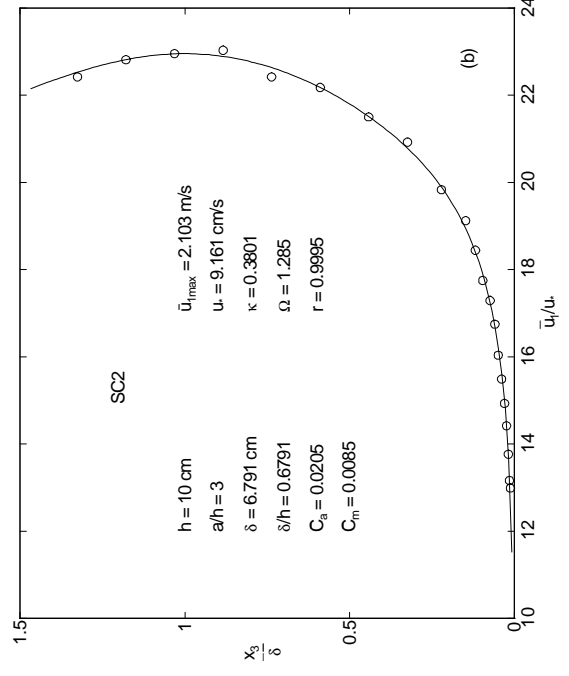
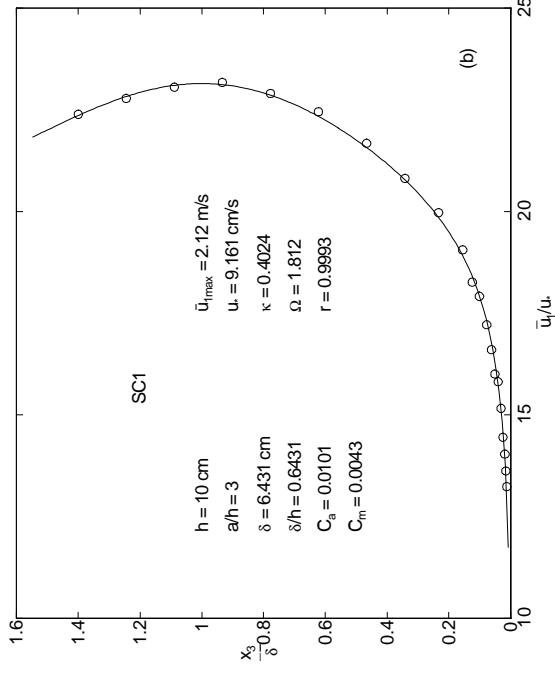


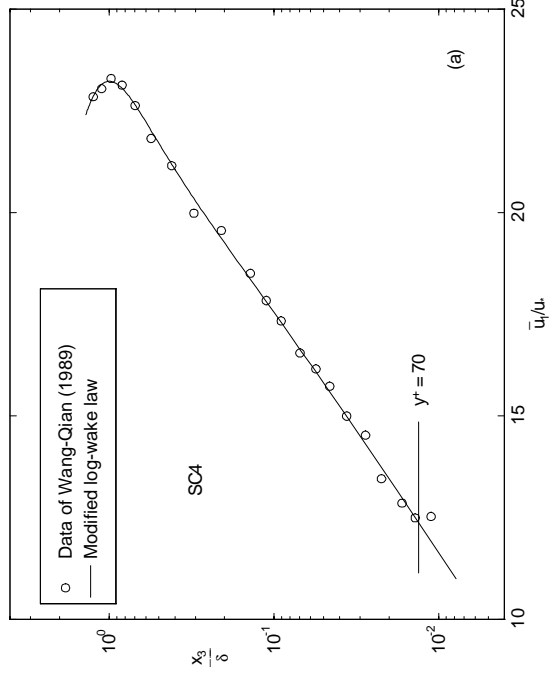
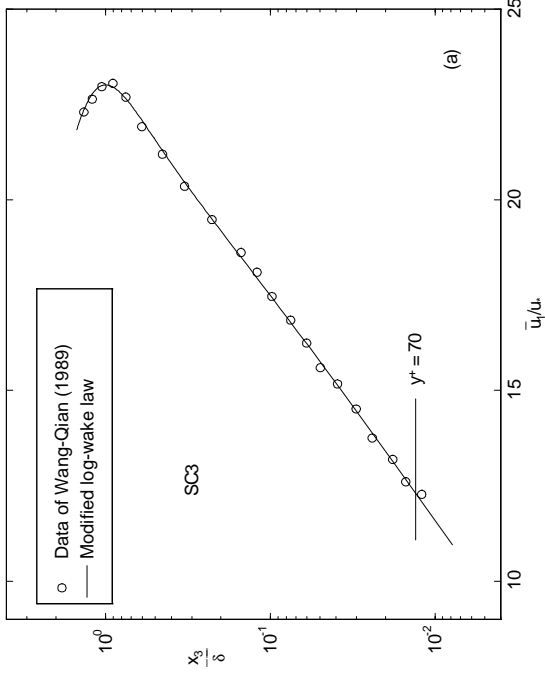
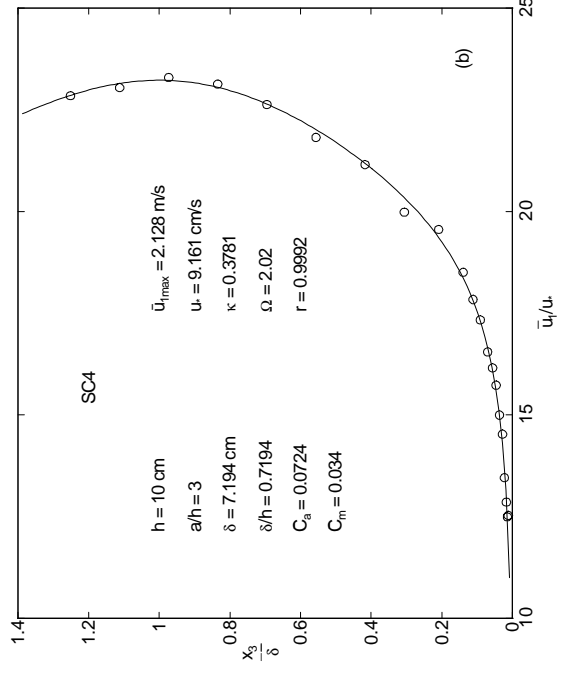
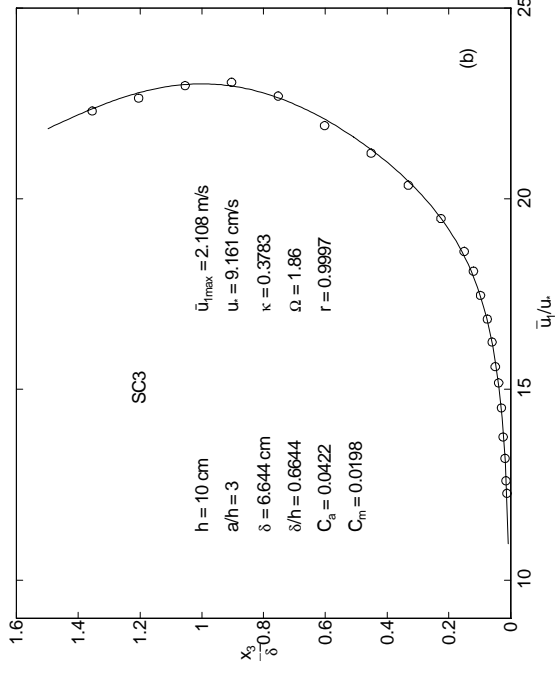


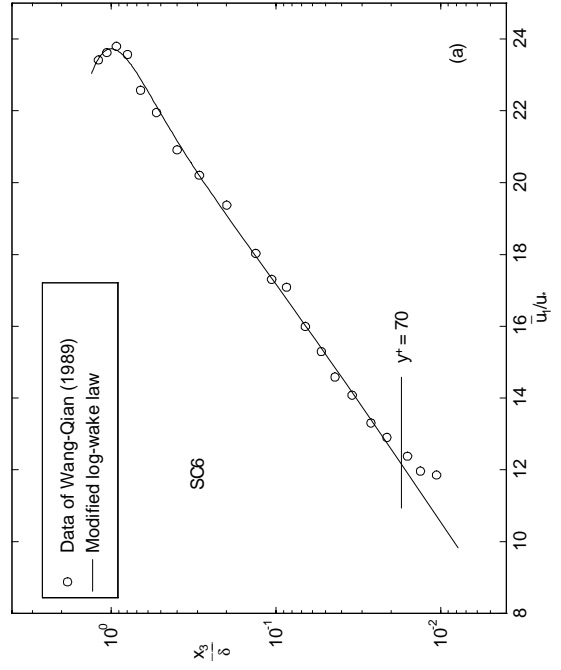
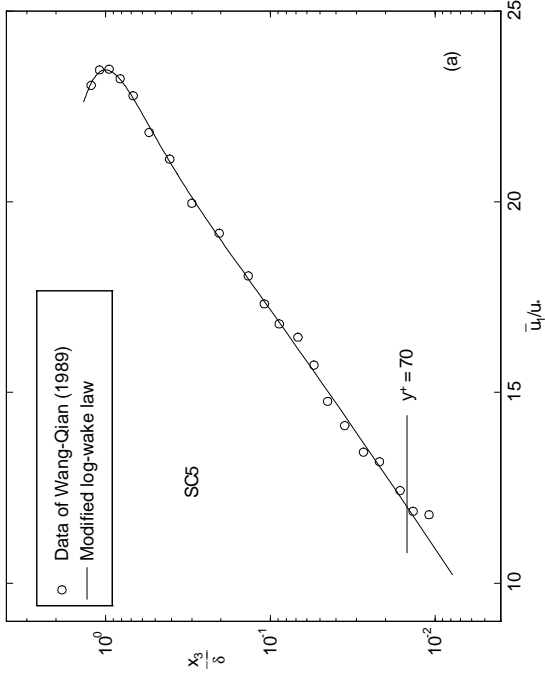
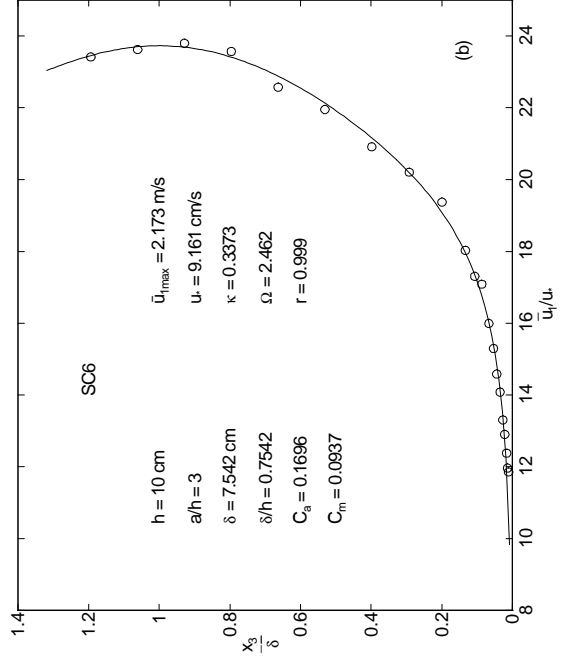
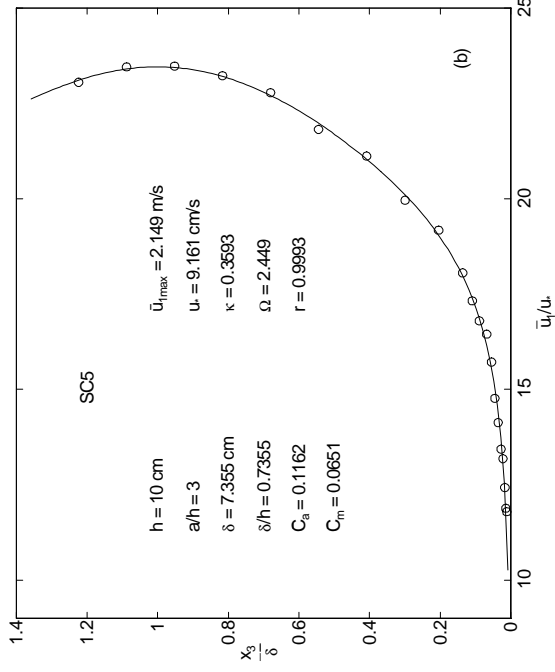


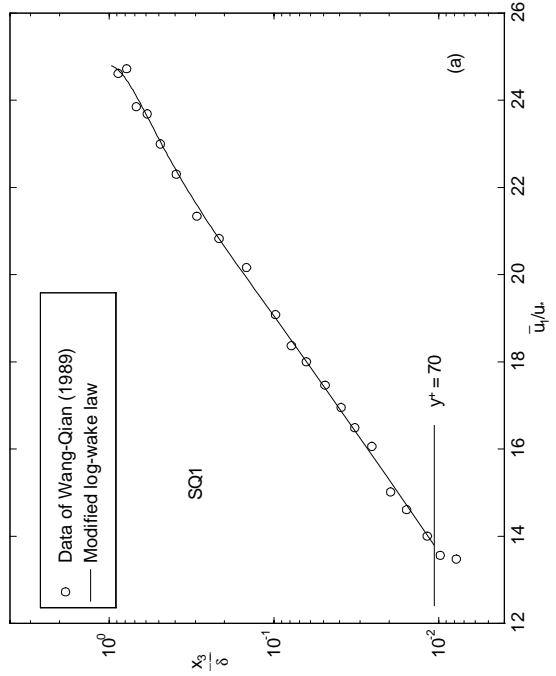
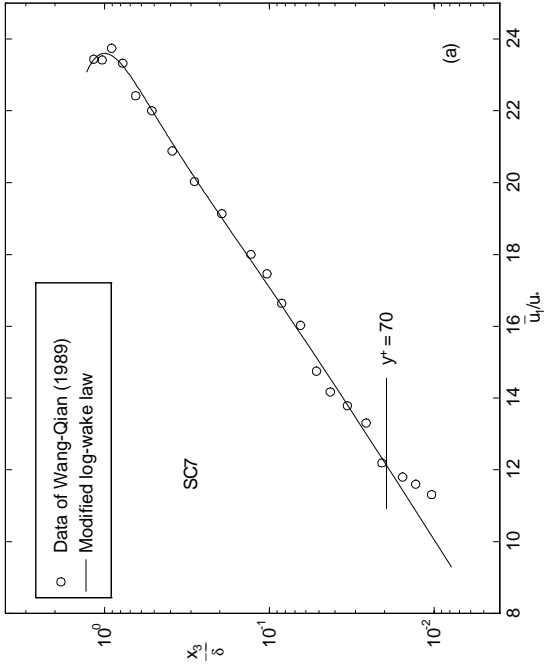
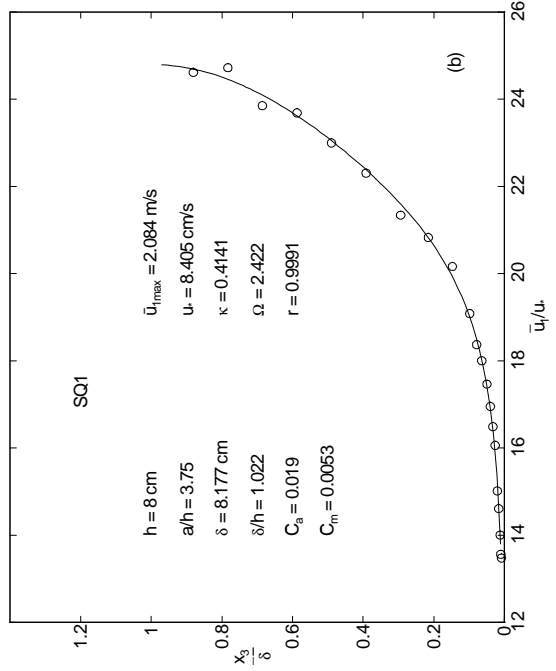
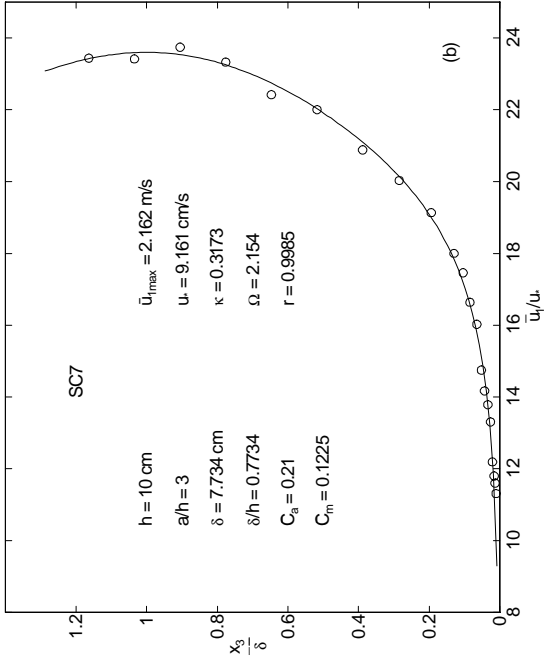


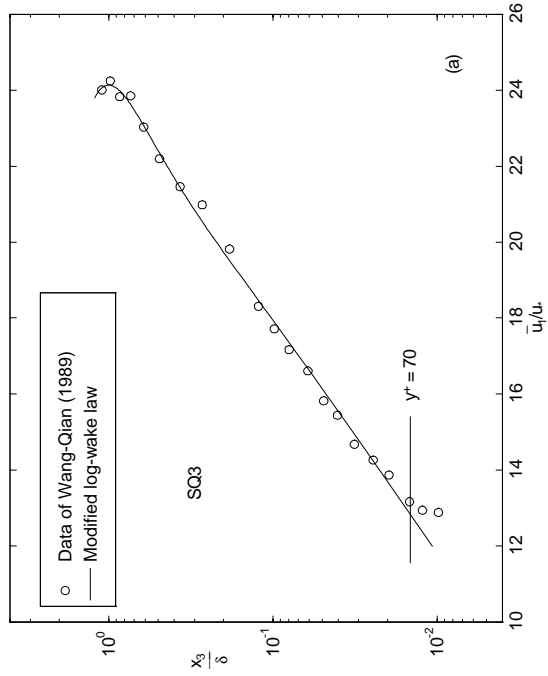
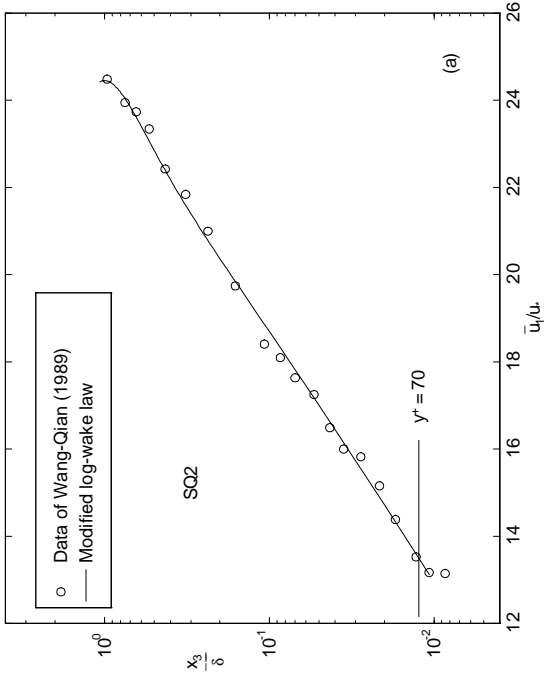
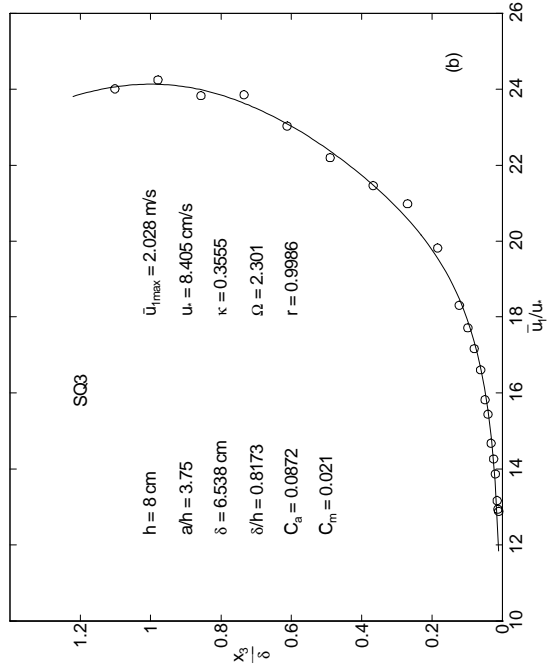
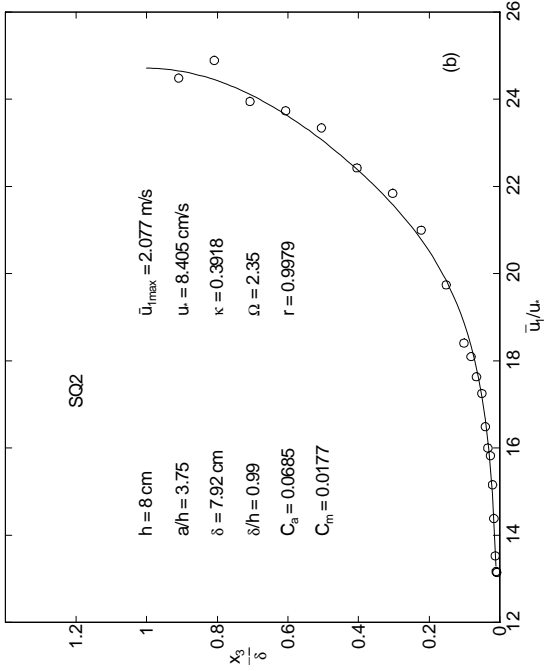












Appendix D

ANALYSIS OF COLEMAN'S EXPERIMENTAL DATA

Coleman (1986) did experiments in a smooth flume which is 356 mm wide and 15 m long. During the experiments, the energy slope S was kept to be 0.002 except the last three runs where $S = 0.0022$. The flow depths are about 171 cm. Runs 1, 21, and 32 are clear water flows. Run 2-20 are with fine sands of $d_s = 0.105$ mm; Runs 22-31 are with middle sands of $d_s = 0.21$ mm; and Runs 33-40 are with coarse sands of $d_s = 0.42$ mm. The temperatures are between 19.5 and 25.3°C. Detailed experimental information can be found in literature (Coleman, 1986). The measurements of velocity and concentration profiles are shown in Table D.1. All velocity profile analyses are attached after the table.

Table D.1: Coleman's (1986) measurement data of velocity and concentration profiles

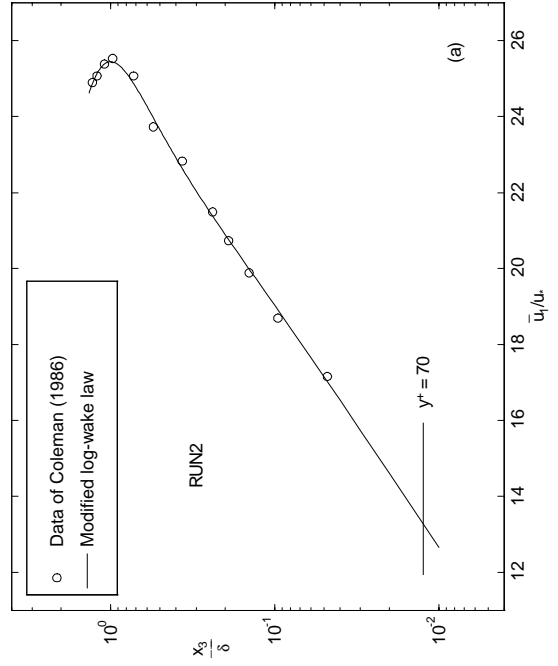
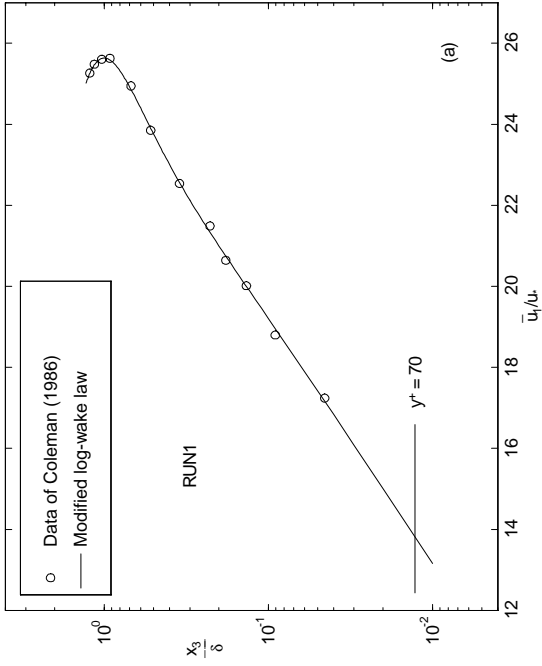
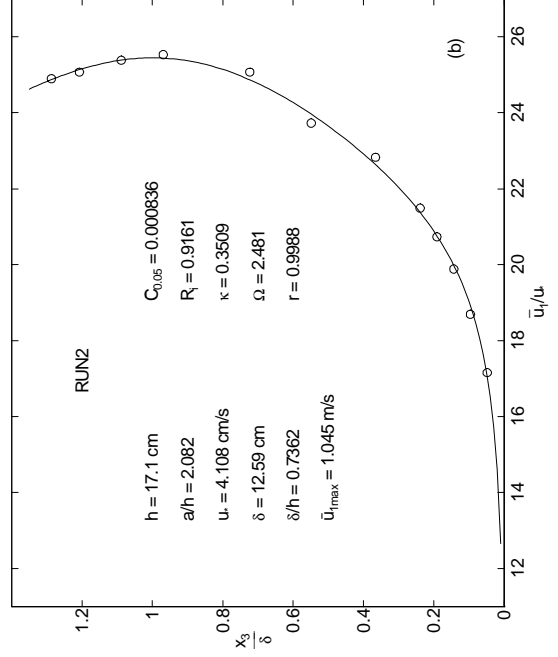
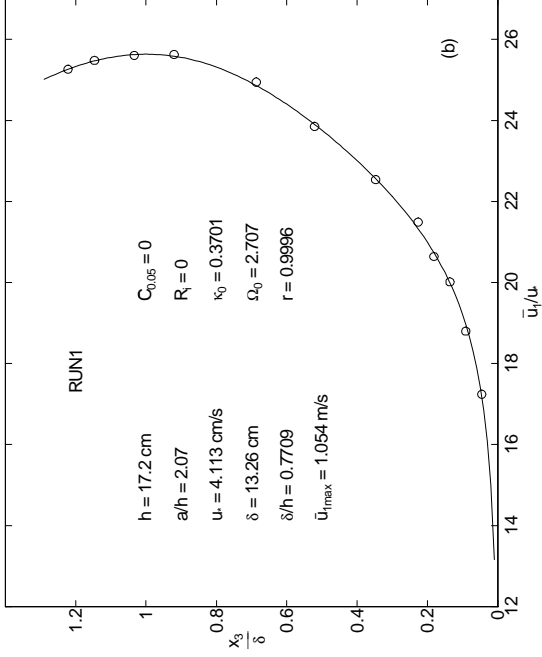
Run No.		x_3 (mm)													
		6	12	18	24	30	46	69	91	122	137	152	162		
1	\bar{u}_1 (m/s)	0.709	0.773	0.823	0.849	0.884	0.927	0.981	1.026	1.054	1.053	1.048	1.039		
2	\bar{C} (1e-4)	8.500	6.400	5.200	4.200	3.700	2.800	2.400	1.400	0.810	0.650	0.500	0.300		
2	\bar{u}_1 (m/s)	0.705	0.768	0.817	0.852	0.883	0.938	0.975	1.030	1.049	1.043	1.030	1.023		
3	\bar{C} (1e-4)	17.000	12.000	9.700	7.600	6.800	5.300	3.900	2.500	1.500	1.100	0.730	0.480		
3	\bar{u}_1 (m/s)	0.680	0.738	0.795	0.836	0.870	0.922	0.963	1.025	1.048	1.039	1.028	1.020		
4	\bar{C} (1e-4)	28.000	19.000	15.000	12.000	10.000	7.500	5.900	3.700	2.200	1.400	1.000	0.560		
4	\bar{u}_1 (m/s)	0.665	0.740	0.802	0.829	0.863	0.922	0.965	1.023	1.049	1.048	1.033	1.024		
5	\bar{C} (1e-4)	40.000	26.000	19.000	16.000	14.000	11.000	7.800	5.000	2.800	2.000	1.300	0.860		
5	\bar{u}_1 (m/s)	0.662	0.717	0.788	0.814	0.852	0.911	0.968	1.028	1.038	1.047	1.030	1.027		
6	\bar{C} (1e-4)	51.000	32.000	24.000	20.000	17.000	12.000	9.600	6.200	3.400	2.300	1.400	0.770		
6	\bar{u}_1 (m/s)	0.652	0.727	0.766	0.805	0.848	0.905	0.951	1.037	1.054	1.049	1.026	1.031		
7	\bar{C} (1e-4)	62.000	40.000	32.000	25.000	21.000	15.000	12.000	7.600	4.300	3.000	1.800	1.100		
7	\bar{u}_1 (m/s)	0.639	0.709	0.770	0.804	0.849	0.924	0.962	1.030	1.061	1.051	1.040	1.027		
8	\bar{C} (1e-4)	77.000	49.000	36.000	30.000	24.000	17.000	14.000	8.600	5.000	3.400	2.000	1.200		
8	\bar{u}_1 (m/s)	0.630	0.696	0.751	0.800	0.831	0.902	0.958	1.012	1.044	1.046	1.033	1.028		
9	\bar{C} (1e-4)	90.000	60.000	42.000	34.000	27.000	19.000	15.000	9.600	5.400	3.500	1.900	1.200		
9	\bar{u}_1 (m/s)	0.621	0.683	0.751	0.804	0.842	0.897	0.945	1.028	1.048	1.050	1.040	1.032		
10	\bar{C} (1e-4)	110.00	66.000	49.000	39.000	32.000	21.000	17.000	11.000	5.500	3.400	2.000	1.000		
10	\bar{u}_1 (m/s)	0.619	0.688	0.759	0.808	0.841	0.912	0.976	1.033	1.061	1.062	1.050	1.045		
11	\bar{C} (1e-4)	120.00	78.000	54.000	41.000	35.000	24.000	18.000	12.000	5.900	3.200	1.800	0.700		
11	\bar{u}_1 (m/s)	0.625	0.688	0.761	0.812	0.855	0.929	0.989	1.050	1.085	1.077	1.070	1.063		
12	\bar{C} (1e-4)	130.00	82.000	56.000	44.000	36.000	25.000	19.000	12.000	7.000	4.000	2.300	1.300		
12	\bar{u}_1 (m/s)	0.598	0.669	0.731	0.796	0.830	0.912	0.964	1.004	1.052	1.058	1.045	1.033		
13	\bar{C} (1e-4)	140.00	90.000	63.000	49.000	40.000	28.000	21.000	14.000	7.400	4.400	2.400	1.300		
13	\bar{u}_1 (m/s)	0.600	0.665	0.747	0.798	0.844	0.914	0.973	1.038	1.070	1.062	1.045	1.039		

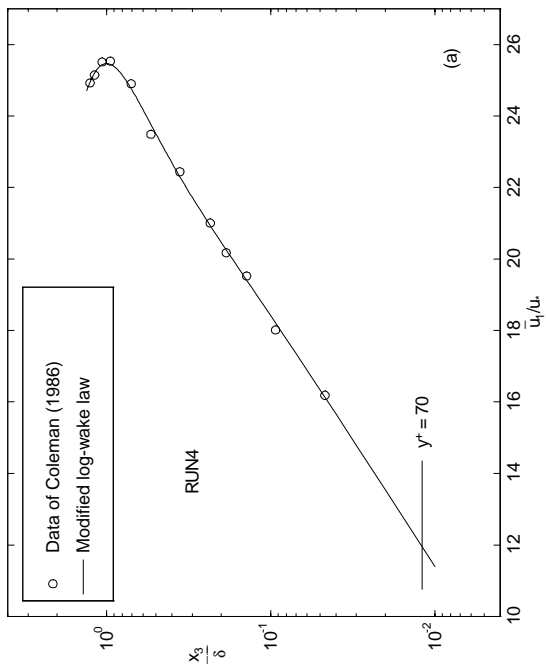
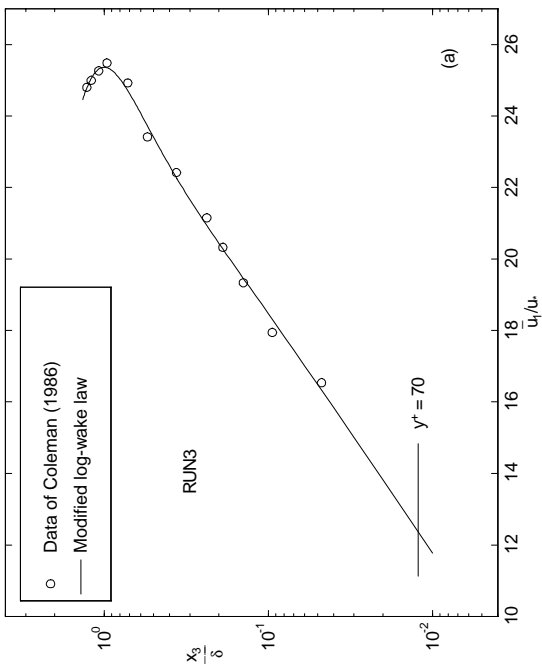
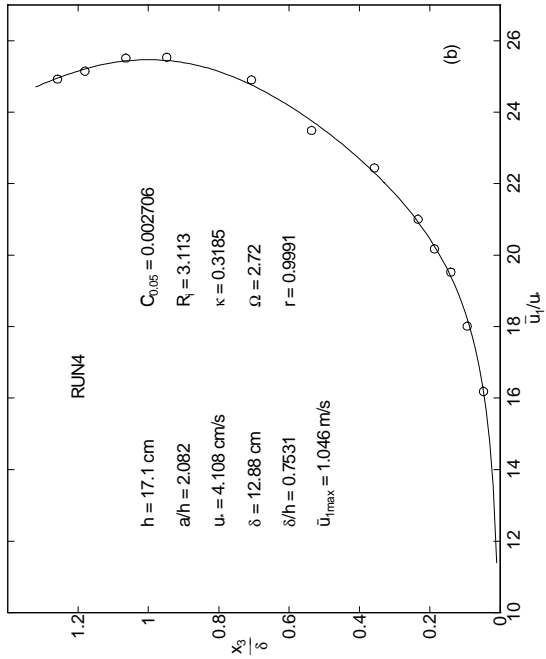
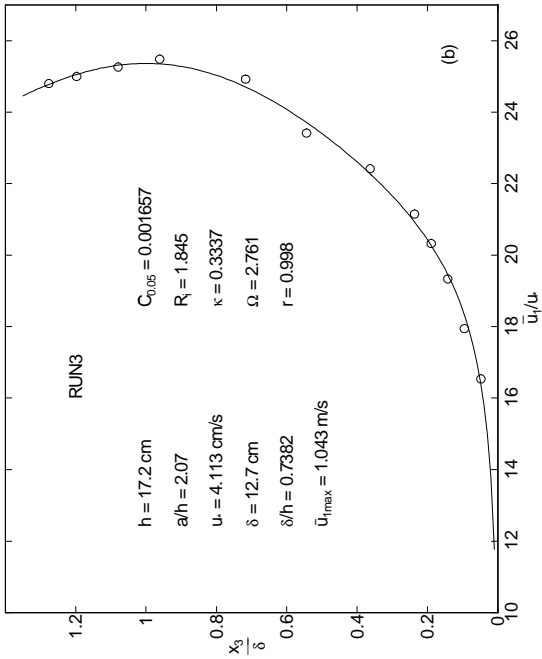
Table D.1 (continued)

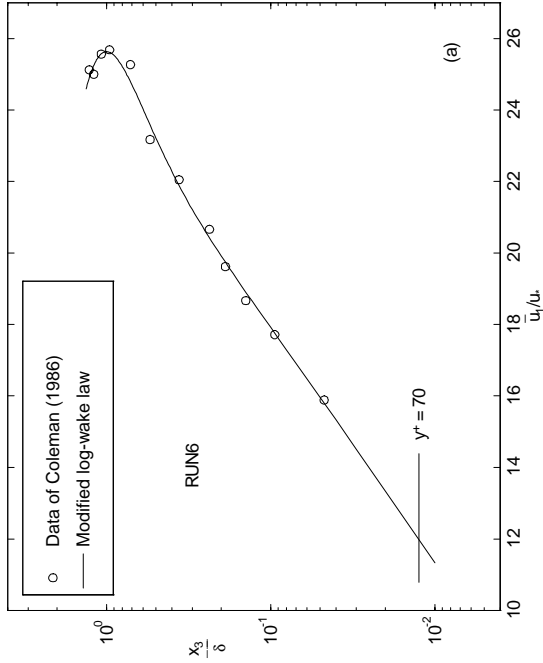
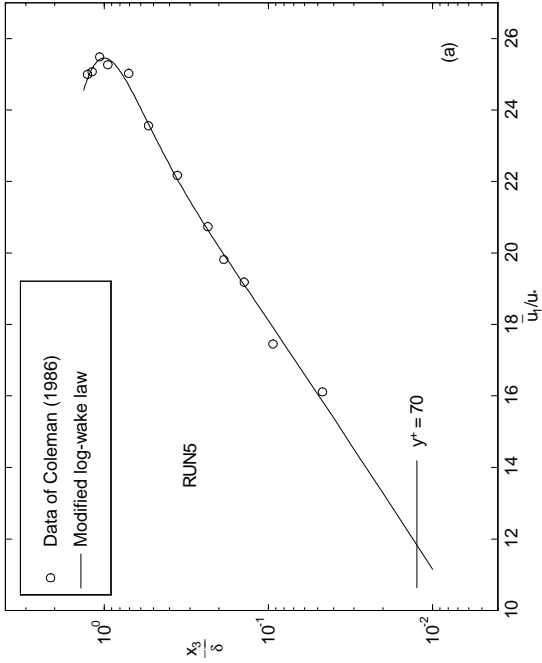
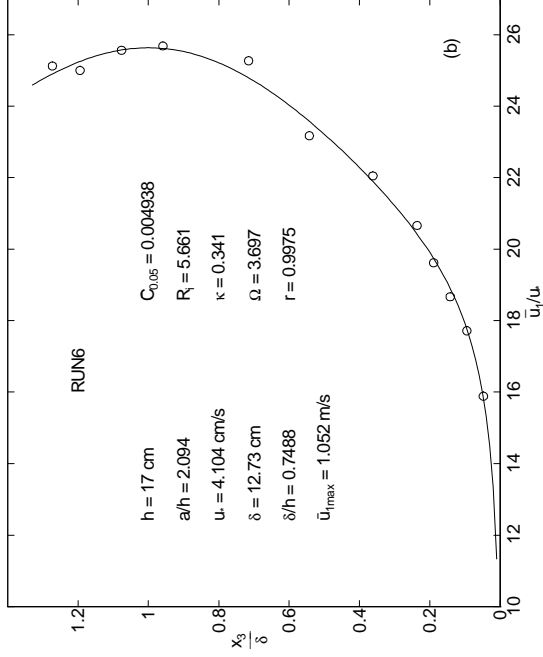
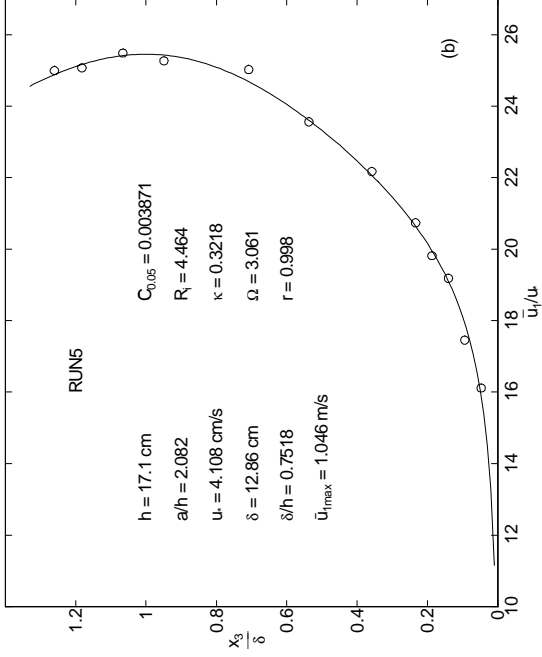
14	$\bar{C}(1e-4)$	150.00	98.000	68.000	52.000	44.000	30.000	23.000	14.000	8.000	4.600	2.400	1.200
14	$\bar{u}_1(\text{ m/s})$	0.598	0.669	0.746	0.800	0.840	0.922	0.971	1.042	1.067	1.062	1.051	1.048
15	$\bar{C}(1e-4)$	170.00	100.00	71.000	54.000	44.000	31.000	24.000	16.000	8.200	4.500	2.300	1.300
15	$\bar{u}_1(\text{ m/s})$	0.588	0.674	0.746	0.799	0.850	0.918	0.980	1.052	1.074	1.070	1.059	1.050
16	$\bar{C}(1e-4)$	180.00	110.00	74.000	56.000	47.000	32.000	25.000	16.000	7.900	4.600	2.200	1.200
16	$\bar{u}_1(\text{ m/s})$	0.583	0.661	0.744	0.804	0.854	0.922	0.978	1.051	1.074	1.070	1.057	1.046
17	$\bar{C}(1e-4)$	190.00	110.00	64.000	58.000	47.000	31.000	24.000	15.000	7.600	4.700	2.100	1.400
17	$\bar{u}_1(\text{ m/s})$	0.586	0.655	0.750	0.804	0.838	0.938	0.976	1.022	1.071	1.071	1.060	1.053
18	$\bar{C}(1e-4)$	190.00	110.00	74.000	56.000	46.000	32.000	24.000	15.000	8.000	5.200	2.500	1.300
18	$\bar{u}_1(\text{ m/s})$	0.579	0.688	0.734	0.780	0.836	0.916	0.966	1.027	1.054	1.053	1.049	1.024
19	$\bar{C}(1e-4)$	210.00	120.00	77.000	59.000	48.000	32.000	25.000	16.000	8.000	4.400	2.200	1.600
19	$\bar{u}_1(\text{ m/s})$	0.576	0.649	0.743	0.798	0.838	0.916	0.976	1.047	1.070	1.070	1.057	1.048
20	$\bar{C}(1e-4)$	230.00	120.00	82.000	61.000	48.000	33.000	26.000	16.000	7.600	4.000	2.000	1.100
20	$\bar{u}_1(\text{ m/s})$	0.570	0.648	0.743	0.791	0.848	0.922	0.986	1.043	1.070	1.068	1.057	1.048
21	$\bar{u}_1(\text{ m/s})$	0.734	0.789	0.827	0.867	0.891	0.936	0.987	1.030	1.048	1.046	1.033	1.028
22	$\bar{C}(1e-4)$	9.800	6.300	4.200	3.300	3.000	2.100	1.600	1.100	0.640	0.500	0.420	0.320
22	$\bar{u}_1(\text{ m/s})$	0.738	0.775	0.814	0.841	0.855	0.916	0.953	1.015	1.026	1.024	1.012	1.008
23	$\bar{C}(1e-4)$	21.000	12.000	8.600	6.800	5.600	3.900	2.900	1.900	1.100	0.900	0.630	0.640
23	$\bar{u}_1(\text{ m/s})$	0.717	0.764	0.816	0.839	0.866	0.918	0.971	1.030	1.052	1.039	1.027	1.021
24	$\bar{C}(1e-4)$	34.000	18.000	13.000	11.000	8.600	6.000	4.500	2.700	1.600	1.200	0.890	0.630
24	$\bar{u}_1(\text{ m/s})$	0.684	0.742	0.794	0.844	0.872	0.922	0.959	1.030	1.056	1.049	1.034	1.024
25	$\bar{C}(1e-4)$	48.000	26.000	18.000	13.000	11.000	7.600	5.900	3.600	2.200	1.500	1.100	0.680
25	$\bar{u}_1(\text{ m/s})$	0.660	0.737	0.790	0.844	0.872	0.934	0.984	1.051	1.073	1.063	1.048	1.040
26	$\bar{C}(1e-4)$	54.000	32.000	22.000	18.000	14.000	9.700	7.800	4.800	2.800	2.100	1.500	1.100
26	$\bar{u}_1(\text{ m/s})$	0.649	0.713	0.775	0.809	0.843	0.899	0.960	1.020	1.045	1.041	1.032	1.027
27	$\bar{C}(1e-4)$	66.000	40.000	26.000	21.000	17.000	12.000	8.900	5.300	2.800	2.000	1.400	0.880

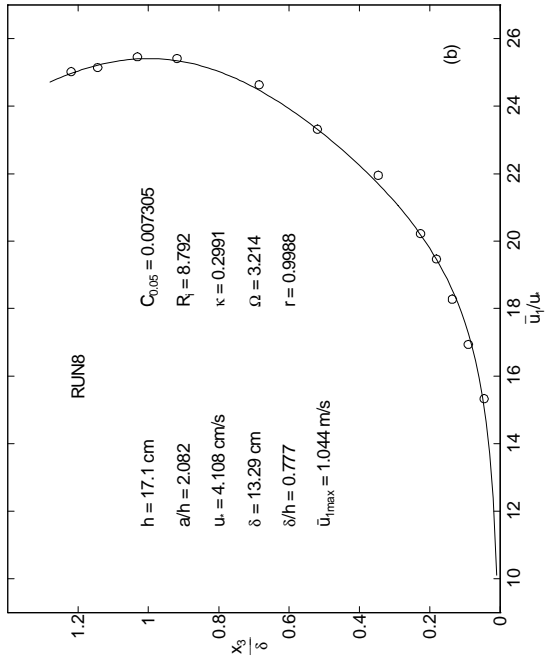
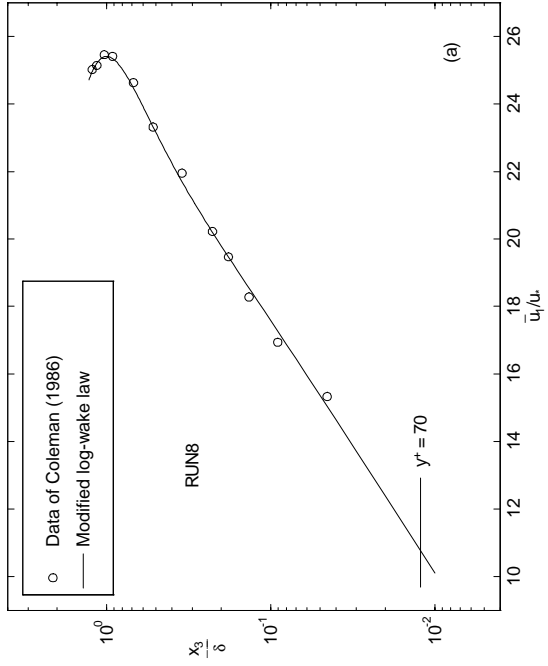
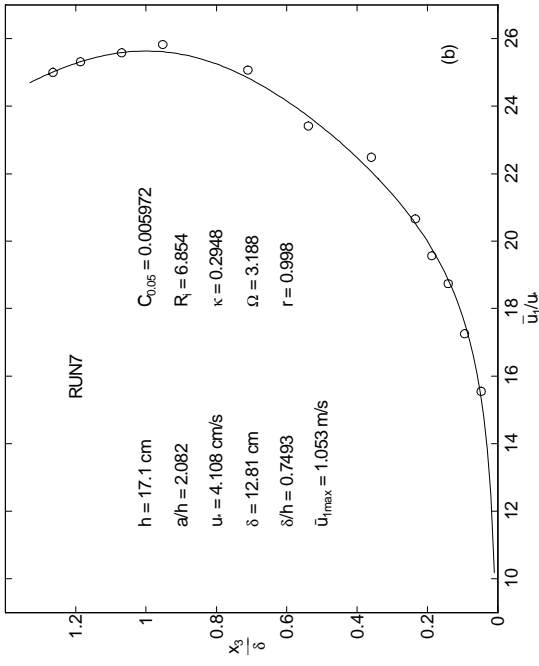
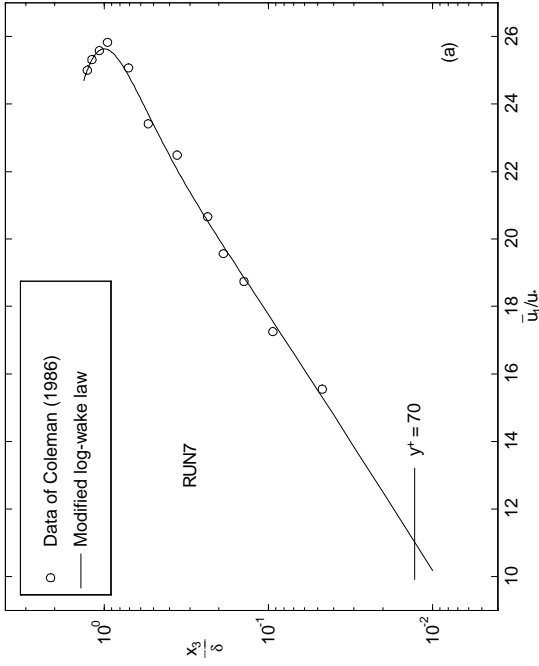
Table D.1 (continued)

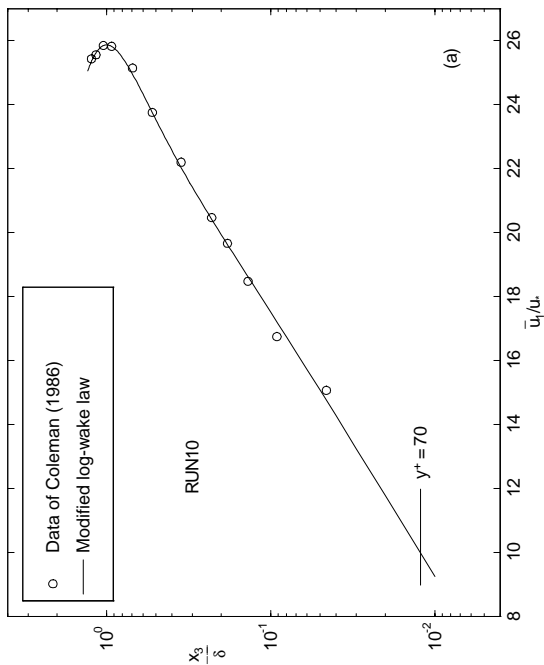
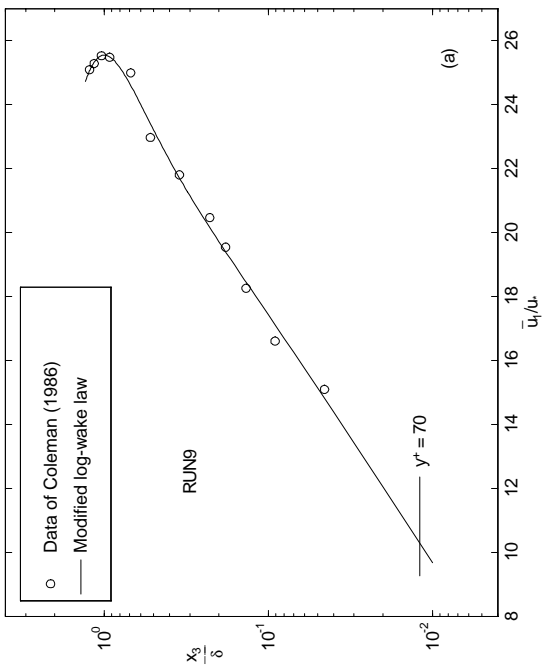
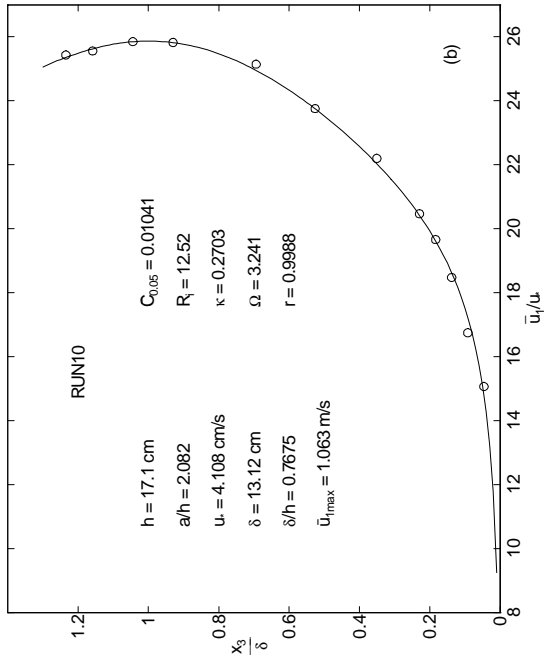
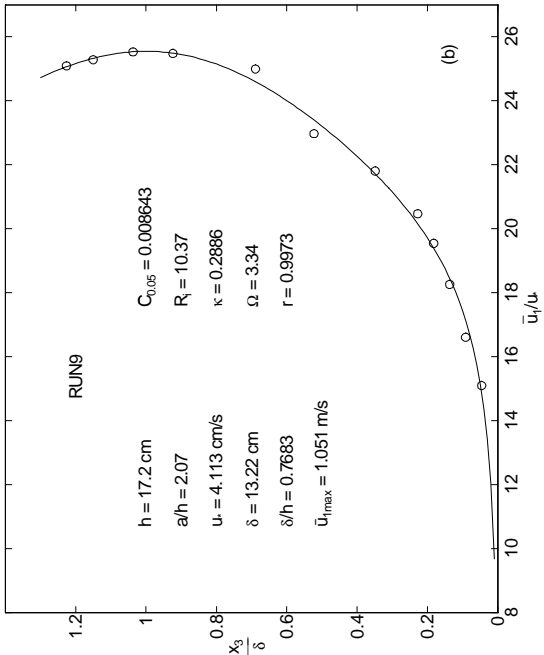
27	\bar{u}_1 (m/s)	0.662	0.720	0.775	0.801	0.863	0.925	0.984	1.042	1.075	1.064	1.052	1.044
28	\bar{C} (1e-4)	80.000	48.000	31.000	23.000	19.000	13.000	9.800	5.900	3.300	2.300	1.700	1.200
28	\bar{u}_1 (m/s)	0.638	0.714	0.771	0.811	0.848	0.910	0.967	1.040	1.065	1.060	1.043	1.044
29	\bar{C} (1e-4)	95.000	52.000	34.000	26.000	21.000	17.000	11.000	6.400	3.400	2.600	1.600	0.980
29	\bar{u}_1 (m/s)	0.648	0.701	0.776	0.823	0.853	0.930	0.991	1.055	1.084	1.082	1.066	1.064
30	\bar{C} (1e-4)	110.00	57.000	39.000	28.000	24.000	16.000	12.000	7.100	3.700	2.700	1.800	1.100
30	\bar{u}_1 (m/s)	0.661	0.713	0.772	0.822	0.876	0.932	0.999	1.064	1.089	1.093	1.076	1.074
31	\bar{u}_1 (m/s)	0.598	0.679	0.743	0.791	0.828	0.899	0.960	1.026	1.063	1.058	1.048	1.042
31	\bar{C} (1e-4)	120.00	63.000	40.000	30.000	24.000	16.000	12.000	7.700	4.100	3.000	2.000	1.500
32	\bar{u}_1 (m/s)	0.689	0.746	0.786	0.821	0.838	0.887	0.964	0.999	1.024	1.025	1.012	1.004
33	\bar{C} (1e-4)	2.700	1.400	0.860	0.660	0.570	0.430	0.340	0.230	0.190	0.160	0.140	0.120
33	\bar{u}_1 (m/s)	0.690	0.746	0.791	0.832	0.853	0.903	0.948	1.027	1.018	1.042	1.027	1.018
35	\bar{C} (1e-4)	5.100	2.400	1.500	1.200	0.970	0.700	0.560	0.320	0.270	0.240	0.190	0.180
35	\bar{u}_1 (m/s)	0.709	0.745	0.788	0.820	0.861	0.906	0.952	1.019	1.046	1.050	1.029	1.012
35	\bar{C} (1e-4)	9.300	4.100	2.200	1.700	1.500	1.100	0.860	0.560	0.420	0.340	0.310	0.250
35	\bar{u}_1 (m/s)	0.688	0.733	0.788	0.826	0.863	0.917	0.960	1.019	1.065	1.060	1.045	1.028
36	\bar{C} (1e-4)	17.000	6.800	3.800	3.000	2.300	1.700	1.200	0.880	0.610	0.480	0.400	0.320
36	\bar{u}_1 (m/s)	0.698	0.740	0.804	0.841	0.881	0.942	0.988	1.055	1.090	1.080	1.068	1.062
37	\bar{C} (1e-4)	19.000	7.800	4.700	3.600	2.900	2.200	1.700	1.100	0.800	0.630	0.540	0.430
37	\bar{u}_1 (m/s)	0.674	0.724	0.796	0.835	0.871	0.920	0.985	1.050	1.086	1.077	1.067	1.058
38	\bar{C} (1e-4)	22.000	11.000	6.000	4.600	4.000	2.700	2.200	1.400	0.960	0.790	0.640	0.550
38	\bar{u}_1 (m/s)	0.716	0.735	0.810	0.847	0.884	0.952	0.998	1.091	1.118	1.110	1.098	1.092
39	\bar{C} (1e-4)	27.000	11.000	6.200	4.900	4.000	3.000	2.300	1.600	1.000	0.880	0.800	0.640
39	\bar{u}_1 (m/s)	0.677	0.745	0.798	0.826	0.871	0.936	0.981	1.068	1.099	1.096	1.084	1.072
40	\bar{C} (1e-4)	26.000	11.000	6.400	4.600	4.200	3.000	2.500	1.600	1.200	0.970	0.800	0.690
40	\bar{u}_1 (m/s)	0.678	0.710	0.792	0.836	0.879	0.936	0.985	1.069	1.107	1.101	1.086	1.080

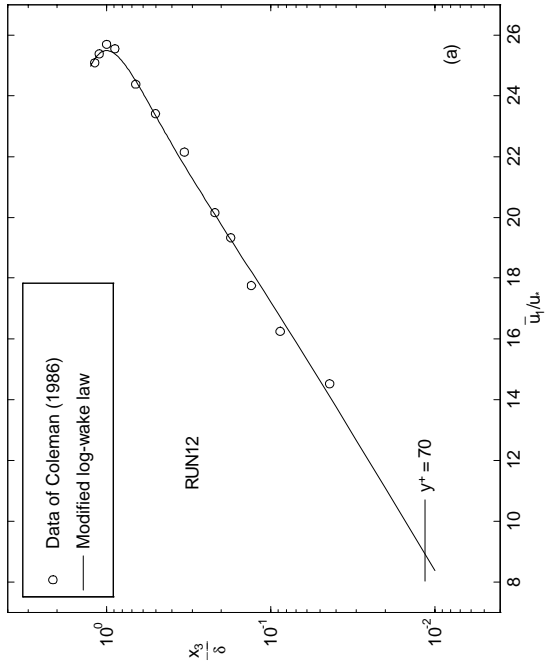
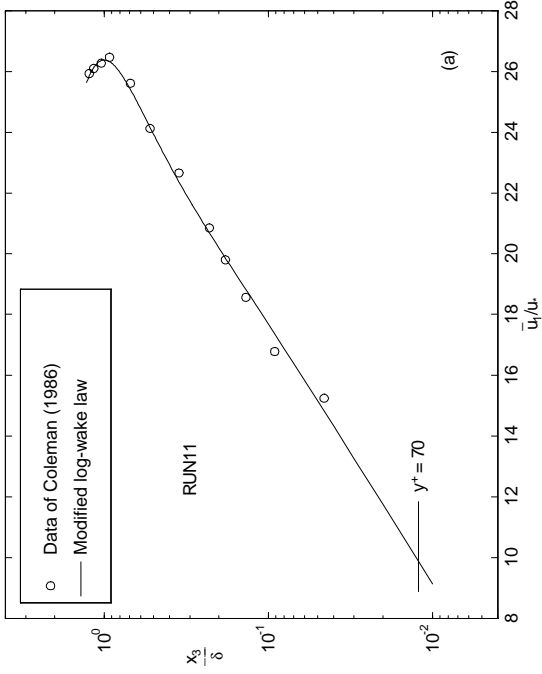
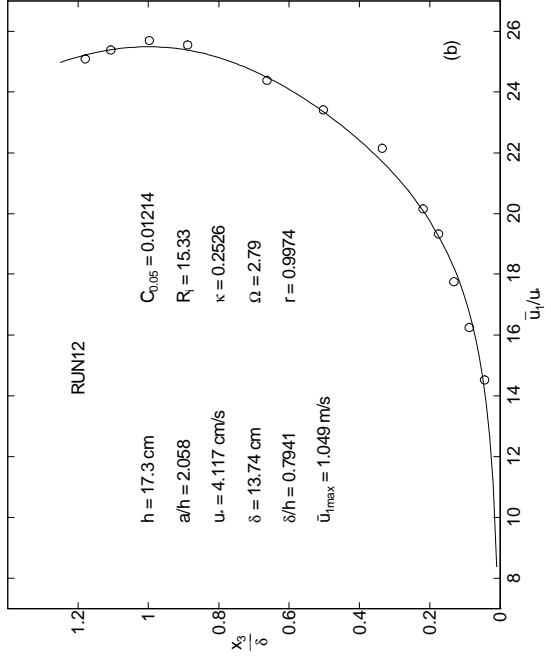
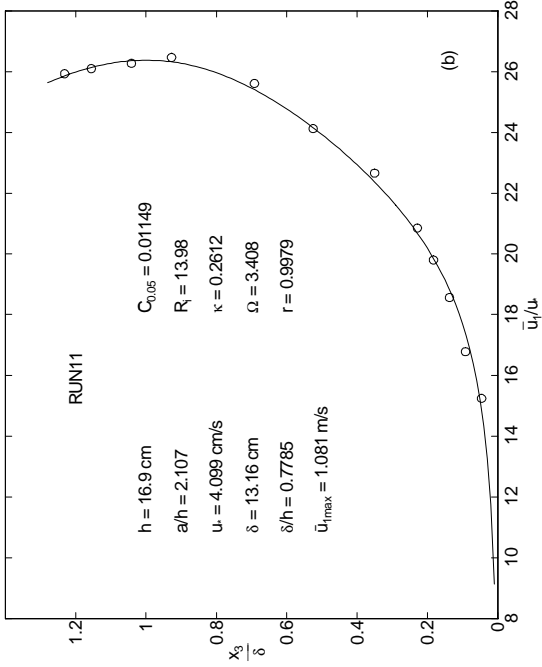


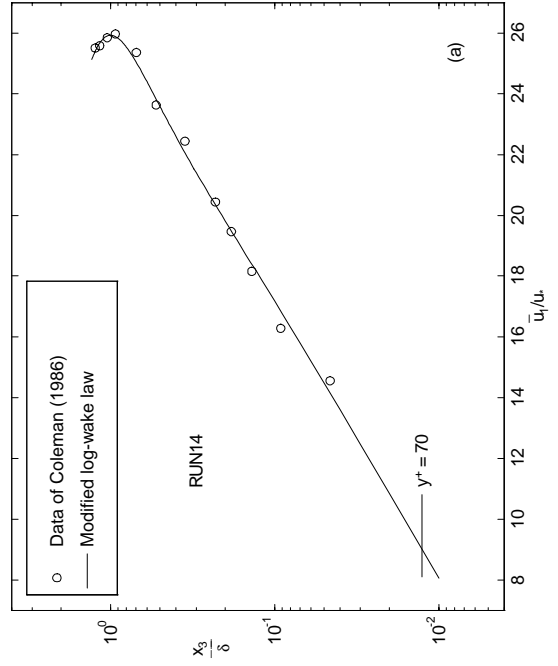
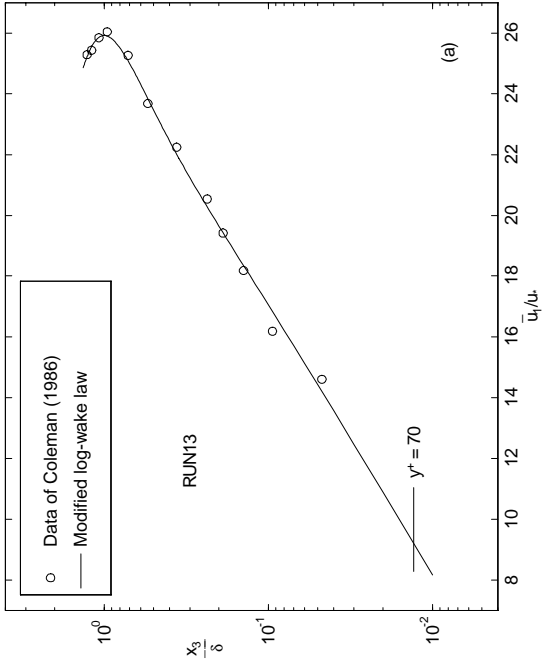
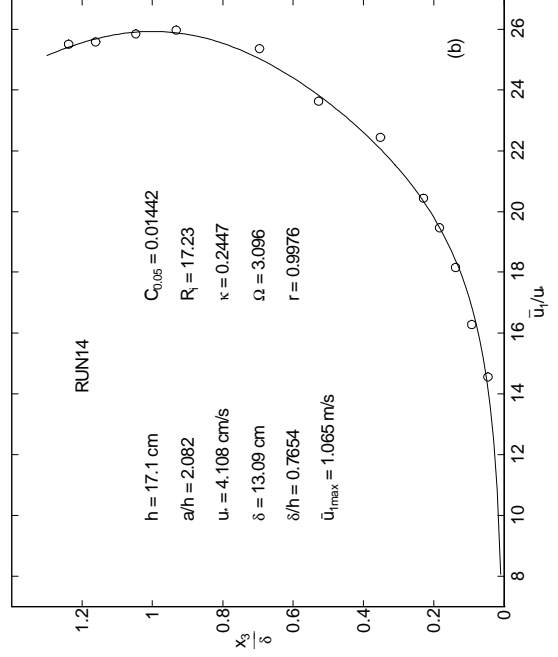
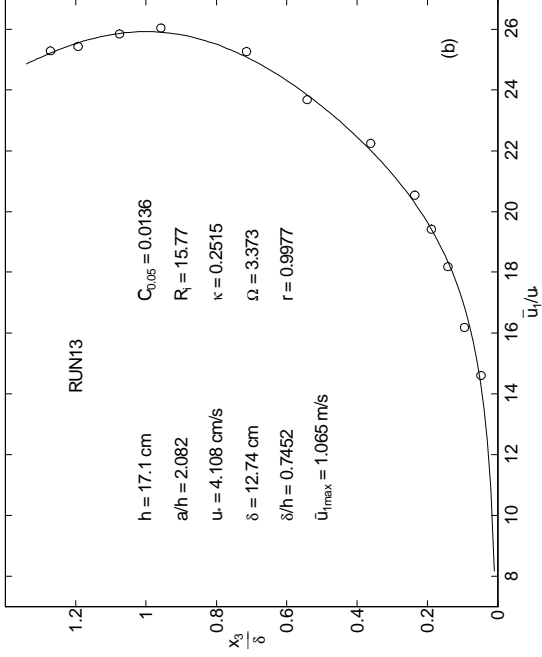


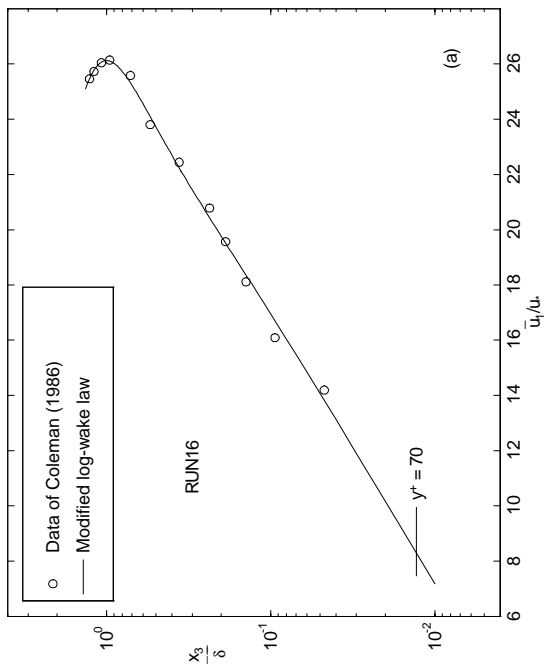
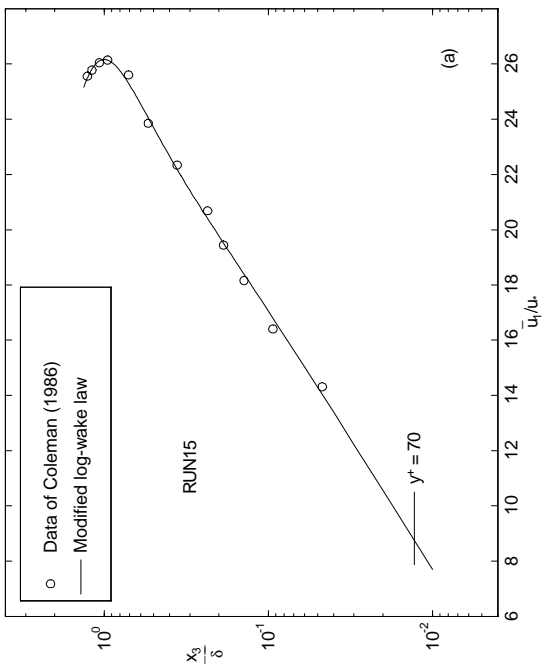
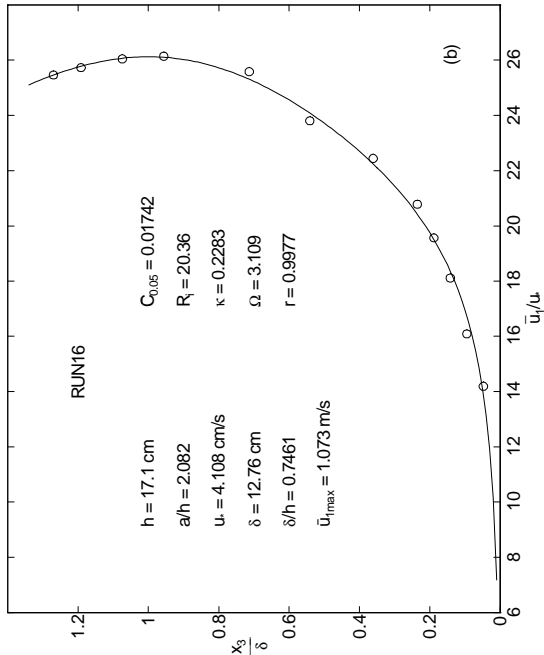
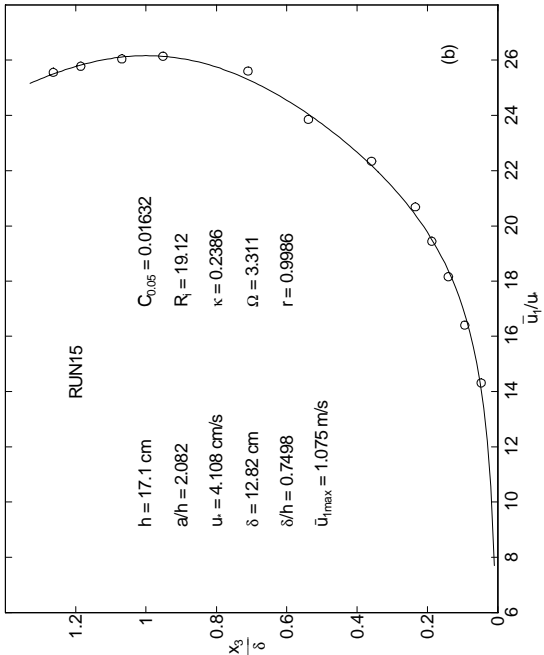


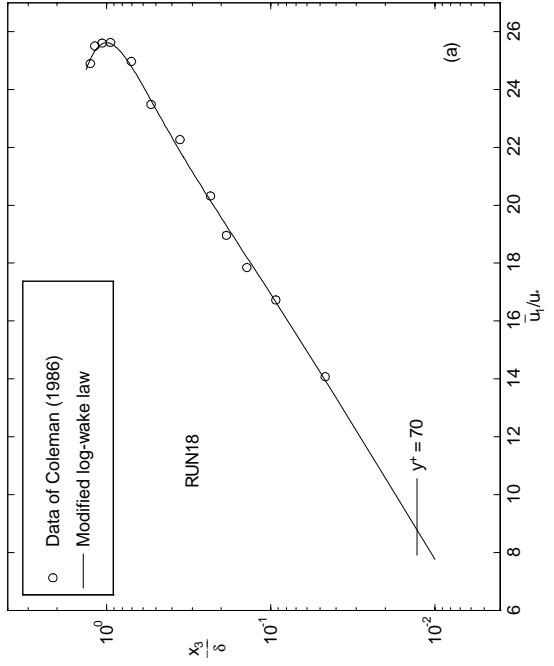
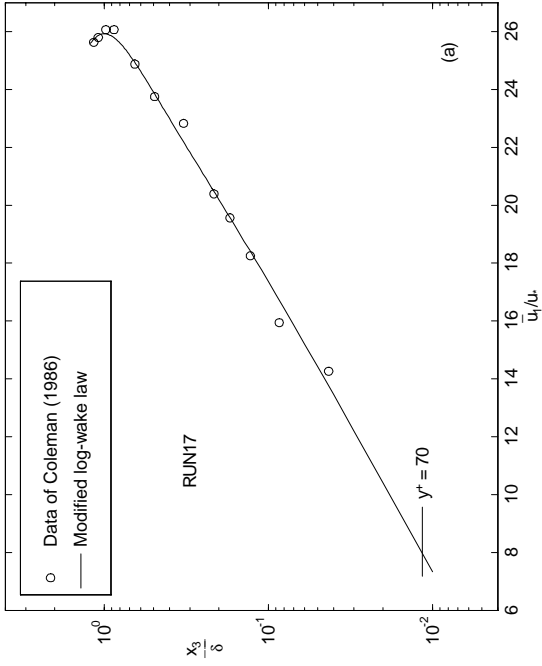
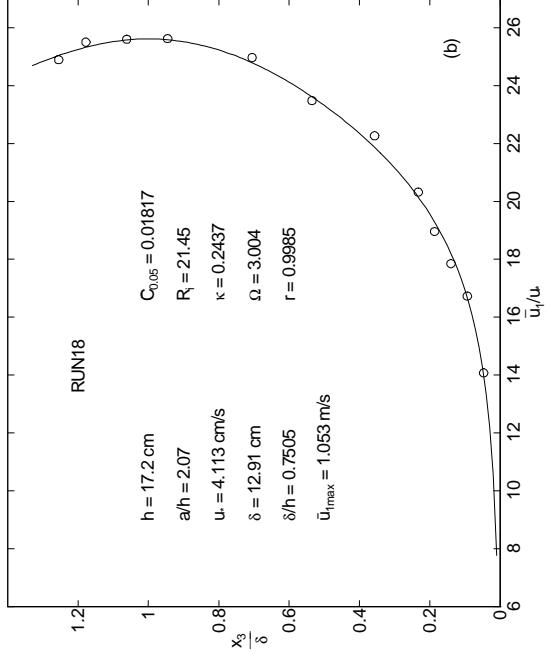
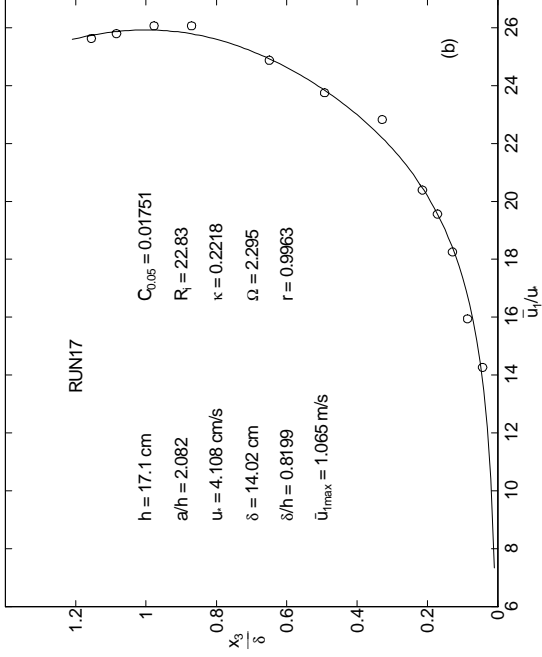


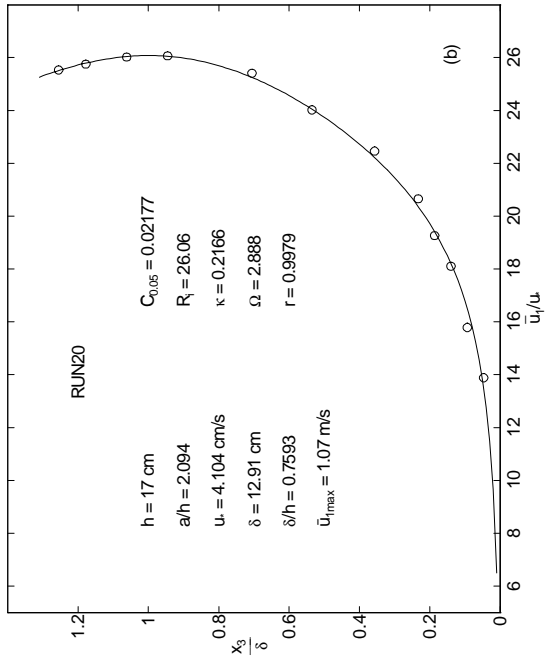
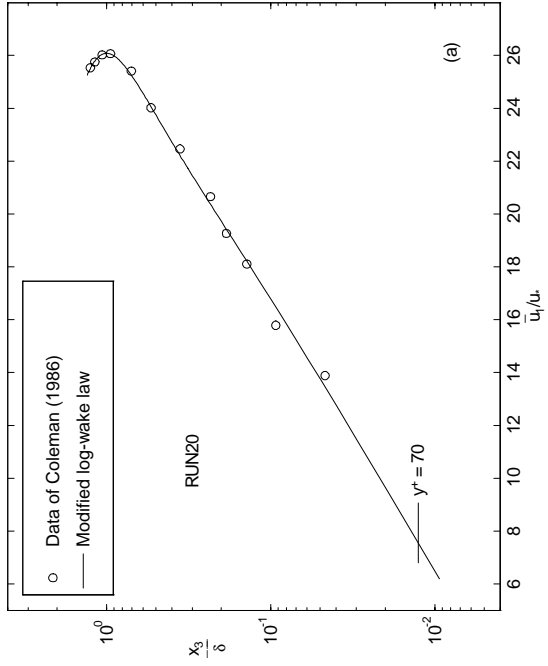
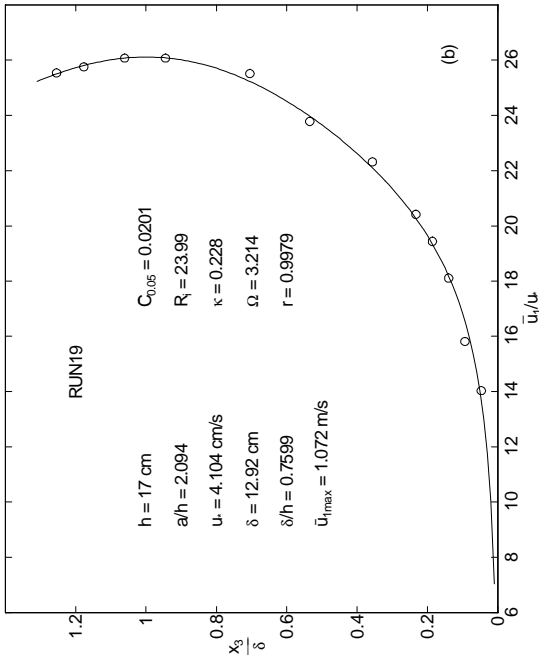
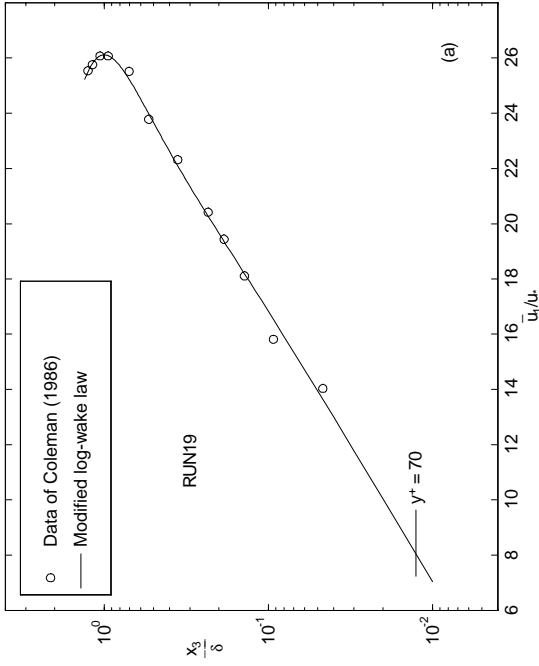


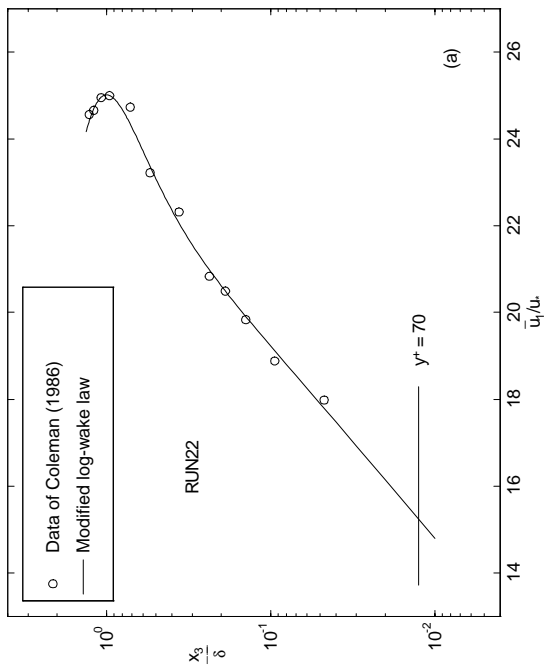
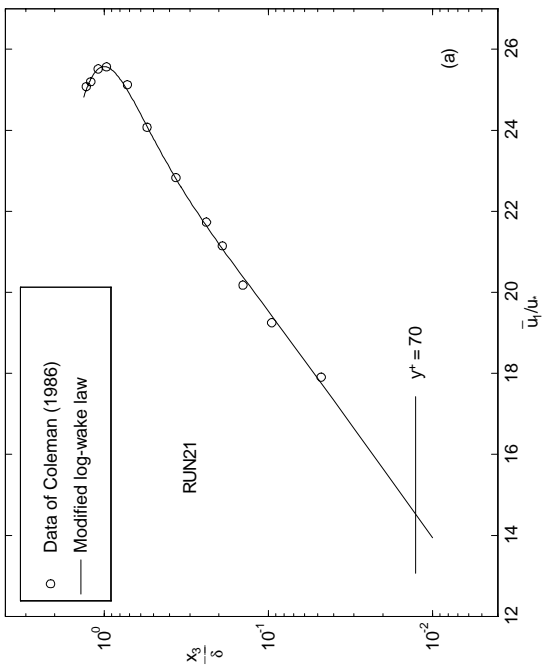
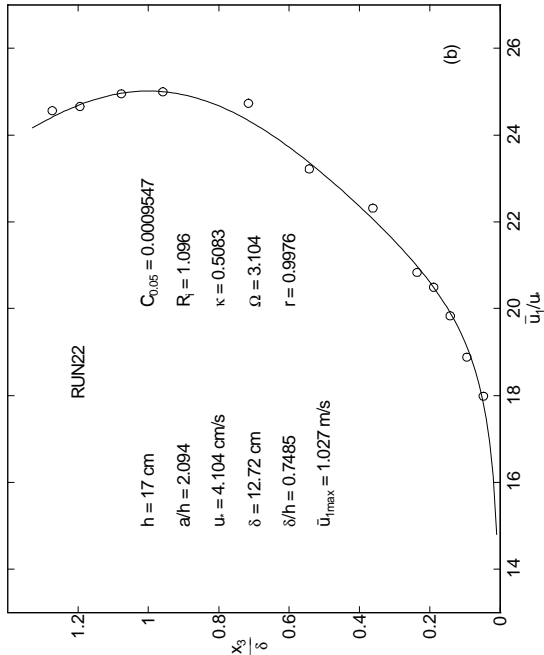
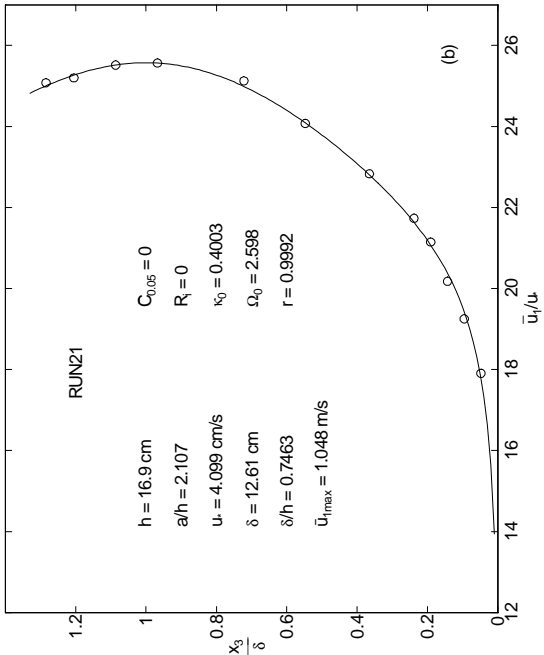


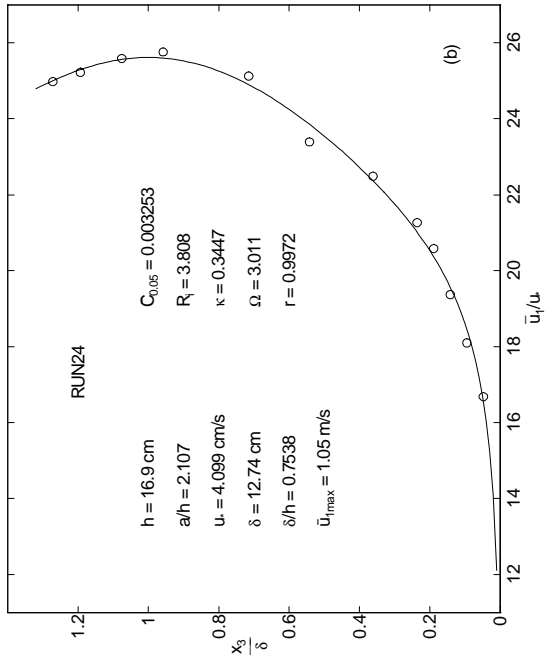
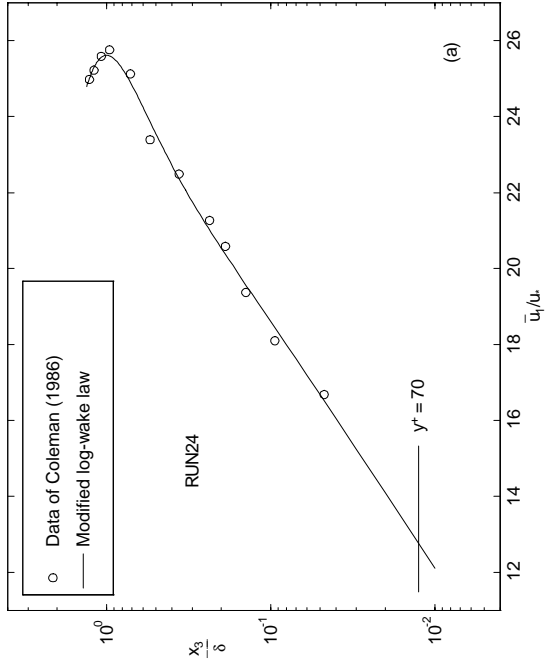
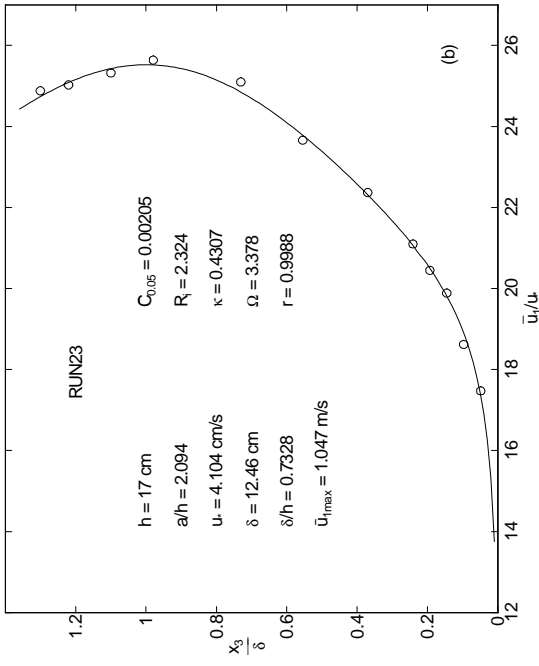
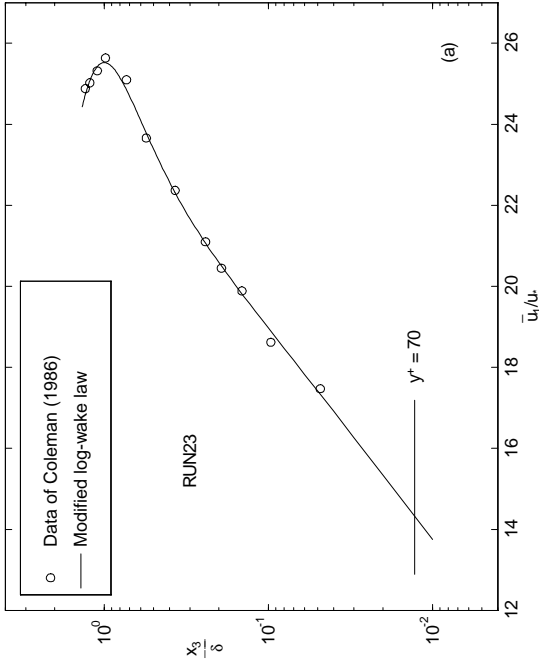


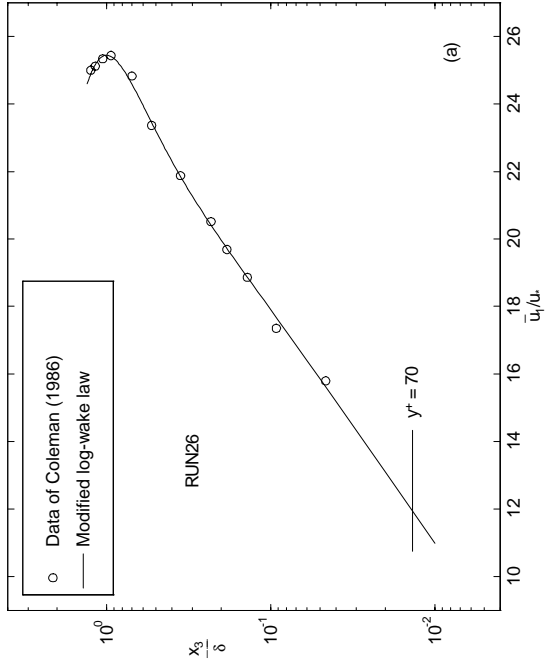
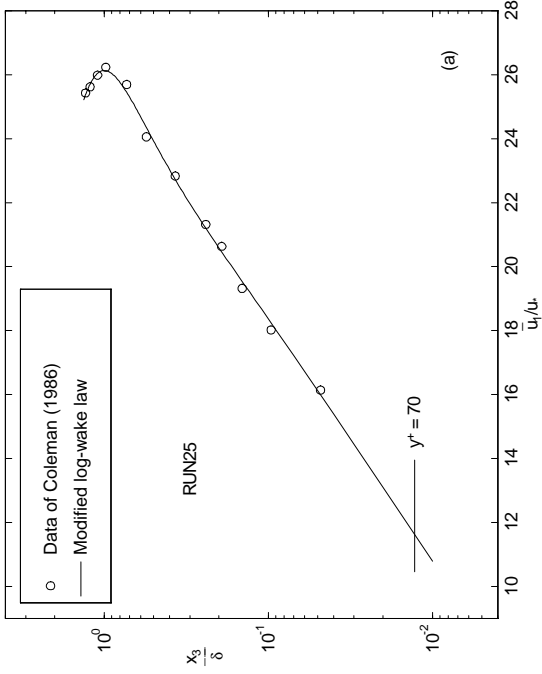
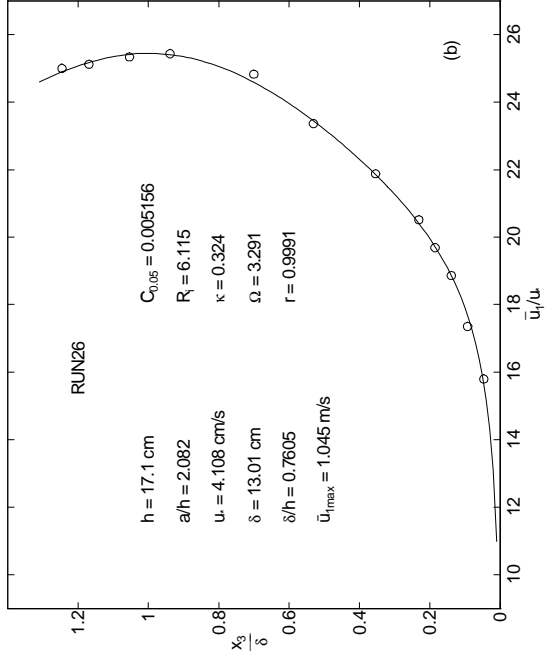
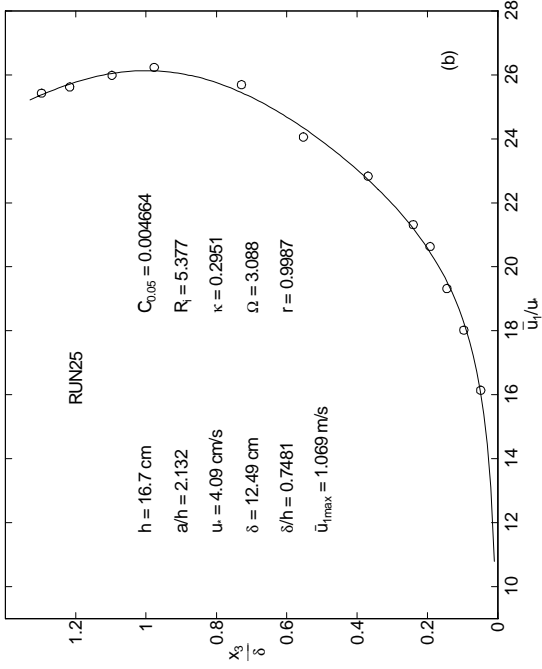


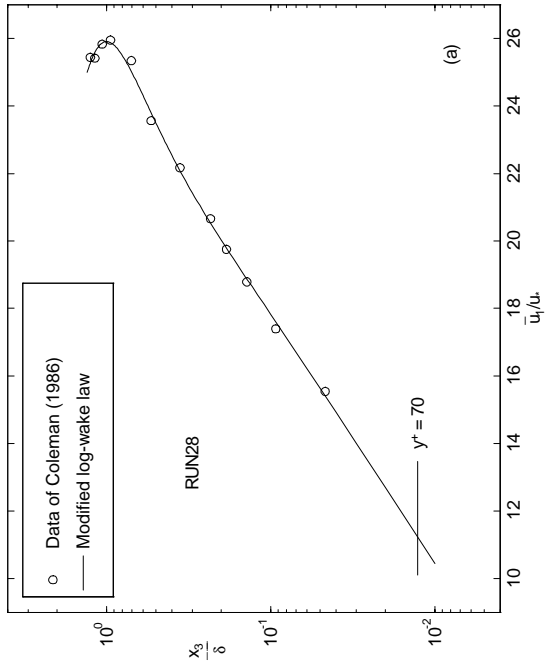
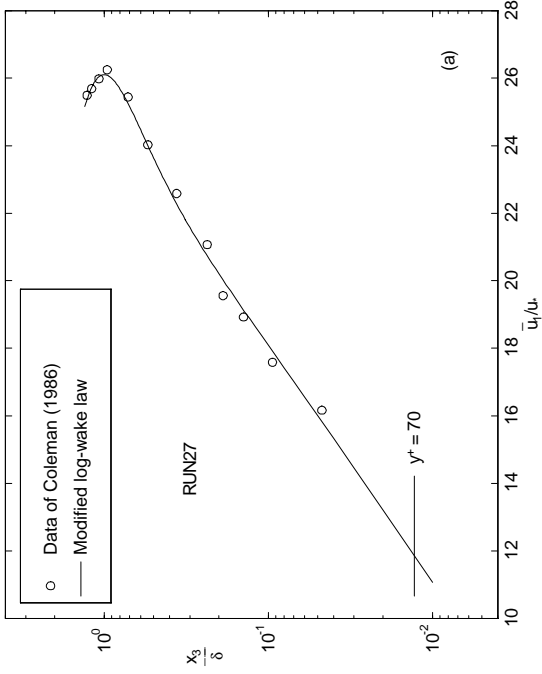
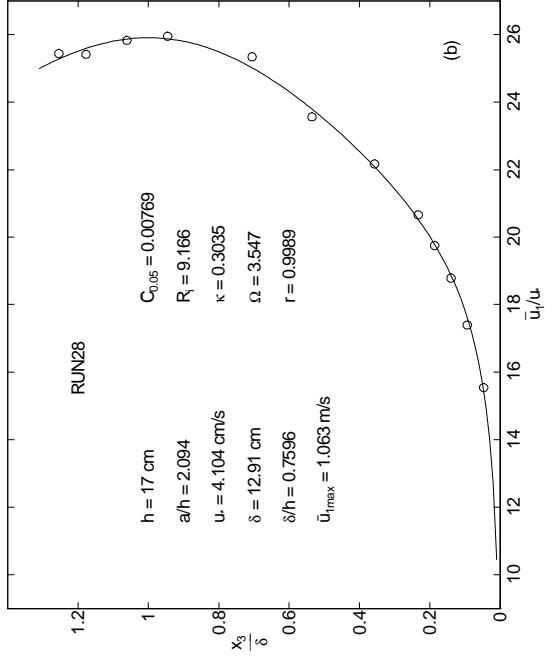
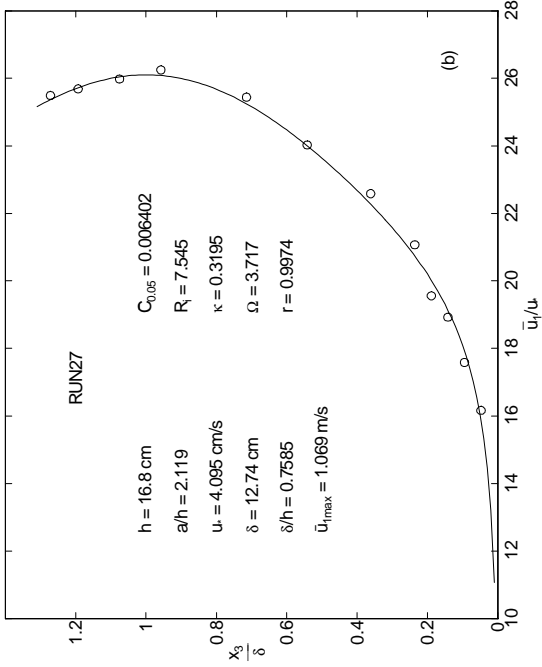


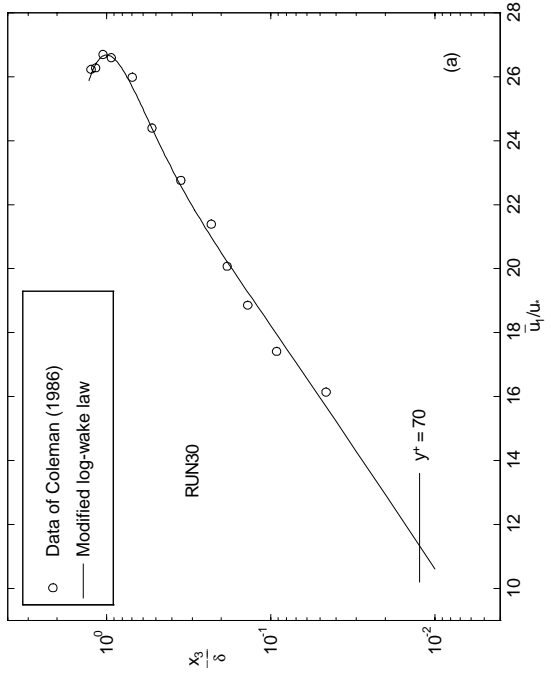
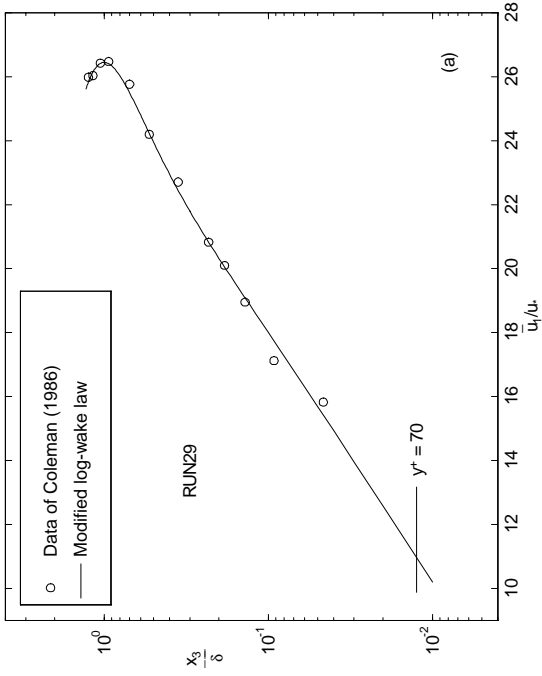
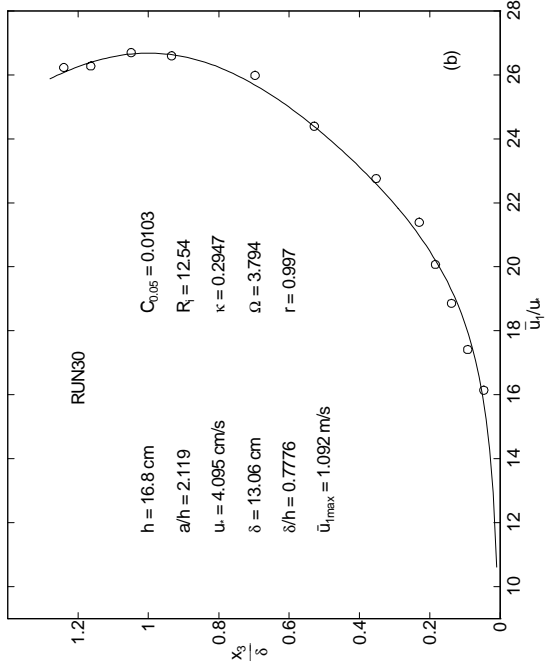
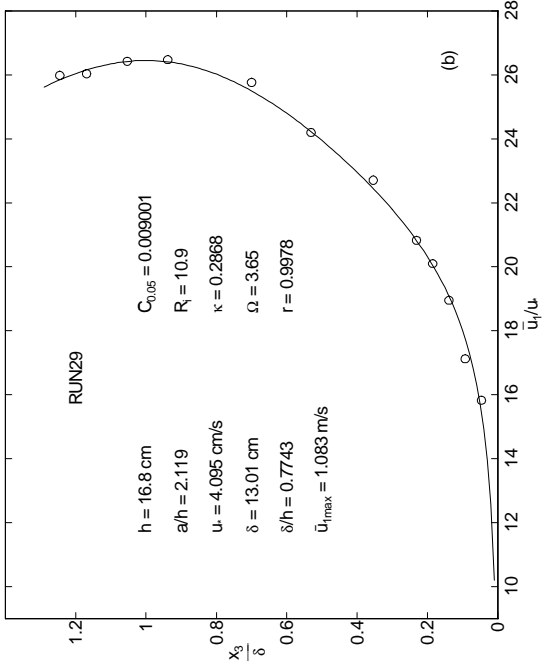


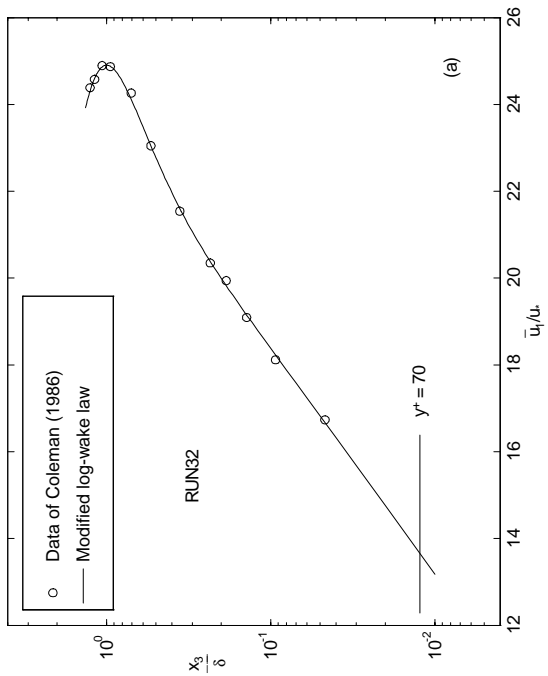
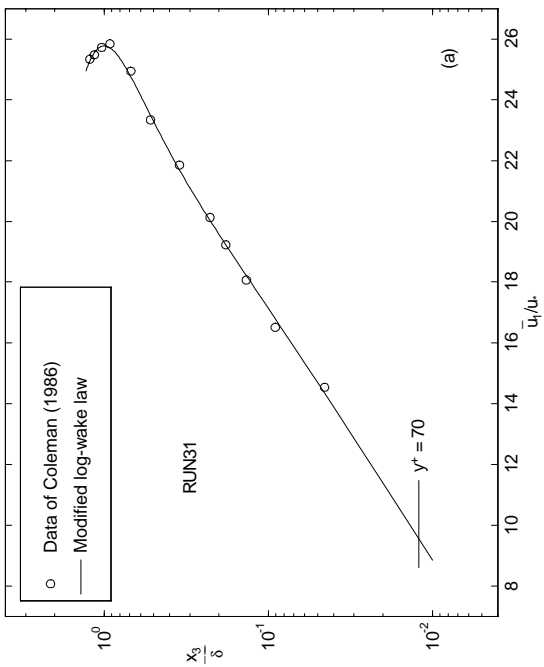
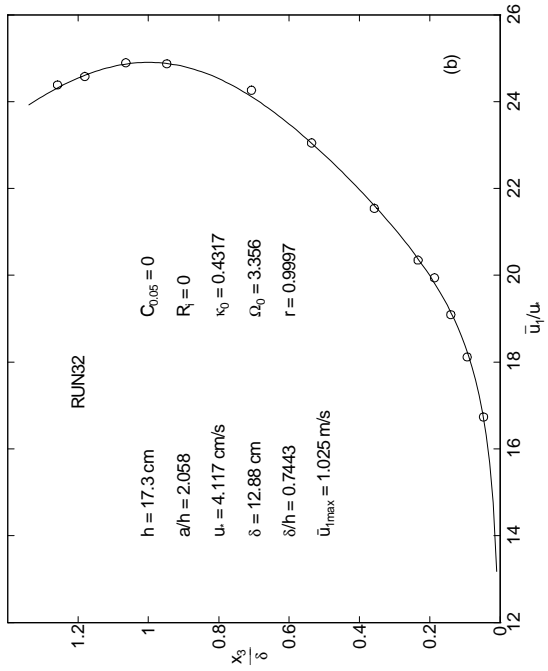
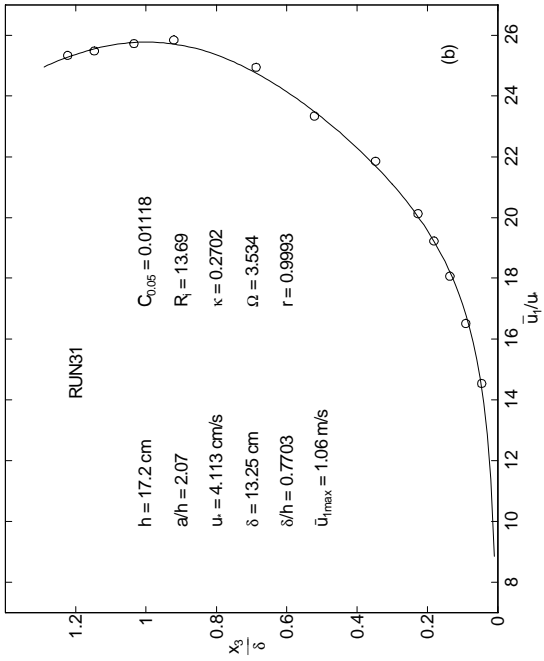


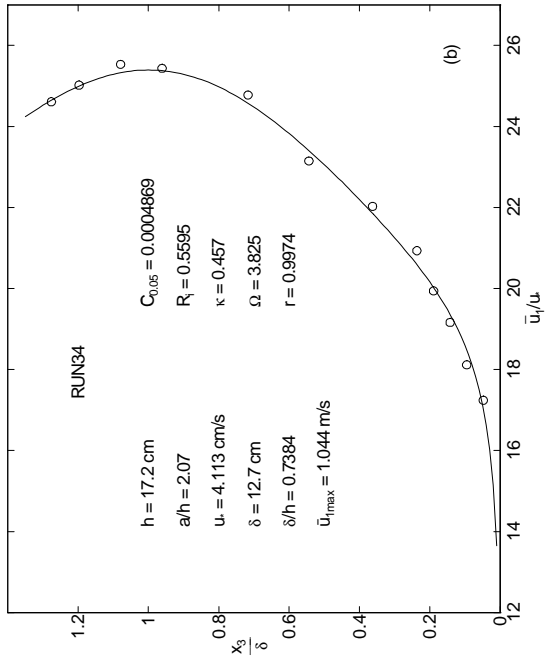
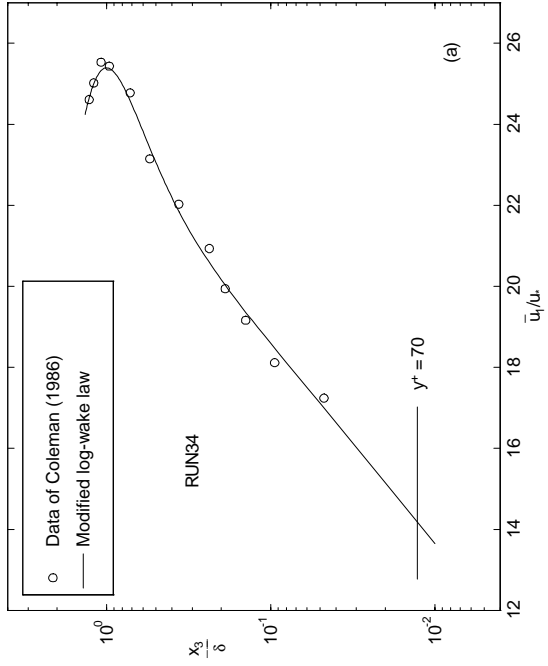
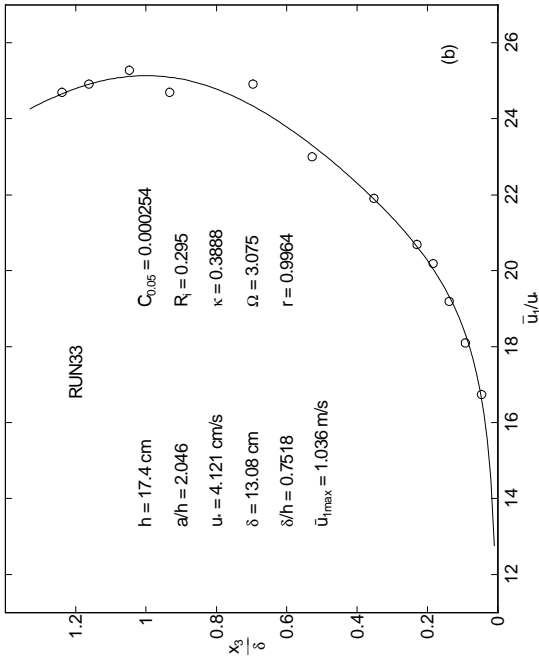
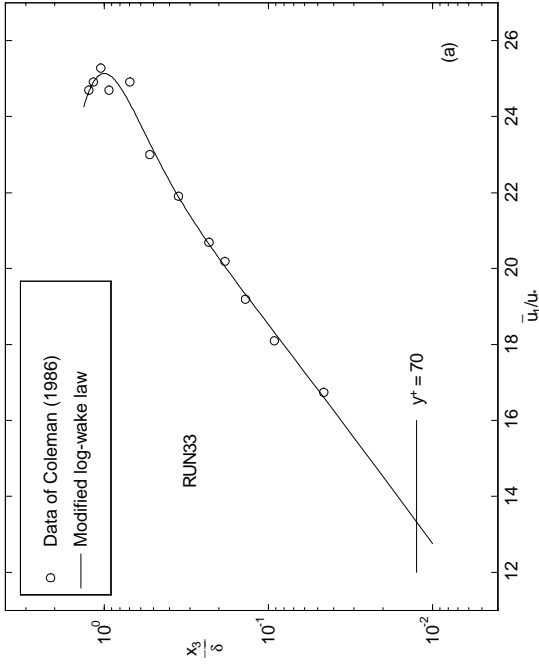


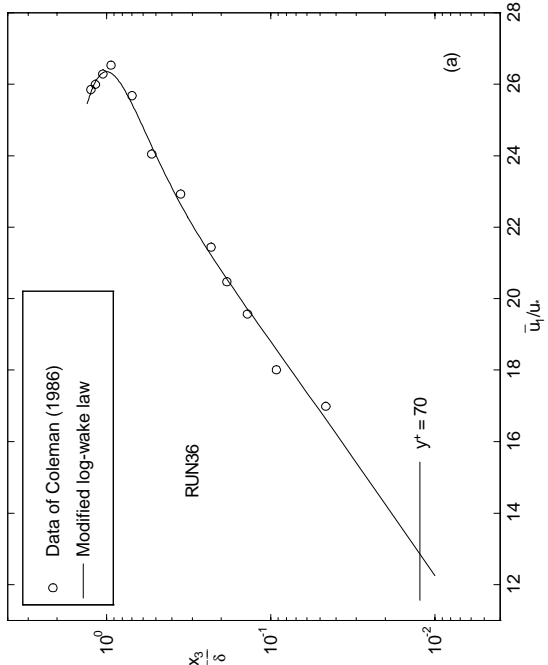
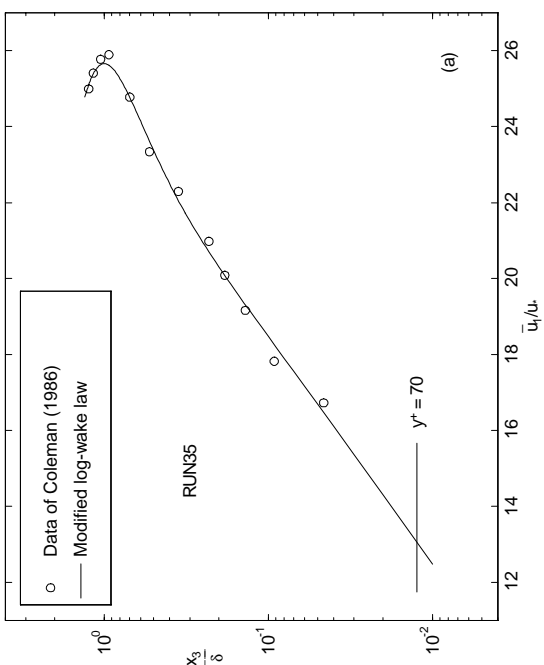
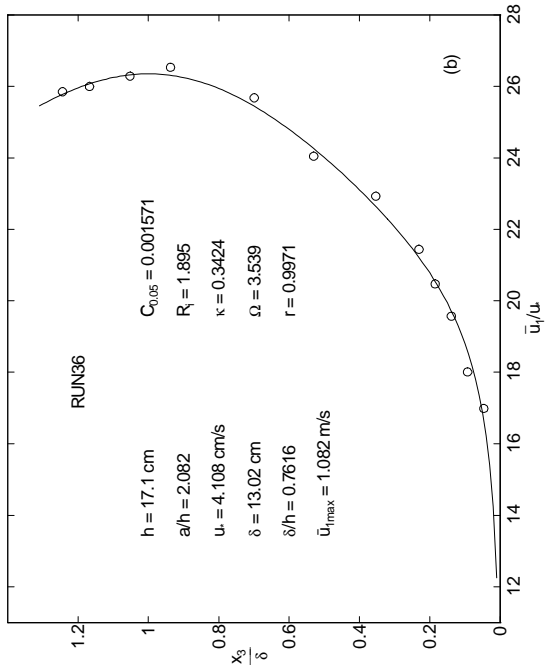
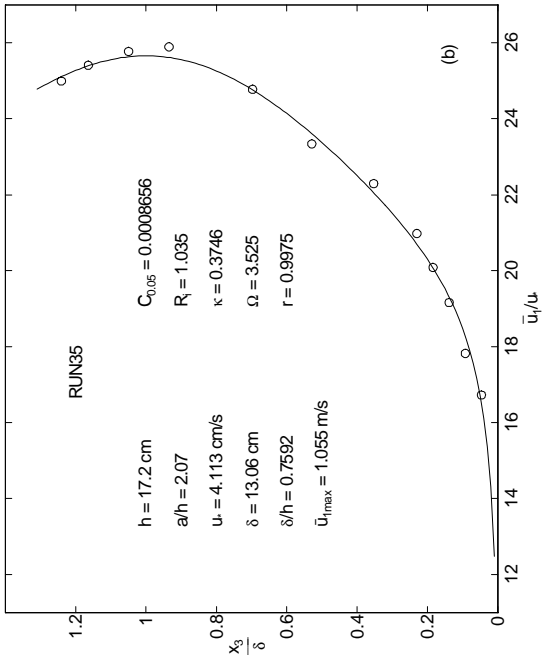


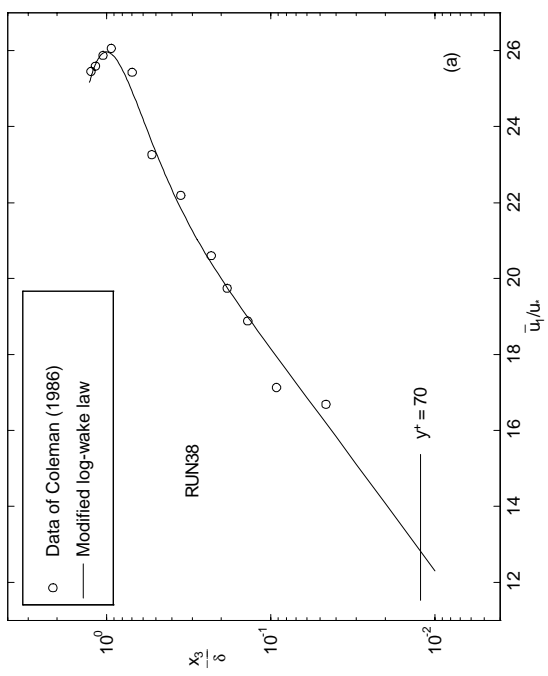
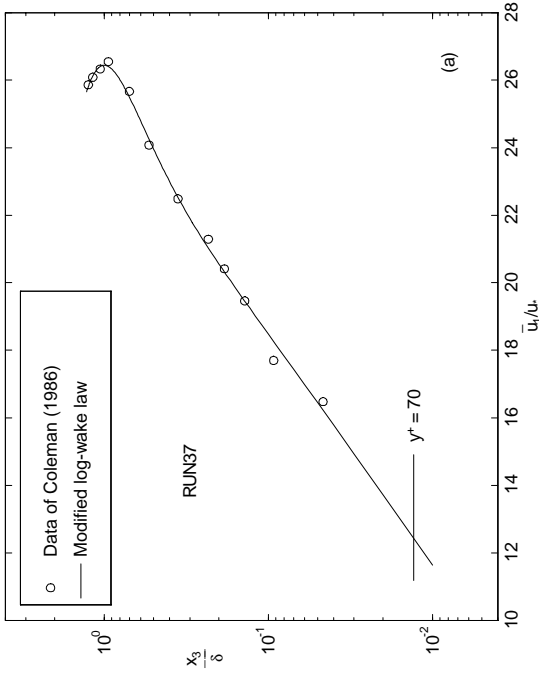
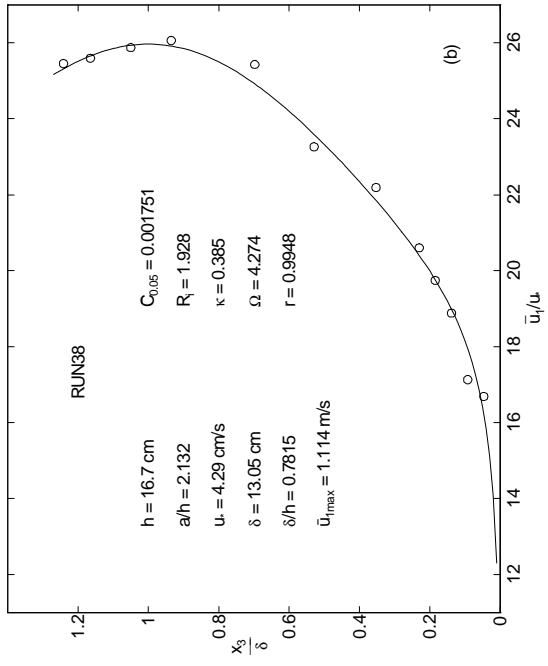
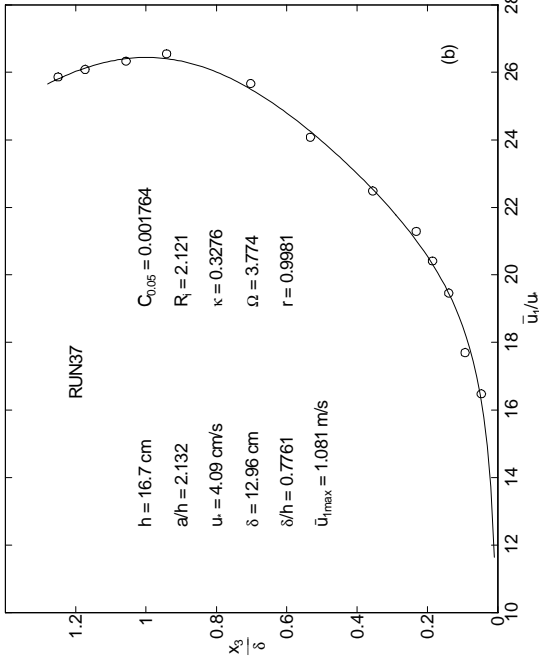


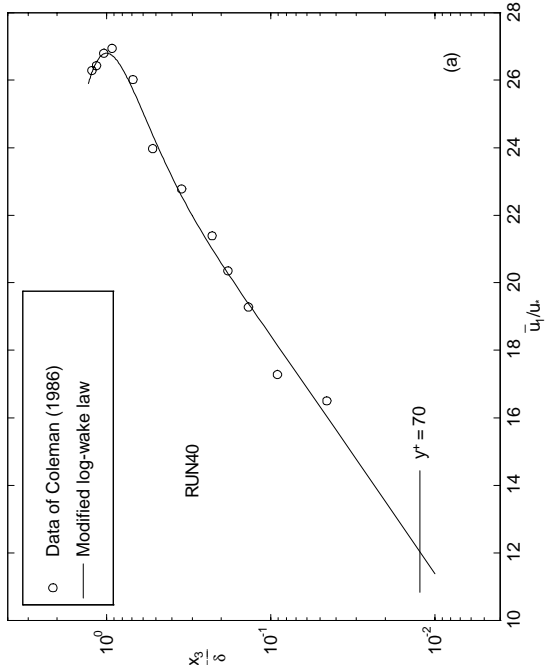
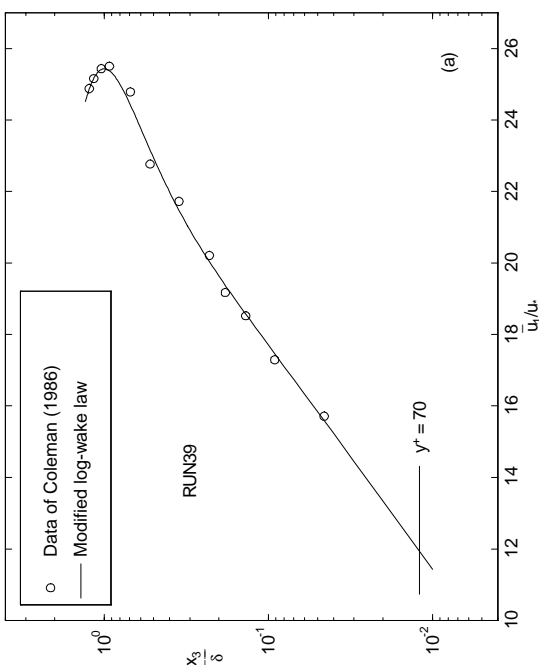
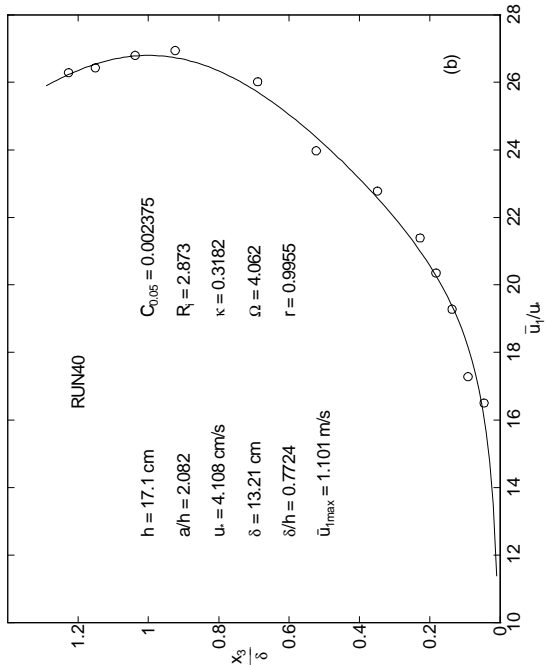
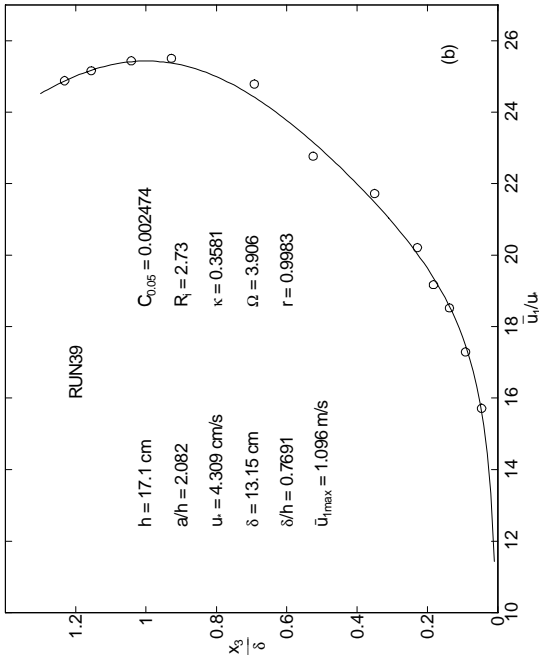












Appendix E

ANALYSIS OF KIRONOTO'S EXPERIMENTAL DATA

Kironoto (1993), under the guidance of Prof. Walter Graf at Swiss Federal Institute of Technology, Lausanne, Switzerland, did experiments on both uniform and non-uniform flows. Only the uniform flow experimental data are cited here. The experimental data include both mean velocity profiles and turbulence intensity distribution, see next page. All velocity profile analyses are attached after the tables.

RUN : UGA3 - Flow parameters

$S_g = 0.00025$	$D = 0.286 \text{ m}$	$U = 0.503 \text{ m/s}$	$U_c = 0.572 \text{ m/s}$	$u_{\infty} = 0.037 \text{ m/s}$
$Br = 9.80$	$\Gamma = 0.04$	$Re = 5.73 \cdot 10^4$	$Fr = 0.30$	$y/D = 2.11$
$\delta = 0.224 \text{ m}$	$\delta_{\infty} = 0.034 \text{ m}$	$\theta = 0.022 \text{ m}$	$H = 1.52$	$\delta_{\infty} = -1.00$

RUN : UGA3 - Velocity distribution

$y \times 10^2$ (m)	u (m/s)	y/δ (-)	y/D (-)	y/δ_{∞} (-)	$(U_c - u)/u_{\infty}$ (-)	u/U_c (-)	u/u_{∞} (-)
0.80	0.262	0.036	0.028	0.352	8.852	0.459	7.113
1.00	0.290	0.045	0.035	0.439	7.942	0.507	7.855
1.30	0.317	0.058	0.048	0.570	7.220	0.555	8.000
1.50	0.324	0.067	0.053	0.657	7.037	0.566	8.776
1.80	0.341	0.081	0.064	0.787	6.573	0.596	9.234
2.00	0.357	0.090	0.071	0.874	6.135	0.624	9.567
2.30	0.362	0.103	0.081	1.004	5.952	0.633	9.816
2.50	0.369	0.112	0.088	1.091	5.758	0.645	9.989
2.80	0.388	0.125	0.099	1.222	5.198	0.679	10.521
3.00	0.388	0.134	0.106	1.309	5.177	0.678	10.510
3.30	0.397	0.148	0.116	1.439	4.995	0.694	10.756
3.80	0.408	0.170	0.134	1.657	4.549	0.713	11.045
4.40	0.420	0.197	0.155	1.917	4.174	0.734	11.377
4.90	0.435	0.219	0.172	2.135	3.674	0.765	11.851
5.90	0.457	0.264	0.208	2.570	3.083	0.800	12.392
7.40	0.485	0.330	0.260	3.222	2.350	0.847	13.130
8.90	0.504	0.397	0.319	3.874	1.833	0.881	13.851
10.40	0.516	0.464	0.365	4.526	1.511	0.902	13.975
11.90	0.529	0.531	0.418	5.178	1.164	0.924	14.324
13.40	0.541	0.598	0.471	5.830	0.833	0.946	14.658
14.90	0.550	0.665	0.524	6.483	0.591	0.962	14.902
16.40	0.556	0.732	0.576	7.135	0.434	0.972	15.080
18.40	0.563	0.821	0.647	8.004	0.231	0.985	15.264
20.40	0.572	0.910	0.717	8.874	0.001	0.999	15.497
22.40	0.572	0.999	0.787	9.743	0.000	1.000	15.402
24.40	0.567	1.089	0.857	10.613	-	0.991	15.357
26.90	0.558	1.200	0.945	11.700	-	0.975	15.114

$K_s = 0.0230$

RUN : UGA3 - Turbulence distribution

$y \times 10^2$ (m)	y/δ (-)	du/dy (1/s)	u' (m/s)	$-\overline{u'v'}$ (m ² /s ²)	u'/u_{∞} (-)	$v_1 \times 10^4$ (m ² /s)	$L \times 10^2$ (m)	$v_1/\delta u_{\infty}$ (-)	U/δ (-)
0.80	0.036	10.495	0.066	0.00131	1.779	1.254	0.346	0.015	0.015
1.30	0.058	7.531	0.071	0.00128	1.936	1.707	0.478	0.020	0.021
1.80	0.080	5.288	0.071	0.00125	1.934	2.373	0.670	0.028	0.030
2.30	0.103	3.767	0.070	0.00122	1.885	3.250	0.929	0.039	0.041
2.80	0.125	2.968	0.067	0.00119	1.822	4.023	1.164	0.048	0.052
3.30	0.147	2.739	0.070	0.00118	1.892	4.248	1.245	0.051	0.056
3.80	0.170	2.562	0.062	0.00113	1.674	4.422	1.314	0.053	0.059
4.40	0.196	2.380	0.057	0.00109	1.552	4.646	1.403	0.056	0.063
4.90	0.219	2.200	0.062	0.00106	1.682	4.846	1.484	0.058	0.066
5.90	0.263	1.802	0.056	0.00100	1.530	5.285	1.667	0.063	0.074
7.40	0.330	1.512	0.053	0.00091	1.430	6.043	1.999	0.073	0.089
8.90	0.397	1.190	0.044	0.00082	1.183	6.911	2.410	0.083	0.107
10.40	0.464	0.937	0.045	0.00073	1.229	7.801	2.885	0.094	0.129
11.90	0.531	0.751	0.038	0.00064	1.037	8.517	3.368	0.102	0.150
13.40	0.598	0.614	0.036	0.00055	0.879	8.929	3.813	0.107	0.170
14.90	0.665	0.502	0.030	0.00046	0.818	9.101	4.258	0.109	0.190
16.40	0.732	0.417	0.032	0.00036	0.859	8.765	4.585	0.105	0.204
18.40	0.821	0.345	0.029	0.00024	0.783	7.063	4.525	0.085	0.202
20.40	0.911	0.320	0.025	0.00012	0.683	3.807	3.449	0.046	0.154
22.40	1.000	-	0.023	0.00000	0.633	-	-	-	-
24.40	1.089	-	0.027	-	0.722	-	-	-	-

$-\overline{u'v'}$ is calculated as $-\overline{u'v'} = u_{\infty}^2 (1 - y/\delta)$

RUN : UGA5 - Flow parameters

$S_c = 0.00025$	$D = 0.285 \text{ m}$	$U = 0.502 \text{ m/s}$	$U_g = 0.576 \text{ m/s}$	$u_w = 0.040 \text{ m/s}$
$Br = 8.00$	$\Pi = -0.05$	$Re = 5.72 \cdot 10^4$	$Fr = 0.30$	$b/D = 2.11$
$\delta = 0.214 \text{ m}$	$\delta_w = 0.034 \text{ m}$	$\theta = 0.022 \text{ m}$	$H = 1.56$	$B_w = -1.00$

RUN : UGA5 - Velocity distribution

$y \times 10^2$ (m)	u (m/s)	y/δ (-)	y/D (-)	y/θ (-)	$(U_c - u)/u_c$ (-)	u/U_c (-)	u/u_c (-)
0.80	0.239	0.039	0.029	0.359	8.315	0.418	6.101
1.00	0.271	0.048	0.036	0.446	7.526	0.473	6.903
1.30	0.304	0.062	0.047	0.576	6.691	0.531	7.749
1.50	0.316	0.071	0.054	0.663	6.377	0.553	8.067
1.80	0.341	0.085	0.064	0.793	5.749	0.597	8.704
2.00	0.349	0.095	0.071	0.880	5.554	0.610	8.902
2.30	0.361	0.109	0.082	1.011	5.263	0.631	9.208
2.50	0.373	0.118	0.089	1.098	4.958	0.652	9.507
2.80	0.385	0.132	0.099	1.228	4.649	0.673	9.821
3.00	0.390	0.141	0.106	1.315	4.525	0.682	9.947
3.30	0.391	0.155	0.117	1.446	4.498	0.684	9.974
3.80	0.411	0.179	0.135	1.663	3.997	0.719	10.483
4.40	0.426	0.207	0.156	1.924	3.615	0.745	10.872
4.90	0.433	0.230	0.173	2.141	3.453	0.757	11.038
5.90	0.455	0.277	0.208	2.576	2.898	0.796	11.614
7.40	0.481	0.347	0.261	3.228	2.249	0.840	12.259
8.90	0.496	0.417	0.314	3.880	1.855	0.868	12.660
10.40	0.514	0.487	0.367	4.533	1.404	0.899	13.118
11.90	0.529	0.557	0.420	5.185	1.042	0.924	13.486
13.40	0.542	0.627	0.472	5.837	0.714	0.947	13.818
14.90	0.549	0.697	0.525	6.489	0.523	0.961	14.012
16.40	0.556	0.767	0.578	7.141	0.357	0.972	14.181
17.90	0.565	0.837	0.631	7.793	0.130	0.988	14.411
19.40	0.568	0.907	0.683	8.446	0.055	0.993	14.488
21.40	0.570	1.000	0.754	9.315	0.000	1.000	14.543
23.40	0.568	1.093	0.824	10.185	-	0.992	14.478
25.40	0.563	1.187	0.894	11.054	-	0.984	14.351
26.90	0.560	1.257	0.947	11.707	-	0.979	14.285

$K_s = 0.0230$

RUN : UGA5 - Turbulence distribution

$y \times 10^2$ (m)	y/δ (-)	du/dy (1/s)	u' (m/s)	$-\overline{u'v'}$ (m ² /s ²)	u'/u_c (-)	$v_r \times 10^4$ (m ² /s)	$\ell \times 10^2$ (m)	$v_r/\delta u_c$ (-)	ℓ/δ (-)
0.80	0.039	11.740	0.074	0.00152	1.675	1.299	0.333	0.015	0.016
1.30	0.062	8.917	0.077	0.00149	1.957	1.668	0.433	0.020	0.020
1.80	0.085	6.588	0.085	0.00145	2.174	2.202	0.578	0.026	0.027
2.30	0.109	4.752	0.082	0.00141	2.085	2.975	0.791	0.035	0.037
2.80	0.132	3.410	0.071	0.00138	1.820	4.037	1.088	0.048	0.051
3.30	0.155	2.561	0.071	0.00134	1.798	5.231	1.429	0.062	0.067
3.80	0.179	2.207	0.067	0.00130	1.702	5.902	1.635	0.070	0.076
4.40	0.207	2.060	0.067	0.00126	1.700	6.049	1.705	0.072	0.080
4.90	0.230	1.971	0.065	0.00122	1.656	6.196	1.773	0.074	0.083
5.90	0.277	1.771	0.058	0.00115	1.488	6.477	1.912	0.077	0.089
7.40	0.347	1.497	0.063	0.00104	1.601	6.921	2.150	0.082	0.100
8.90	0.417	1.253	0.055	0.00093	1.395	7.383	2.427	0.088	0.113
10.40	0.487	1.040	0.050	0.00081	1.288	7.828	2.743	0.093	0.128
11.90	0.557	0.859	0.043	0.00070	1.102	8.185	3.087	0.097	0.144
13.40	0.627	0.701	0.039	0.00059	0.998	8.446	3.471	0.101	0.162
14.90	0.697	0.558	0.036	0.00048	0.916	8.621	3.931	0.103	0.183
16.40	0.767	0.431	0.031	0.00037	0.786	8.586	4.463	0.102	0.208
17.90	0.837	0.317	0.030	0.00026	0.764	8.171	5.077	0.097	0.237
19.40	0.907	0.224	0.027	0.00015	0.692	6.608	5.431	0.079	0.254
21.40	1.000	0.120	0.028	0.00000	0.714	0.000	0.000	0.000	0.000
23.40	1.093	-	0.027	-	0.897	-	-	-	-
25.40	1.187	-	0.031	-	0.792	-	-	-	-

$-\overline{u'v'}$ is calculated as $-\overline{u'v'} = u_c^2(1-y/\delta)$

RUN : UGB3 - Flow parameters

$S_a = 0.00050$	$D = 0.280$ m	$U = 0.405$ m/s	$U_c = 0.465$ m/s	$u_{10} = 0.032$ m/s
$Re = 8.90$	$\Pi = -0.03$	$Re = 4.70 \cdot 10^4$	$Fr = 0.23$	$b/D = 2.97$
$\xi = 0.229$ m	$\xi_c = 0.038$ m	$\theta = 0.023$ m	$H = 1.53$	$F_{a0} = -1.00$

RUN : UGB3 - Velocity distribution

$y \times 10^2$ (m)	u (m/s)	y/δ (-)	y/D (-)	y/ξ (-)	$(U_c - u)/u_c$ (-)	u/U_c (-)	u/u_c (-)
0.95	0.210	0.041	0.033	0.413	8.001	0.452	5.589
1.30	0.244	0.057	0.046	0.570	6.952	0.524	7.638
1.80	0.267	0.079	0.063	0.787	6.221	0.574	8.369
2.30	0.288	0.101	0.080	1.004	5.561	0.619	9.029
2.80	0.305	0.123	0.098	1.222	4.988	0.658	9.602
3.30	0.314	0.144	0.115	1.439	4.735	0.675	9.855
3.80	0.318	0.166	0.133	1.657	4.635	0.682	9.954
4.40	0.327	0.192	0.154	1.817	4.326	0.704	10.264
4.90	0.349	0.214	0.171	2.135	3.648	0.750	10.941
5.40	0.354	0.236	0.189	2.352	3.505	0.760	11.084
5.90	0.357	0.258	0.208	2.570	3.388	0.768	11.202
7.40	0.382	0.323	0.258	3.222	2.610	0.821	11.980
8.90	0.392	0.389	0.310	3.874	2.303	0.842	12.286
10.40	0.409	0.454	0.363	4.526	1.762	0.879	12.828
11.40	0.420	0.498	0.398	4.981	1.430	0.902	13.160
12.90	0.431	0.564	0.450	5.613	1.093	0.925	13.497
14.90	0.444	0.651	0.520	6.483	0.688	0.953	13.901
18.90	0.457	0.738	0.589	7.352	0.250	0.963	14.340
18.90	0.465	0.825	0.659	8.222	0.006	1.000	14.583
20.90	0.465	0.913	0.729	9.091	0.011	0.999	14.579
22.90	0.465	1.000	0.798	9.961	0.000	1.000	14.580
24.90	0.455	1.087	0.868	10.830	-	0.977	14.256
25.90	0.453	1.131	0.903	11.265	-	0.974	14.209
26.90	0.450	1.175	0.938	11.700	-	0.967	14.115
27.90	0.449	1.218	0.972	12.135	-	0.965	14.081
28.40	0.446	1.240	0.990	12.352	-	0.958	13.970

$K = 0.0230$

RUN : UGB3 - Turbulence distributions

$y \times 10^2$ (m)	y/δ (-)	du/dy (1/s)	u' (m/s)	v' (m/s)	$-\overline{u'v'}$ (m ² /s ²)	u'/u_c (-)	v'/u_c (-)	$-\overline{u'v'}/u_c^2$ (-)	$-\overline{u'v'}/u_c v'$ (-)	$v_t \times 10^4$ (m ² /s)	$L \times 10^2$ (m)	v_t/u_c (-)	L/δ (-)
0.95	0.041	6.057	0.065	0.034	0.00090	2.034	1.055	0.886	0.413	1.489	0.496	0.018	0.022
1.30	0.057	5.127	0.065	0.035	0.00099	2.029	1.086	0.975	0.442	1.935	0.814	0.024	0.027
1.80	0.079	4.298	0.063	0.036	0.00096	1.965	1.113	0.945	0.432	2.237	0.721	0.027	0.031
2.30	0.101	3.573	0.063	0.035	0.00096	1.981	1.107	0.962	0.438	2.739	0.875	0.033	0.038
2.80	0.123	2.950	0.062	0.037	0.00109	1.939	1.157	1.072	0.478	3.897	1.119	0.045	0.049
3.30	0.144	2.430	0.062	0.035	0.00101	1.934	1.108	0.992	0.463	4.153	1.307	0.051	0.057
3.80	0.166	2.013	0.058	0.035	0.00087	1.803	1.083	0.855	0.438	4.324	1.488	0.053	0.064
4.40	0.192	1.847	0.060	0.032	0.00087	1.892	1.017	0.853	0.444	3.271	1.789	0.064	0.078
4.90	0.214	1.456	0.058	0.035	0.00098	1.821	1.085	0.958	0.485	6.697	2.145	0.082	0.094
5.40	0.236	1.367	0.059	0.034	0.00086	1.862	1.055	0.844	0.430	6.285	2.144	0.077	0.094
5.90	0.258	1.323	0.057	0.032	0.00084	1.780	0.992	0.824	0.467	6.339	2.189	0.077	0.095
7.40	0.323	1.200	0.043	0.029	0.00048	1.319	0.901	0.469	0.389	3.973	1.820	0.049	0.079
8.90	0.389	1.080	0.048	0.030	0.00070	1.490	0.940	0.893	0.495	6.525	2.458	0.080	0.107
10.40	0.454	0.969	0.040	0.028	0.00045	1.269	0.863	0.438	0.400	4.595	2.178	0.056	0.095
11.40	0.498	0.900	0.042	0.028	0.00053	1.303	0.881	0.518	0.452	5.859	2.551	0.072	0.111
12.90	0.564	0.792	0.039	0.025	0.00038	1.210	0.770	0.373	0.400	4.787	2.458	0.058	0.107
14.90	0.651	0.630	0.039	0.025	0.00038	1.211	0.779	0.378	0.401	6.110	3.114	0.075	0.136
16.90	0.738	0.447	0.034	0.024	0.00030	1.069	0.751	0.289	0.372	6.805	3.902	0.083	0.170
18.90	0.825	0.243	0.029	0.021	0.00017	0.909	0.661	0.170	0.282	7.103	5.408	0.087	0.236
20.90	0.913	-	0.026	0.020	0.00008	0.771	0.615	0.081	0.172	-	-	-	-
22.90	1.000	-	0.025	0.018	0.00000	0.788	0.558	0.000	0.000	-	-	-	-
24.90	1.087	-	0.027	0.017	-0.00002	0.844	0.527	-0.026	-	-	-	-	-
25.90	1.131	-	0.025	0.015	0.00000	0.791	0.467	0.000	-	-	-	-	-
26.90	1.175	-	0.027	0.013	0.00000	0.837	0.423	0.000	-	-	-	-	-
27.90	1.218	-	0.026	0.012	0.00001	0.822	0.373	0.013	-	-	-	-	-
28.40	1.240	-	0.028	0.010	0.00002	0.874	0.323	0.019	-	-	-	-	-

$-\overline{u'v'}$ is measured

RUN : UGB5 - flow parameters

$S_g = 0.00050$	$D = 0.290 \text{ m}$	$U = 0.396 \text{ m/s}$	$U_c = 0.463 \text{ m/s}$	$u_{*0} = 0.034 \text{ m/s}$
$Br = 7.50$	$\Gamma = -0.08$	$Re = 4.63 \cdot 10^5$	$Fr = 0.23$	$b/D = 2.07$
$\delta = 0.229 \text{ m}$	$\delta_* = 0.042 \text{ m}$	$\theta = 0.027 \text{ m}$	$H = 1.58$	$R_* = -1.00$

RUN : UGB5 - Velocity distribution

$y \times 10^2$ (m)	u (m/s)	y/δ (-)	y/D (-)	y/k_s (-)	$(U_c - u)/u_*$ (-)	u/U_c (-)	u/u_* (-)
0.70	0.173	0.731	0.024	0.304	8.405	0.375	5.043
1.30	0.207	0.057	0.045	0.565	7.427	0.448	8.020
1.80	0.241	0.079	0.062	0.783	6.427	0.522	7.020
2.30	0.270	0.100	0.080	1.000	5.602	0.583	7.945
2.80	0.295	0.122	0.097	1.217	4.862	0.638	8.585
3.30	0.303	0.144	0.114	1.435	4.654	0.654	8.794
3.80	0.316	0.166	0.131	1.652	4.273	0.682	9.175
4.40	0.331	0.192	0.152	1.913	3.824	0.716	9.624
4.90	0.340	0.214	0.170	2.130	3.570	0.735	9.777
5.40	0.340	0.236	0.187	2.348	3.565	0.735	9.883
5.90	0.351	0.258	0.204	2.565	3.255	0.759	10.193
7.40	0.370	0.323	0.256	3.217	2.681	0.801	10.767
8.90	0.383	0.389	0.308	3.870	2.320	0.827	11.128
10.40	0.390	0.454	0.360	4.522	2.119	0.842	11.329
11.40	0.398	0.498	0.394	4.957	1.885	0.860	11.563
12.90	0.409	0.563	0.446	5.609	1.549	0.885	11.899
14.90	0.429	0.651	0.516	6.478	0.982	0.927	12.465
16.90	0.443	0.738	0.585	7.348	0.573	0.957	12.874
18.90	0.450	0.825	0.654	8.217	0.355	0.974	13.093
20.90	0.458	0.913	0.723	9.087	0.140	0.990	13.308
22.90	0.463	1.000	0.792	9.957	0.000	1.000	13.448
24.90	0.461	1.087	0.862	10.826	-	0.998	13.415
26.90	0.463	1.175	0.931	11.696	-	1.000	13.459

$K_s = 0.0230$

RUN : UGB5 - Turbulence distribution

$y \times 10^2$ (m)	y/δ (-)	du/dy (1/s)	u' (m/s)	$-\overline{u'v'}$ (m ² /s ²)	u'/u_* (-)	$v_t \times 10^4$ (m ² /s)	$\mathcal{L} \times 10^2$ (m)	$v_t/\delta u_*$ (-)	\mathcal{L}/δ (-)
0.70	0.031	8.329	0.054	0.00118	1.566	1.423	0.413	0.017	0.018
1.30	0.057	6.980	0.064	0.00131	1.857	1.880	0.519	0.023	0.023
1.80	0.079	5.769	0.062	0.00126	1.795	2.191	0.616	0.027	0.027
2.30	0.100	4.694	0.063	0.00129	1.835	2.742	0.764	0.033	0.033
2.80	0.122	3.758	0.059	0.00144	1.703	3.831	1.010	0.047	0.044
3.30	0.144	2.959	0.058	0.00133	1.686	4.502	1.233	0.055	0.054
3.80	0.166	2.297	0.056	0.00114	1.641	4.973	1.471	0.061	0.064
4.40	0.192	1.685	0.053	0.00114	1.546	6.738	2.004	0.083	0.087
4.90	0.214	1.326	0.056	0.00130	1.655	9.796	2.718	0.120	0.119
5.40	0.236	1.105	0.056	0.00113	1.625	10.247	3.045	0.125	0.133
5.90	0.258	1.022	0.060	0.00111	1.746	10.821	3.254	0.132	0.142
7.40	0.323	0.978	0.052	0.00062	1.517	6.354	2.549	0.078	0.111
8.90	0.389	0.928	0.050	0.00092	1.443	9.965	3.277	0.122	0.143
10.40	0.454	0.873	0.049	0.00058	1.424	6.644	2.759	0.081	0.120
11.40	0.498	0.833	0.045	0.00089	1.305	8.301	3.157	0.101	0.138
12.90	0.563	0.769	0.043	0.00050	1.252	6.447	2.895	0.079	0.126
14.90	0.651	0.675	0.043	0.00050	1.252	7.475	3.328	0.091	0.145
16.90	0.738	0.570	0.038	0.00040	1.101	7.006	3.506	0.086	0.153
18.90	0.825	0.456	0.036	0.00023	1.058	4.978	3.304	0.061	0.144
20.90	0.913	0.332	0.032	0.00011	0.938	3.278	3.142	0.040	0.137
22.90	1.000	0.198	0.028	0.00000	0.815	0.000	0.000	0.000	0.000
24.90	1.087	-	0.027	-0.00003	0.797	-	-	-	-
26.90	1.175	-	0.023	0.00000	0.683	-	-	-	-

$-\overline{u'v'}$ is calculated (assumed to be similar with the $-\overline{u'v'}$ profile of run UGB3) as $-\overline{u'v'}|_k = (-\overline{u'v'})_k \left(\frac{u_*|_k}{u_*|_0} \right)^2$

RUN : UPA3 - Flow parameters

$Se = 0.0010$	$D = 0.115 \text{ m}$	$U = 0.463 \text{ m/s}$	$U_c = 0.576 \text{ m/s}$	$u_w = 0.034 \text{ m/s}$
$Br = 0.75$	$\Pi = 0.06$	$Re = 2.2 \times 10^4$	$Fr = 0.46$	$b/D = 5.22$
$\delta = 0.115 \text{ m}$	$\delta_w = 0.019 \text{ m}$	$\theta = 0.013 \text{ m}$	$H = 1.45$	$\beta_w = -1.00$

RUN : UPA3 - Velocity distribution

$y \times 10^2$ (m)	u (m/s)	y/δ (-)	y/D (-)	y/k_s (-)	$(U_c - u)/u_w$ (-)	u/U_c (-)	u/u_w (-)
0.25	0.243	0.022	0.022	0.521	9.834	0.422	7.187
0.45	0.284	0.039	0.039	0.938	8.628	0.493	8.393
0.65	0.328	0.057	0.057	1.354	7.331	0.569	9.691
0.85	0.341	0.074	0.074	1.771	6.952	0.592	10.069
1.05	0.360	0.091	0.091	2.188	6.373	0.626	10.648
1.25	0.380	0.109	0.109	2.604	5.805	0.659	11.217
1.55	0.399	0.135	0.135	3.229	5.218	0.693	11.803
1.75	0.409	0.152	0.152	3.646	4.950	0.709	12.071
2.05	0.419	0.178	0.178	4.271	4.633	0.728	12.388
2.25	0.422	0.196	0.196	4.688	4.559	0.732	12.462
2.55	0.436	0.222	0.222	5.313	4.135	0.757	12.886
3.05	0.459	0.265	0.265	6.354	3.454	0.797	13.567
3.55	0.470	0.309	0.309	7.396	3.144	0.815	13.877
4.05	0.478	0.352	0.352	8.438	2.891	0.830	14.131
5.05	0.494	0.439	0.439	10.521	2.432	0.857	14.590
6.05	0.510	0.526	0.526	12.604	1.953	0.885	15.069
7.05	0.532	0.613	0.613	14.688	1.308	0.923	15.715
8.05	0.537	0.700	0.700	16.771	1.165	0.932	15.856
9.05	0.554	0.787	0.787	18.854	0.644	0.962	16.378
10.05	0.564	0.874	0.874	20.938	0.370	0.978	16.851
10.55	0.570	0.917	0.917	21.979	0.175	0.990	16.846
11.50	0.576	1.000	1.000	23.958	0.000	1.000	17.021

$K_S = 4.799 \times 10^{-3}$

RUN : UPA3 - Turbulence distributions

$y \times 10^2$ (m)	y/δ (-)	du/dy (1/s)	u' (m/s)	v' (m/s)	$-\overline{u'v'}$ (m ² /s ²)	u'/u_w (-)	v'/u_w (-)	$-\overline{u'v'}/u_w^2$ (-)	$-\overline{u'v'}/u_w v'$ (-)	$v' \times 10^4$ (m ² /s)	$\zeta \times 10^2$ (m)	$v'/\delta u_w$ (-)	ζ/δ (-)
0.65	0.057	14.497	0.066	0.037	0.00111	1.937	1.093	0.970	0.458	0.766	0.230	0.020	0.020
1.05	0.091	8.279	0.063	0.034	0.00097	1.848	1.008	0.843	0.452	1.166	0.375	0.030	0.033
1.55	0.135	5.047	0.063	0.034	0.00107	1.865	0.998	0.938	0.504	2.128	0.649	0.055	0.056
2.05	0.178	4.249	0.063	0.032	0.00097	1.854	0.934	0.847	0.489	2.283	0.733	0.059	0.064
2.55	0.222	3.560	0.057	0.032	0.00091	1.684	0.951	0.795	0.497	2.566	0.850	0.066	0.074
3.05	0.265	2.950	0.058	0.032	0.00094	1.710	0.934	0.820	0.513	3.182	1.039	0.082	0.090
3.55	0.309	2.449	0.051	0.029	0.00067	1.516	0.843	0.588	0.460	2.748	1.059	0.071	0.092
4.05	0.352	2.046	0.051	0.030	0.00082	1.522	0.884	0.715	0.531	4.000	1.398	0.103	0.122
5.05	0.439	1.537	0.047	0.027	0.00067	1.386	0.797	0.581	0.526	4.329	1.678	0.111	0.148
6.05	0.526	1.423	0.046	0.026	0.00060	1.345	0.756	0.520	0.511	4.182	1.714	0.107	0.149
7.05	0.613	1.454	0.042	0.024	0.00051	1.247	0.764	0.444	0.506	3.496	1.551	0.090	0.135
8.05	0.700	1.396	0.037	0.023	0.00039	1.094	0.666	0.339	0.466	2.784	1.412	0.072	0.123
9.05	0.787	1.247	0.033	0.020	0.00027	0.978	0.584	0.232	0.406	2.131	1.307	0.055	0.114
10.05	0.874	1.009	0.033	0.018	0.00022	0.965	0.533	0.191	0.372	2.167	1.466	0.056	0.127
10.55	0.917	0.856	0.030	0.017	0.00012	0.881	0.491	0.104	0.240	1.389	1.274	0.036	0.111

$-\overline{u'v'}$ is measured

RUN : UPAS - Flow parameters

$S_G = 0.0010$	$D = 0.115 \text{ m}$	$U = 0.481 \text{ m/s}$	$U_c = 0.579 \text{ m/s}$	$u_* = 0.033 \text{ m/s}$
$Br = 9.0$	$\Pi = 0.16$	$Re = 2.21 \cdot 10^3$	$Fr = 0.45$	$b/D = 5.22$
$\delta = 0.115 \text{ m}$	$\delta_* = 0.019 \text{ m}$	$\theta = 0.013 \text{ m}$	$H = 1.46$	$\beta_* = -1.00$

RUN : UPAS - Velocity distribution

$y \times 10^2$ (m)	u (m/s)	y/δ (-)	y/D (-)	y/k_s (-)	$(U_c - u)/u_*$ (-)	u/U_c (-)	u/u_* (-)
0.25	0.244	0.022	0.022	0.521	10.260	0.421	7.459
0.45	0.288	0.039	0.039	0.938	8.906	0.498	8.822
0.65	0.316	0.057	0.057	1.354	8.058	0.545	9.671
0.85	0.344	0.074	0.074	1.771	7.198	0.594	10.530
1.05	0.360	0.091	0.091	2.188	6.701	0.622	11.027
1.25	0.370	0.109	0.109	2.604	6.397	0.639	11.331
1.55	0.389	0.135	0.135	3.229	5.826	0.671	11.902
1.75	0.398	0.152	0.152	3.646	5.532	0.688	12.196
2.05	0.419	0.178	0.178	4.271	4.908	0.723	12.820
2.25	0.420	0.196	0.196	4.688	4.869	0.725	12.856
2.55	0.438	0.222	0.222	5.313	4.305	0.757	13.423
3.05	0.450	0.265	0.265	6.354	3.955	0.777	13.773
3.55	0.461	0.309	0.309	7.396	3.616	0.796	14.112
4.05	0.476	0.352	0.352	8.438	3.157	0.822	14.571
5.05	0.490	0.439	0.439	10.521	2.731	0.846	14.997
6.05	0.511	0.526	0.526	12.604	2.085	0.882	15.643
7.05	0.527	0.613	0.613	14.688	1.598	0.910	16.130
8.05	0.537	0.700	0.700	16.771	1.276	0.928	16.452
9.05	0.550	0.787	0.787	18.854	0.880	0.950	16.848
10.05	0.565	0.874	0.874	20.938	0.418	0.976	17.310
10.55	0.574	0.917	0.917	21.979	0.158	0.961	17.570
11.50	0.579	1.000	1.000	23.958	0.000	1.000	17.728

$K_s = 4.799 \times 10^{-3}$

RUN : UPAS - Turbulence distributions

$y \times 10^2$ (m)	y/δ (-)	du/dy (1/s)	u' (m/s)	$-\overline{u'v'}$ (m ² /s ²)	u'/u_* (-)	$v_1 \times 10^4$ (m ² /s)	$\zeta \times 10^2$ (m)	$v_1/\delta u_*$ (-)	ζ/δ (-)
0.65	0.057	13.344	0.076	0.00103	2.324	0.776	0.241	0.021	0.021
1.05	0.091	7.930	0.070	0.00090	2.144	1.134	0.378	0.030	0.033
1.55	0.135	5.094	0.063	0.00100	1.933	1.999	0.632	0.053	0.055
2.05	0.178	4.284	0.059	0.00090	1.821	2.109	0.702	0.056	0.061
2.55	0.222	3.643	0.058	0.00085	1.776	2.329	0.800	0.062	0.070
3.05	0.265	3.080	0.057	0.00087	1.738	2.839	0.960	0.076	0.083
3.55	0.309	2.595	0.057	0.00063	1.732	2.415	0.965	0.064	0.084
4.05	0.352	2.190	0.052	0.00076	1.596	3.481	1.261	0.093	0.110
5.05	0.439	1.614	0.053	0.00062	1.617	3.840	1.542	0.102	0.134
6.05	0.526	1.353	0.045	0.00055	1.386	4.097	1.740	0.109	0.151
7.05	0.613	1.406	0.045	0.00047	1.373	3.368	1.548	0.090	0.135
8.05	0.700	1.521	0.041	0.00036	1.258	2.380	1.251	0.083	0.109
9.05	0.787	1.450	0.038	0.00025	1.090	1.027	1.078	0.045	0.094
10.05	0.874	1.221	0.033	0.00020	1.017	1.668	1.169	0.044	0.102
10.55	0.917	1.035	0.031	0.00011	0.952	1.070	1.017	0.028	0.088

$-\overline{u'v'}$ is calculated (assumed to be similar with the $-\overline{u'v'}$ profile of run UPAC) as: $[-\overline{u'v'}]_y = [-\overline{u'v'}]_{y_0} \left(\frac{u_* y_0}{u_* y}\right)^2$

RUN : UPB3 - Flow parameters

$Sa = 0.00078$	$D=0.101$ m	$U=0.465$ m/s	$U_c=0.581$ m/s	$u_c=0.037$ m/s
$Br = 7.50$	$\Pi=0.03$	$Re=1.88 \cdot 10^4$	$Fr = 0.47$	$h/D = 5.94$
$\delta = 0.101$ m	$\delta_c = 0.017$ m	$\theta = 0.012$ m	$H = 1.48$	$\beta_c = -1.00$

RUN : UPB3 - Velocity distribution

$y \times 10^2$ (m)	u (m/s)	y/δ (-)	y/D (-)	y/k_s (-)	$(U_c-u)/u_c$ (-)	u/U_c (-)	u/u_c (-)
0.25	0.225	0.025	0.025	0.521	9.147	0.401	6.114
0.45	0.270	0.045	0.045	0.938	7.924	0.461	7.337
0.65	0.306	0.064	0.064	1.354	6.939	0.545	8.322
0.85	0.327	0.084	0.084	1.771	6.366	0.583	8.895
1.05	0.351	0.104	0.104	2.188	5.708	0.626	9.553
1.25	0.363	0.124	0.124	2.604	5.397	0.646	9.884
1.55	0.390	0.153	0.153	3.229	4.648	0.695	10.613
1.75	0.402	0.173	0.173	3.646	4.336	0.716	10.925
2.05	0.416	0.203	0.203	4.271	3.951	0.741	11.310
2.25	0.420	0.223	0.223	4.688	3.842	0.748	11.420
2.55	0.429	0.252	0.252	5.313	3.604	0.764	11.657
3.05	0.446	0.302	0.302	6.354	3.142	0.794	12.119
3.55	0.453	0.351	0.351	7.396	2.937	0.808	12.324
4.05	0.473	0.401	0.401	8.438	2.406	0.842	12.856
5.05	0.492	0.500	0.500	10.521	1.874	0.877	13.388
6.05	0.505	0.599	0.599	12.604	1.518	0.901	13.743
7.05	0.520	0.698	0.698	14.688	1.113	0.927	14.148
8.05	0.539	0.797	0.797	16.771	0.611	0.980	14.650
9.05	0.553	0.896	0.896	18.854	0.211	0.986	15.051
10.1	0.561	1.000	1.000	21.042	0.060	1.000	15.251

$K_s = 4.800 \times 10^{-3}$

RUN : UPB3 - Turbulence distributions

$y \times 10^2$ (m)	y/δ (-)	du/dy (1/s)	u' (m/s)	v' (m/s)	$-\overline{u'v'}$ (m ² /s ²)	u'/u_c (-)	v'/u_c (-)	$-\overline{u'v'}/u_c^2$ (-)	$-\overline{u'v'}/u_c v'$ (-)	$v_t \times 10^4$ (m ² /s)	$\ell \times 10^2$ (m)	$v_t/\delta u_c$ (-)	ℓ/δ (-)
0.65	0.064	15.110	0.067	0.038	0.00120	1.813	1.041	0.890	0.472	0.796	0.229	0.021	0.023
1.05	0.104	9.046	0.066	0.038	0.00126	1.807	1.020	0.935	0.507	1.397	0.393	0.038	0.039
1.55	0.153	5.635	0.062	0.035	0.00106	1.689	0.946	0.782	0.489	1.875	0.577	0.051	0.057
2.05	0.203	4.511	0.060	0.033	0.00104	1.640	0.901	0.768	0.520	2.301	0.714	0.062	0.071
2.55	0.252	3.573	0.058	0.031	0.00092	1.586	0.848	0.682	0.507	2.579	0.850	0.069	0.084
3.05	0.302	2.822	0.058	0.032	0.00096	1.570	0.870	0.710	0.519	3.398	1.097	0.092	0.109
3.55	0.351	2.258	0.052	0.030	0.00085	1.414	0.824	0.629	0.540	3.787	1.292	0.101	0.128
4.05	0.401	1.880	0.049	0.030	0.00076	1.331	0.811	0.583	0.522	4.046	1.467	0.109	0.145
5.05	0.500	1.095	0.046	0.027	0.00067	1.241	0.733	0.460	0.505	7.685	1.479	0.099	0.146
6.05	0.599	1.776	0.045	0.025	0.00060	1.233	0.697	0.442	0.521	1.400	1.375	0.090	0.136
7.05	0.698	1.715	0.035	0.023	0.00036	0.963	0.628	0.264	0.436	2.076	1.101	0.056	0.109
8.05	0.797	1.502	0.034	0.023	0.00030	0.934	0.615	0.219	0.382	1.973	1.146	0.050	0.113
9.05	0.896	1.138	0.032	0.022	0.00017	0.878	0.610	0.123	0.229	1.459	1.132	0.039	0.112

$-\overline{u'v'}$ is measured

RUN : UPB5 - Flow parameters

$So = 0.00075$	$D = 0.101 \text{ m}$	$U = 0.469 \text{ m/s}$	$U_c = 0.562 \text{ m/s}$	$u_w = 0.036 \text{ m/s}$
$Br = 7.85$	$\Pi = 0.01$	$Re = 1.91 \cdot 10^3$	$Fr = 0.47$	$b/D = 5.94$
$\delta = 0.101 \text{ m}$	$\delta_w = 0.017 \text{ m}$	$\theta = 0.011 \text{ m}$	$H = 1.48$	$\beta_w = -1.00$

RUN : UPB5 - Velocity distribution

$y \times 10^2$ (m)	u (m/s)	y/δ (-)	y/D (-)	y/δ_w (-)	$(U_c - u)/u_w$ (-)	u/U_c (-)	u/u_w (-)
0.25	0.233	0.025	0.025	0.521	9.245	0.414	6.541
0.45	0.278	0.045	0.045	0.938	7.966	0.495	7.820
0.65	0.310	0.064	0.064	1.354	7.088	0.551	8.698
0.85	0.339	0.084	0.084	1.771	6.269	0.603	9.518
1.05	0.355	0.104	0.104	2.188	5.828	0.631	9.958
1.25	0.374	0.124	0.124	2.604	5.271	0.666	10.516
1.55	0.397	0.153	0.153	3.229	4.636	0.706	11.151
1.75	0.402	0.173	0.173	3.646	4.482	0.718	11.304
2.05	0.422	0.203	0.203	4.271	3.945	0.750	11.841
2.25	0.431	0.223	0.223	4.688	3.690	0.766	12.097
2.55	0.434	0.252	0.252	5.313	3.590	0.773	12.197
3.05	0.449	0.302	0.302	6.354	3.167	0.799	12.620
3.55	0.464	0.351	0.351	7.396	2.756	0.825	13.031
4.05	0.472	0.401	0.401	8.438	2.537	0.839	13.250
5.05	0.493	0.500	0.500	10.521	1.942	0.877	13.845
6.05	0.510	0.599	0.599	12.604	1.471	0.907	14.315
7.05	0.526	0.698	0.698	14.688	1.026	0.935	14.760
8.05	0.543	0.797	0.797	16.771	0.541	0.966	15.246
9.05	0.552	0.896	0.896	18.854	0.284	0.982	15.502
10.05	0.562	1.000	1.000	21.042	0.000	1.000	15.787

$K_s = 4.800 \times 10^{-3}$

RUN : UPB5 - Turbulence distributions

$y \times 10^2$ (m)	y/δ (-)	du/dy (1/s)	v' (m/s)	$-\overline{u'v'}$ (m ² /s ²)	u'/u_w (-)	$v_t \times 10^4$ (m ² /s)	$\ell \times 10^2$ (m)	v_t/δ_w (-)	ℓ/δ (-)
0.65	0.064	15.086	0.060	0.00113	1.694	0.748	0.223	0.020	0.022
1.05	0.104	9.918	0.063	0.00119	1.764	1.195	0.347	0.032	0.034
1.55	0.153	5.647	0.056	0.00099	1.569	1.755	0.557	0.048	0.055
2.05	0.203	3.806	0.055	0.00097	1.549	2.558	0.820	0.069	0.081
2.55	0.252	3.174	0.055	0.00086	1.537	2.723	0.926	0.074	0.092
3.05	0.302	2.659	0.047	0.00090	1.316	3.382	1.128	0.092	0.112
3.55	0.351	2.262	0.046	0.00080	1.292	3.527	1.249	0.096	0.124
4.05	0.401	1.980	0.042	0.00071	1.179	3.603	1.349	0.098	0.134
5.05	0.500	1.769	0.041	0.00058	1.149	3.292	1.364	0.089	0.135
6.05	0.599	1.739	0.035	0.00056	0.973	3.218	1.360	0.087	0.135
7.05	0.698	1.605	0.032	0.00033	0.901	2.083	1.139	0.056	0.113
8.05	0.797	1.364	0.032	0.00028	0.890	2.038	1.222	0.055	0.121
9.05	0.896	1.017	0.030	0.00016	0.847	1.531	1.227	0.042	0.121

$-\overline{u'v'}$ is calculated (assumed to be similar with the $-\overline{u'v'}$ profile of run UPB3) as: $-\overline{u'v'} = -\overline{u'v'}_0 \left(\frac{u_w - u}{u_w} \right)^2$

RUN : UPC3 - Flow parameters

$Se = 0.00025$	$D = 0.119 \text{ m}$	$U = 0.338 \text{ m/s}$	$U_c = 0.402 \text{ m/s}$	$u_w = 0.022 \text{ m/s}$
$Br = 9.50$	$\Pi = 0.15$	$Re = 1.61 \cdot 10^4$	$Fr = 0.31$	$b/D = 5.04$
$\delta = 0.119 \text{ m}$	$\delta_w = 0.019 \text{ m}$	$\theta = 0.013 \text{ m}$	$H = 1.45$	$B_w = -1.00$

RUN : UPC3 - Velocity distribution

$y \times 10^2$ (m)	u (m/s)	y/δ (-)	y/D (-)	y/k_s (-)	$(U_c - u)/u_w$ (-)	u/U_c (-)	u/u_w (-)
0.25	0.167	0.021	0.021	0.521	10.739	0.415	7.617
0.45	0.203	0.038	0.038	0.938	9.079	0.505	8.277
0.65	0.222	0.055	0.055	1.354	7.882	0.571	10.474
0.85	0.243	0.071	0.071	1.771	7.273	0.604	11.084
1.05	0.256	0.088	0.088	2.188	6.681	0.636	11.675
1.25	0.265	0.105	0.105	2.604	6.255	0.659	12.101
1.55	0.272	0.130	0.130	3.229	5.935	0.677	12.422
1.75	0.281	0.147	0.147	3.646	5.539	0.698	12.818
2.05	0.289	0.172	0.172	4.271	5.178	0.718	13.178
2.25	0.295	0.189	0.189	4.688	4.882	0.734	13.474
2.55	0.302	0.214	0.214	5.313	4.571	0.751	13.785
3.05	0.310	0.256	0.256	6.354	4.207	0.771	14.149
3.55	0.319	0.298	0.298	7.396	3.804	0.793	14.552
4.05	0.322	0.340	0.340	8.438	3.496	0.826	15.160
5.05	0.343	0.424	0.424	10.521	2.714	0.852	15.642
6.05	0.361	0.508	0.508	12.604	1.892	0.897	16.464
7.05	0.369	0.592	0.592	14.688	1.511	0.918	16.845
8.05	0.377	0.676	0.676	16.771	1.144	0.938	17.212
9.05	0.385	0.761	0.761	18.854	0.762	0.959	17.595
10.05	0.393	0.845	0.845	20.938	0.430	0.977	17.926
11.05	0.398	0.929	0.929	23.021	0.163	0.991	18.193
11.90	0.402	1.000	1.000	24.792	0.000	1.000	18.356

$k_s = 4.798 \times 10^{-3}$

RUN : UPC3 - Turbulence distribution

$y \times 10^2$ (m)	y/δ (-)	du/dy (1/s)	u' (m/s)	v' (m/s)	$-\overline{u'v'}$ (m ² /s ²)	u'/u_w (-)	v'/u_w (-)	$-\overline{u'v'}/u_w^2$ (-)	$-\overline{u'v'}/u_w v'$ (-)	$v_t \times 10^4$ (m ² /s)	$\ell \times 10^2$ (m)	$v_t/\delta u_w$ (-)	ℓ/δ (-)
0.65	0.055	10.438	0.044	0.025	0.00047	2.011	1.151	0.986	0.426	0.453	0.208	0.017	0.018
1.05	0.088	5.769	0.045	0.024	0.00048	2.046	1.100	1.000	0.444	0.831	0.380	0.032	0.032
1.55	0.130	2.764	0.041	0.023	0.00046	1.870	1.032	0.953	0.493	1.653	0.773	0.063	0.065
2.05	0.172	2.241	0.041	0.021	0.00040	1.854	0.975	0.833	0.461	1.706	0.854	0.065	0.072
2.55	0.214	2.177	0.040	0.020	0.00038	1.816	0.925	0.790	0.471	1.740	0.894	0.067	0.075
3.05	0.256	2.019	0.038	0.020	0.00035	1.713	0.911	0.725	0.484	1.722	0.923	0.066	0.078
3.55	0.298	1.868	0.036	0.020	0.00034	1.627	0.900	0.708	0.484	1.819	0.987	0.070	0.083
4.05	0.340	1.723	0.036	0.019	0.00032	1.634	0.883	0.663	0.470	1.845	1.035	0.071	0.087
5.05	0.424	1.453	0.033	0.018	0.00030	1.500	0.819	0.615	0.501	2.031	1.182	0.078	0.099
6.05	0.508	1.209	0.029	0.017	0.00025	1.312	0.780	0.525	0.512	2.081	1.312	0.080	0.110
7.05	0.592	0.991	0.029	0.016	0.00020	1.335	0.708	0.420	0.444	2.030	1.431	0.078	0.120
8.05	0.676	0.811	0.026	0.015	0.00018	1.199	0.668	0.384	0.479	2.270	1.673	0.087	0.141
9.05	0.761	0.679	0.024	0.014	0.00014	1.093	0.619	0.282	0.416	1.990	1.712	0.076	0.144
10.05	0.845	0.596	0.022	0.011	0.00007	0.995	0.499	0.148	0.299	1.193	1.415	0.046	0.119
11.05	0.929	0.561	0.020	0.009	0.00004	0.909	0.413	0.093	0.248	0.795	1.190	0.031	0.100

$-\overline{u'v'}$ is measured

RUN : UPC5 - Flow parameters

$S_G = 0.00025$	$D = 0.119 \text{ m}$	$U = 0.339 \text{ m/s}$	$U_c = 0.404 \text{ m/s}$	$u_* = 0.023 \text{ m/s}$
$Br = 9.00$	$\Pi = 0.12$	$Re = 1.61 \cdot 10^7$	$Fr = 0.31$	$b/D = 5.04$
$\delta = 0.119 \text{ m}$	$\delta_* = 0.019 \text{ m}$	$\theta = 0.013 \text{ m}$	$H = 1.45$	$\beta_* = -1.00$

RUN : UPC5 - Velocity distribution

$y \times 10^2$ (m)	u (m/s)	y/δ (-)	y/D (-)	y/k_s (-)	$(U_c - u)/u_*$ (-)	w/U_c (-)	u/u_* (-)
0.25	0.172	0.021	0.021	0.521	10.223	0.426	7.574
0.45	0.207	0.038	0.038	0.938	8.668	0.513	9.129
0.65	0.224	0.055	0.055	1.354	7.927	0.555	9.871
0.85	0.237	0.071	0.071	1.771	7.376	0.586	10.421
1.05	0.251	0.088	0.088	2.188	6.743	0.621	11.054
1.25	0.265	0.105	0.105	2.604	6.146	0.655	11.651
1.55	0.271	0.130	0.130	3.229	5.860	0.671	11.938
1.75	0.281	0.147	0.147	3.646	5.432	0.695	12.365
2.05	0.292	0.172	0.172	4.271	4.921	0.724	12.877
2.25	0.299	0.189	0.189	4.688	4.623	0.740	13.175
2.55	0.306	0.214	0.214	5.313	4.308	0.758	13.489
3.05	0.316	0.256	0.256	6.354	3.860	0.782	13.912
3.55	0.320	0.298	0.298	7.396	3.682	0.793	14.115
4.05	0.332	0.340	0.340	8.438	3.157	0.823	14.640
5.05	0.345	0.424	0.424	10.521	2.592	0.854	15.206
6.05	0.358	0.508	0.508	12.604	2.023	0.886	15.774
7.05	0.367	0.592	0.592	14.688	1.616	0.909	16.181
8.05	0.374	0.676	0.676	16.771	1.339	0.925	16.458
9.05	0.387	0.761	0.761	18.854	0.741	0.958	17.056
10.05	0.397	0.845	0.845	20.938	0.293	0.984	17.504
11.05	0.399	0.929	0.929	23.021	0.223	0.987	17.574
11.90	0.404	1.000	1.000	24.792	0.000	1.000	17.797

4.798×10^{-2}

RUN : UPC5 - Turbulence distributions

$y \times 10^2$ (m)	y/δ (-)	du/dy (1/s)	u' (m/s)	$-\overline{u'v'_1}$ (m ² /s ²)	u'/u_* (-)	$v'_1 \times 10^4$ (m ² /s)	$\ell \times 10^2$ (m)	$v'_1/\delta u_*$ (-)	ℓ/δ (-)
0.25	0.021	14.136	0.043	-	1.892	-	-	-	-
0.65	0.055	9.359	0.045	0.00051	1.981	0.543	0.241	0.027	0.020
1.05	0.088	5.926	0.043	0.00052	1.893	0.869	0.383	0.032	0.032
1.55	0.130	3.526	0.042	0.00049	1.868	1.392	0.628	0.052	0.053
2.05	0.172	2.859	0.038	0.00043	1.669	1.501	0.725	0.056	0.061
2.55	0.214	2.417	0.039	0.00041	1.696	1.684	0.835	0.062	0.070
3.05	0.256	2.038	0.034	0.00037	1.496	1.832	0.948	0.068	0.080
3.55	0.298	1.719	0.032	0.00037	1.430	2.124	1.112	0.079	0.093
4.05	0.340	1.464	0.032	0.00034	1.411	2.333	1.262	0.086	0.106
5.05	0.424	1.137	0.031	0.00032	1.348	2.789	1.566	0.103	0.132
6.05	0.508	1.058	0.031	0.00027	1.351	2.555	1.554	0.095	0.131
7.05	0.592	1.066	0.028	0.00022	1.231	2.028	1.379	0.075	0.116
8.05	0.676	1.012	0.025	0.00020	1.086	1.955	1.390	0.072	0.117
9.05	0.761	0.894	0.023	0.00015	1.031	1.624	1.348	0.060	0.113
10.05	0.845	0.714	0.020	0.00008	0.895	1.070	1.224	0.040	0.103
11.05	0.929	0.470	0.019	0.00005	0.835	1.020	1.473	0.038	0.124

$-\overline{u'v'_1}$ is calculated (assumed to be similar with the $-\overline{u'v'_1}$ profile of run UPC3) as, $[-\overline{u'v'_1}]_y = [-\overline{u'v'_1}]_b \left(\frac{[u_*]_y}{[u_*]_b} \right)^2$

RUN : UPD3 - Flow parameters

$S_0 = 0.00125$	$D = 0.087 \text{ m}$	$U = 0.447 \text{ m/s}$	$U_c = 0.550 \text{ m/s}$	$u_* = 0.035 \text{ m/s}$
$Br = 7.80$	$\Pi = 0.12$	$Re = 1.56 \cdot 10^4$	$Fr = 0.48$	$b/D = 6.90$
$\delta = 0.087 \text{ m}$	$\delta_* = 0.016 \text{ m}$	$\theta = 0.011 \text{ m}$	$H = 1.52$	$\delta_n = -1.00$

RUN : UPD3 - Velocity distribution

$y \times 10^2$ (m)	u (m/s)	y/δ (-)	y/D (-)	y/k_s (-)	$(U_c - u)/u_*$ (-)	u/U_c (-)	u/u_* (-)
0.25	0.213	0.029	0.029	0.521	9.617	0.388	6.097
0.45	0.270	0.052	0.052	0.938	7.988	0.492	7.727
0.65	0.303	0.075	0.075	1.354	7.066	0.550	8.648
0.85	0.329	0.098	0.098	1.771	6.328	0.597	9.389
1.05	0.342	0.121	0.121	2.188	5.948	0.621	9.766
1.25	0.365	0.144	0.144	2.604	5.297	0.663	10.417
1.55	0.377	0.178	0.178	3.229	4.949	0.685	10.765
1.75	0.391	0.201	0.201	3.646	4.544	0.711	11.170
2.05	0.405	0.236	0.236	4.271	4.152	0.736	11.562
2.25	0.408	0.259	0.259	4.688	4.054	0.742	11.660
2.55	0.419	0.293	0.293	5.313	3.754	0.761	11.960
3.05	0.440	0.351	0.351	6.354	3.144	0.800	12.570
3.55	0.451	0.408	0.408	7.396	2.832	0.820	12.883
4.05	0.461	0.466	0.466	8.438	2.549	0.838	13.165
5.05	0.486	0.580	0.580	10.521	1.834	0.883	13.880
6.05	0.504	0.695	0.695	12.604	1.319	0.916	14.395
7.05	0.530	0.810	0.810	14.688	0.582	0.963	15.132
7.55	0.535	0.868	0.868	15.729	0.426	0.973	15.289
8.05	0.543	0.925	0.925	16.771	0.195	0.988	15.519
8.70	0.550	1.000	1.000	18.125	0.000	1.000	15.714

$k_s = 4.798 \times 10^{-3}$

RUN : UPD3 - Turbulence distributions

$y \times 10^2$ (m)	y/δ (-)	du/dy (1/s)	u' (m/s)	v' (m/s)	$-\overline{u'v'}$ (m ² /s ²)	u'/u_* (-)	v'/u_* (-)	$-\overline{u'v'}/u_*^2$ (-)	$-\overline{u'v'}/u_*v'$ (-)	$v'_t \times 10^4$ (m ² /s)	$L \times 10^2$ (m)	$v'/\delta u_*$ (-)	L/δ (-)
0.65	0.075	15.740	0.065	0.037	0.00103	1.851	1.071	0.890	0.449	0.693	0.210	0.023	0.024
1.05	0.121	8.814	0.086	0.035	0.00111	1.889	1.009	0.910	0.477	1.293	0.388	0.042	0.045
1.55	0.178	4.888	0.081	0.032	0.00095	1.733	0.925	0.776	0.484	1.953	0.633	0.064	0.073
2.05	0.236	4.098	0.059	0.032	0.00094	1.676	0.903	0.765	0.505	2.286	0.747	0.075	0.088
2.55	0.293	3.456	0.054	0.030	0.00082	1.551	0.847	0.666	0.508	2.362	0.827	0.078	0.095
3.05	0.351	2.944	0.050	0.030	0.00079	1.430	0.857	0.644	0.525	2.680	0.954	0.088	0.110
3.55	0.408	2.580	0.049	0.028	0.00067	1.397	0.802	0.548	0.489	2.620	1.012	0.086	0.116
4.05	0.466	2.305	0.048	0.027	0.00064	1.369	0.780	0.520	0.487	2.764	1.095	0.091	0.126
5.05	0.580	2.183	0.041	0.026	0.00049	1.184	0.742	0.404	0.460	2.265	1.019	0.074	0.117
6.05	0.695	2.171	0.037	0.023	0.00035	1.046	0.659	0.283	0.411	1.598	0.858	0.052	0.099
7.05	0.810	1.889	0.033	0.022	0.00026	0.929	0.643	0.216	0.362	1.400	0.861	0.046	0.099
7.55	0.868	1.646	0.036	0.022	0.00018	1.026	0.633	0.148	0.228	1.100	0.817	0.036	0.094

$-\overline{u'v'}$ is measured

RUN : UPD5 - Flow parameters

$Sc = 0.0u125$	$D = 0.087 \text{ m}$	$U = 0.443 \text{ m/s}$	$U_c = 0.545 \text{ m/s}$	$u_{\infty} = 0.037 \text{ m/s}$
$Br = 7.00$	$\Pi = 0.07$	$Re = 1.54 \cdot 10^3$	$Fr = 0.48$	$b/D = 6.9$
$\delta = 0.087 \text{ m}$	$\delta_{\infty} = 0.016 \text{ m}$	$\theta = 0.011 \text{ m}$	$H = 1.54$	$\beta_{\infty} = -1.00$

6.19

RUN : UPD5 - Velocity distribution

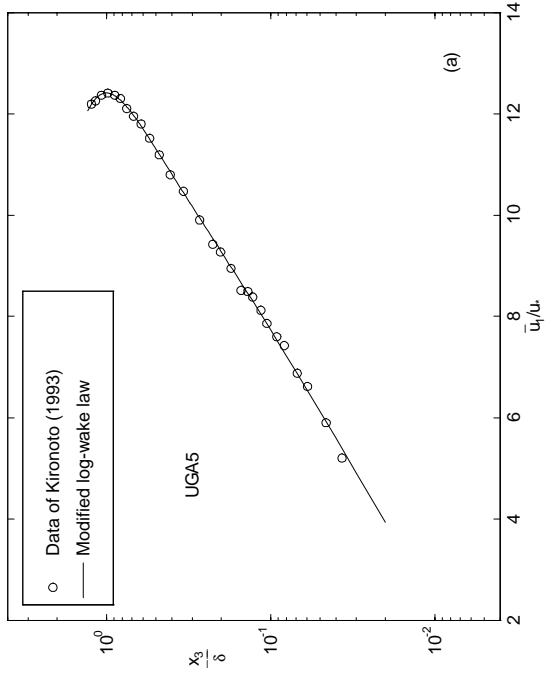
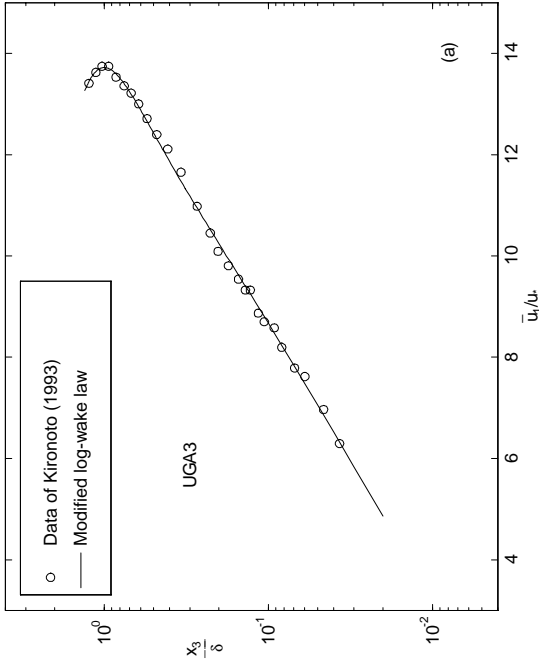
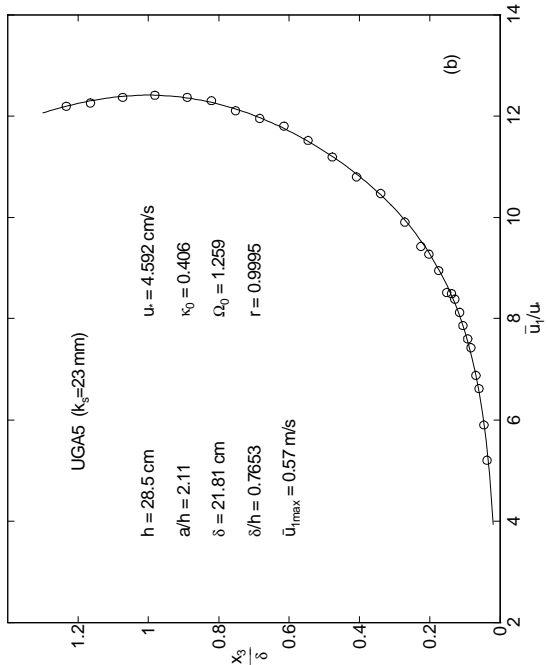
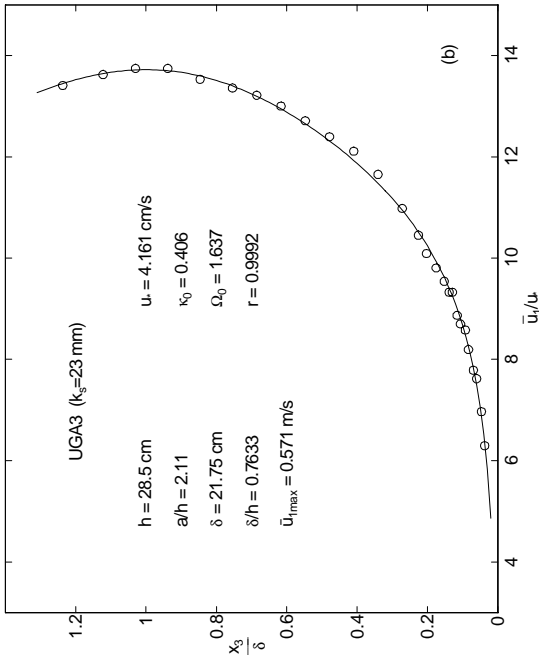
$y \times 10^2$ (m)	u (m/s)	y/δ (-)	y/D (-)	y/k_s (-)	$(U_c - u)/u_{\infty}$ (-)	u/U_c (-)	u/u_{∞} (-)
0.25	0.206	0.029	0.029	0.521	9.104	0.379	5.547
0.45	0.255	0.052	0.052	0.938	7.810	0.467	6.841
0.65	0.286	0.075	0.075	1.354	6.958	0.525	7.693
0.85	0.317	0.098	0.098	1.771	6.140	0.581	8.510
1.05	0.334	0.121	0.121	2.188	5.673	0.613	8.978
1.25	0.355	0.144	0.144	2.604	5.117	0.651	9.534
1.55	0.375	0.178	0.178	3.229	4.582	0.687	10.068
1.75	0.386	0.201	0.201	3.646	4.278	0.708	10.373
2.05	0.402	0.236	0.236	4.271	3.847	0.737	10.803
2.25	0.407	0.259	0.259	4.688	3.699	0.747	10.951
2.55	0.420	0.293	0.293	5.313	3.365	0.770	11.286
3.05	0.435	0.351	0.351	6.354	2.968	0.797	11.682
3.55	0.448	0.408	0.408	7.396	2.617	0.821	12.033
4.05	0.461	0.466	0.466	8.438	2.265	0.845	12.386
5.05	0.488	0.580	0.580	10.521	1.547	0.894	13.104
6.05	0.503	0.695	0.695	12.604	1.125	0.923	13.526
7.05	0.525	0.810	0.810	14.688	0.540	0.963	14.111
7.55	0.530	0.868	0.868	15.729	0.395	0.973	14.256
8.05	0.539	0.925	0.925	16.771	0.172	0.988	14.478
8.70	0.545	1.000	1.000	18.125	0.000	1.000	14.651

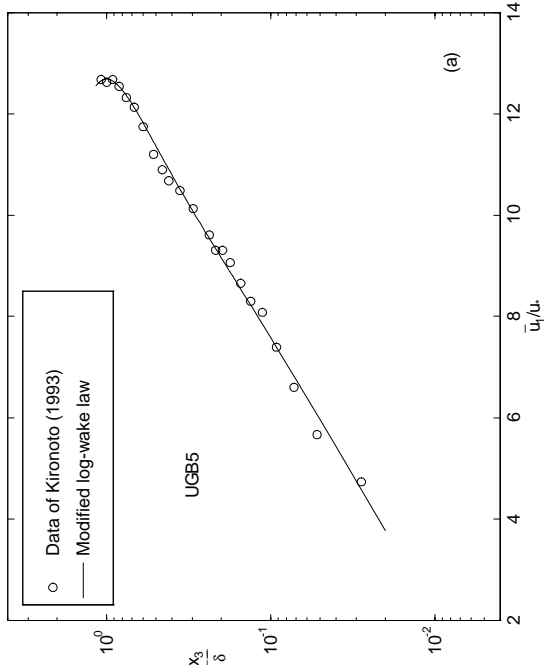
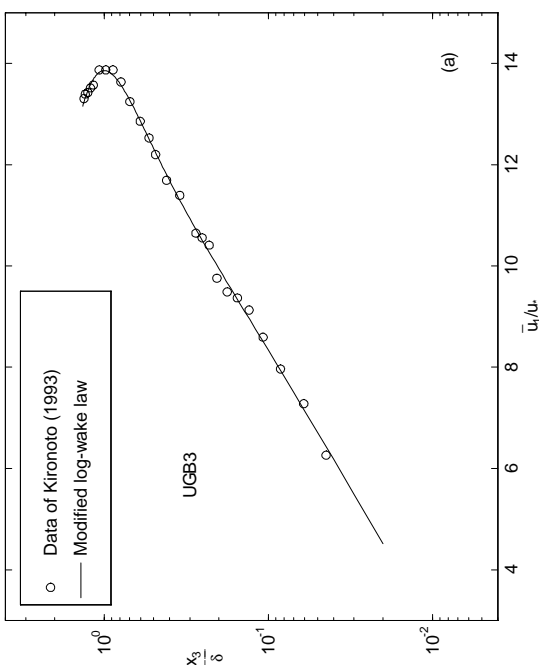
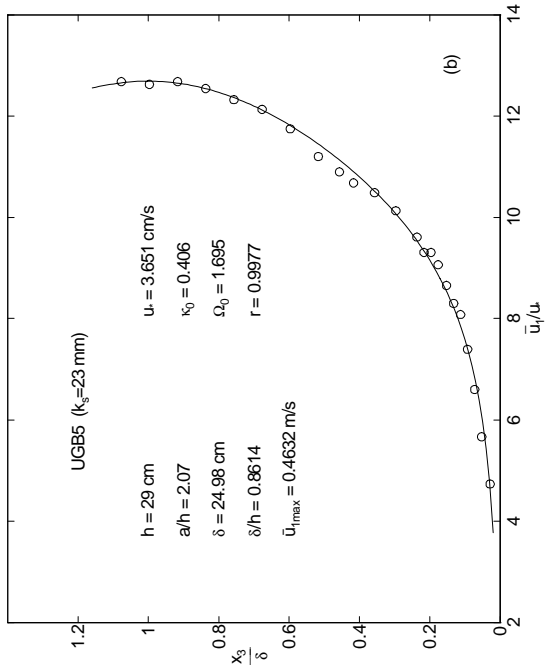
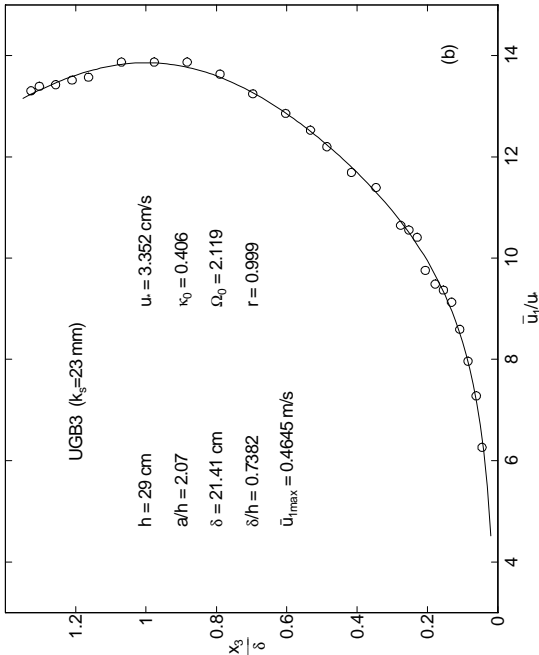
$K_S = 4.798 \times 10^{-3}$

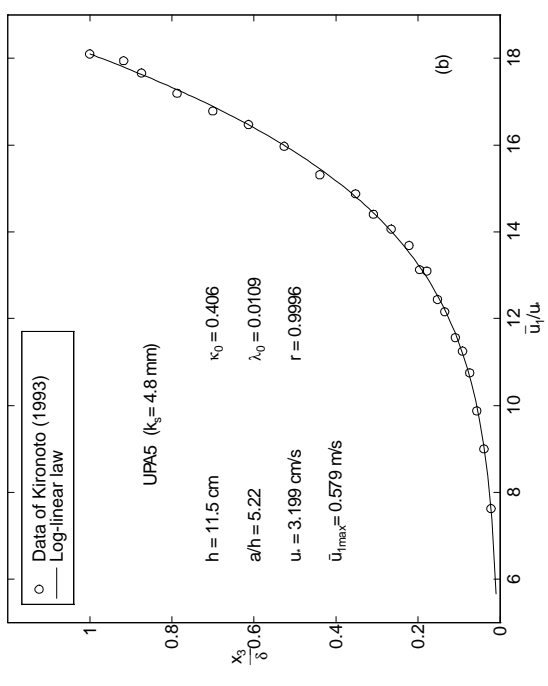
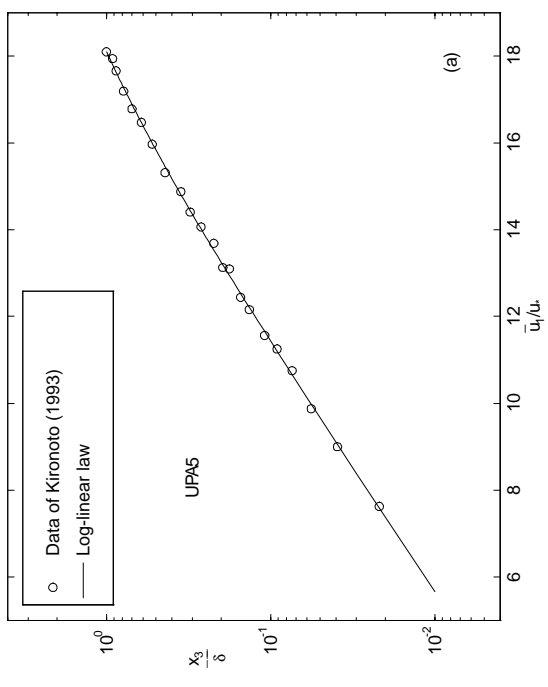
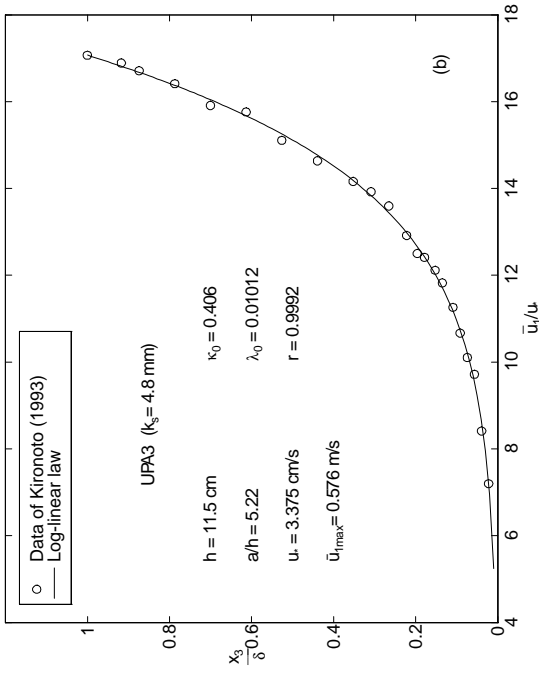
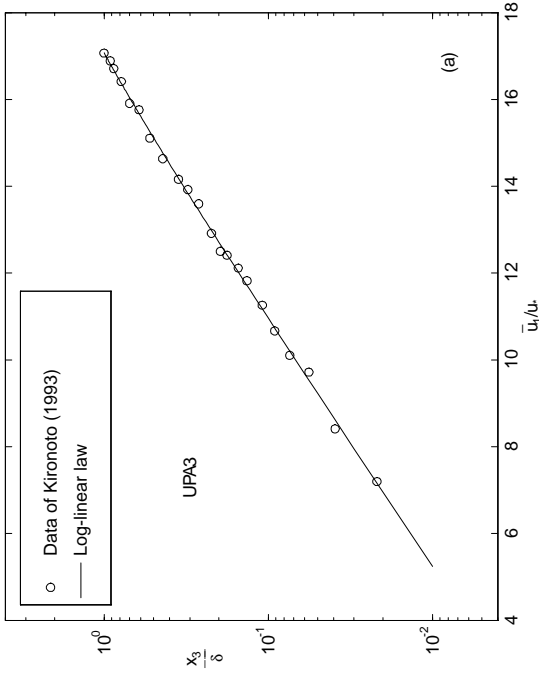
RUN : UPD5 - Turbulence distributions

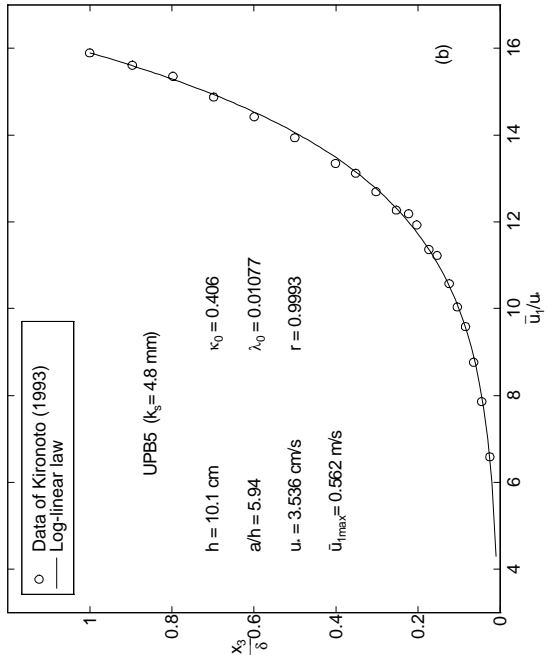
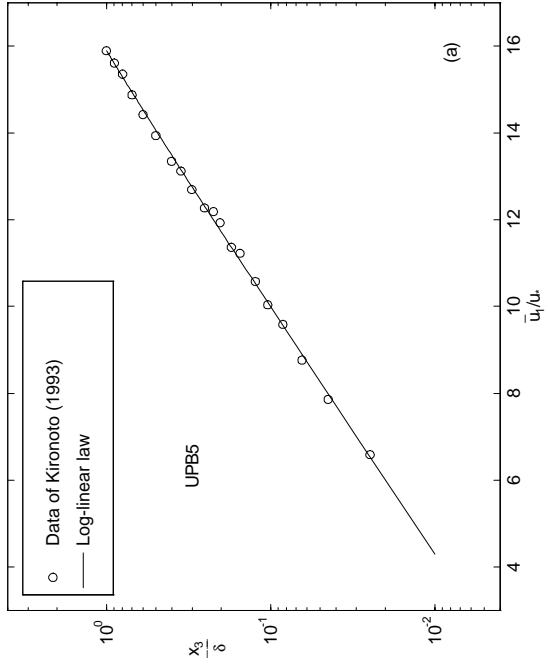
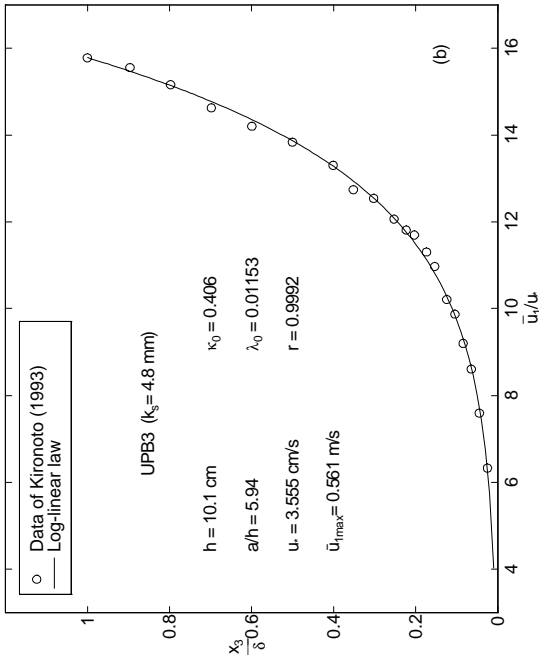
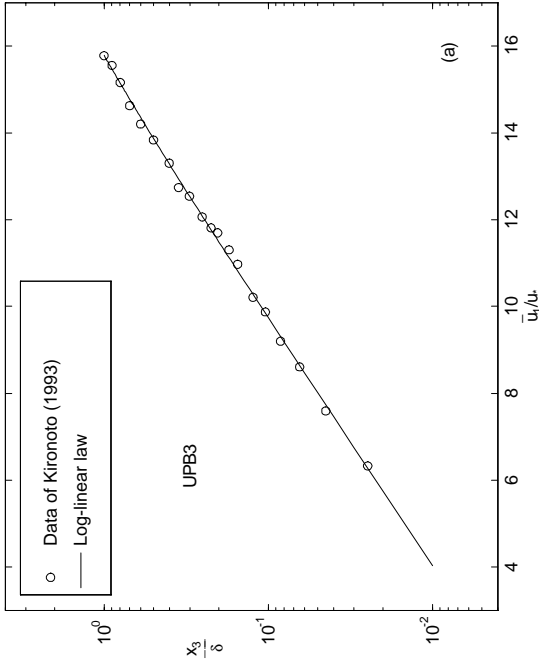
$y \times 10^2$ (m)	y/δ (-)	du/dy (1/s)	u' (m/s)	$-\overline{u'v'}$ (m ² /s ²)	u'/u_{∞} (-)	$v_t \times 10^4$ (m ² /s)	$\ell \times 10^2$ (m)	$v_t/\delta u_{\infty}$ (-)	ℓ/δ (-)
0.45	0.052	19.534	0.061	-	1.628	-	-	-	-
0.65	0.075	15.771	0.063	0.00123	1.704	0.781	0.223	0.024	0.026
1.05	0.121	9.910	0.066	0.00126	1.768	1.270	0.358	0.039	0.041
1.55	0.178	5.706	0.060	0.00107	1.615	1.883	0.574	0.058	0.066
2.05	0.236	4.385	0.054	0.00106	1.458	2.414	0.742	0.075	0.085
2.55	0.293	3.549	0.052	0.00092	1.390	2.598	0.856	0.080	0.098
3.05	0.351	2.937	0.049	0.00089	1.321	3.035	1.017	0.094	0.117
3.55	0.408	2.549	0.047	0.00076	1.261	2.972	1.080	0.092	0.124
4.05	0.466	2.385	0.046	0.00072	1.241	3.017	1.125	0.093	0.129
5.05	0.580	2.224	0.039	0.00056	1.053	2.511	1.063	0.078	0.122
6.05	0.695	1.978	0.038	0.00039	1.020	1.982	1.001	0.061	0.115
7.05	0.810	1.645	0.035	0.00030	0.928	1.816	1.051	0.056	0.121
7.55	0.868	1.447	0.036	0.00020	0.968	1.413	0.988	0.044	0.114

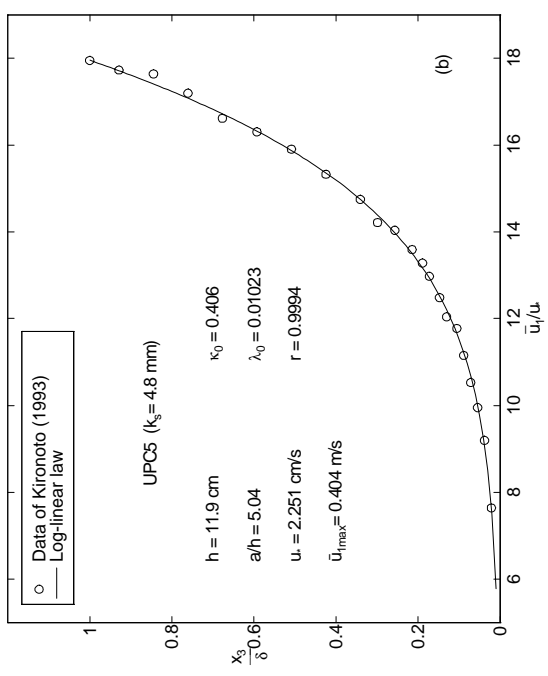
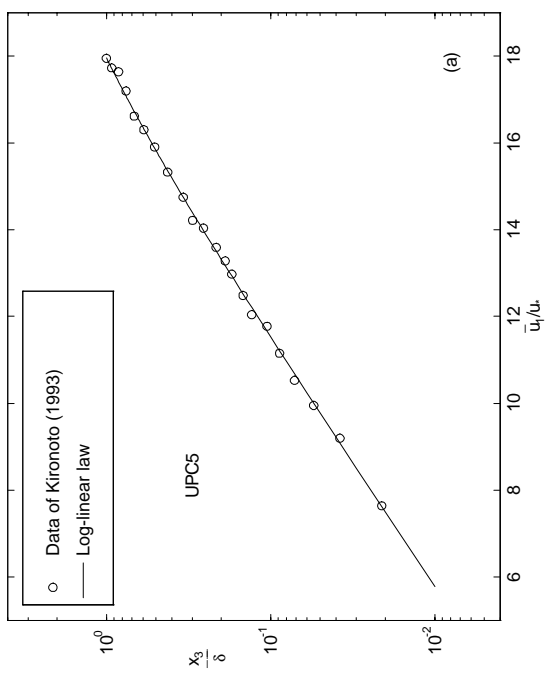
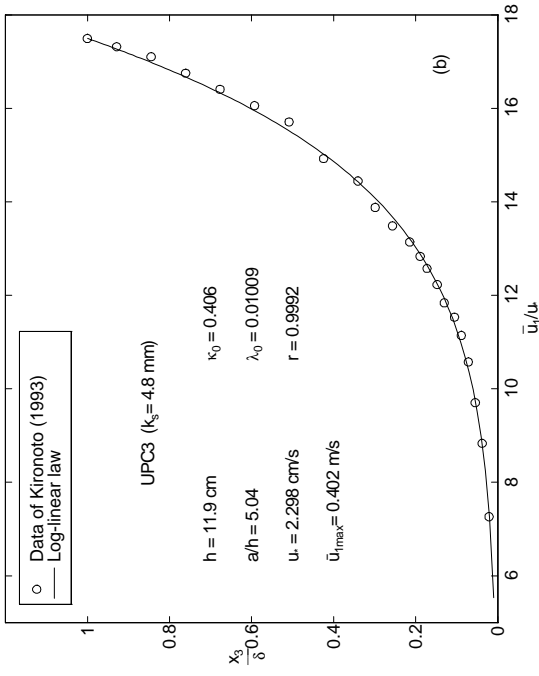
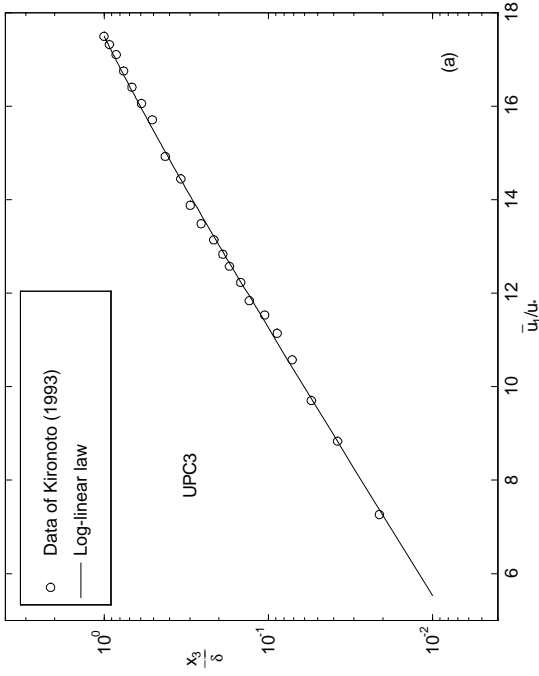
$-\overline{u'v'}$ is calculated (assumed to be similar with the $-\overline{u'v'}$ profile of run UPD3) as: $[-\overline{u'v'}]_k = [-\overline{u'v'}]_0 \left(\frac{[u_{\infty}]_k}{[u_{\infty}]_0} \right)^2$

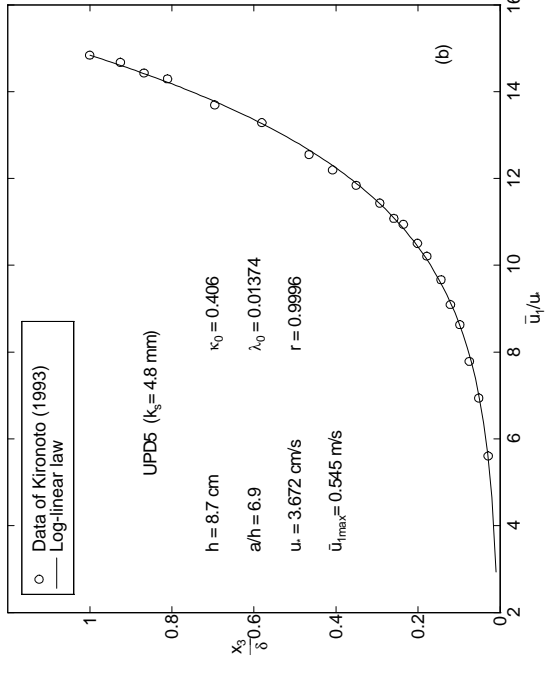
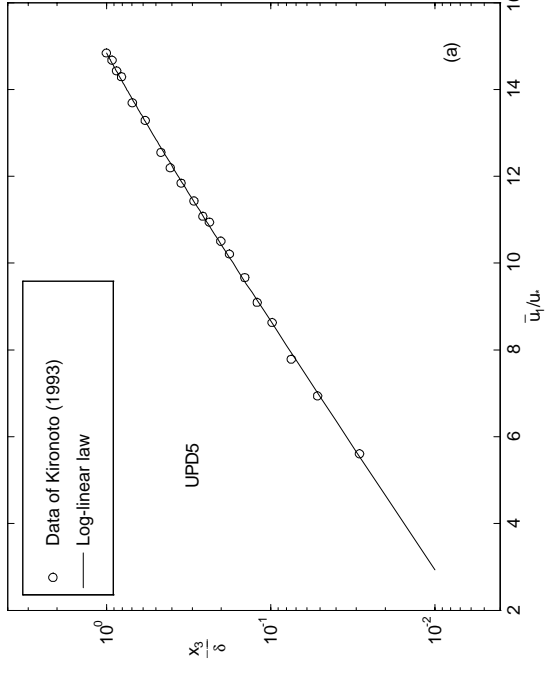
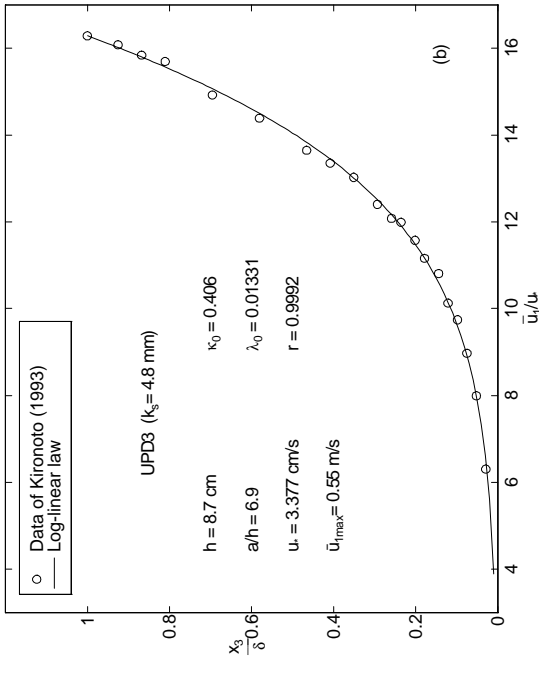
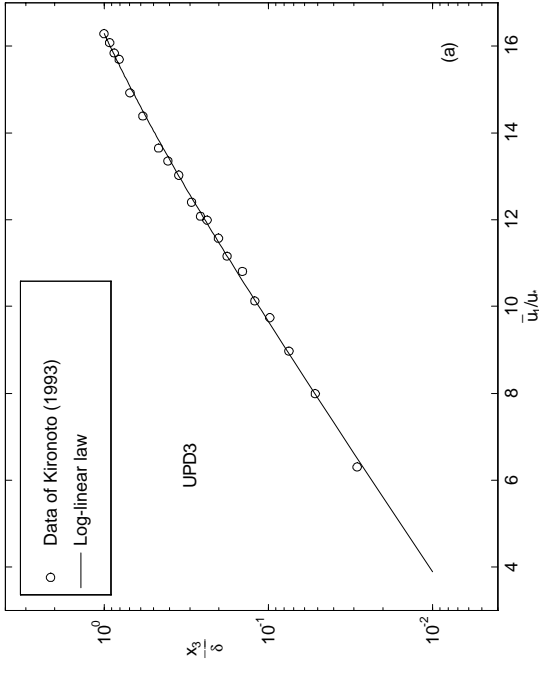












Appendix F

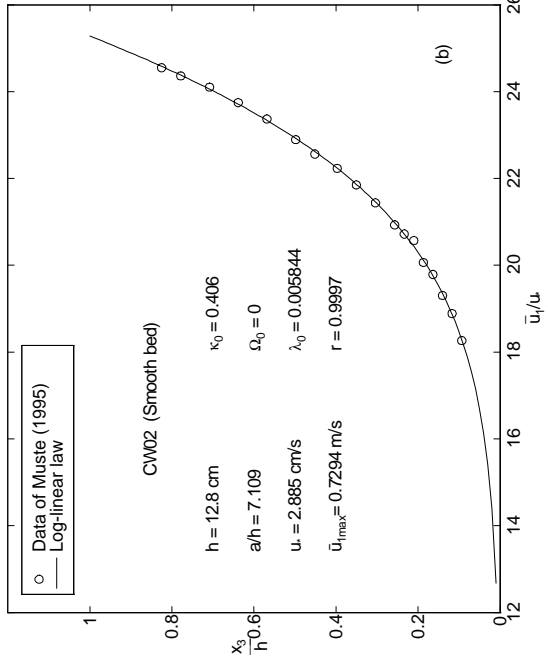
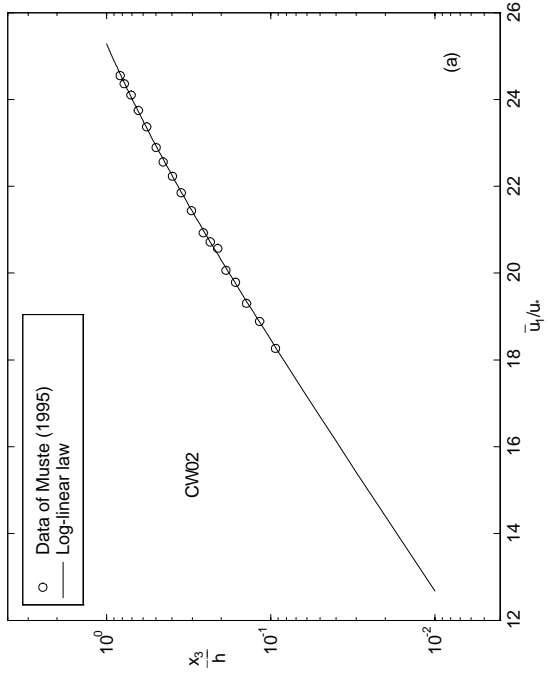
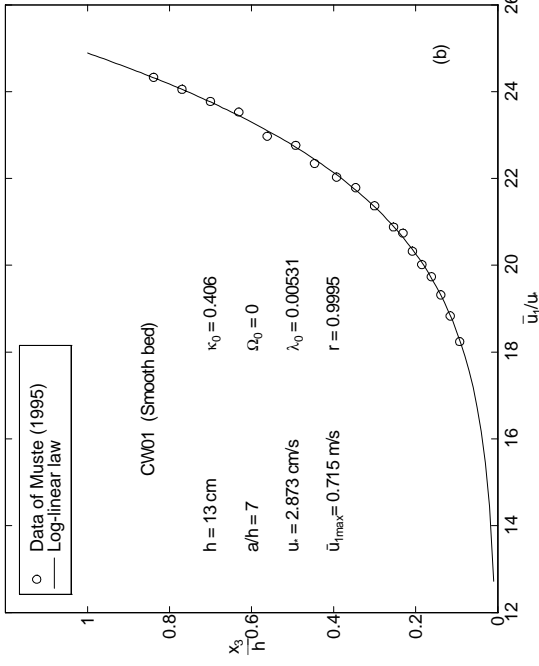
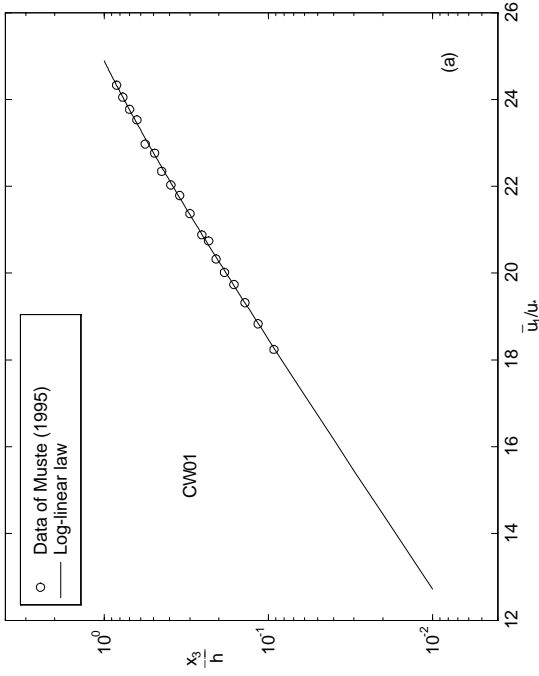
ANALYSIS OF MUSTE'S EXPERIMENTAL DATA

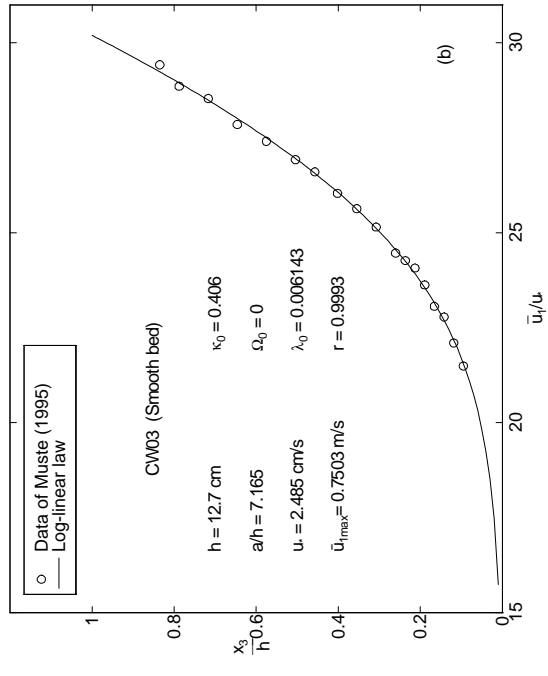
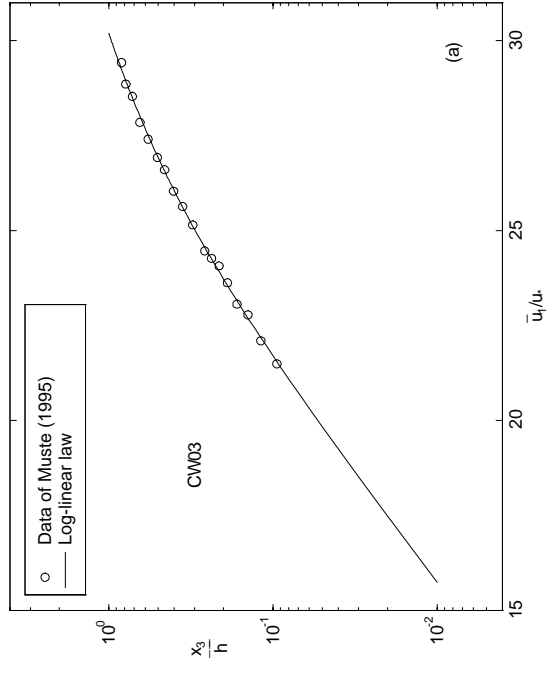
Muste (1995) did three runs of clear water experiments and three runs of sediment-laden experiments in a smooth wide flume with 30 m long, 0.91 m wide and 0.45 deep. He measured both fluid and sediment particles velocities in sediment-laden flows. However, only the three clear water experiments are cited here. The experimental conditions and measurement data are shown in Table F.1. The three velocity profile analyses are attached after the table.

Table F.1: Muste's (1995)^a measurements of velocity profiles

CW01		CW02		CW03	
$h = 13 \text{ cm}$		$h = 12.8 \text{ cm}$		$h = 12.7 \text{ cm}$	
$S = 7.41\text{E-}4$		$S = 7.71\text{E-}4$		$S = 8.11\text{E-}4$	
x_3/h	\bar{u}_1 (m/s)	x_3/h	\bar{u}_1 (m/s)	x_3/h	\bar{u}_1 (m/s)
0.0923	0.5240	0.0933	0.5270	0.0945	0.5340
0.1154	0.5410	0.1167	0.5450	0.1181	0.5490
0.1385	0.5550	0.1400	0.5570	0.1417	0.5660
0.1615	0.5670	0.1634	0.5709	0.1654	0.5730
0.1846	0.5750	0.1867	0.5790	0.1890	0.5870
0.2077	0.5840	0.2100	0.5936	0.2126	0.5980
0.2308	0.5960	0.2334	0.5980	0.2362	0.6030
0.2538	0.6000	0.2567	0.6040	0.2598	0.6080
0.3000	0.6140	0.3034	0.6187	0.3071	0.6250
0.3462	0.6260	0.3501	0.6306	0.3543	0.6370
0.3923	0.6330	0.3967	0.6416	0.4016	0.6470
0.4462	0.6420	0.4512	0.6511	0.4567	0.6610
0.4923	0.6540	0.4979	0.6607	0.5039	0.6690
0.5615	0.6600	0.5679	0.6744	0.5748	0.6810
0.6308	0.6760	0.6379	0.6853	0.6457	0.6920
0.7000	0.6830	0.7079	0.6955	0.7165	0.7090
0.7692	0.6910	0.7779	0.7030	0.7874	0.7170
0.8385	0.6990	0.8246	0.7084	0.8346	0.7310

^a Data were obtained by private communication.





Appendix G

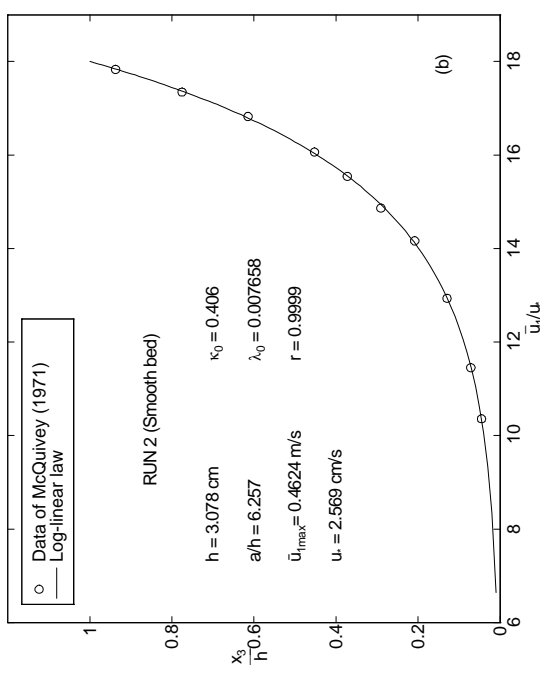
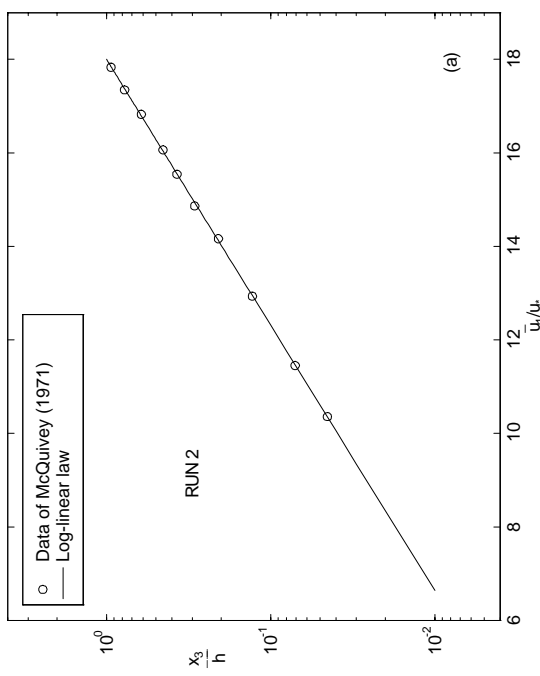
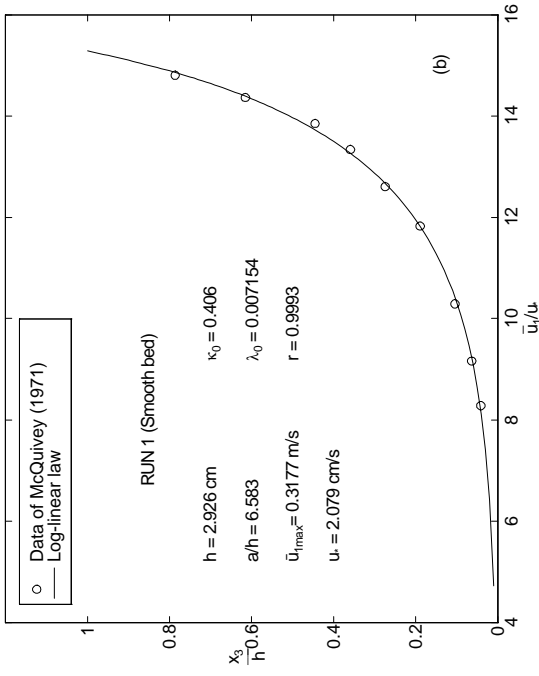
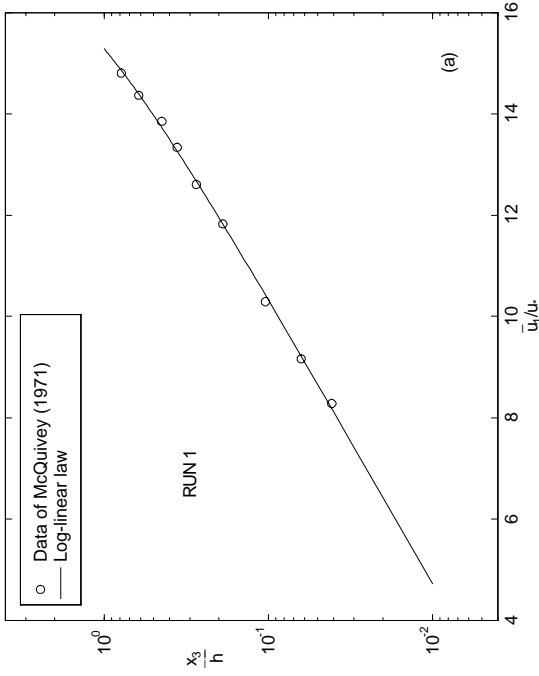
ANALYSIS OF McQUIVEY'S EXPERIMENTAL DATA

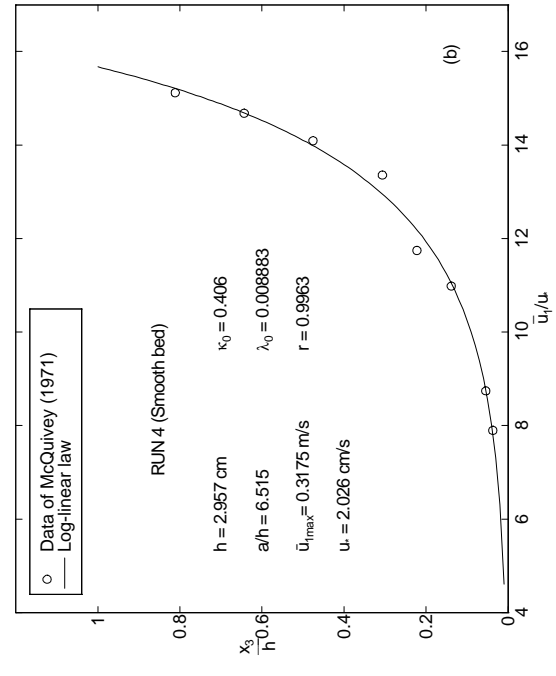
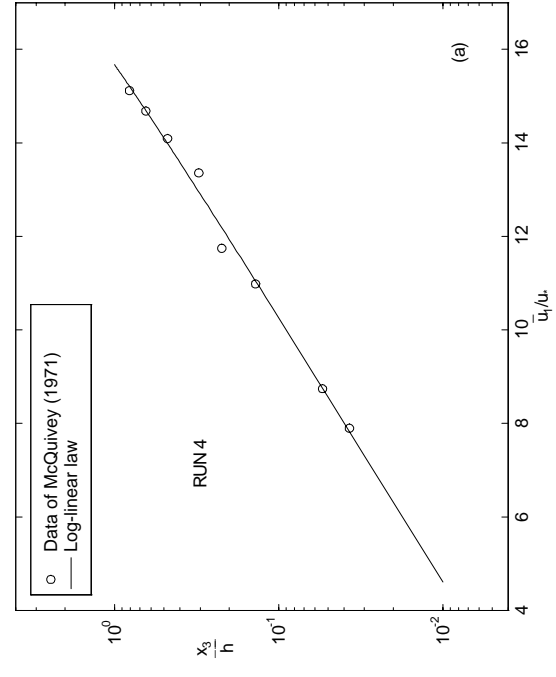
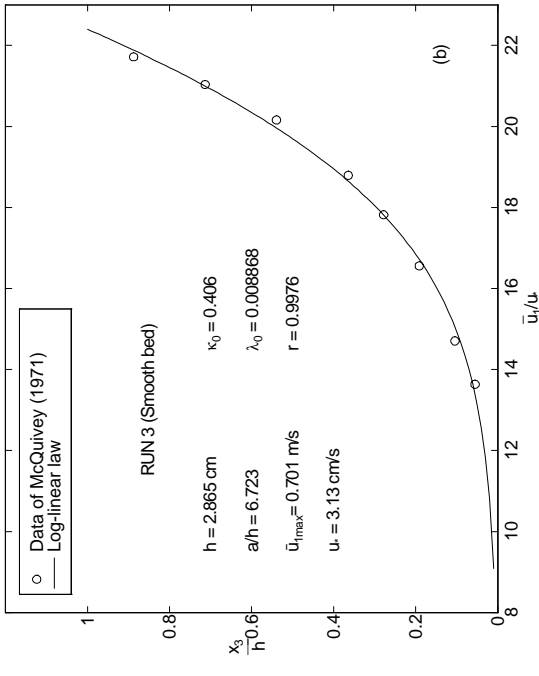
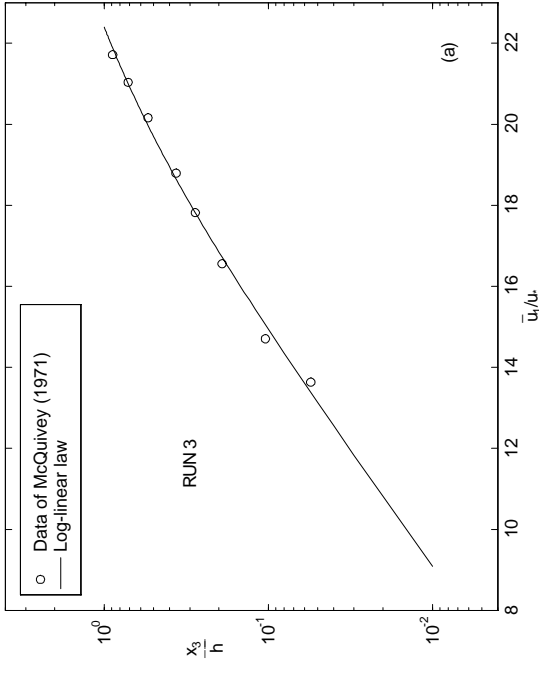
McQuivey (1971) collected a lot of experimental data. The data in a 20 centimeter-wide flume with a rigid boundary are cited and analyzed here, see attached table and figures.

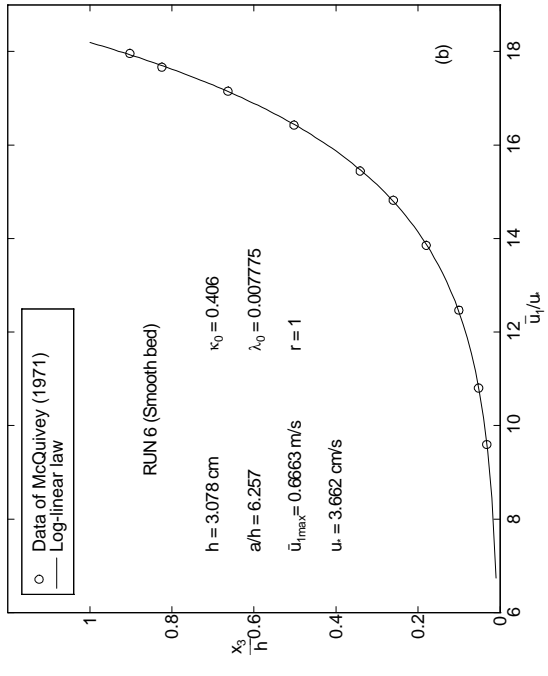
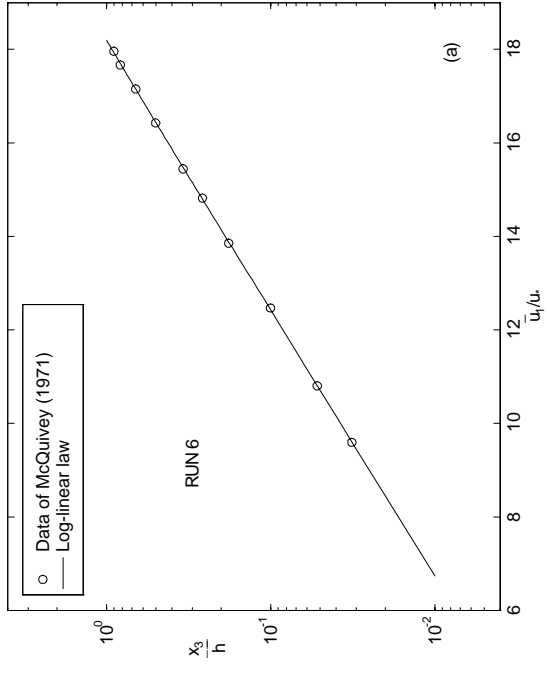
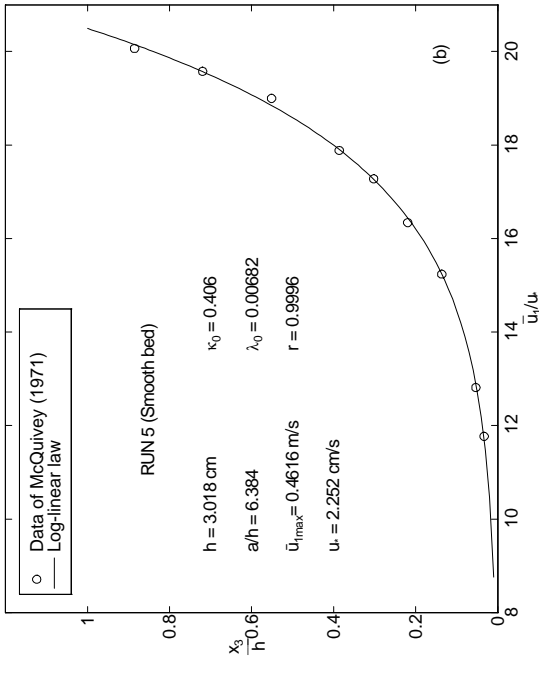
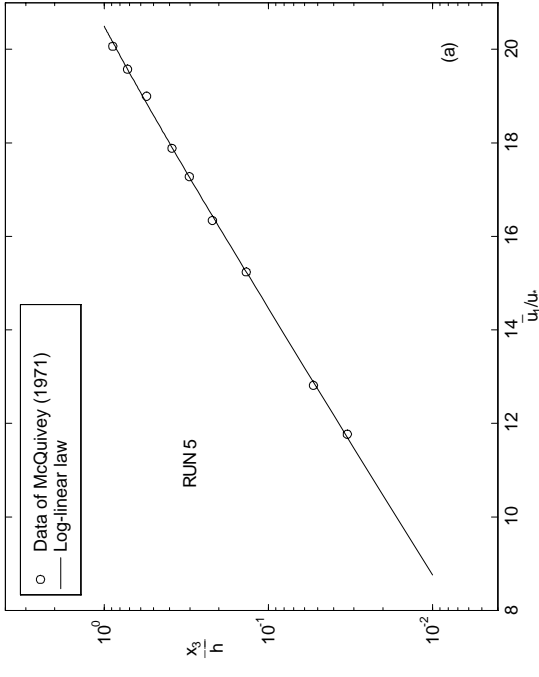
TABLE 1a. — 20-centimeter-wide flume, rigid boundary

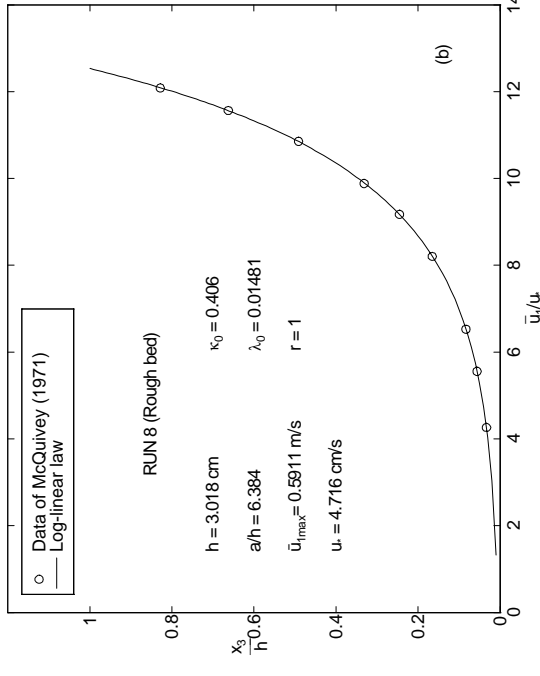
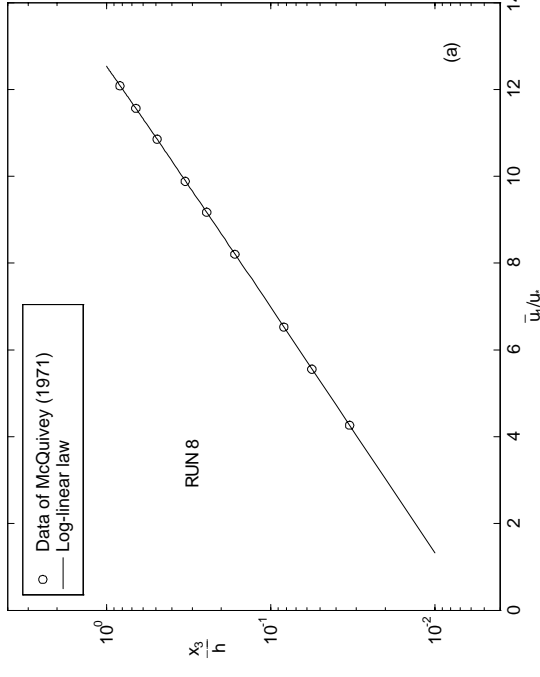
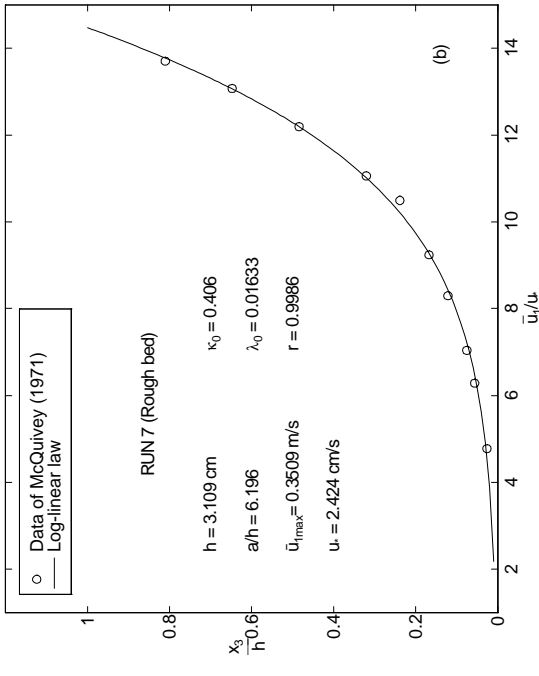
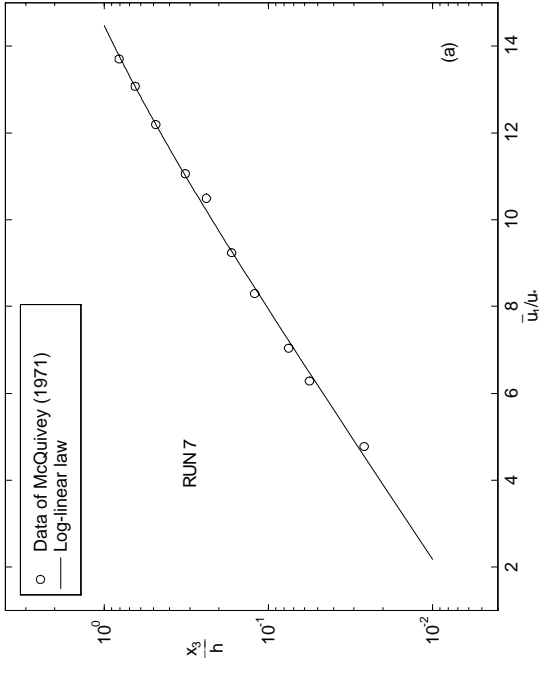
Mean flow parameters and variables		T/D	T (fps)	\bar{u}^* (fps)	$\sqrt{u^2}/\bar{u}$	$\sqrt{v^2}/u_*$
Smooth boundary, channel centerline, cylindrical hot-film sensor						
$S = 0.89 \times 10^3$	$u_* = 0.046$ fps	0.786	1.010	0.0559	0.0554	1.215
$W = 0.632$ ft	$\tau = 0.0053$ lb/ft ²	.615	.980	.0660	.0674	1.435
$Q = 0.054$ cfs	$v = 0.920 \times 10^3$ ft ² /sec	.445	.945	.0714	.0756	1.552
$T = 27.2$ °C	$R = 9,500$.159	.910	.0786	.0864	1.709
$D = 0.096$ ft	$F = 0.506$.274	.860	.0821	.0955	1.785
$\bar{V} = 0.89$ fps	$C/\bar{q} = 19.35$.189	.807	.0921	.1141	2.002
		.104	.702	.1087	.1548	2.363
		.063	.625	.1195	.1912	2.598
		.041	.565	.1296	.2294	2.817
$S = 1.70 \times 10^3$	$u_* = 0.0648$ fps	.937	1.503	.0592	.0394	.914
$W = 0.632$ ft	$\tau = 0.0106$ lb/ft ²	.775	1.462	.0656	.0449	1.012
$Q = 0.087$ cfs	$v = 0.920 \times 10^3$ ft ² /sec	.614	1.418	.0752	.0530	1.160
$T = 27.2$ °C	$R = 15,000$.452	1.354	.0878	.0648	1.355
$D = 0.101$ ft	$F = 0.76$.372	1.310	.0987	.0753	1.523
$\bar{V} = 1.365$ fps	$C/\bar{q} = 21.10$.290	1.253	.1110	.0886	1.713
		.208	1.194	.1200	.1005	1.852
		.129	1.090	.1320	.1211	2.037
		.071	.965	.1480	.1534	2.284
		.045	.875	.1670	.1913	2.577
$S = 3.50 \times 10^3$	$u_* = 0.089$ fps	.887	2.230	.0857	.0384	.963
$W = 0.632$ ft	$\tau = 0.019$ lb/ft ²	.713	2.160	.1027	.0476	1.154
$Q = 0.118$ cfs	$v = 0.909 \times 10^3$ ft ² /sec	.539	2.070	.1140	.0551	1.281
$T = 27.8$ °C	$R = 20,500$.364	1.930	.1266	.0656	1.422
$D = 0.094$ ft	$F = 1.14$.278	1.830	.1391	.0760	1.563
$\bar{V} = 1.98$ fps	$C/\bar{q} = 22.30$.191	1.700	.1632	.0960	1.834
		.104	1.510	.1806	.1196	2.029
		.055	1.400	.2121	.1515	2.383
Smooth boundary, channel centerline, wedge hot-film sensor						
$S = 0.87 \times 10^3$	$u_* = 0.0456$ fps	.811	1.005	.0470	.0370	1.031
$W = 0.632$ ft	$\tau = 0.0047$ lb/ft ²	.643	.976	.0520	.0430	1.140
$Q = 0.054$ cfs	$v = 1.01 \times 10^3$ ft ² /sec	.475	.937	.0587	.0520	1.287
$T = 23.3$ °C	$R = 8,500$.306	.888	.0688	.0660	1.509
$D = 0.097$ ft	$F = 0.50$.222	.811	.0775	.0770	1.700
$\bar{V} = 0.88$ fps	$C/\bar{q} = 19.35$.138	.730	.0874	.0900	1.917
		.054	.581	.1050	.1560	2.303
		.037	.525	.1100	.1760	2.412
$S = 1.82 \times 10^3$	$u_* = 0.0664$ fps	.885	1.483	.0506	.0260	.762
$W = 0.632$ ft	$\tau = 0.011$ lb/ft ²	.719	1.447	.0611	.0330	.920
$Q = 0.085$ cfs	$v = 1.01 \times 10^3$ ft ² /sec	.551	1.404	.0702	.0400	1.057
$T = 23.3$ °C	$R = 13,500$.386	1.322	.0782	.0480	1.178
$D = 0.099$ ft	$F = 0.76$.302	1.277	.0850	.0550	1.295
$\bar{V} = 1.36$ fps	$C/\bar{q} = 20.50$.219	1.208	.0952	.0650	1.434
		.136	1.126	.1056	.0780	1.590
		.053	.947	.1370	.1250	2.063
		.033	.870	.1531	.1580	2.306
$S = 3.50 \times 10^3$	$u_* = 0.0904$ fps	.902	2.158	.0572	.0270	.632
$W = 0.632$ ft	$\tau = 0.021$ lb/ft ²	.824	2.123	.0628	.0300	.694
$Q = 0.121$ cfs	$v = 1.01 \times 10^3$ ft ² /sec	.663	2.061	.0702	.0340	.776
$T = 23.3$ °C	$R = 19,000$.502	1.974	.0849	.0430	.939
$D = 0.101$ ft	$F = 1.05$.341	1.856	.0997	.0540	1.103
$\bar{V} = 1.90$ fps	$C/\bar{q} = 21.00$.260	1.781	.1033	.0580	1.143
		.180	1.665	.1195	.0680	1.322
		.100	1.498	.1522	.0850	1.684
		.052	1.298	.1787	.122	1.977
		.032	1.153	.1982	.163	2.192

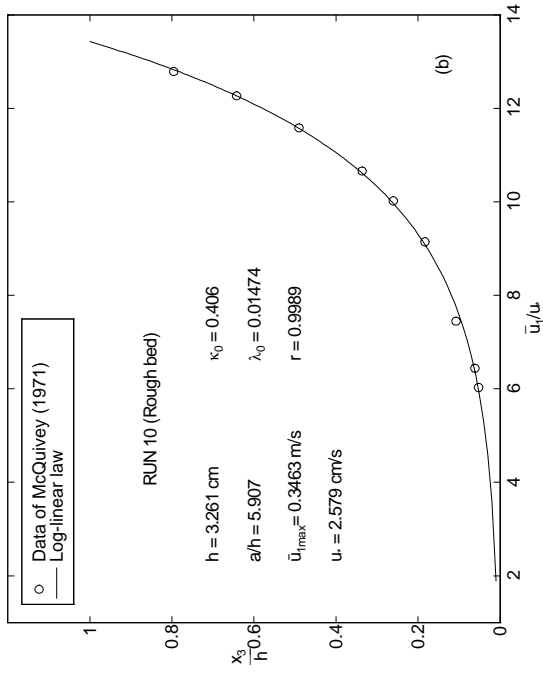
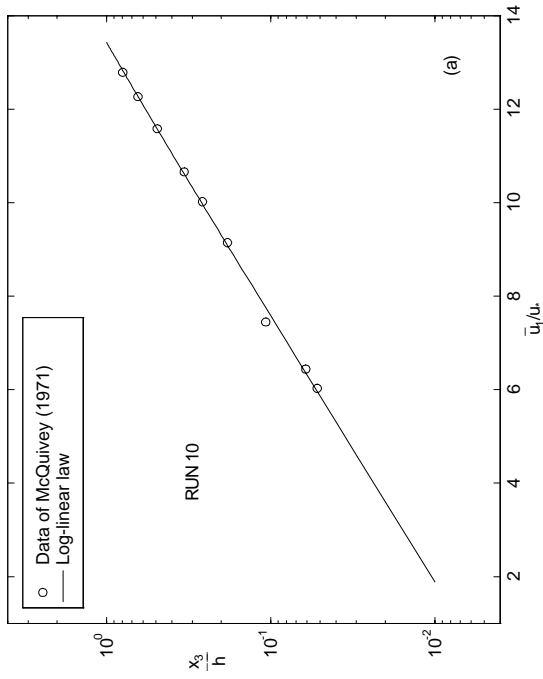
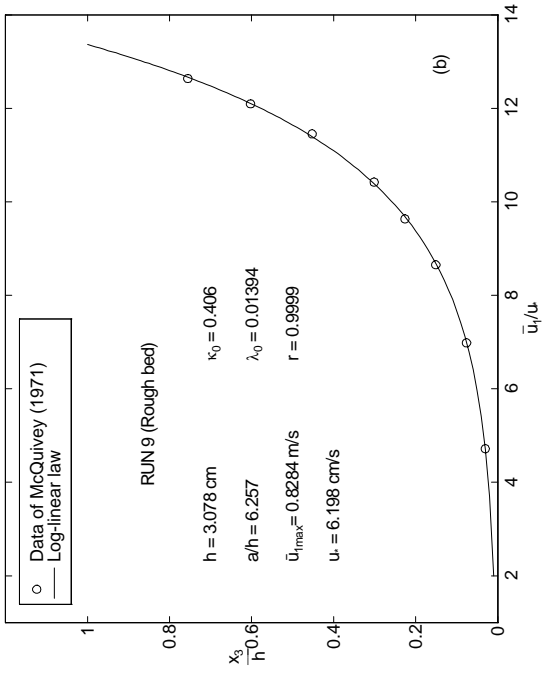
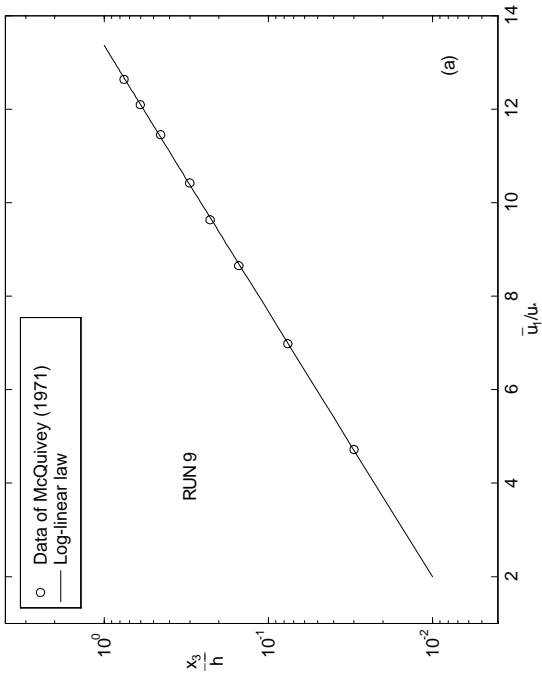
Mean flow parameters and variables		T/D	T (fps)	\bar{u}^* (fps)	$\sqrt{u^2}/\bar{u}$	$\sqrt{v^2}/u_*$
Shot roughness, channel centerline, cylindrical hot-film sensor						
$S = 1.80 \times 10^3$	$u_* = 0.0670$ fps	0.810	1.090	0.0686	0.0629	1.024
$W = 0.632$ ft	$\tau = 0.011$ lb/ft ²	.647	1.040	.0790	.0760	1.179
$Q = 0.062$ cfs	$v = 1.00 \times 10^3$ ft ² /sec	.484	.970	.0932	.0961	1.391
$T = 23.9$ °C	$R = 9,400$.320	.880	.1082	.1230	1.615
$D = 0.102$ ft	$F = 0.52$.238	.835	.1211	.1450	1.808
$\bar{V} = 0.930$ fps	$C/\bar{q} = 13.85$.167	.735	.1303	.1773	1.945
		.121	.660	.1381	.2092	2.061
		.075	.560	.1541	.2752	2.300
		.056	.500	.1623	.3246	2.422
		.026	.380	.2092	.5811	3.122
$S = 5.07 \times 10^3$	$u_* = 0.111$ fps	.995	1.940	.1036	.0534	.935
$W = 0.632$ ft	$\tau = 0.031$ lb/ft ²	.828	1.870	.1183	.0633	1.068
$Q = 0.099$ cfs	$v = 1.01 \times 10^3$ ft ² /sec	.662	1.790	.1237	.0691	1.113
$T = 23.6$ °C	$R = 14,800$.491	1.680	.1357	.0808	1.222
$D = 0.099$ ft	$F = 0.86$.331	1.530	.1603	.1048	1.444
$\bar{V} = 1.58$ fps	$C/\bar{q} = 13.50$.245	1.420	.1836	.1293	1.654
		.165	1.270	.2070	.1630	1.865
		.083	1.010	.2450	.2406	2.189
		.056	.860	.2741	.3187	2.469
		.033	.660	.3225	.4886	2.905
Shot roughness, channel centerline, wedge hot-film sensor						
$S = 1.80 \times 10^3$	$u_* = 0.068$ fps	.795	1.082	.0512	.0473	.752
$W = 0.632$ ft	$\tau = 0.012$ lb/ft ²	.642	1.058	.0633	.0610	.930
$Q = 0.065$ cfs	$v = 1.04 \times 10^3$ ft ² /sec	.490	.980	.0745	.0760	1.096
$T = 24.4$ °C	$R = 10,200$.336	.902	.0873	.0968	1.284
$D = 0.107$ ft	$F = 0.50$.260	.848	.0990	.1167	1.456
$\bar{V} = 0.960$ fps	$C/\bar{q} = 13.65$.183	.774	.1130	.1460	1.662
		.107	.650	.1110	.1762	1.632
		.061	.545	.1480	.2716	2.176
		.052	.510	.1580	.3098	2.324
$S = 5.00 \times 10^3$	$u_* = 0.1193$ fps	.810	1.982	.0740	.0370	.620
$W = 0.632$ ft	$\tau = 0.037$ lb/ft ²	.655	1.903	.0855	.0450	.716
$Q = 0.105$ cfs	$v = 1.04 \times 10^3$ ft ² /sec	.499	1.801	.1086	.0620	.910
$T = 24.4$ °C	$R = 16,600$.343	1.658	.1319	.0800	1.103
$D = 0.105$ ft	$F = 0.84$.265	1.573	.1458	.0930	1.222
$\bar{V} = 1.58$ fps	$C/\bar{q} = 13.00$.187	1.439	.1592	.1110	1.334
		.109	1.183	.1843	.1560	1.545
		.062	1.030	.2202	.2140	1.846
		.053	.972	.2388	.2460	2.002
$S = 8.44 \times 10^3$	$u_* = 0.1444$ fps	.840	2.493	.0800	.0320	.554
$W = 0.632$ ft	$\tau = 0.053$ lb/ft ²	.677	2.401	.0960	.0400	.664
$Q = 0.134$ cfs	$v = 1.04 \times 10^3$ ft ² /sec	.517	2.278	.1160	.0510	.803
$T = 24.4$ °C	$R = 20,800$.355	2.090	.1440	.0690	.997
$D = 0.101$ ft	$F = 1.10$.274	1.976	.1560	.0790	1.080
$\bar{V} = 2.10$ fps	$C/\bar{q} = 13.85$.194	1.824	.1860	.1020	1.288
		.113	1.506	.2120	.1410	1.468
		.065	1.191	.2880	.2070	1.994
		.055	1.120	.3100	.2480	2.147

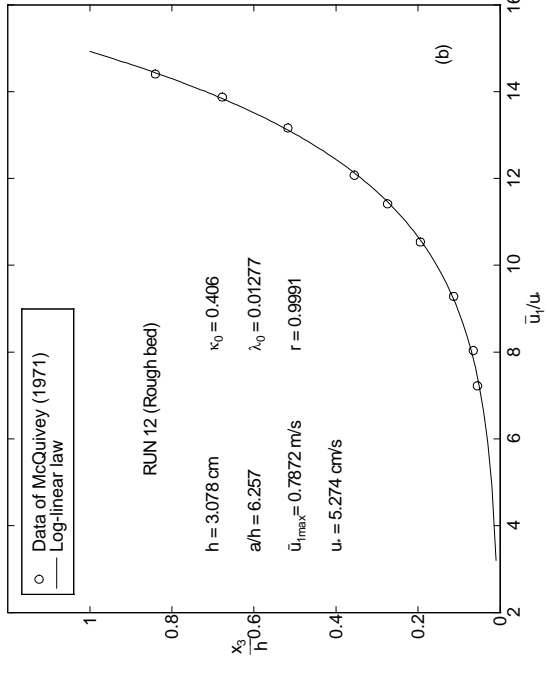
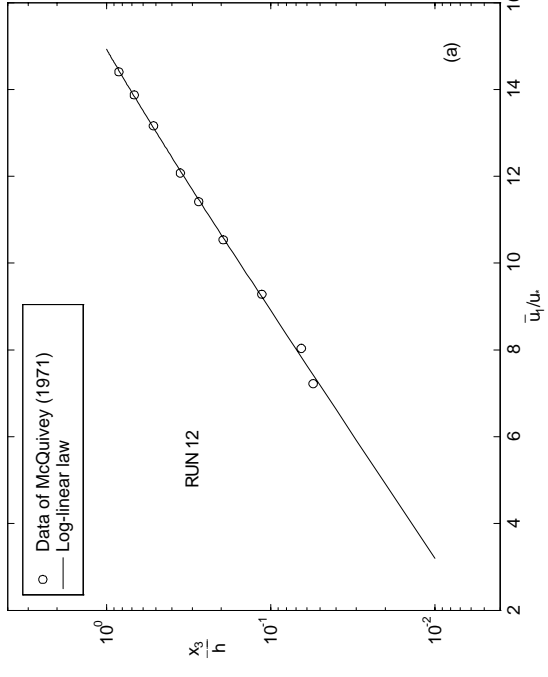
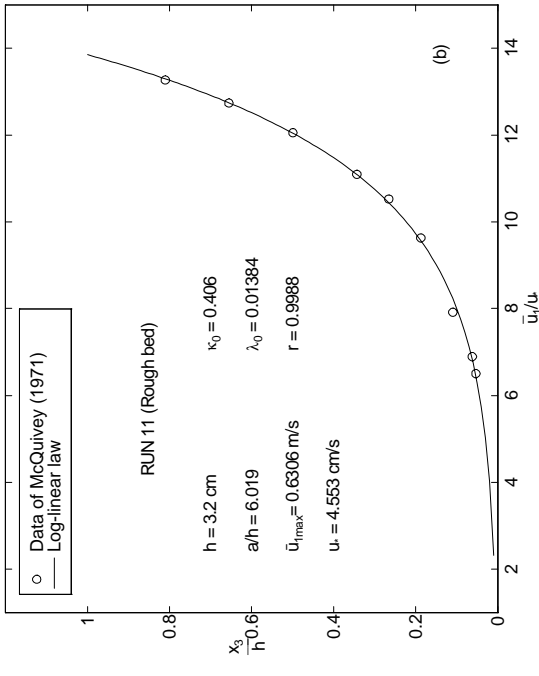
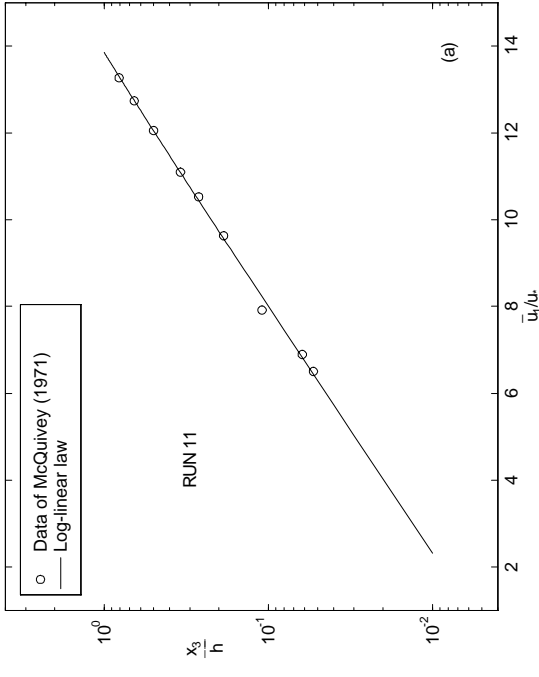












Appendix H

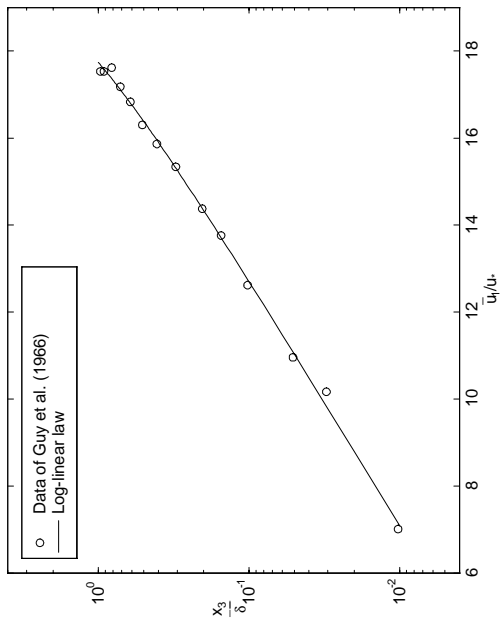
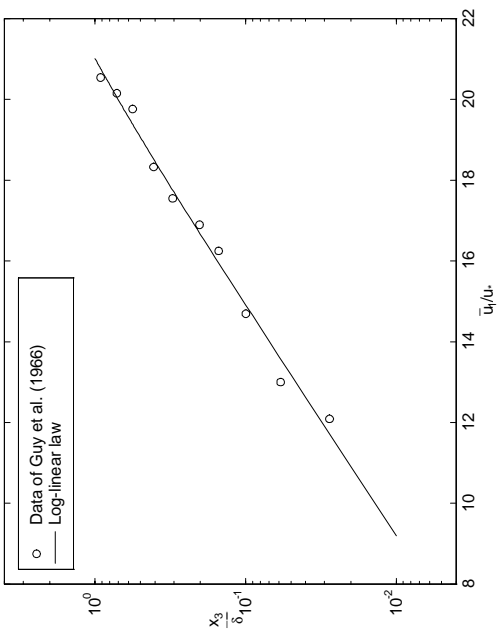
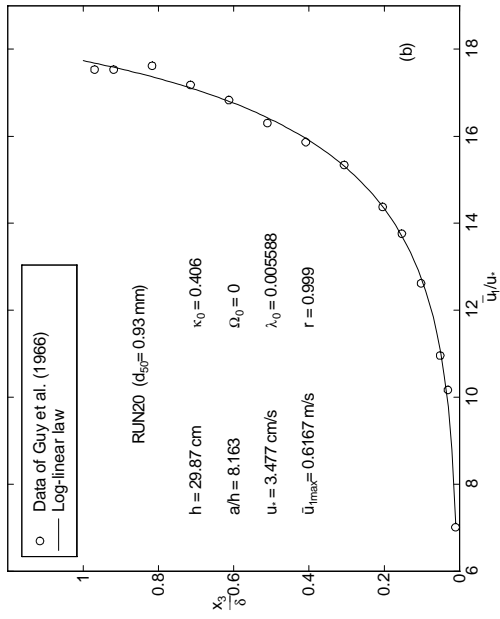
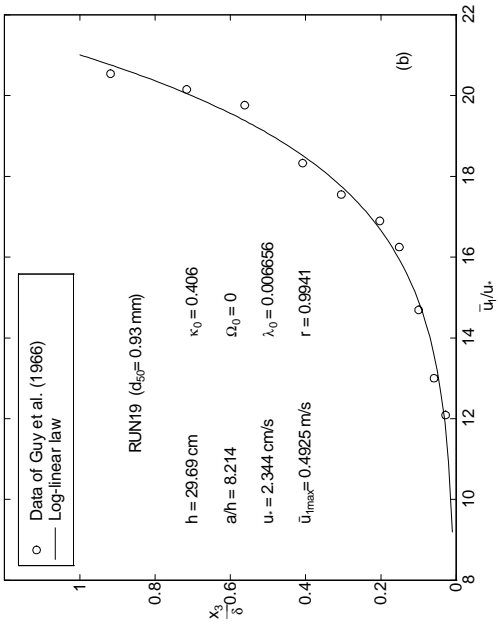
ANALYSIS OF GUY, SIMONS AND RICHARDSON'S EXPERIMENTAL DATA

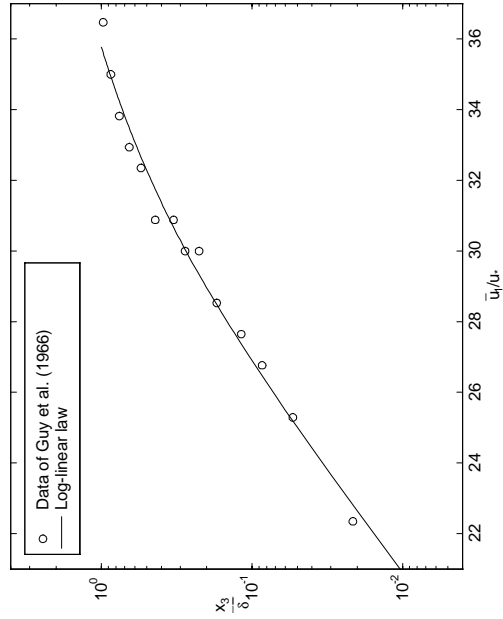
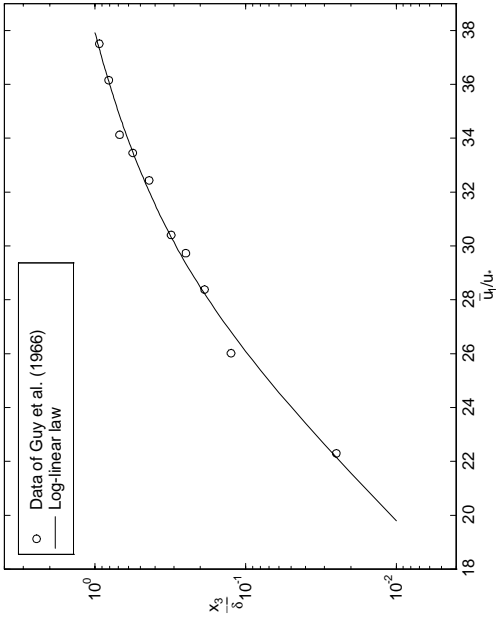
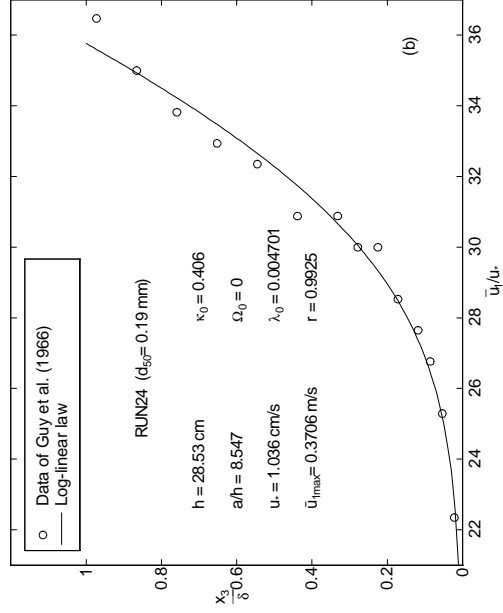
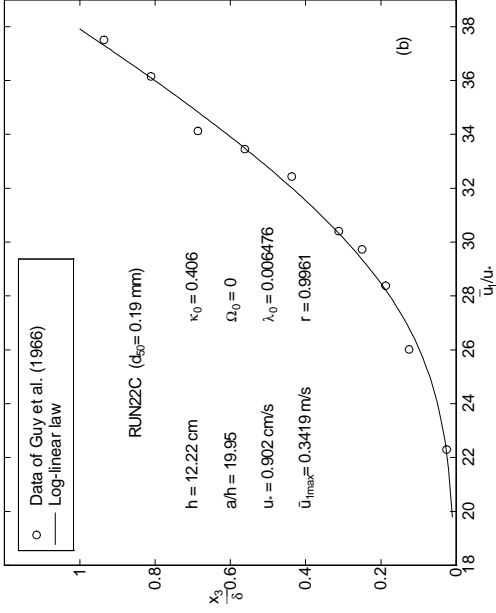
Eight velocity profile measurements over plane beds by Guy, Simons and Richardson (1966) are cited. The flow conditions and measurement data are listed in Table H.1. The analyses of velocity profile are attached after the table.

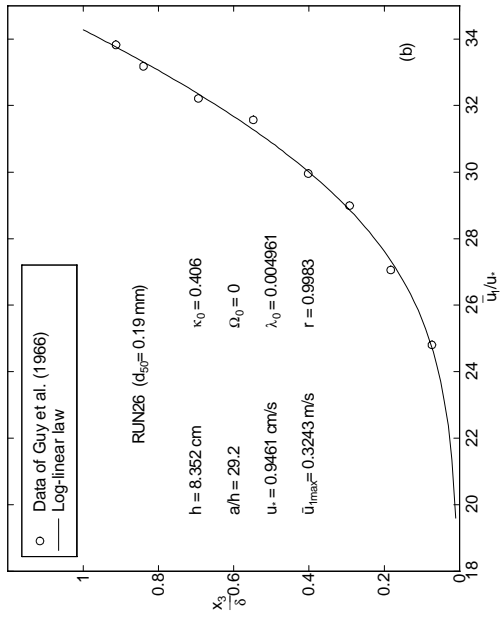
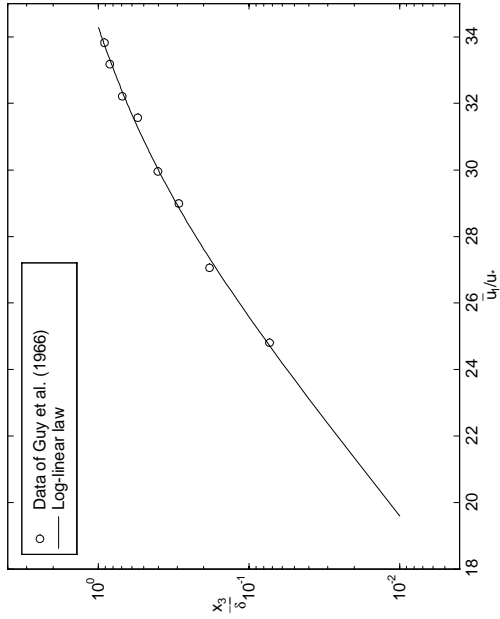
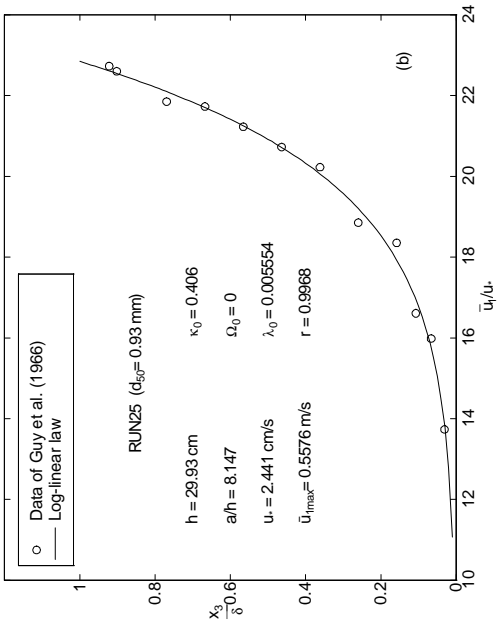
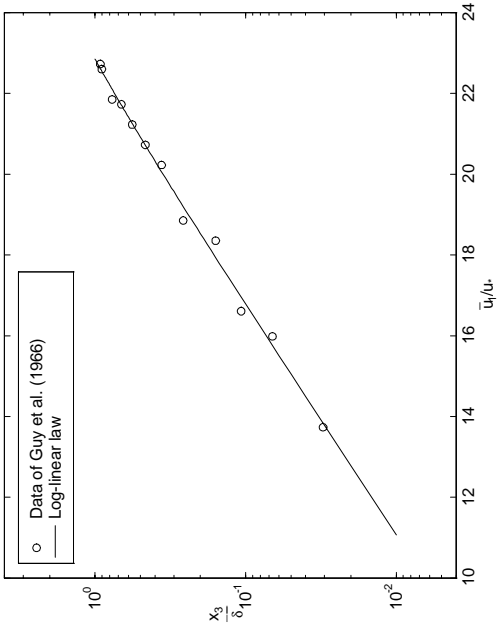
Table H.1: Selected experimental data of Guy, Simons and Richardson (1966)

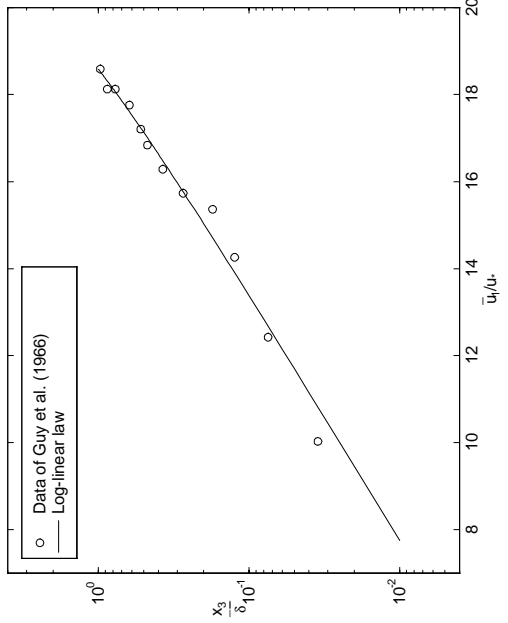
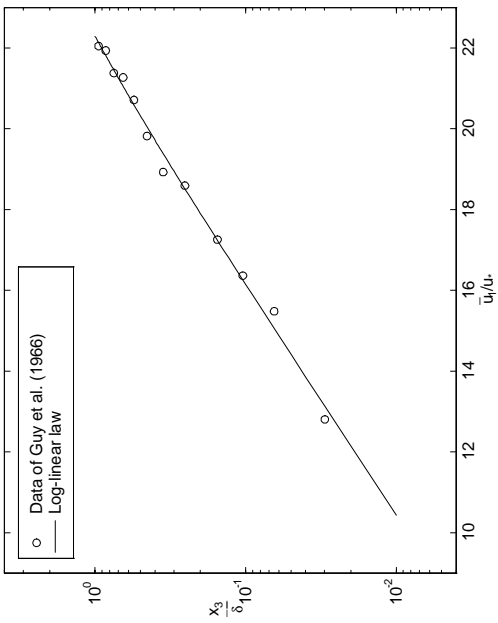
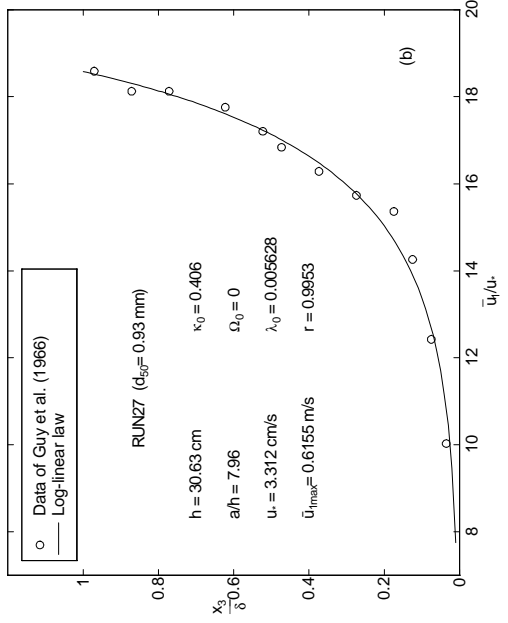
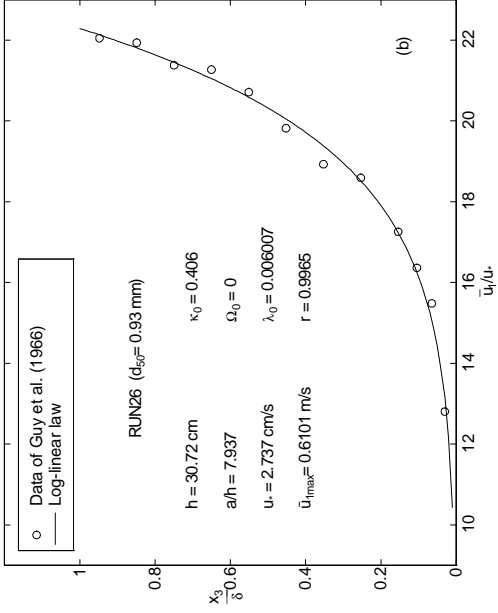
Table12-22C ^a	Table12-24	Table12-26	Table16-19	Table16-20	Table16-25	Table16-26	Table16-27
$d_{50} = 0.19$ mm $h = 12.22$ cm $S = 1.8E - 4$	$d_{50} = 0.19$ mm $h = 28.53$ cm $S = 5.5E - 5$	$d_{50} = 0.19$ mm $h = 8.352$ cm $S = 1.7E - 4$	$d_{50} = 0.93$ mm $h = 29.69$ cm $S = 1.3E - 4$	$d_{50} = 0.93$ mm $h = 29.87$ cm $S = 2.8E - 4$	$d_{50} = 0.93$ mm $h = 29.93$ cm $S = 2.2E - 4$	$d_{50} = 0.93$ mm $h = 30.72$ cm $S = 2.2E - 4$	$d_{50} = 0.93$ mm $h = 30.63$ cm $S = 2.8E - 4$
x_3/h							
\bar{u}_1 (m/s)							
0.935	0.972	0.912	0.918	0.969	0.922	0.947	0.970
0.810	0.865	0.839	0.716	0.918	0.901	0.848	0.871
0.686	0.759	0.693	0.562	0.816	0.769	0.749	0.771
0.561	0.652	0.547	0.408	0.714	0.667	0.650	0.622
0.436	0.545	0.401	0.305	0.612	0.565	0.551	0.522
0.312	0.438	0.292	0.202	0.510	0.463	0.451	0.473
0.249	0.331	0.182	0.151	0.408	0.362	0.352	0.373
0.187	0.278	0.073	0.100	0.306	0.260	0.253	0.274
0.125	0.224		0.059	0.204	0.158	0.154	0.174
0.025	0.171		0.028	0.153	0.107	0.104	0.124
	0.118			0.102	0.066	0.064	0.075
	0.085			0.051	0.031	0.030	0.035
	0.053			0.031	0.031	0.030	0.035
	0.021			0.010	0.010	0.010	0.005
				0.244	0.244	0.244	0.2100

^a Table12-22C means RUN 22 of Table 12 in the literature.









Appendix I

MEASUREMENT DATA IN THE YELLOW RIVER AND THE YANGTZE RIVER¹

Measurements of velocity and concentration profiles
at Hua-Yuan-Kou Hydrologic Station, the Yellow
River, China

Time: 7/27/83
 $h = 3.3$ m
 $S = 3.7 \times 10^{-4}$

Time: 8/15/83
 $h = 2.4$ m
 $S = 7.2 \times 10^{-4}$

ξ	\bar{u}_1 (m/s)	\bar{C} (kg/m ³)	ξ	\bar{u}_1 (m/s)	\bar{C} (kg/m ³)
0.97	2.33	10.40	0.97	2.33	11.80
0.80	2.00	12.00	0.80	2.00	12.30
0.60	1.60	16.30	0.60	1.60	12.80
0.40	1.36	20.20	0.40	1.36	13.30
0.30	1.14	22.00	0.30	1.14	13.50
0.20	0.98	23.80	0.20	0.98	15.30
0.10	0.82	27.10	0.10	0.82	18.80
0.03	0.65	30.00	0.03	0.65	39.30

¹Provided by Prof. Yu-jia Hui, Tsinghua University, Beijing, China

Time: 8/15/83
 $h = 2.5$ m
 $S = 7.2 \times 10^{-4}$

ξ	\bar{u}_1 (m/s)	\bar{C} (kg/m ³)
0.96	3.09	11.40
0.80	2.96	10.40
0.60	2.70	13.50
0.40	2.41	14.30
0.30	2.25	17.40
0.20	2.01	18.90
0.10	1.74	24.00
0.04	1.53	29.00

Time: 8/15/83
 $h = 2.5$ m
 $S = 7.2 \times 10^{-4}$

ξ	\bar{u}_1 (m/s)	\bar{C} (kg/m ³)
0.96	3.11	8.14
0.80	2.96	12.20
0.60	2.74	14.00
0.40	2.46	16.00
0.30	2.31	17.10
0.20	2.10	19.80
0.10	1.86	20.30
0.04	1.64	24.90

Time: 8/15/83
 $h = 2.3$ m
 $S = 7.2 \times 10^{-4}$

ξ	\bar{u}_1 (m/s)	\bar{C} (kg/m ³)
0.96	3.34	7.15
0.80	3.18	7.63
0.60	3.03	11.20
0.40	2.84	15.60
0.30	2.65	18.40
0.20	2.48	19.00
0.10	2.29	23.40
0.04	1.97	22.60

Time: 8/14/83
 $h = 2.4$ m
 $S = 7.8 \times 10^{-4}$

ξ	\bar{u}_1 (m/s)	\bar{C} (kg/m ³)
0.96	3.34	7.50
0.80	3.18	11.20
0.60	2.93	11.60
0.40	2.70	15.10
0.30	2.53	15.80
0.20	2.39	16.50
0.10	2.15	18.40
0.04	1.99	24.80

Time: 8/14/83
 $h = 2.3$ m
 $S = 7.7 \times 10^{-4}$

ξ	\bar{u}_1 (m/s)	\bar{C} (kg/m ³)
0.96	3.38	7.62
0.80	3.11	10.20
0.60	3.02	10.90
0.40	2.62	14.60
0.30	2.48	16.30
0.20	2.27	18.00
0.10	2.01	20.80
0.04	1.81	27.20

Time: 8/15/83
 $h = 2.5$ m
 $S = 8.0 \times 10^{-4}$

ξ	\bar{u}_1 (m/s)	\bar{C} (kg/m ³)
0.96	3.38	3.95
0.80	3.11	8.38
0.60	3.02	10.50
0.40	2.62	12.40
0.30	2.48	14.00
0.20	2.27	15.90
0.10	2.01	14.60
0.04	1.81	19.70

Measurements of velocity and concentration profiles at Feng-Jie Hydrologic Station, the Yangtze River, China

Time: 8/25/76
 $h = 28.7$ m
 $S = 1 \times 10^{-4}$

ξ	\bar{u}_1 (m/s)	\bar{C} (kg/m ³)
0.9983	2.87	1.74
0.8000	2.81	1.84
0.4000	2.57	2.03
0.2000	2.21	2.19
0.1000	1.96	2.35
0.0174	1.43	2.97
0.0035	1.10	4.18

Time: 9/02/76
 $h = 37.1$ m
 $S = 7.5 \times 10^{-5}$

ξ	\bar{u}_1 (m/s)	\bar{C} (kg/m ³)
0.9987	2.74	1.31
0.8000	2.70	1.45
0.4000	2.41	1.65
0.2000	2.28	1.67
0.1000	1.88	1.63
0.0135	1.65	2.34
0.0027	1.33	4.01

Time: 9/03/76
 $h = 34.2$ m
 $S = 8.3 \times 10^{-5}$

ξ	\bar{u}_1 (m/s)	\bar{C} (kg/m ³)
0.9985	2.64	1.60
0.8000	2.61	1.66
0.4000	2.28	1.74
0.2000	2.10	1.72
0.1000	1.87	1.82
0.0146	1.56	1.93
0.0029	1.31	4.71

Time: 7/19
 $h = 42.2$ m
 $S = 5.8 \times 10^{-5}$

ξ	\bar{u}_1 (m/s)	\bar{C} (kg/m ³)
0.9988	2.82	1.41
0.8000	2.82	1.70
0.4000	2.46	1.83
0.2000	2.22	1.93
0.1000	2.03	2.26
0.0118	1.63	2.26
0.0024	1.41	4.93

Time: 8/21/81
 $h = 44.4$ m
 $S = 5.1 \times 10^{-5}$

ξ	\bar{u}_1 (m/s)	\bar{C} (kg/m ³)
0.9989	2.91	2.94
0.8000	2.83	3.58
0.4000	2.59	3.97
0.2000	2.35	4.16
0.0023	1.71	4.15

Time: 5/21/81
 $h = 15.4$ m
 $S = 1.16 \times 10^{-4}$

ξ	\bar{u}_1 (m/s)	\bar{C} (kg/m ³)
0.9989	2.77	0.75
0.8000	2.72	0.88
0.4000	2.45	0.98
0.2000	2.16	1.31
0.0023	1.59	1.59

Time: 8/27/76
 $h = 33.6$ m
 $S = 7.6 \times 10^{-5}$

ξ	\bar{u}_1 (m/s)	\bar{C} (kg/m ³)
0.9985	2.90	2.52
0.8000	2.88	2.53
0.4000	2.58	2.85
0.2000	2.29	3.16
0.1000	2.02	3.24
0.0149	1.79	4.64
0.0030	1.53	8.86

Time: 8/19/81
 $h = 32.3$ m
 $S = 7.5 \times 10^{-5}$

ξ	\bar{u}_1 (m/s)	\bar{C} (kg/m ³)
0.9985	2.85	1.29
0.8000	2.79	1.37
0.4000	2.51	1.67
0.2000	2.30	1.77
0.0031	1.62	1.89

Time: 8/21/81
 $h = 44.4$ m
 $S = 5.1 \times 10^{-5}$

ξ	\bar{u}_1 (m/s)	\bar{C} (kg/m ³)
0.9989	2.91	
0.8000	2.83	
0.4000	2.59	
0.2000	2.35	
0.0023	1.71	

Time: 7/21/76
 $h = 45.9$ m
 $S = 5 \times 10^{-5}$

ξ	\bar{u}_1 (m/s)	\bar{C} (kg/m ³)
0.9989	2.94	1.57
0.8000	2.85	2.03
0.4000	2.58	2.18
0.2000	2.34	2.19
0.1000	2.08	2.77
0.0109	1.89	3.00
0.0022	1.57	3.87

Time: 8/21/81
 $h = 44.4$ m
 $S = 5.1 \times 10^{-5}$

ξ	\bar{u}_1 (m/s)	\bar{C} (kg/m ³)
0.9988	2.91	2.94
0.8000	2.83	3.58
0.4000	2.59	3.97
0.2000	2.35	4.16
0.0024	1.71	4.15